

**Mineralogical and geochemical variations in the UG2 reef at  
Booyssendal and Zondereinde mines, with implications for  
beneficiation of PGM**

by

Michael-John McCall

Thesis presented for the degree of Master of Science in the Faculty of Science at  
Stellenbosch University



Supervisor: Dr Jodie Miller

March 2016

## **Declaration**

By submitting this thesis electronically, I declare that the entirety of the work contained therein is my own, original work, that I am the sole author thereof (save to the extent explicitly otherwise stated), that reproduction and publication thereof by Stellenbosch University will not infringe any third party rights and that I have not previously in its entirety or in part submitted it for obtaining any qualification.

March 2016

Copyright © 2016 Stellenbosch University

All rights reserved

## Abstract

The layered intrusion of the Bushveld Complex, South Africa hosts the world's largest concentration of platinum group elements (PGE), which are principally mined from three mineralised horizons namely, the Merensky reef, the Upper Group Two (UG2) reef and the Platreef. The PGE contents of these horizons are conventionally beneficiated via comminution, froth flotation and smelting techniques. The mineralogical and geochemical characteristics of the platiniferous reefs, and any variations thereof, are known to be intimately connected with the performance of the above-mentioned techniques. In particular, the chromite-rich UG2 reef presents a variety of complications, for example the ore/gangue relationships, mineral chemistry and textural characteristics, which can impact upon its beneficiation potential.

This study was primarily aimed at evaluating and constraining the mineralogical and geochemical characteristics of two UG2 reef mining cuts from Booyendal mine (eastern Bushveld Complex) and Zondereinde mine (western Bushveld Complex). The results of comprehensive petrographic (2-D and 3-D), compositional and geochemical investigations were then placed within the context of the milling and flotation process in order to comment on the impact that any variability might have during the beneficiation of the PGE contents. In addition to these aims, the validity of results obtained from 3-D microfocus X-Ray Computed Tomography ( $\mu$ XCT) were assessed within the context of this study.

In this study it was found that the main ore zone from each UG2 reef sample is characterised by cumulate chromite grains with variable characteristics depending on the grain size, composition, degree of compaction and grain shape. The Zondereinde UG2 reef in particular was interpreted as having experienced a significant degree of compaction due to the lack of intercumulate silicate phases within the chromitite units. All mineral phases within both UG2 reef sample sets exhibit variable alteration features which results in the replacement of primary silicates by hydrous silicate minerals. PGE grade is commonly distributed with a top- and bottom-loaded profile in the main chromitite layers. Some PGE exist as platinum group minerals (PGM) with average grain sizes of less than 3  $\mu$ m, associated predominantly with nickel and copper

sulphide minerals. The Booyendal UG2 reef is dominated by a PGE-sulphide assemblage whereas Zondereinde is dominated by PGE-alloys.

The mineralogical and geochemical characteristics further described in this study can be utilised to refine the milling regime and flotation parameters in order to maximise plant efficiencies. It is suggested that the Booyendal UG2 reef's lesser degree of compaction within the chromitite horizons and predominance of PGE-sulphide mineral compositions may yield better liberation and faster recoveries of PGM contents when compared to the Zondereinde UG2 reef. In the case of the Zondereinde UG2 reef, the homogeneity of chromite textures might serve to simplify the refinement of milling regimes so as to not over- or under-grind the reef contents. This, coupled with a strong association of PGM with comparably higher sulphide mineral proportions will benefit the beneficiation process.

The interpretation of results obtained from 3-D  $\mu$ XCT proved the technique to be a powerful tool in terms of the broad-scale characterisation of chromite textures and PGM distribution. The technique however suffers from resolution limitations when attempting to accurately discern individual PGM grains. This is interpreted to be an artefact of the typically small grain size of PGM from the UG2 reef.

## **Keywords**

Bushveld Complex, UG2, Platinum Group Mineral, 3-D X-Ray Computed Tomography, Scanning Electron Microscope, QEMSCAN, X-Ray Diffraction, Beneficiation



## Acknowledgements

First and foremost, I would like to extend my sincere gratitude to Dr Jodie Miller for her support during this project. Her guidance, kindness and expertise has lead me up to this point and without her, I would not have been able to undertake this project nor would I have come close to producing a product of this standard. Secondly, I would like to thank Dr Ian Basson for both his financial and technical support throughout the duration of the project. Knowing that I had him in my corner gave me the confidence to focus on, and tackle the task at hand.

I would also like to thank Dr Megan Becker and Gaynor Yorath for their assistance with all things QEMSCAN, Madelaine Frazenburg for her expertise and patience during SEM work and Dr Anton du Plessis for his help with the 3-D  $\mu$ XCT component of the work. The kindness, willingness to help and the understanding of these particular people knows no bounds. Many thanks go to Damian Smith from Northam Platinum, for without his assistance, this project would never have been realised.

Additionally, I would like to thank all those who were present on my journey through the minefield that is a M.Sc. project. Thank you for standing by me in times of weakness and frustration; your help, kind words of encouragement and understanding made a real difference.

## Contents

Declaration .....	i
Abstract .....	ii
Keywords .....	iii
Acknowledgements .....	iv
Abbreviations .....	viii
Mineral List.....	ix
Chapter 1: INTRODUCTION .....	1
1.1. General Introduction.....	1
1.2. Aims and Objectives .....	4
1.3. Platinum-group Mineralisation.....	6
1.3.1. Variations in Platinum-group Mineralogy .....	8
1.3.2. Precious Metal Beneficiation .....	8
Chapter 2: THE BUSHVELD COMPLEX.....	11
2.1. Lithostratigraphy.....	12
2.1.1. Critical Zone .....	13
2.2. The UG2 Reef .....	14
2.2.1. Relationships between Mineral Phases.....	15
2.2.2. Variations in Reef Characteristics.....	16
2.3. Sample Locations.....	17
2.3.1. Booyendal.....	17
2.3.2. Zondereinde .....	18
Chapter 3: METHODS.....	20
3.1. Introduction .....	20
3.2. Sample Preparation .....	20
3.3. Petrographic and SEM Analysis.....	23

3.4. XRD Mineralogical Analysis .....	23
3.5. QEMSCAN Analysis.....	24
3.6. Geochemical Analysis.....	24
3.7. X-Ray Computed Tomography.....	25
Chapter 4: BOOYSENDAL UG2 .....	27
4.1. Structure and Bulk Mineralogy .....	28
4.2. Textural Relationships.....	30
4.2.1. Silicates .....	30
4.2.2. Chromite .....	32
4.2.3. Sulphides.....	34
4.2.4. PGM .....	36
4.3. Mineral Chemistry and Relative Proportions .....	40
4.3.1. Chromite .....	40
4.3.2. Sulphides.....	41
4.3.3. PGM .....	43
4.4. Bulk Rock Geochemistry .....	46
4.4.1. Differentiation between Mining Units .....	46
4.4.2. Stratigraphic Variation .....	47
4.5. 3-D $\mu$ XCT Analysis.....	50
4.5.1. Chromite Texture and 3-D Distribution of PGM .....	50
4.5.2. PGM Grain Size Characteristics .....	52
Chapter 5: ZONDEREINDE UG2 .....	52
5.1. Structure and Bulk Mineralogy .....	54
5.2. Textural Relationships.....	56
5.2.1. Silicates .....	56
5.2.2. Chromite .....	58

5.2.3. Sulphides.....	61
5.2.4. PGM .....	63
5.3. Mineral Chemistry and Relative Proportions .....	67
5.3.1. Chromite .....	67
5.3.2. Sulphides.....	68
5.3.3. PGM .....	70
5.4. Bulk Rock Geochemistry .....	73
5.4.1. Differentiation between Mining Units .....	73
5.4.2. Stratigraphic Variation .....	74
5.5. 3-D $\mu$ XCT Analysis.....	77
5.5.1. Chromite Texture and 3-D Distribution of PGM .....	77
5.5.2. PGM Grain Size Characteristics .....	79
Chapter 6: DISCUSSION .....	80
6.1. Mineralogical and Textural Characterisation of UG2.....	80
6.1.1. Booyendal.....	80
6.1.2. Zondereinde .....	82
6.2. Relationship between Chromite, Sulphides and PGE Grade .....	84
6.3. Two-Dimensional vs. Three-Dimensional Analysis .....	87
6.4. Implications for PGM Beneficiation .....	90
Chapter 7: CONCLUSIONS .....	93
7.1. Conclusions.....	93
7.2. Recommendations .....	95
References.....	97
Appendix A.....	106

## Abbreviations

3-D $\mu$ XCT	Three-dimensional microfocus X-ray Computed Tomography
4PGE	Four platinum-group elements (Pt, Pd, Rh, Ru)
Alt	Alteration phase
Au	Gold
BMS	Base Metal Sulphide/s
CAF	Central Analytical Facility
Chr	Chromite
Cu	Copper
ECD	Equivalent circular diameter
ED	Energy dispersive
ESD	Equivalent spherical diameter
FW	Footwall
HW	Hanging wall
ICP-OES	Inductively Coupled Plasma Optical Emission Spectrometer
Ir	Iridium
IRUP	Iron-rich ultramafic pegmatoid
MLA	Mineral Liberation Analyser/Analysis
NC	No core
Ni	Nickel
Opx	Orthopyroxene
Os	Osmium
Pd	Palladium
PGE	Platinum-group element/s
PGM	Platinum-group metals/minerals
Plag	Plagioclase
PSD	Position sensitive detector
Pt	Platinum
QEMSCAN	Quantitative evaluation of minerals by SEM
Rh	Rhodium
RLM	Reflected light microscopy
RLS	Rustenburg Layered Suite
Ru	Ruthenium
S	Sulphur
SEM	Scanning Electron Microscopy
SG	Specific gravity
Sil	Silicate
Wt. %	Weight per cent
XRD	X-Ray diffraction
Z	Average atomic number
Zn	Zinc
$\mu$ m	Micrometre

**Mineral List**

Anorthite (Plagioclase)	$\text{CaAl}_2\text{Si}_2\text{O}_8$
Antigorite (Serpentine)	$(\text{Mg,Fe})_3\text{Si}_2\text{O}_5(\text{OH})_4$
Apatite	$\text{Ca}_5(\text{PO}_4)_3(\text{F,Cl,OH})$
Biotite	$\text{K}(\text{Mg,Fe})_3\text{AlSi}_3\text{O}_{10}(\text{OH,F})_2$
Braggite	$(\text{Pt,Pd})\text{S}$
Calcite	$\text{CaCO}_3$
Chalcocite	$\text{Cu}_2\text{S}$
Chalcopyrite	$\text{CuFeS}_2$
Clinochlore (Chlorite)	$(\text{Mg,Fe})_5\text{Al}(\text{AlSi}_3)\text{O}_{10}(\text{OH})_8$
Clinochrysotile (Serpentine)	$\text{Mg}_3\text{Si}_2\text{O}_5(\text{OH})_4$
Cooperite	$\text{PtS}$
Enstatite (Orthopyroxene)	$\text{Mg}_2\text{Si}_2\text{O}_6$
Forsterite (Olivine)	$\text{Mg}_2\text{SiO}_4$
Galena	$\text{PbS}$
Hornblende	$\text{Ca}_2[\text{Mg}_4(\text{Al,Fe})]\text{Si}_7\text{AlO}_{22}$
Illite (Mica)	$(\text{K,H}_3\text{O})(\text{Al,Mg,Fe})_2(\text{Si,Al})_4\text{O}_{10}(\text{OH})_2$
Isoferroplatinum	$(\text{Pt,Pd})(\text{Fe,Cu})$
Laurite	$\text{RuS}_2$
Magnesio-chromite	$\text{MgCr}_2\text{O}_4$
Malanite	$\text{Cu}(\text{Pt,Ir})_2\text{S}_4$
Millerite	$\text{NiS}$
Muscovite (Mica)	$\text{KAl}_2(\text{Si}_3\text{Al})\text{O}_{10}(\text{OH,F})_2$
Pentlandite	$(\text{Fe,Ni})_9\text{S}_8$
Pyrite	$\text{FeS}_2$
Pyrrhotite	$\text{Fe}_{(1-x)}\text{S}$ ( $x=0-0.17$ )
Rutile/Anatase	$\text{TiO}_2$
Sperrylite	$\text{PtAs}_2$
Talc	$\text{Mg}_3\text{Si}_4\text{O}_{10}(\text{OH})_4$
Tetraferroplatinum	$\text{PtFe}$
Titanite (Sphene)	$\text{CaTiSiO}_5$
Tremolite (Amphibole)	$\text{Ca}_2\text{Mg}_5\text{Si}_8\text{O}_{22}(\text{OH})_2$
Uvarovite	$\text{Ca}_3\text{Cr}_2(\text{SiO}_4)_3$

## Chapter 1: INTRODUCTION

### 1.1. General Introduction

The Bushveld Complex, South Africa, is the world's largest known concentration of platinum group elements (PGE), chromium and vanadium (Cawthorn, 2005; Naldrett et al., 2009). Since the discovery of PGE mineralisation more than 90 years ago, the Bushveld Complex has been the subject of extensive and ongoing research (see review by Cawthorn 1999), and yet there are still many aspects on which researchers are unable to reach consensus. Two areas which continue to attract considerable debate are the mechanics behind the formation of chromitite layers as well as the accumulation of PGE within these layers (Godel et al., 2010). The formation of chromitite layers within the Rustenburg Layered Suite (RLS) is generally attributed to either gravity settling or influxes of magma with different compositions (see review by Schouwstra et al., 2000). The debate around PGE accumulation has focused on the formation and mineralisation of the Merensky and UG2 reefs, which collectively comprise ~90 per cent (%) of the total platinum and palladium resources in the Bushveld Complex (Vermaak, 1995).

There are two models which are generally thought to have been responsible for PGE enrichment in the Merensky and UG2 reefs. The first model is based on an orthomagmatic origin for PGE enrichment (Ballhaus and Sylvester, 2000; Godel et al., 2007). In this model PGE-rich sulphide blebs form in-situ during the initial fractionation of the host magmas. This model is supported by recent observations of nano-scale PGE inclusions found within base metal sulphides (BMS) (Wirth et al., 2013). The nano-scale PGE inclusions in the BMS are interpreted to represent an early phase of platinum group mineral (PGM) precipitation from a silicate melt. This would suggest that nano-scale PGM were entrained within the sulphide fraction before crystallisation of the magma. The second model proposes that BMS act as collectors of PGE which are subsequently transported upwards through a partially solidified crystal pile via post-magmatic fluid infiltration. These fluids then get trapped by impermeable chromitite layers, such as the Merensky and UG2 reefs (Boudreau and McCallum, 1992). Evaluating these two models has been complicated by the variability in reef characteristics throughout the Bushveld Complex (Penberthy and Merkle, 1999).

One of the most impressive aspects of the Bushveld Complex is the broad scale homogeneity and lateral continuity of the mineralised reefs (Cawthorn, 1999). The UG2 and Merensky Reefs are known to be laterally continuous on the scale of hundreds of kilometres and maintain relatively uniform compositions and thicknesses over much of this length (Schouwstra et al., 2000; Eales and Cawthorn, 1996). However, in spite of these overall similarities, important variations are known to exist within the mineralised reefs including variations in mineral compositions, phase abundances, textures and/or the mode of occurrence of minerals. These variations are linked to both primary (magmatic) and secondary (recrystallization) mechanisms (Kinloch, 1982). Some of these variations manifest in regional domains. For example, PGM within the Merensky reef adjacent to the Pilanesberg Alkaline Complex (western limb) are dominated by Pt-Fe alloy compositions, whereas other areas show a strong predominance for PGE-sulphide assemblages (Kinloch, 1982). PGM phases in the UG2 reef also vary between sulphide- or alloy-dominated assemblages. Other important mineralogical variations in the UG2 include the variable replacement of primary silicate phases with quartz, albite, sphene and low temperature alteration minerals such as talc, serpentine, chlorite and epidote (Penberthy and Merkle, 1999). The variable nature of the UG2 impacts not only on our understanding of the PGE collection models but also on how the PGE are beneficiated.

Variable reef characteristics directly impact PGE beneficiation processes such as flotation and smelting (Becker et al., 2008). In particular, the very high chromite contents coupled with low proportions of BMS make it a more challenging target for PGM recovery. This is further complicated by our relatively poor understanding of the distribution and occurrence of PGE within the reef. Traditionally, PGE were thought to only be hosted in PGMs and the type, proportion and location of the PGMs had a direct impact on the amount of PGE ultimately recovered (Xiao and Laplante, 2004). In recent years there has been an acknowledgement that not all PGE occur as PGM and that some PGE occur as nano-particles and within solid-solution in BMS (Wirth et al., 2013; Cawthorn et al., 2002). To ensure a high degree of PGM liberation and recovery of this component of the PGE budget requires fine to ultra-fine grinding. However this process introduces complications with the beneficiation of the PGM including the possible increase in the proportions of naturally floating gangue (e.g. talc) and a decrease in average grain size which may cause rheological issues during flotation



(Becker et al., 2013). The key to understanding the impact of these processes lies in better understanding the exact in-situ nature of PGM mode of occurrence and distribution within targeted mineralised horizons.

The fine-scale mineralogical and textural variation of PGM and chromite within the UG2 reef has always been difficult to evaluate because of two main factors. These are the very fine grain size of typical PGM (generally less than 10  $\mu\text{m}$ ) (Junge et al., 2015), and the extremely heterogeneous distribution of PGM within the mineralised horizons, often referred to as the “nugget” effect. The second of these factors has been more difficult to evaluate because most studies conducted on PGM beneficiation have tended to use milled samples to evaluate PGM populations. In these cases, the primary characteristics of the reef are destroyed and the results may be skewed by the selective bias caused by the variable responses of different minerals during the flotation/concentration stages (Penberthy et al., 2000).

A number of analytical developments in recent years have allowed for the re-examination of the PGM populations and distribution within mineralised horizons such as the UG2 reef. The first of these was the development of the auto-SEM techniques such as MLA and QEMSCAN which have been successful in providing large statistical databases on ore characteristics which have helped to improve the beneficiation process. QEMSCAN, developed by CSIRO in Australia, provides an automatic, offline pixel by pixel mineralogical analysis of samples by using a combination of EDX analysis and BSE images to build an image of a sample based on the chemical composition of the mineral contents (Xiao and Laplante, 2004). More recently, the advent of three-dimensional microfocus X-ray computed tomography (3-D  $\mu\text{XCT}$ ) has allowed visualisation of geological samples in the third dimension, potentially providing unrivalled insights into the 3-D distribution of mineral phases within mineralised reefs like the UG2.

In this study, focused mineralogical and geochemical data are used to understand variations in both the PGM populations and the textural environment in which the PGM occur on both the eastern and western limbs of the Bushveld Complex. All the samples come from the Northam Platinum mining leases of either Zondereinde (western Bushveld Complex) or Booyendal (eastern Bushveld Complex). Data collected

include bulk mineralogy, mineral compositions, grain shape and size statistics, and the 2-D (QEMSCAN) and 3-D ( $\mu$ XCT) distribution of PGM. The data were then linked using geochemical indicators to variations in reef characteristics and placed in context of the beneficiation process that is required to concentrate PGEs. The combination of 2-D and 3-D analysis with detailed textural information allowed the evaluation of each technique to better understand the nature of PGE mineralisation in each reef type.

## 1.2. Aims and Objectives

The study was undertaken to describe and compare mineralogical and geochemical characteristics of UG2 reef samples from Booyendal and Zondereinde mines (Northam Platinum). Along with an in-depth investigation into the typical mining cut at each location, this study is complemented with a discussion on the possible influences of variations in reef characteristics on PGM beneficiation processes. In addition to these aims, results obtained via traditional 2-D techniques are compared with those obtained from 3-D  $\mu$ XCT. Therefore the aims of this study are four-fold and are outlined below.

1. To describe the mineralogical and textural characteristics of each UG2 mining cut.
  - What is the bulk mineralogy (size, shape and texture for dominant minerals) of the reef and how does it vary between the various mining units?
  - How do the major mineral groups (i.e. silicates, oxides, sulphides and PGM) associate themselves within the UG2 reef?
  - How do the proportions of each mineral group vary with stratigraphic height?
  - How are chromite and PGM grains distributed in 3-D within each of the main ore bearing units?
  
2. To determine the chemical characteristics of each UG2 mining cut.
  - What are the compositions of major oxide, base metal sulphide and PGM minerals?
  - How is the PGM budget characterised in terms of mineral speciation?

- What are the bulk geochemical characteristics and how does this relate to mineralogical changes in the UG2 reef?
- What is the distribution of PGE and base metals in the UG2 reef and do any correlations exist between PGE grade and other geochemical features?

3. To assess how reef characteristics might influence the performance of PGM beneficiation processes.

- How might mineralogical/textural variations influence beneficiation techniques such as grinding regimes for PGM liberation and froth flotation for PGM recovery?

4. To discuss the possible advantages and shortcomings of 2-D and 3-D imaging techniques within the context of PGM characterisation.

- What are the advantages and disadvantages of 2-D and 3-D imaging techniques for the characterisation of the UG2 reef?
- How might 2-D and 3-D techniques be successfully combined to improve the characterisation of PGM?

### 1.3. Platinum-group Mineralisation

All chromitite layers throughout the critical zone (CZ) of the Rustenburg Layered Suite (RLS) are known to contain elevated PGE concentrations (Lee, 1996; Scoon and Tieglar, 1994). Average PGE grades within the UG2 reef are in the region of 4-9 ppm however, this may vary from location to location throughout the Bushveld Complex (Schouwstra et al., 2000; Voordouw et al., 2010). Typically, sulphide melts that give rise to Ni-Cu ores have platinum and palladium contents of between 0.36-1.6 ppm and 0.5-2.5 ppm respectively, meaning that the UG2 reef has an anomalously high PGE/BMS ratio (Gain, 1985). The PGE budget of the UG2 reef is described by Penberthy and Merkle (1999) in two categories. This first is as discrete platinum-group minerals whilst the second is as platinum-group elements that exist within solid solution of BMS. PGE that exist within the crystal lattice or within solid solution with BMS are considered an important component of the PGE budget for the Bushveld Complex (Kinloch 1982). Furthermore, a recent study by Wirth et al (2013) found that PGE which were generally accepted to exist within solid solution of BMS may actually exist as nano-particles or inclusions (<50 nm in size). These nano-particles are invisible to many conventional microscopy techniques due to their small grain sizes. The PGE-sulphide and -arsenide nano-particles were found to occur as inclusions within pentlandite, pyrrhotite and pyrite as idiomorphic, plate-like crystals but not within chalcopyrite (Wirth et al., 2013). The texture of the nano-particles suggests that they crystallised before solidification of the sulphide melt and the formation of the BMS host, suggesting an orthomagmatic origin for PGE enrichment.

PGE contents that are hosted as discrete PGM form a variety of sulphide assemblages such as cooperite, braggite, malanite and laurite or PGE-alloys such as ferroplatinum, PGE-telluride, -bismuthinide, -arsenide, -bismuthotelluride or -sulpharsenide assemblages (Penberthy et al., 2000). The PGM budget of 'normal UG2 reef' is described as having >90 % PGE-sulphides whereas 'atypical UG2 reef', or reef affected by post magmatic processes, usually contains a higher proportion of PGE-Fe alloys and PGE-bismuthotelluride minerals (Penberthy and Merkle, 1999). When comparing 'normal' and 'atypical' reef types there are no major changes in either grain size or the mode of occurrence of PGM. Average grain sizes are reported to be in the region of 10-30  $\mu\text{m}$  (ranging from <1-50  $\mu\text{m}$ ), however some abnormally large grains

up to 200  $\mu\text{m}$  in size have also been identified (Junge et al., 2014; Penberthy and Merkle, 1999; Schouwstra et al., 2000).

Typically the vertical distribution of PGE + Au in the UG2 reef can be described as top- and bottom-loaded with decreasing proportions of grade towards the centre of the chromitite layers (Penberthy and Merkle, 1999). The distribution of PGE throughout stratigraphic height, although highly variable, does follow some recognisable trends which may allow for the testing of geological models and interpretations for the formation of the mineralised reef (Cawthorn, 2011). There is typically no grade associated with the hanging wall, but some PGE have been found to exist in association with small amounts of 'xenolithic' chromite fragments in the pegmatoidal footwall just below the main chromitite layer (Cawthorn, 2011).

According to Penberthy and Merkle (1999), generally the UG2 reef of the Swartklip facies (north-western Bushveld Complex) exhibits higher PGE grades with a thinner reef width, whilst the UG2 reef of the Rustenburg facies (south-western Bushveld Complex) is thicker but has a lower overall PGE grade, coupled with higher Pt/Pd ratios. When compared to the eastern limb, the UG2 reef of the western limb is thicker but suffers from lower average PGE grades. Interestingly, even though average grades are lower over thicker intervals, there are higher proportions of extractable PGE over the entire width of the UG2 reef. This may be due to a higher proportion of PGE grade contained within discrete PGM rather than PGE which exist in solid solution or PGM which exist as nano-particles in BMS.

PGE grade is known to decrease with increasing proximity to the Steelpoort fault (eastern Bushveld Complex) as well as other localised reef disturbances such as potholes and iron-rich ultramafic pegmatoids (IRUP) (Gauert et al., 1995). A UG3 chromitite layer, which is primarily restricted to the northern region of the eastern limb is characterised by a large Pt/Pd ratio (Cawthorn, 2011). The absence of this layer elsewhere is attributed to its amalgamation with the main UG2 reef (Gain, 1985; Reid and Basson, 2002).

### 1.3.1. Variations in Platinum-group Mineralogy

There are geological anomalies which influence the distribution and mineralogy of PGM (Penberthy and Merkle, 1999; Reid and Basson, 2002; Scoon and Mitchell, 1994; Smith et al., 2013). These anomalies occur on both a local and regional scale throughout the Bushveld Complex. Variations from 'typical' or 'normal' UG2 reef are attributed to the interaction with fluids at low-intermediate temperatures, local disturbances such as IRUP, potholes and faulting or otherwise as a result of other less well-defined hydrothermal activity or erosional processes (Gauert et al., 1995; Penberthy and Merkle, 1999; Viljoen and Scoon, 1985). Many of these can result in the truncation of the well-mineralised bottom portion of the UG2 reef ultimately redistributing the PGE contents.

The interaction of iron-rich fluids with PGE may result in a change in PGM composition to Pt-Fe alloys, PGE-sulpharsenides, PGE-bismuthotellurides and other non-sulphide phases (Penberthy and Merkle, 1999). Kinloch (1982) drew the comparison between the Driekop dunite pipe as a smaller scale representation of the Bushveld Complex in terms of the influence of volatiles on PGM compositions especially when it comes to the presence of Pt-Fe alloys. Additionally, potholes are seen to serve as a proxy for fluid movement which is thought to be responsible for the increase in the Pt-Fe alloy/PGE-sulphide ratio, as well as changes in the primary BMS assemblage (Kinloch, 1982). Platinum is a siderophilic element which has the tendency to alloy with iron under conditions of high oxygen fugacity ( $fO_2$ ). Higher  $fO_2$  is observed in areas where fluid movement is present; these areas also see an increase in the proportion of PGE within solid solution of other non PGE-phases (Kinloch 1982).

### 1.3.2. Precious Metal Beneficiation

Typically, PGE from the UG2 reef are beneficiated by means of multistage milling and froth flotation (Corrans et al., 1982, Overbeek et al., 1985). The milling schedule of an ore is a crucial component of the beneficiation process as over-grinding wastes energy and may result in excessive fines production, whilst under-grinding results in poor liberation and hence poor recovery of PGM. Milling regimes are crucial to efficient liberation likely that some of the greatest losses of PGM occur during this early stage of the beneficiation process (Xiao and Laplante, 2004). Froth flotation is a process

whereby minerals are separated based on their chemical and physical characteristics. In the case of PGM flotation, hydrophobic minerals, such as BMS and PGM, are collected on air bubbles (froth) that rise to the surface of the flotation cell whilst hydrophilic minerals such as silicates and oxides sink to the bottom (Will and Munn, 1997). The recovery of PGM is influenced by several factors some of which include grain size, association, composition and the degree of liberation of the BMS and PGM fractions (Chetty et al., 2009; Lotter et al., 2008; Penberthy and Merkle, 1999; Schouwstra et al., 2000).

Froth flotation performance is based on bulk sulphide flotation principles (Xiao and Laplante, 2004). According to Penberthy and Merkle (1999), PGM that are associated with BMS report to the fast floating concentrates with chalcopyrite being the fastest floating BMS species. Liberated PGM grains report to the fast floating concentrates but at a slower rate than PGM associated with BMS (Penberthy et al., 2000). A study of the flotation potential of PGM with different compositions by Chetty et al. (2009) found that PGE-sulphide contents are concentrated first, with decreasing proportions down the test flotation cell bank, whilst PGE-Bi-Te and -As minerals peaked in the later cells. The speed at which different liberated PGM grains are recovered, from fastest to slowest, (with larger grains being preferentially floated) are braggite, cooperite, malanite, ferroplatinum and laurite (Penberthy and Merkle, 1999). PGM grains that are associated with composite BMS/gangue particles tend to report to either the slow floating concentrates or tailings. PGM that are hosted within chromite, typically laurite, or within solid solution with silicate minerals are essentially unrecoverable using the above-mentioned techniques (Kinloch 1982).

The chemistry of the flotation cell used to beneficiate PGM from the UG2 is of great importance. Micro-flotation tests by Wesseldijk et al. (1999) showed that the reagent suite used and pH conditions present during flotation influenced the recovery of chromite. This is especially important as the practical upper limit for chromite content, as a source of MgO, within the final concentrate is 2.5 - 3 % due to the increasing effect magnesium has on the liquidus temperature during smelting (Ekmekçi et al., 2003; Lotter et al., 2008). Chromite, being hydrophilic, does not float naturally and it is thought that the main mechanisms for chromite recovery is by entrainment or via the flotation of composite particles (Ekmekçi et al., 2003; Hay and Roy, 2010; Wesseldijk

et al., 1999). Another major source of MgO within mafic deposits is olivine, orthopyroxene and associated hydrous alteration minerals such as serpentine, talc and chlorite (Lotter et al., 2008). The addition of a Cu-sulphate activator increases the floatability of orthopyroxene and plagioclase but decreases that of talc (Martinovic, 2005).

It is common to find hydrous alteration minerals along grain boundaries and cleavage planes of primary orthopyroxene within the UG2 reef (Becker et al., 2006; Li et al., 2004). Phyllosilicate minerals such as talc and serpentine form from the low temperature alteration of anhydrous minerals such as orthopyroxene or olivine (Becker et al., 2013) with some of these hydrous minerals being naturally floatable (e.g. talc and chlorite). Therefore, understanding the inter-relationships of ore to gangue minerals, distribution and mode of occurrence is critical in terms of minimising inadvertent recovery (Becker et al., 2013). The problems associated with increased orthopyroxene and/or alteration mineral flotation are; 1) the dilution of the flotation concentrate, 2) the reduction of pay-metal grades, 3) the increase of MgO contents in the concentrate and 4) decreased froth stability (Becker et al., 2009; Hay and Roy, 2010). This undesirable "MgO flotation" can be minimised through the use of depressants such as carboxy-methyl cellulose (CMC) or guar gum (Lotter et al., 2008).

The small grain size of PGM, low sulphide contents, high chromite content and the natural floatability of some gangue minerals make the UG2 reef a complex ore from which to beneficiate PGM efficiently (Lotter et al., 2008; Rule and Schouwstra, 2011; Schouwstra et al., 2000). Inefficient recovery due to variations in ore characteristics has prompted further interrogation into understanding where and why loss of grade occurs in order to maximise recovery (Penberthy et al., 2000). This can be done by compiling statistically relevant and reliable mineralogical data on the type, texture, mode of occurrence and size of PGM, BMS, oxide and silicate minerals and relating these characteristics to the known behaviour of the minerals during froth flotation (Penberthy and Merkle, 2000; Schouwstra et al., 2000).



## Chapter 2: THE BUSHVELD COMPLEX

The Palaeoproterozoic Bushveld Complex (Fig. 1) is a sequence of layered ultramafic and mafic igneous rocks that were intruded into the Transvaal Supergroup at ~2.06 Ga (Buick et al., 2001; Walraven et al., 1990). In the northern limb of the Potgietersrus area the Bushveld Complex overlies Archean granite basement rocks (Armitage et al., 2002). The rock types are dominantly noritic but span a compositional and mineralogical range from harzburgite and pyroxenite through to leuconorite and anorthosite. It is thought to extend 450 km east-west and 350 km north-south (Naldrett et al., 2008), is approximately 7-9 km thick (Eales and Cawthorn, 1996) and covers (discontinuously) an area of ca. 65 000 km<sup>2</sup> (Cawthorn and Webb, 2001). The stratigraphy of the Bushveld Complex dips towards the centre of the intrusion at 10-20°. This is thought to be the result of isostatic adjustment of the crust in response to the large density contrast between the mafic rocks (~3.02 g/cm<sup>3</sup>) of the Bushveld Complex and the surrounding host rocks (~2.6 g/cm<sup>3</sup>) (Cawthorn and Webb, 2001; Webb et al., 2004). Despite its age, it is not thought to have undergone any significant metamorphism or deformation other than tectonic subsidence (Eales and Cawthorn, 1996).

Presently, the Bushveld Complex crops out in five distinct areas, or so-called limbs; the eastern, western, far western, northern and south eastern (McLaren and de Villiers, 1982). The main focus of mining activity has been situated on the eastern and western limbs because of large surface outcrops along strike of the Merensky and UG2 reefs. Although often referred to separately, the eastern and western limbs are believed to be connected at depth (Cawthorn and Webb, 2001; Cawthorn et al., 2008; Webb et al., 2004). The western limb is divided into northern and southern compartments, termed the Swartklip and Rustenburg facies respectively.

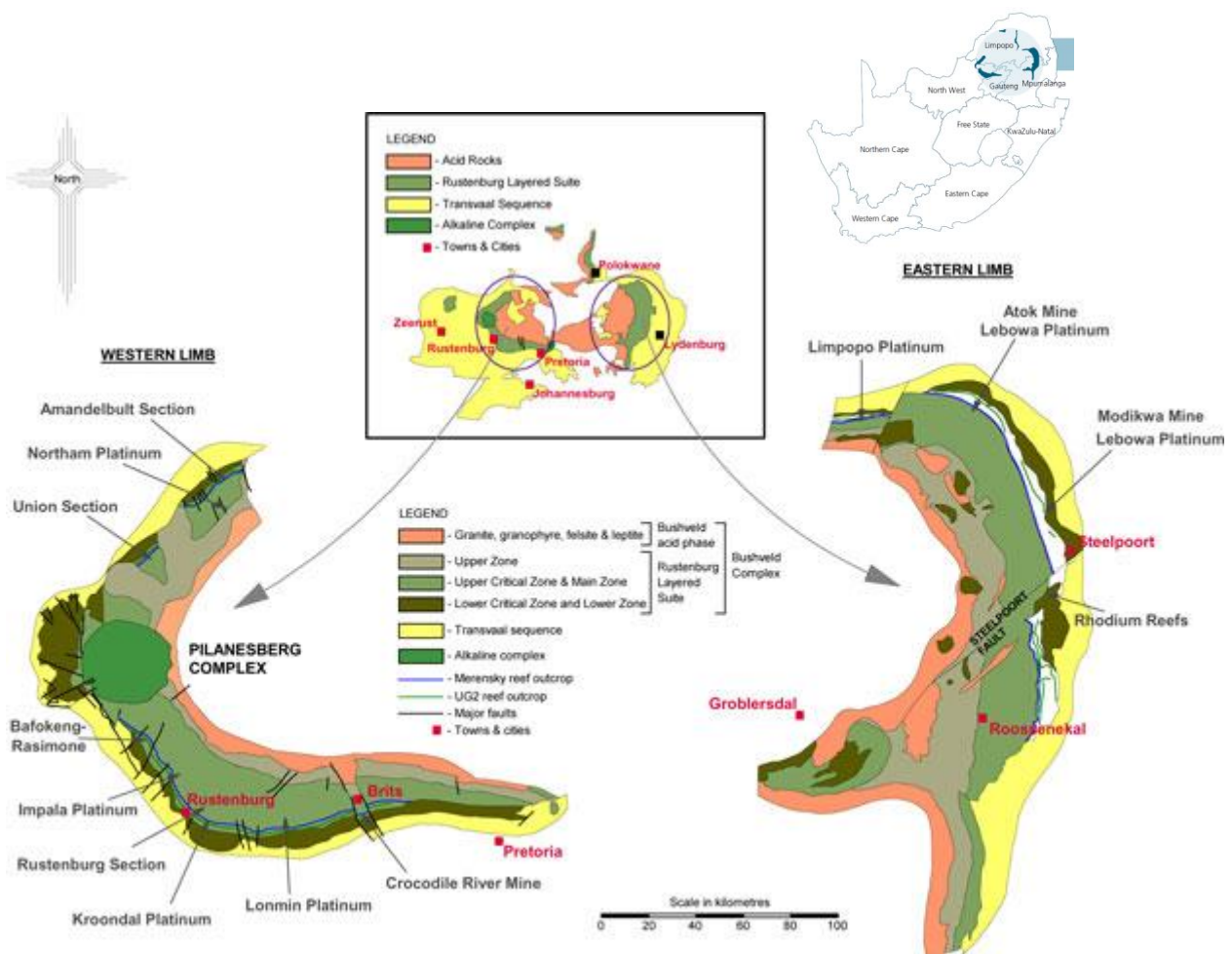


Figure 1 - Geological map of the Bushveld Complex (Stone and Chunnnett, 2007)

## 2.1. Lithostratigraphy

The Bushveld Complex is made up of five main lithostratigraphic suites of rocks: (1) a suite of intrusive mafic sills, (2) the Rooiberg lavas, (3) the Rustenburg Layered Suite (RLS), (4) the Rashoop Granophyre Suite and (5) the Lebowa Granite Suite (Fig. 1). PGE, chromium and vanadium mineralisation are associated with the mafic and ultramafic rocks of the Rustenburg Layered Suite. The RLS can be subdivided, based on the mineralogy of the rocks, into five zones, from bottom to top as the Marginal Zone, the Lower Zone, the Critical Zone (CZ), the Main Zone and the Upper Zone. The Marginal Zone and Lower Zone tend to be dominated by ultramafic lithologies (dunite, harzburgite and pyroxenite). The CZ is dominated by repeated cycles of pyroxenite to anorthosite separated by chromitite layers. The Main Zone is dominated by gabbronorite whilst the Upper Zone, which is more iron-rich than the other zones, contains magnetite as a dominant mineral phase (Eales and Cawthorn, 1996; Lee, 1996).

### 2.1.1. Critical Zone

The critical zone is between 1300-1800 m thick and comprises chromitite, pyroxenite, harzburgite, norite and anorthosite lithologies (Naldrett et al., 2008). PGE contents increase from the Marginal Zone up to a maximum in the Upper CZ and show an immediate decrease in PGE content just above this zone (Barnes and Maier, 2002a). The PGE mineralisation of the CZ shows a strong spatial association with the multiple chromitite layers that occur within the CZ. The chromitite layers are conventionally divided into seven lower group (LG), four middle group (MG) and two or three upper group (UG) layers (Eales and Cawthorn, 1996). The average thicknesses of these chromitite reefs can range from 2-90cm (Eales and Costin, 2012). The upper portion of the CZ contains both the Merensky and Upper Group Chromitite 2 (UG2) reefs (Fig. 2) which are synonymous with high grades of PGE. However, the Platreef, situated just below the Main Zone in the northern limb of the Bushveld Complex, is also well mineralised (Cawthorn, 1999).

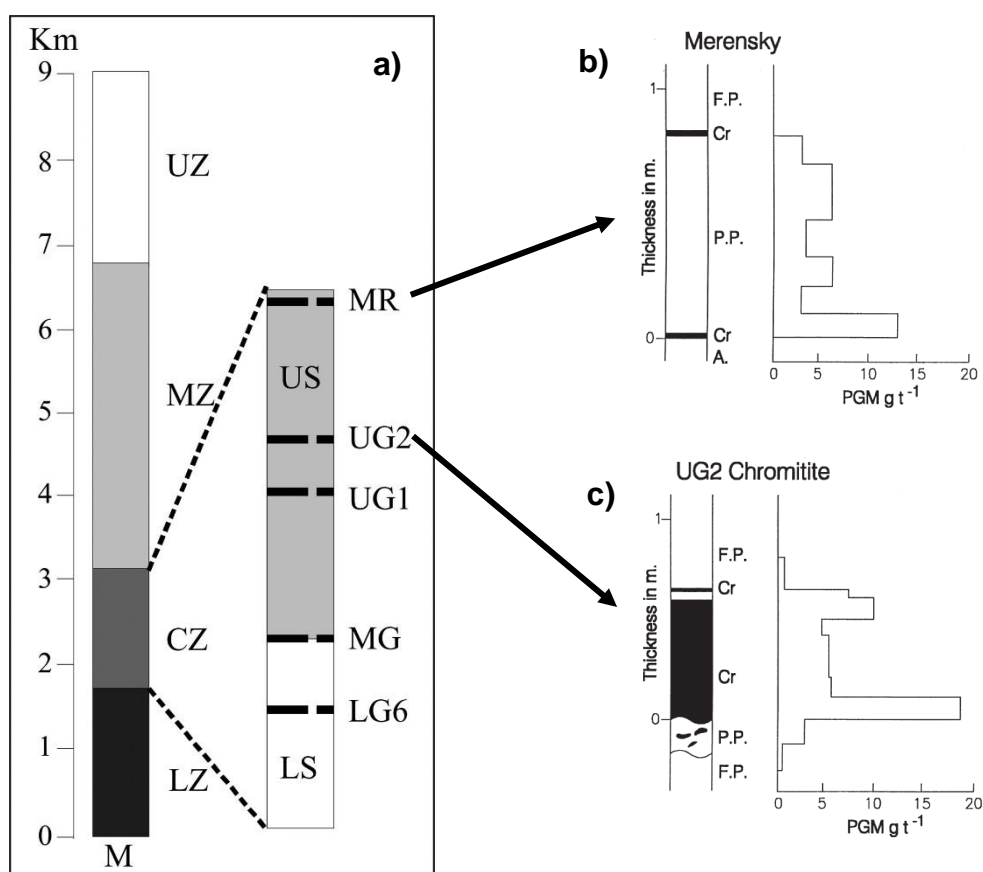


**Figure 2** - Generalised stratigraphic profiles for a) Rustenburg Layered Suite (Lenaz et al., 2007), b) Merensky and c) UG2 reefs (with PGE grade distribution for Merensky and UG2 reefs) (Cawthorn, 1999). (UZ – Upper Zone, MZ - Main Zone, LZ – Lower Zone, M – Marginal Zone, F.P. – Feldspathic pyroxenite, P.P. – Pegmatoidal pyroxenite, A. – Anorthosite).

## 2.2. The UG2 Reef

The UG2 reef can be situated anywhere between 20-400 m below the Merensky reef and may range in thickness between 0.4-2.5 m, but is only rarely observed with thicknesses over 1 m (Cawthorn et al., 2011; Schouwstra, 2000). It can be traced along surface for nearly the entire 400km strike length of the eastern and western limbs of the Bushveld Complex (McLaren and De Villiers, 1982). The reef package, which is cemented predominantly by intercumulus plagioclase grains, has average chromite contents of 30-35 % (Schouwstra, 2000) but within individual chromitite layers proportions may increase to 75-90 % (Mathez and Mey, 2005). Over a regional context, the UG2 reef is generally characterised by a pegmatoidal footwall, a main layer which is a combination of 2 or more (up to 9) chromitite layers, overlain by melanoritic host rocks that contain a thin chromitite leader (Voordouw et al., 2010).

In detail, the UG2 reef of the eastern limb is often associated with a pyroxenite hanging wall whereas the UG2 reef of the western limb is overlain by an olivine-enriched pyroxenite (Cawthorn et al., 2011). The footwall of the UG2 reef on both limbs is either a pegmatoidal pyroxenite or anorthositic rock type (Cawthorn et al., 2011). The hanging wall usually has rare to no chromite whereas the footwall may contain 'xenolithic' chromite grains (Mondal and Mathez, 2007). The pegmatoidal texture of the footwall rocks suggests that its formation post-dates the formation of the main UG2 chromitite layer (Penberthy and Merkle, 1999). Chromitite stringers, sometimes up to seven independent stringers, occur between 0.5-1 m above the main UG2 chromitite layer and are usually well mineralised (Cawthorn, 2011). When pyroxenite partings, which sometimes separate the main chromitite unit from the multiple overlying chromitite stringers, are absent, the reef thickness increases and a 'top peak' of PGE grade appears to have moved downwards towards the middle of the reef (Penberthy and Merkle, 1999). This is described by Gain (1985) as an artefact of the amalgamation of multiple independent chromitite stringers with the main chromitite unit.

The UG2 chromitites have been divided into 10 sub-layers based on variations in chromite chemistry with decreasing Mg# (defined as the cation ratio;  $Mg/(Mg+Fe)$ ) from the bottom to the top, excluding the basal sub-layer, and a concomitant increase in Cr# (defined as the cation ratio;  $Cr/(Cr+Al)$ ) and  $TiO_2$  contents (Junge et al., 2014). The

formation of sub-layers are thought to be a result of magmatic differentiation of individual chromitite layers which then coalesced to form a massive chromitite layer (Gain, 1985; Junge et al., 2014). Annealed and compacted chromite textures, where chromite grain boundaries between adjacent grains are essentially destroyed, are described by Junge et al. (2014) and Mathez and Mey (2005) as a characteristic feature of the bottom part of the main UG2 layer.

### *2.2.1. Relationships between Mineral Phases*

An understanding of the various relationships between ore and gangue minerals is vital to hypothesise not only what mechanisms may have been responsible for the formation of PGE mineralisation but to also efficiently beneficiate the PGE contents. The ubiquitous association of discrete PGM with BMS throughout the Bushveld Complex is well documented (Cawthorn, 2011; Kinloch, 1982; Penberthy and Merkle, 1999; Penberthy et al., 2000; Schouwstra et al., 2000). Descriptions of the associations of PGM state that >60 volume % of PGM from the UG2 reef are intimately associated with BMS, particularly pentlandite (Penberthy and Merkle, 1999). PGM tend to be locked within or occur on the outside boundary of BMS but are also hosted by silicate and chromite gangue (either within or at grain boundaries) (Godel et al., 2010; Kinloch, 1982; Penberthy et al., 2000). Some studies have suggested that BMS acted as collectors of PGE and PGM during the crystallisation of large layered intrusions, especially PGE with a chalcophile affinity such as palladium (Gain, 1985). However, Penberthy and Merkle (1999) attribute the formation of discrete PGM to the expulsion of PGE from BMS phases during crystallisation which then situate themselves on the outer boundary of the host BMS.

Data on the western limb was used to establish a link between high ferroplatinum contents and the tendency for PGM to be enclosed within silicate phases, whereas a Pt-Pd sulphide/telluride dominated PGM budget was seen in close association with BMS phases (Kinloch, 1982). It is thought that PGE-sulphide dominant assemblages are indicative of 'normal' UG2 reef and PGM contents which are predominantly alloys, such as ferroplatinum or bismuth-tellurides, represent reef packages which have undergone some degree of post-magmatic modification (Penberthy and Merkle, 1999).

### 2.2.2. *Variations in Reef Characteristics*

Variations within the UG2 reef manifest themselves as differences in chromite composition, thicknesses of the UG2 chromitites, the vertical distribution of PGM, PGE grade and relative proportions of PGE, mineralogy of PGM and BMS and the extent and type of alteration caused by late to post-magmatic processes (Cawthorn et al., 2002; Cawthorn, 2011; Kinloch, 1982, Lee, 1996; Penberthy and Merkle, 1999; Schouwstra et al., 2000; Voordouw et al., 2010). These differences may be observed as regional trends or as local anomalies (Penberthy and Merkle, 1999). Due to textural and compositional differences observed towards the middle of the UG2 reef, it is suggested that the UG2 reef is not a single layer but is rather made up of multiple composite layers (Lee, 1996). This interpretation is based on three upward depletion trends observed in PGE contents. This is further supported by Cawthorn (2011) who suggest that the UG2 reef was formed by three magma emplacement events which may or may not be separated by silicate rock lithologies.

In comparison to the Merensky reef, the BMS contents of the UG2 reef are low, with copper and nickel proportions in the region of 0.05 % (McLaren and de Villiers, 1982; Lee, 1996), suggesting a sulphide-poor magma (Cawthorn, 2011). Penberthy and Merkle (1999) reported sulphur contents of 0.01-0.08 weight per cent (wt. %) in their study of the UG2 reef, with sulphide mineralisation, in order of decreasing abundance, comprising pentlandite, chalcopyrite and pyrrhotite ( $\pm$ pyrite). Naldrett et al. (1989) suggest that ~60 % of the original BMS budget, in the form of primary pyrrhotite, has been removed or altered. This is supported by Li et al. (2004) with observations of actinolite and carbonates growing on BMS grains suggesting that the reef package has been affected by fluid interaction. A change in the BMS assemblages from a pentlandite, chalcopyrite, pyrrhotite, and  $\pm$ pyrite dominated BMS budget to a millerite, pyrite and chalcopyrite dominated BMS budget was observed in the Brits-Marikana area between 'normal' and 'altered' UG2 reef samples, respectively (Penberthy and Merkle, 1999). The change in mineralogy was attributed to sulphur and iron loss as a result of sulphide-chromite interactions caused by fluid ingress during reef disturbances. This phenomena results in the predominance of Ni-rich BMS in areas subjected to fluid interaction (e.g. fault zones). In the case of 'altered' UG2 reef, this may lead to the removal of BMS or the isolation of PGM within phyllosilicate phases.



BMS that have been redistributed as a consequence of fluid ingress and primary silicate mineral alteration result in BMS grains becoming enveloped by secondary hydrous silicate phases (Penberthy and Merkle, 1999).

Observations of phyllosilicate minerals such as talc and serpentine along fractures and joints are synonymous with hydrothermal alteration textures (Gain, 1985). A mine-scale investigation by Voordouw et al. (2010) found that secondary hydrous silicate phases constituted up to 50 % of the total silicate proportion within the UG2 reef package. A more recent study identified up to 8 wt. % talc and chlorite minerals in samples from the UG2 reef (Becker et al., 2013). The proportions of these secondary hydrous minerals may differ either locally or regionally throughout the Bushveld Complex depending on the extent of fluid interaction that has affected the reef package.

### **2.3. Sample Locations**

A brief overview of the localities from which the samples were taken for this study is outlined below. The samples are representative of what is known as 'normal facies' UG2 reef from Booyendal mine in the southern sector of the eastern limb and 'undisrupted reef' from Zondereinde mine of the Swartklip facies on the western limb.

#### *2.3.1. Booyendal*

Booyendal mine (Fig. 3) is situated on the border of the Mpumalanga and Limpopo provinces, ~35 km west of the town of Lydenburg. The operation is owned by Northam Platinum Limited and has been in production since 1 July 2013. The mining lease area contains both the Merensky and UG2 reefs with an outcrop strike length of 14.5 km. The stratigraphic distance between the Merensky and UG2 reefs is approximately 175 m and these ore bodies dip at ~10° to the west in the area. Currently, mining operations are underway within the northern sector of the mine lease area where the critical zone stratigraphy is fully developed. Thinning of Bushveld Complex stratigraphy within the southern sector is attributed to basement highs, which in turn have caused disruptions of the internal structure of the mineralised reefs.

The structure of the UG2 reef at Booyensdal mine is divided into an upper Leader Chromitite (UL) and a lower Main Chromitite (UM) that are typically merged into one continuous chromitite layer of ~140cm. However, they may also be separated by silicate partings. The chromitite units are immediately overlain by a 3.5-5.0 m thick pyroxenite layer which can contain up to seven thin chromitite stringers (UT0-UT5 and UPC). The structure of the UG2 reef within the area is consistent with that of the western limb whilst the Merensky reef is similar to the northern part of the eastern limb. Whilst the area is reported to be affected by some degree of faulting and jointing, it has been found that typically the structures are not fluid bearing and lack any widespread alteration zones (Northam Annual Intergrated Report, 2015, [www.northam.co.za](http://www.northam.co.za)).

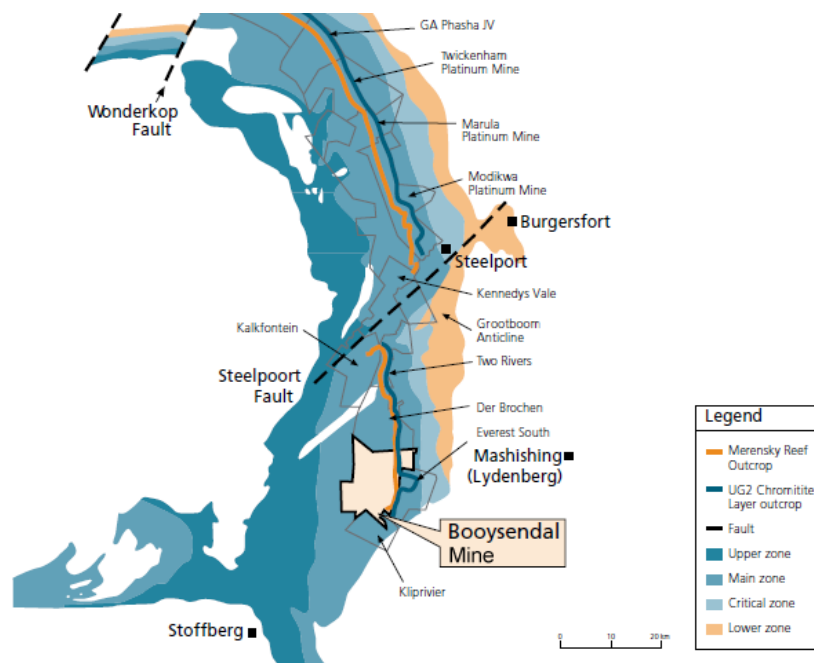


**Figure 3** – Geological overview of the eastern limb with the location of Booyensdal mine indicated (Northam Platinum Limited).

### 2.3.2. Zondereinde

Zondereinde mine is situated ~20 km south of the town of Thabazimbi, Limpopo province (Fig. 4). The mining operation is owned by Northam Platinum Limited and although mining in the area dates back to 1987, Zondereinde was established in 1993. Mining operations exploit both the Merensky and UG2 reefs which have a strike length of 8 km across the mine lease area. The stratigraphic separation between the



Merensky and UG2 reefs is anywhere between 20-40 m. In comparison to the Merensky reef, the UG2 reef is relatively unaffected by reef disturbances such as faults, some of which are ground-water bearing. At Zondereinde, the UG2 reef consists of three chromitite layers separated by silicic lithologies; a major 80 cm thick layer and two overlying leader chromitite layers of about 20cm in thickness. Typically, the main chromitite layer contains a higher average PGE grade than the two thinner overlying chromitite layers (Northam Annual Intergrated Report, 2015, [www.northam.co.za](http://www.northam.co.za)).

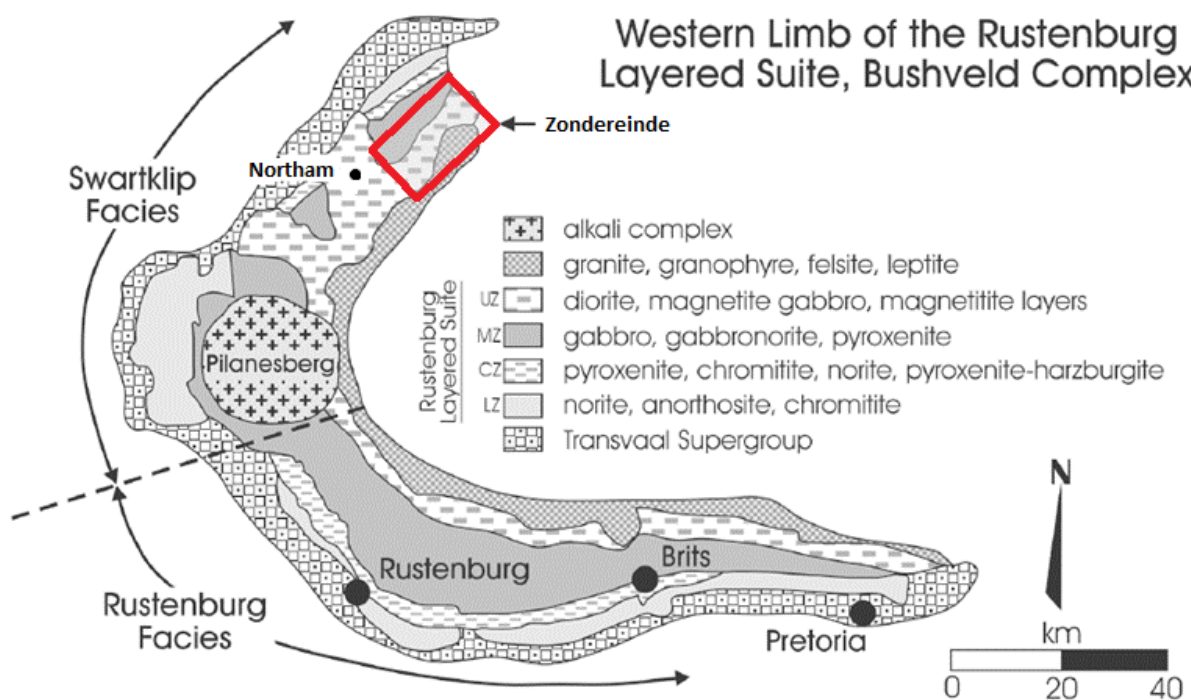


**Figure 4 - Geological map of the western limb of the Bushveld Complex with the location of Zondereinde mine indicated (after Viljoen 1994, 1999).**

## Chapter 3: METHODS

### 3.1. Introduction

Two sets of continuous 30mm drill core through UG2 mining sections were received from Northam Platinum Limited; one from Booyseindal Mine (eastern Bushveld) and one from Zondereinde Mine (western Bushveld). Both sections are representative of the normal “mining cut” at the respective mines. The total lengths of the Booyseindal and Zondereinde mining cuts were 2.94 m and 3.10 m respectively. The original core length provided by each mine is illustrated in Figure 5. The mineralogy and texture of each of the cores were analysed via reflected light microscopy (RLM), scanning electron microscopy (SEM), quantitative evaluation of minerals by scanning electron microscopy (QEMSCAN), 3-D microfocus X-Ray computed tomography (3-D  $\mu$ XCT), X-Ray diffraction (XRD) and various geochemical assay techniques (Table 1). The preparation of the core for these analyses is outlined below followed by a description of the analytical techniques employed in this study.

**Table 1** - Number of samples used for each analytical technique.

	RLM	SEM	QEMSCAN	$\mu$ XCT	XRD	Assay
<b>Booyseindal</b>	50	20	4	11	18	18
<b>Zondereinde</b>	31	11	3	15	23	23

### 3.2. Sample Preparation

Both core sets were logged on receipt and photos were taken of the intact core lengths. Both cores were then halved perpendicular to the layering using a standard rock saw. One half of each core was split into samples of known length and prepared for milling (Fig. 6a). Samples were weighed, dried, crushed to 80 % passing 2 mm and then milled in a ring and puck pulveriser to 85 % passing 75  $\mu$ m. These pulp samples were used for analysis of 5PGE+Au, major element oxides and base metal contents at SGS, Johannesburg. Other samples, taken from the same pulp samples as above, were prepared for qualitative and semi-quantitative XRD at iThemba labs, Faure (see section 3.5.).

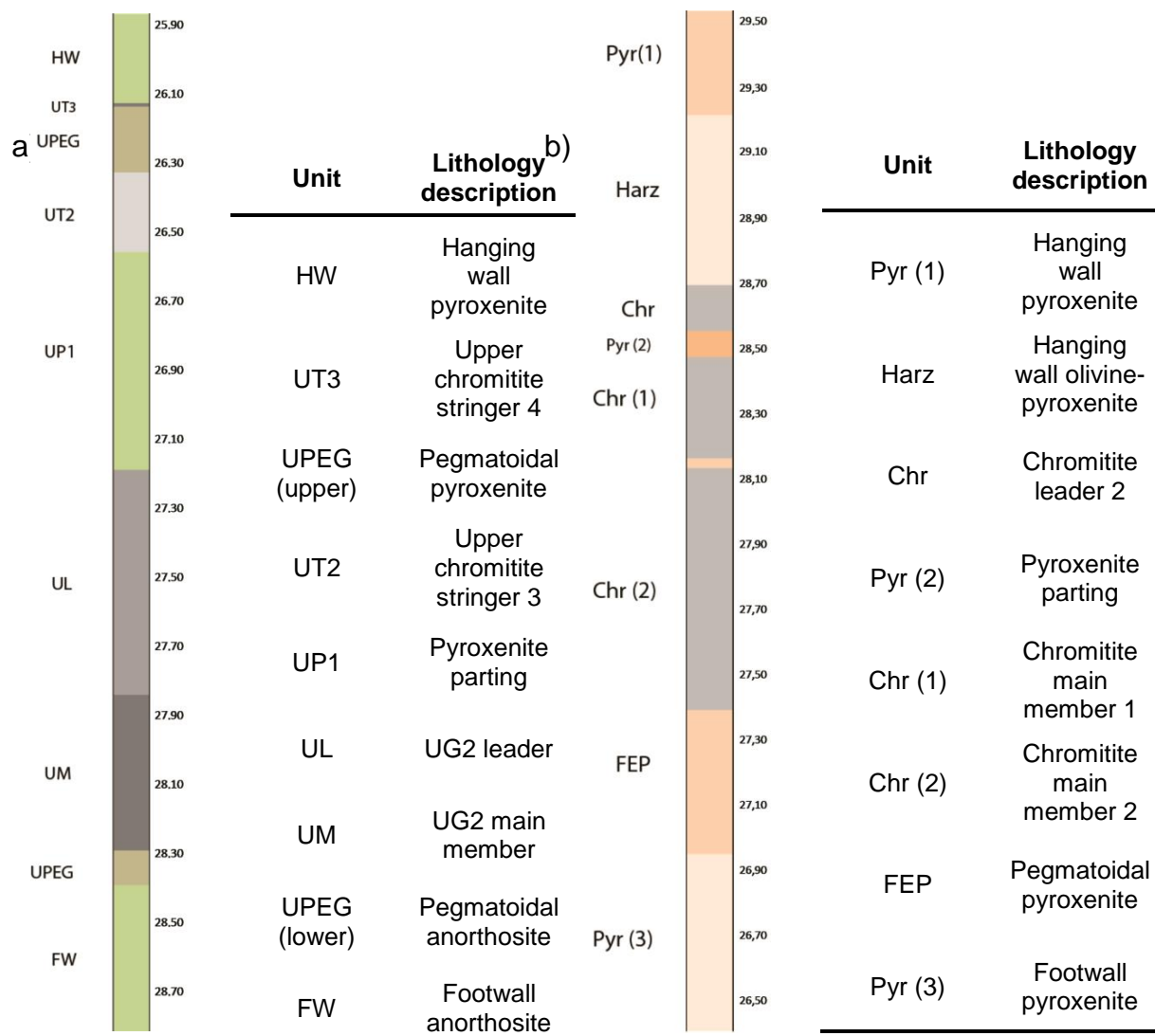


**Figure 5** – Complete core sets with unit subdivisions for a) Booyensdal and b) Zondereinde.

The remaining half-cores from each set were further halved in order to produce two quarter cores (Fig. 6a and b). One quarter core from each core set was trimmed using a small circular saw to produce rounded ‘mini-core’ lengths that would be used for high resolution  $\mu$ XCT (Fig. 6b). The last quarter from each core set were trimmed into 2 cm blocks to be later made into polished block mounts (Fig. 6c). The blocks have a known paleo-vertical direction (“up” towards the collar of the drill hole) and represent a snapshot of intervals ~10 cm apart throughout the length of each core (Fig. 7). The top surface represents a section view, perpendicular to the cumulate layering of the core set (i.e. from the bottom to the top of the UG2 reef). Table 1 details the number of samples which were prepared for each technique in this study. The thin pyroxenite parting which separates the Chr (1) and Chr (2) units of the Zondereinde core was lost

during processing due to the brittle nature of the rocks and no data are available from this unit.

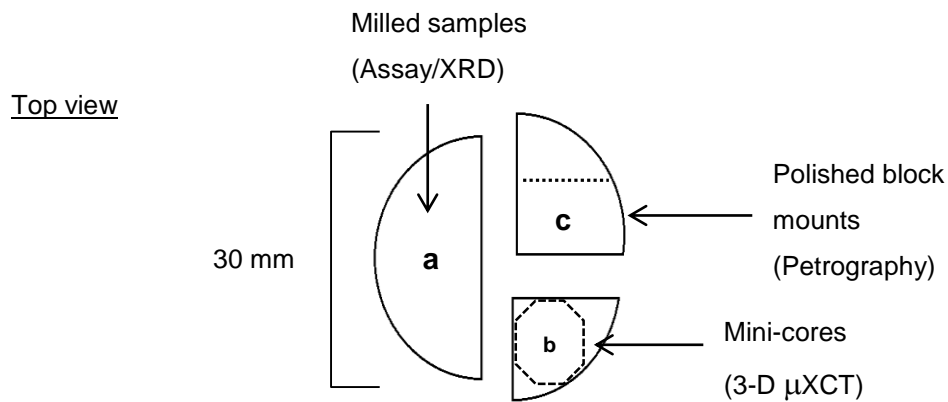


**Figure 6** - Schematic illustration of how each core set was initially prepared, with the analytical method for each piece indicated in brackets (top view).

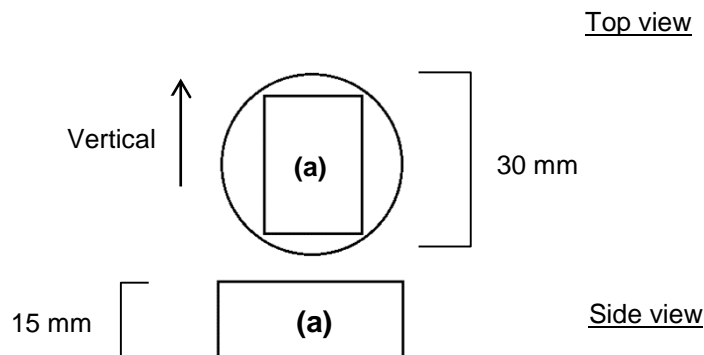


**Figure 7** - Schematic illustration of a polished block mount (see Figure 6c) (top and side views).

### 3.3. Petrographic and SEM Analysis

Initial petrographic investigations were done using RLM on 50 Booyendal and 31 Zondereinde polished block mounts. Individual mineral compositions were determined on a Zeiss EVO MA15VP SEM equipped with an Oxford X-Max EDS Silicon Drift Detector and coupled to a Link ISIS energy dispersive (ED) spectrometry system. The beam energy was set to 20 kV with a current range of -19 to -20.5 nA. Beam stability was periodically checked against the Faraday cup. The working distance between the sample surface and X-ray source was 8.5 mm. Internal Astimex scientific mineral standards for various elements were used for calibration and verification of analyses and are listed in the Table 14. Pure Co was analysed periodically to correct for detector drift on the ED detector.

Oxide and sulphide minerals were classified according to the proportion of each elemental constituent (e.g. Ni, Cr, Fe and S) and cross-checked with ideal molecular proportions for minerals that are known to exist within the Bushveld Complex and especially the UG2 reef. PGM phases were classified according to their major element proportions (e.g. Pt, Pd, Fe and S). A minimum value of 1-2 wt. % was used for the inclusion of an element into the mineral composition's nomenclature.

### 3.4. XRD Mineralogical Analysis

Small portions of milled samples were sent to iThemba labs, Somerset West for XRD analysis to obtain the bulk mineralogy of the various units within each core set. Analysis was done on a Bruker AXS with a D8 Advance diffractometer and a PSD Lynx-Eye detector. The samples were scanned with Cu-K $\alpha$  radiation (40 kV, 40 mA) from 3° to 90° (2 $\theta$ ) with a 0.027° step size. Phases were identified using the International Centre for Diffraction Data "Powder diffraction file" on Bruker's EVA software. Phase abundances are estimated based on the intensity of the relevant peaks and are only semi-quantitative (major vs. minor), i.e. the larger the peak on the diffraction pattern, the greater the abundance of the identified mineral phases when compared to the overall distribution of peak intensities.

### **3.5. QEMSCAN Analysis**

High grade sections of interest were selected for quantitative and qualitative mineralogical characterisation with QEMSCAN. Analysis was conducted on a FEI QEMSCAN 650F at the Centre for Minerals Research, University of Cape Town. Spectra were analysed with two Bruker XFlash 6130 EDS (SDD) detectors at a one micron pixel spacing with the electron beam settings calibrated at 25 kV and 5 nA. These settings were periodically checked (every 2 hours) for consistency. BSE signals were standardized at the start of each sample's analysis to quartz, copper metal and gold metal (BSE signals (grey levels) of 42,130 and 232 respectively). The focus of the analysis was to determine statistics on the mode of occurrence, texture and composition of BMS and PGM grains. Therefore the QEMSCAN was calibrated to conduct a Trace Mineral Search (TMS) to map mineral fields (500 micron<sup>2</sup>) which contained minerals with a BSE signal (grey level) greater than 150. This means that data on the relative proportions of the bulk mineral assemblage of the samples i.e. silicates and oxides phases is not statistically relevant. This was done so that there was as much information on the BMS and PGM populations as possible within the time and budget constraints of the project. The correct identification of minerals is reliant on a well-developed mineral reference file, known as a Species Identification Protocol (SIP) file. Raw data were processed and assessed using iDiscover software to accurately constrain the mineral characteristics and account for any instrumental errors. The post-processing procedure includes user-intensive data refinement to eliminate bad analyses and to constrain mineral compositions and their associational characteristics.

### **3.6. Geochemical Analysis**

Milled core sections were sent to SGS South Africa for chemical assay data on 5PGE + Au, major elements, base metal (Cu, Ni, Zn) and sulphur. The samples were analysed for 5 PGE (Pt, Pd, Rh, Ru, Ir) + Au via Ni-sulphide fire-assay followed by ICP-OES finish. Major element concentrations were determined via XRF using a borate fusion process. Base metal concentrations were determined by two acid "partial" digestion and analysed via ICP-OES while total S was determined using a

Leco analyser. Sulphur contents of the UG2 reef are known to be very low and the latter technique did not produce usable data as S contents were below the detection limits of the method (0.01 %).

**Table 2** - Analytical details for assay procedures.

Code	Elements	Method	Analysis	Lower detection limit
FAI363	Pt,Pt,Rh,Ru,Ir,Au	Ni-S fire assay	ICP-OES	0.02 ppm (Ir: 0.1 ppm)
ICP12B	Cu, Ni, Zn	Two-acid partial digestion	ICP-OES	0.5 ppm (Ni: 1 ppm)
XRF79V	SiO <sub>2</sub> , Al <sub>2</sub> O <sub>3</sub> , CaO, MgO, Fe <sub>2</sub> O <sub>3</sub> , K <sub>2</sub> O, MnO, Na <sub>2</sub> O, P <sub>2</sub> O <sub>5</sub> , TiO <sub>2</sub> , V <sub>2</sub> O <sub>5</sub> , Cr <sub>2</sub> O <sub>3</sub>	Borate fusion	XRF	0.01 % (Si,Al,Mg,Na:0.05 %)
CSA06V	S	Leco	Combustion Infrared Detection	0.01 %

### 3.7. X-Ray Computed Tomography

Mini core sections (Fig. 6b) were scanned with a General Electric Phoenix V|Tome|X L240 X-ray computed tomography scanner housed at the Central Analytical Facility at Stellenbosch University. The samples were scanned at a voxel resolution of 10  $\mu\text{m}$ . The various scanning parameters are detailed in Table 3.

**Table 3** - Scanning parameters for 3-D  $\mu\text{XCT}$  analysis.

Sample type	# samples	Voltage (kV)	Current ( $\mu\text{A}$ )	# images	Voxel resolution ( $\mu\text{m}^3$ )
Mini core	27	150	70	2200-2800	10

X-ray computed tomography is a non-destructive technique used to produce images of the internal structure of a solid. X-rays are passed through the object, in this case samples from the UG2 reef, and are attenuated based on a sample's properties. In the case of geological samples, specific gravity (SG) and average atomic number (Z) are the two most important characteristics (Ketcham and Carlson, 2001; Cnudde and Boone, 2013). The variation in attenuation for each image is mapped onto a detector screen behind the target whilst the sample is step rotated through 360°. These images

are then reconstructed in sequential order to produce image stacks. The result is a 3-D representation of the solid which can be digitally manipulated in order to extract various statistical and visual datasets (Ketcham and Carlson, 2001). Optimal scanning calibration is essential to ensure that data are acquired accurately, artefacts are minimised and the resolution is sufficient for the required analysis (Cnudde and Boone, 2013). Mineral phases with similar chemical and physical properties are grouped together based on grey scale values obtained during 3-D  $\mu$ XCT analysis (e.g. silicates, sulphides/oxides and PGM).

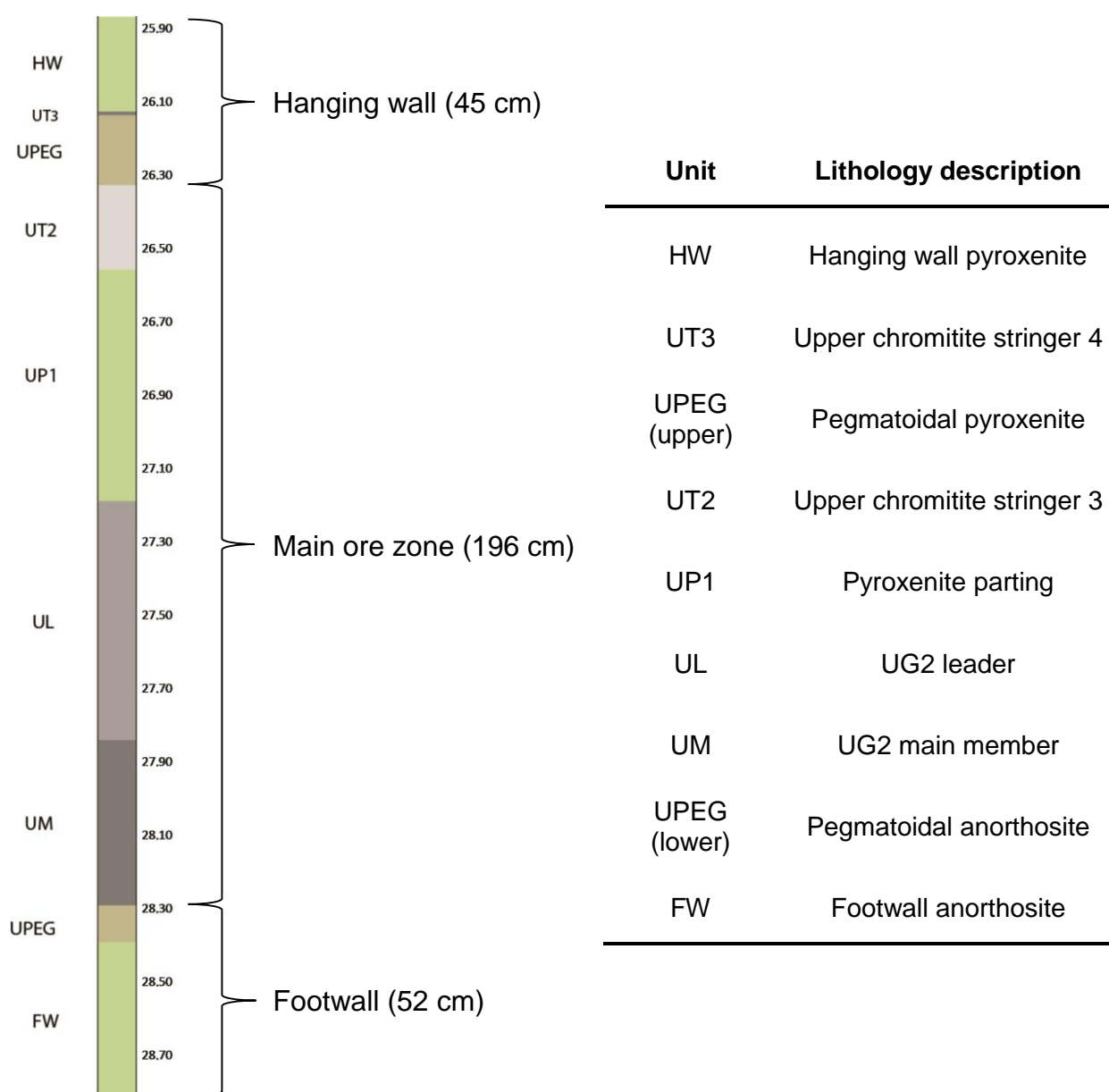
Mineral phases were identified based on the correlation between known mineralogy of the samples identified during petrographic investigation and the X-ray absorption differences obtained from the CT scanner. An attenuation histogram is displayed by the image processing software which allows for the segregation of phases with differing physical and chemical properties. In the case of the UG2 samples, mineral peaks with the lowest attenuation values are assumed to be silicates (lowest SG and Z value), followed by sulphides/oxides and then PGM (highest SG and Z value). SG and Z values for minerals commonly found within the UG2 reef are reported in Table 15.

Image stacks were processed to produce a 3-D volume of the solids using Datos reconstruction software and the post processing and analysis of images was done with VGStudio Max 2.2 software package. Processing is user-intensive and results may vary from user to user. Therefore, a sound geological knowledge in conjunction with a good technical knowledge of how the 3-D  $\mu$ XCT scanner works is necessary to provide realistic data.



## Chapter 4: BOOYSENDAL UG2

The core set is representative of a 'normal UG2' reef mining cut from Booyseendal mine, eastern Bushveld Complex. The hanging wall is pyroxenitic, the footwall anorthositic and the main ore zone is dominated by chromitite layers. The core is divided into nine units based on distinct mineralogical contrasts between layers. Figure 8 details the gross structure of the core whilst Figure 9 illustrates the position from which samples were taken and for which analytical technique it was used.



**Figure 8** – Schematic illustration of the Booyseendal core set as received from Northam Platinum. The core is divided into 3 broad sections namely; hanging wall, main ore zone and footwall based on the prevalence of PGE grade within the various units.

#### 4.1. Structure and Bulk Mineralogy

From top to bottom, the core set consists of a 45 cm hanging wall followed by 196 cm of the main ore zone and a 52 cm footwall (Figure 8). The hanging wall comprises 26 cm of pyroxenite (HW), overlying a thin (~0.5 cm) chromitite stringer (UT3) on top of a 19 cm pegmatoidal pyroxenite layer (UPEG (upper)). The HW and UPEG (upper) are similar rock types. However, the UPEG (upper) exhibits a larger average grain size giving it a pegmatoidal texture. XRD results report that the HW and UPEG (upper) are dominated by enstatite and anorthite grains with minor phyllosilicates, talc and illite.

The main ore zone is dominated by chromitite units but also contains a thick pyroxenite layer which divides the UT2 from the UL. The four units of the main ore zone are: (1) a 23 cm upper chromitite stringer (UT2); (2) a 63 cm thick pyroxenite parting (UP1); (3) a 65 cm UG2 leader chromitite layer (UL); and (4) a 45 cm main chromitite layer (UM). There is no pyroxenite parting separating the UL and UM units. The absence of this parting makes the delineation of the contact between the UL and UM difficult to identify with the naked eye. Geologists at Booyendal mine use the disappearance of vermicular oikocrysts of clinopyroxene to delineate the transition from UL to the UM unit. The UM unit contains less abundant clinopyroxene which have a sub-circular habit. The differentiation of these two units will be investigated throughout the rest of this chapter and discussed in Section 6.1.1. The chromitite units of the main ore zone are dominated by Fe-rich magnesio-chromite but also contain minor proportions of an unnamed “copper-magnesium-manganese oxide”, enstatite and anorthite. The bulk mineralogy of the UP1 unit is similar to the silicic units of the hanging wall in that it is dominated by enstatite and anorthite with minor proportions of talc and illite.

The footwall is divided into 2 units; a 10 cm pegmatoidal pyroxenite (UPEG-lower) which immediately underlies the main ore zone and 42 cm of footwall anorthosite (FW). The footwall units are dominated by enstatite and anorthite with minor proportions of illite.

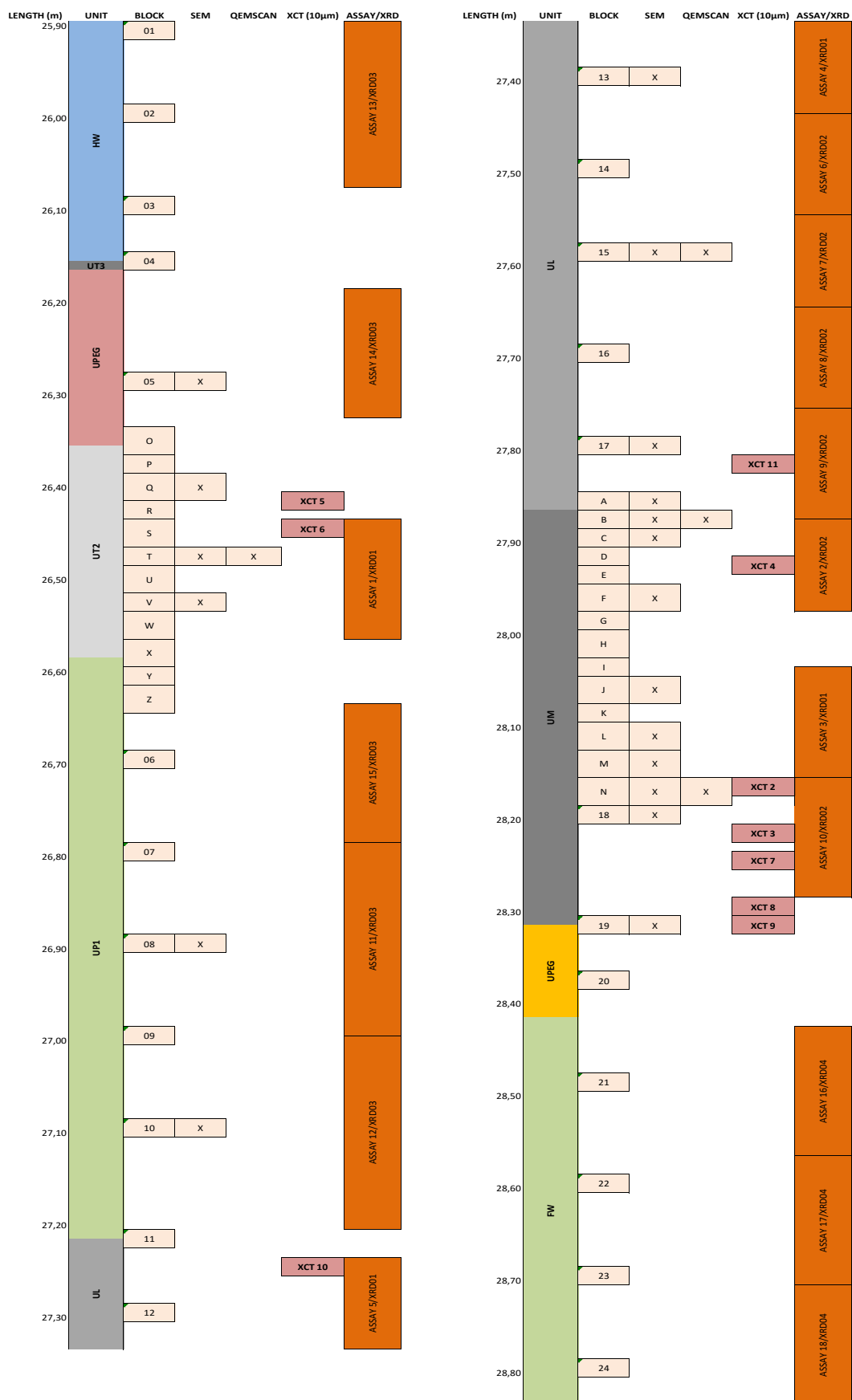


**Figure 9** - Schematic illustration of sample localities for petrographic, compositional, geochemical and 3-D analytical techniques.

## 4.2. Textural Relationships

The HW and UPEG (upper) units are dominated by cumulus orthopyroxene grains (>50 modal %) with intercumulus plagioclase. The average grain size of orthopyroxene from the UPEG (upper) is larger than those found within the HW unit. Although chromite grains are rare, they tend to accumulate in small groups/chains of grains which may exhibit annealed grain boundaries. The UT3 chromitite stringer consists of a layer of mostly annealed chromite grains within a plagioclase-rich matrix. The chromitite units of the main ore zone (UT2, UL and UM) exhibit many different textures based upon mineral proportions and grain size differences which will be discussed in section 4.3.2. below. These units are dominated by Fe-rich magnesio-chromite with lesser intercumulus plagioclase, subhedral to rounded orthopyroxene grains and hydrous silicate alteration phases. The UPEG (lower) unit contains minor amounts of chromite which is associated with the highest proportions of visible sulphide grains seen anywhere in the mining cut as well as pegmatoidal orthopyroxene grains. The FW unit is defined by an absence of chromite, a large proportion of plagioclase and rare sulphide minerals. Throughout the mining cut, the effect of hydrous alteration minerals is maximised in areas which have increased silicate contents, especially where orthopyroxene is present.

### 4.2.1. *Silicates*

Orthopyroxene grains within the HW unit range in size from 1-4 mm whilst in the UPEG (upper) unit, orthopyroxene grains are 3-7 mm in size. In both of these units, the grains have a euhedral/subhedral shape. Plagioclase grains occur intercumulus to orthopyroxene with grain sizes of 0.5-3 mm in the HW unit and 0.5-2 mm in the UPEG (upper) unit. Alteration minerals occur along cleavage planes or as replacement textures (sometimes almost entire replacement) of orthopyroxene grains (Fig. 10a), as very thin (micron-scale) rims around chromite or enveloping BMS grains. There was a noticeable increase in the proportion of alteration within the UPEG (upper) unit in comparison to the overlying units (HW and UT3) (Fig. 10b). The UP1 unit is the most silicic of the main ore zone rock types. The unit is dominated by 0.5-2 mm elongate and rounded grains of orthopyroxene. Plagioclase is also a major phase forming a wide size range of intercumulate grains (1-5 mm). Many of the orthopyroxene grains have undergone partial replacement resulting in hydrous silicate alteration features

along cleavage planes and grain boundaries (Fig. 10c). The alteration features also occur along grain boundaries of chromite, enclosing BMS grains and as the replacement of intercumulate plagioclase (Fig. 10d). The modal proportion of hydrous silicate phases increases towards the top of this unit. Within the chromitite units (UT2, UL and UM) the silicate contents display similar characteristics as above but are found in much lower proportions especially in the UL and lower UM units. The UPEG (lower) unit is characterised by large orthopyroxene grains (2-6 mm) and intercumulus plagioclase. Hydrous silicate alteration features affect all minerals within the UPEG (lower) unit as patchy accumulations of altered orthopyroxene and plagioclase, rims around chromite grains and enclosing sulphide minerals. The FW unit is a plagioclase-rich lithology which also hosts euhedral/subhedral orthopyroxene grains with a wide variety of grain sizes (0.3-6 mm). The FW unit does not seem to be as severely affected by alteration features when compared to the overlying units.

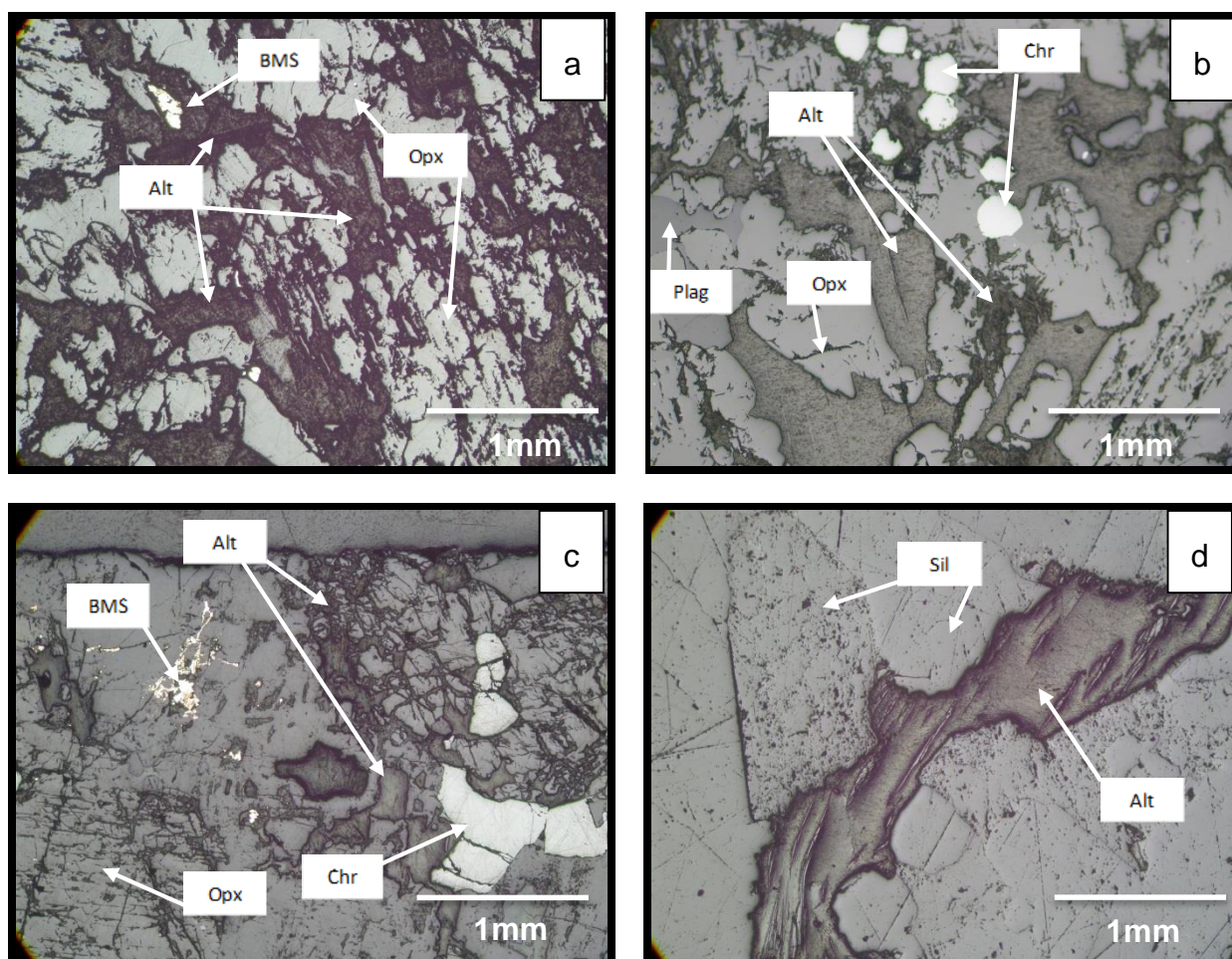


**Figure 10** - Examples of silicate alteration mineral features. **(a)** pervasive alteration of primary opx along cleavage planes (UPEG-upper), **(b)** alteration of plag and opx grains resulting in different alteration mineral assemblages, also affecting chromite (UPEG-upper), **(c)** patchy replacement of primary opx along cleavage planes and as partial replacement of plag, also affecting chromite (UPEG-lower), **(d)** replacement texture of plag occurring interstitial to primary silicates (FW).



#### 4.2.2. Chromite

Chromite within the hanging wall units occur predominantly as sporadic accumulations of small (0.1-0.3 mm) grains often closely associated with sulphide mineralisation (Fig. 11a). The thin UT3 stringer contains small (0.1-0.3 mm), annealed chromite grains with a disseminated texture and relatively high sulphide mineral contents along the top and bottom contacts of the stringer. Chromite minerals within the UT2, UL and UM units display varying textures throughout the stratigraphic intervals. The UT2 unit is defined by patchy, band-like accumulations of either large grained (~1 mm) interlocking or smaller disseminated chromite grains (Fig. 11b). Smaller, rounded chromite grains may exhibit annealing textures where chromite mineral boundaries are lost when two or more grains are in contact (Figs. 11c & d), whilst the larger grains tend to form an interlocking 'puzzle-like' texture of blocky chromite grains (Fig. 11e).

The UP1 unit contains horizontal banding of chromite grains, especially grains which are of the larger sized fraction (1-2 mm), within the upper section of the unit. The chromite grains form chain-like accumulations which cross-cut the silicate fraction and very often have annealed grain boundaries producing uncharacteristic and irregular grain shapes (Fig. 11f). The chromite contents decrease towards the bottom of the unit where they occur as irregularly shaped, small, annealed grains and euhedral shapes within a plagioclase matrix. Rounded, euhedral chromite grains within the UL unit exhibit an extensive degree of annealing, especially the smaller grains. Grain sizes are noticeably smaller in the UT2 and UL units in comparison to the UM unit (maximum sizes of ~0.5 mm (UT2, UL) and ~1 mm (UM)). The UM unit has variable amounts of chromite, with the highest proportions in the bottom half of the unit. Where the chromite content is high (from the bottom to the middle of the UM unit) the grains form thick layers of interlocking grains with almost no intercumulate silicate phase (Fig. 11e). Chromite grains within the footwall units are found within the UPEG (lower) unit in appreciable amounts relative to other siliceous units. They can be described as rounded to euhedral in shape and occur as sporadic accumulations throughout the unit. There is a lower degree of annealing within this chromite fraction.

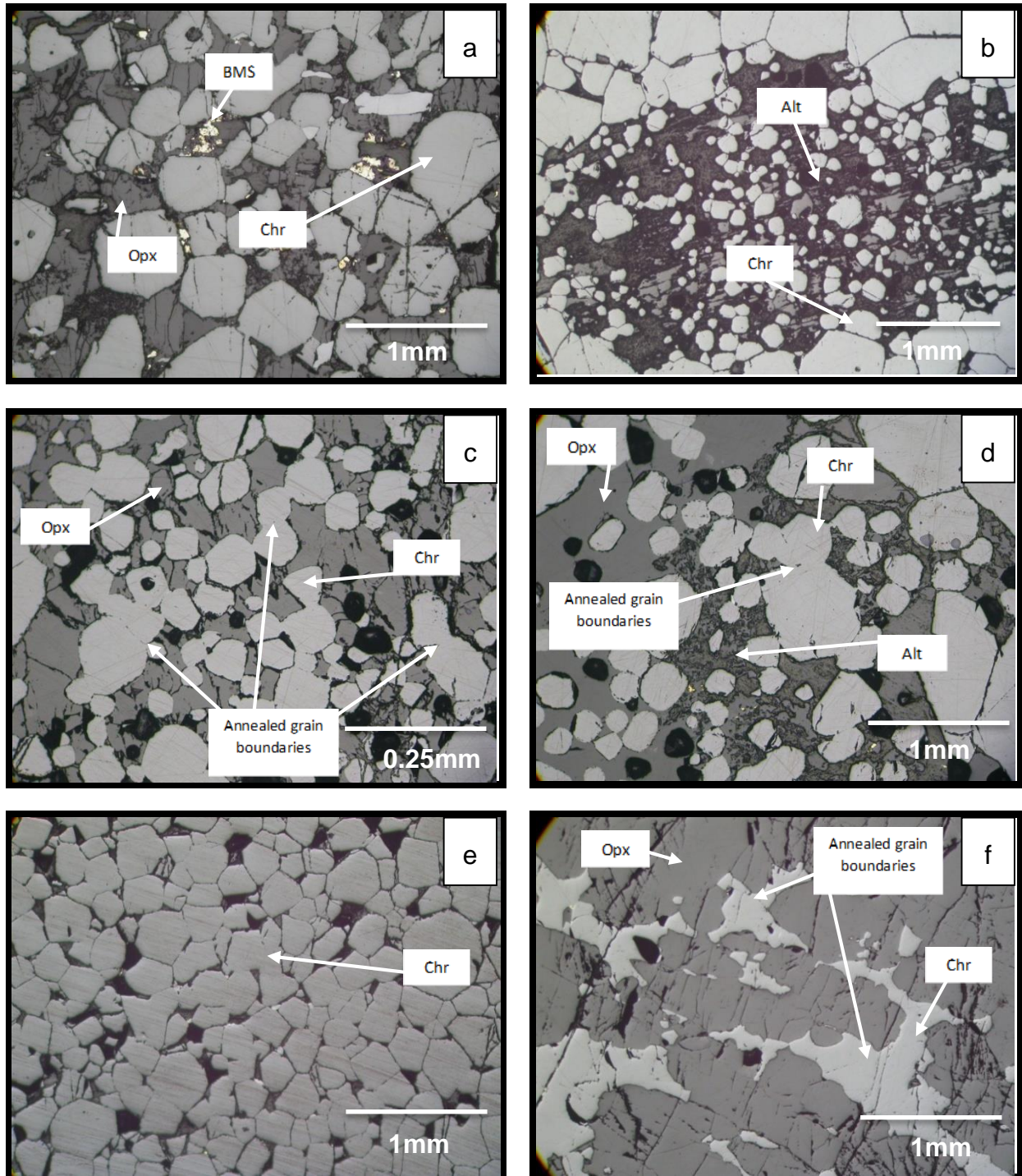


**Figure 11** - Examples of chromite mineral textures and associations throughout the Booyensdal samples. **(a)** euhedral chromite grains with a disseminated texture in close association with BMS grains occurring on chromite grain boundaries. Alteration phases are observed completely enveloping BMS grains and occurring as thin coatings on the grain boundaries of chromite (UPEG-lower). **(b)** pockets of small chromite grains with the interstitial silicate mineral assemblage almost completely replaced by alteration phases (UT2), **(c)** variable grain sizes of chromite occurring with a disseminated texture (UL), **(d)** chromite grains with annealed grain boundaries in close association with alteration phases along chromite grain boundaries (UL), **(e)** compacted chromite with almost no grain boundary annealing with BMS phases locked at the interstices of chromite grain boundaries (UM), **(f)** chain-like banding of chromite with annealed grain boundaries (UP1).

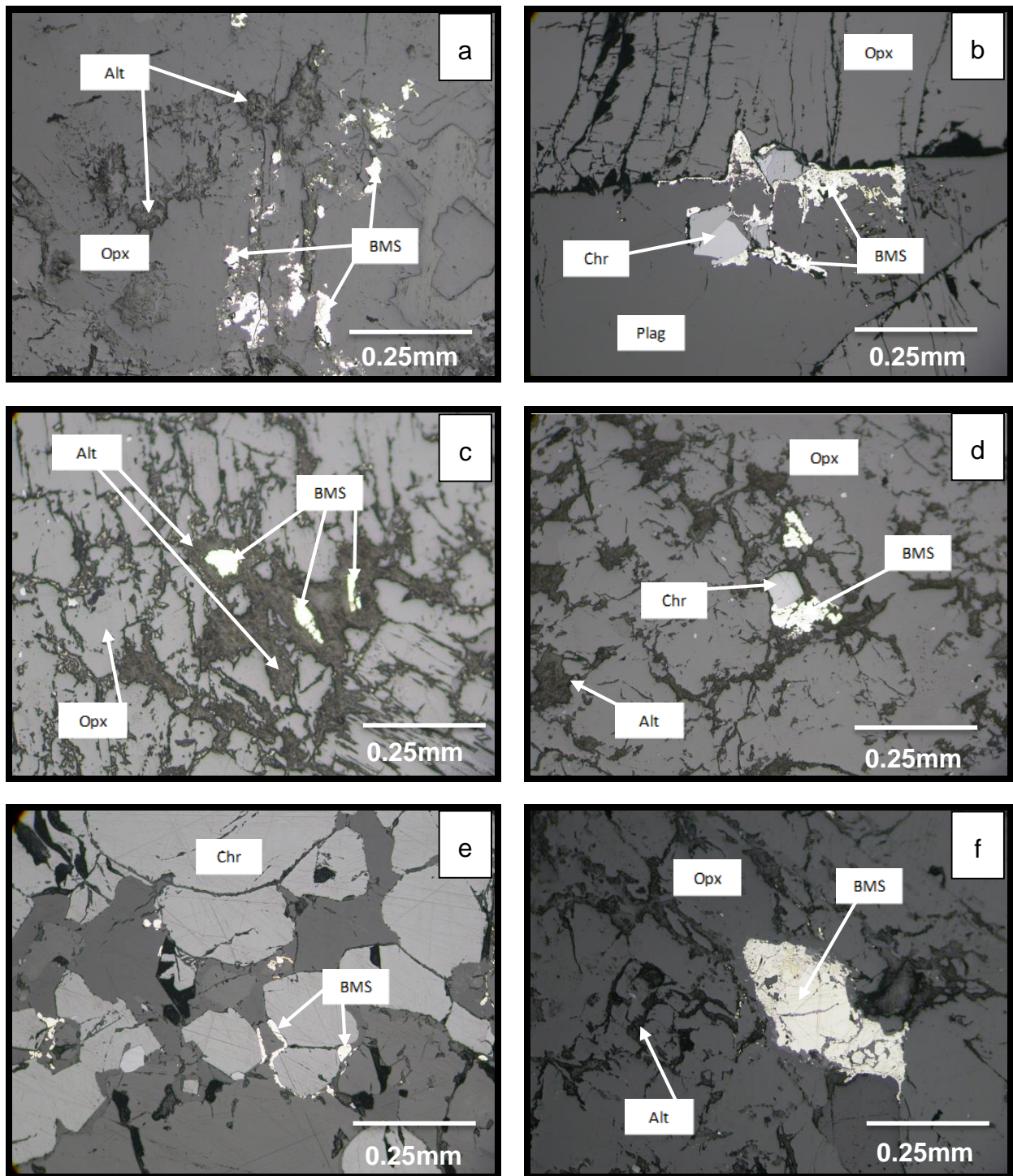
#### 4.2.3. Sulphides

Sulphide mineralisation in the hanging wall section occurs as small (<0.1-0.3 mm) irregularly shaped grains (Fig. 12a) or as discrete aggregates of BMS often closely associated with chromite (Figs. 12b). Sulphide proportions increase substantially at the top and bottom contacts of the thin UT3 stringer. There is also a close association of BMS with alteration phases that exist within the hanging wall. When this association is present, the BMS grains tend to be completely enclosed by alteration phases (Fig. 12c).

BMS are closely associated with chromite in the main ore zone. The small (<0.1-0.3 mm) sporadic aggregations of nickel-iron-copper sulphide assemblages increase from the bottom to the top of the UT2 unit, whereas they decrease upwards within the other three units of the main ore zone (UP1, UL and UM). Sulphide mineralisation is lowest within the UP1 unit and this unit also displays a decreasing trend in the proportions of BMS towards the top of the unit. The minerals occur as discrete aggregates of BMS phases with highly irregular to rounded shapes (Fig. 12d). The sulphide aggregates of the main ore zone preferentially occur with chromite either locked in the interstices between or on the outside grain boundary (Fig. 12e), but there are also BMS associated with the silicate fraction in places (Fig. 12f).

The UPEG (lower) unit is unique due to its higher than average sulphide proportion when compared to other units within the mining cut (except the UT2 unit). The BMS exist in close association with chromite grains, often observed 'draped' or attached to the outside boundary of the chromite grain (Fig. 12e). The BMS, whether occurring as individual grains or as an aggregate of BMS, have a slightly larger average grain size in the UPEG (lower) unit (<0.1-0.5 mm). The FW unit contains only rare grains of BMS occurring as a fine dusting of minute (~0.1 mm) grains hosted by silicate minerals.

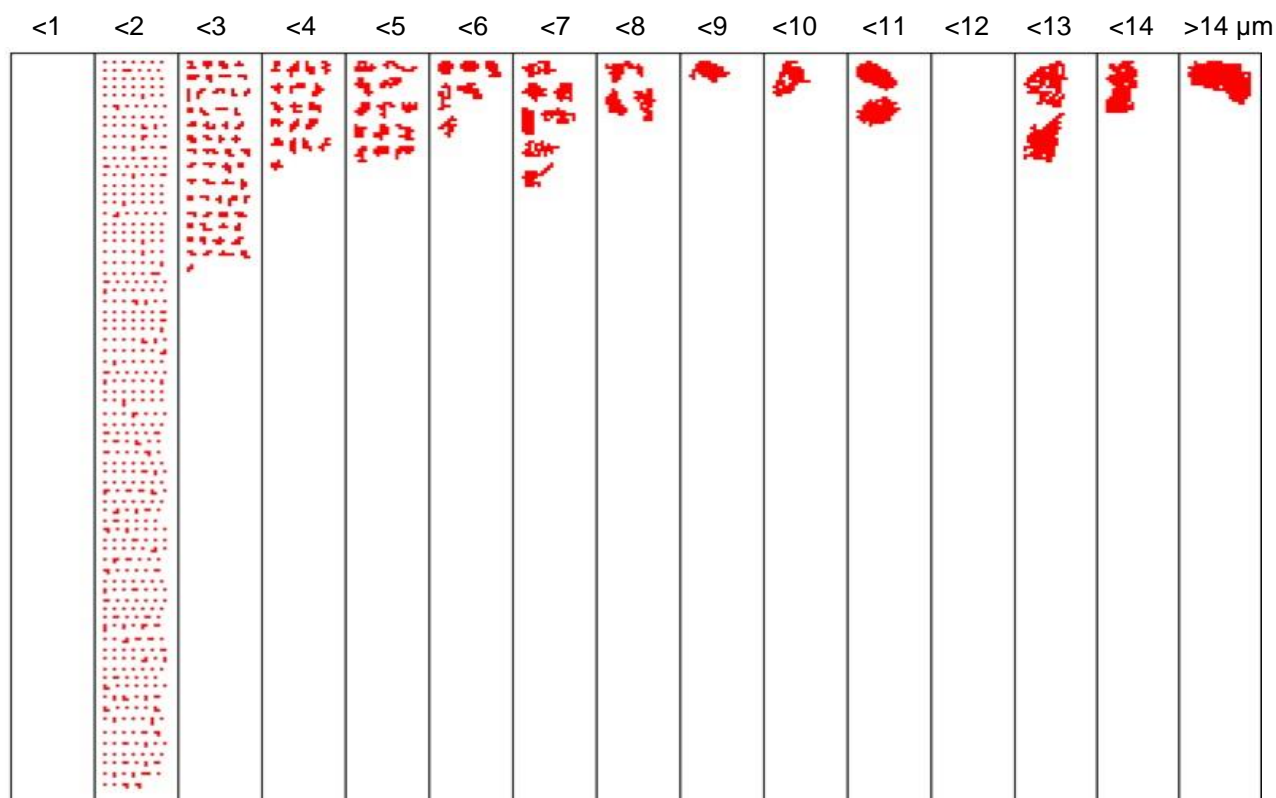




**Figure 12** - Examples of sulphide mineral textures and associations throughout the Booyendal mining cut. **(a)** fine-grained aggregate of BMS in a silicate mineral matrix (HW), **(b)** BMS grains coating the outside boundary of opx and chromite grains (HW), **(c)** BMS grains occurring within alteration mineral pockets which have affected primary opx (UPEG-upper), **(d)** BMS grain situated within alteration minerals and a single chromite grain (UP1), **(e)** BMS grains coating the outside boundary of chromite (UPEG-lower), **(f)** BMS grain in association with opx and plag (HW).

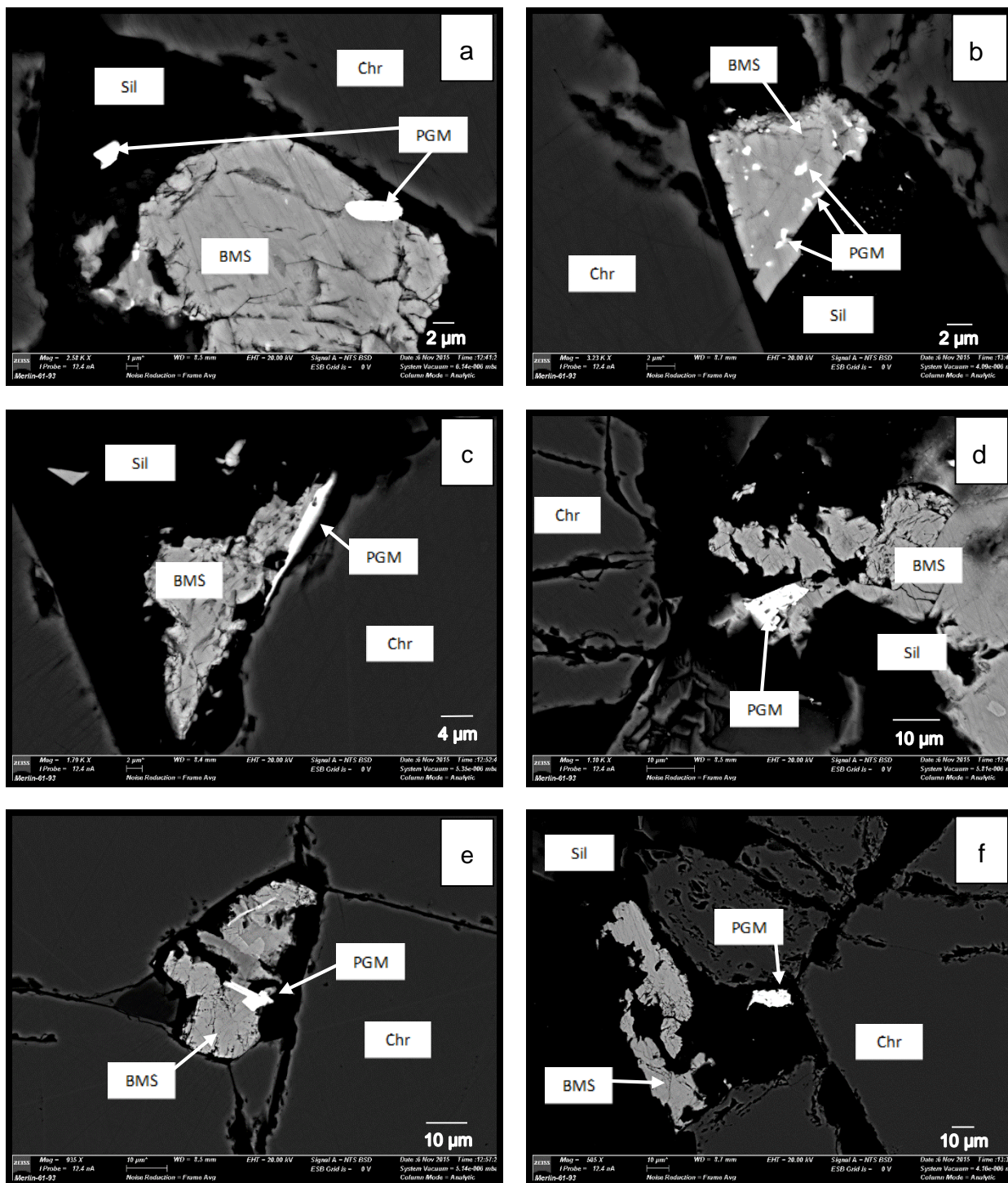
#### 4.2.4. PGM

A total of 610 discrete PGM grains were identified during QEMSCAN analysis. The majority of PGM are  $<3\ \mu\text{m}$  in size (Fig. 13). The greatest proportion of grains ( $\sim 80\%$ ) fall within the category of  $1\text{--}2\ \mu\text{m}$ , with a trend of decreasing abundance with increasing grain size. The " $<1\ \mu\text{m}$ " category is not populated as the resolution of analysis was set at a  $1\ \mu\text{m}$  pixel spacing meaning that some grains that are identified in the  $1\text{--}2\ \mu\text{m}$  fraction may in fact be smaller than  $1\ \mu\text{m}$ . Grain shapes of the PGM vary throughout the size ranges and tend to form sub-rounded (Fig. 14b) and blocky (Fig. 14d & f) to elongate shapes (Fig. 14c & e), although some grains may be described as highly irregular.



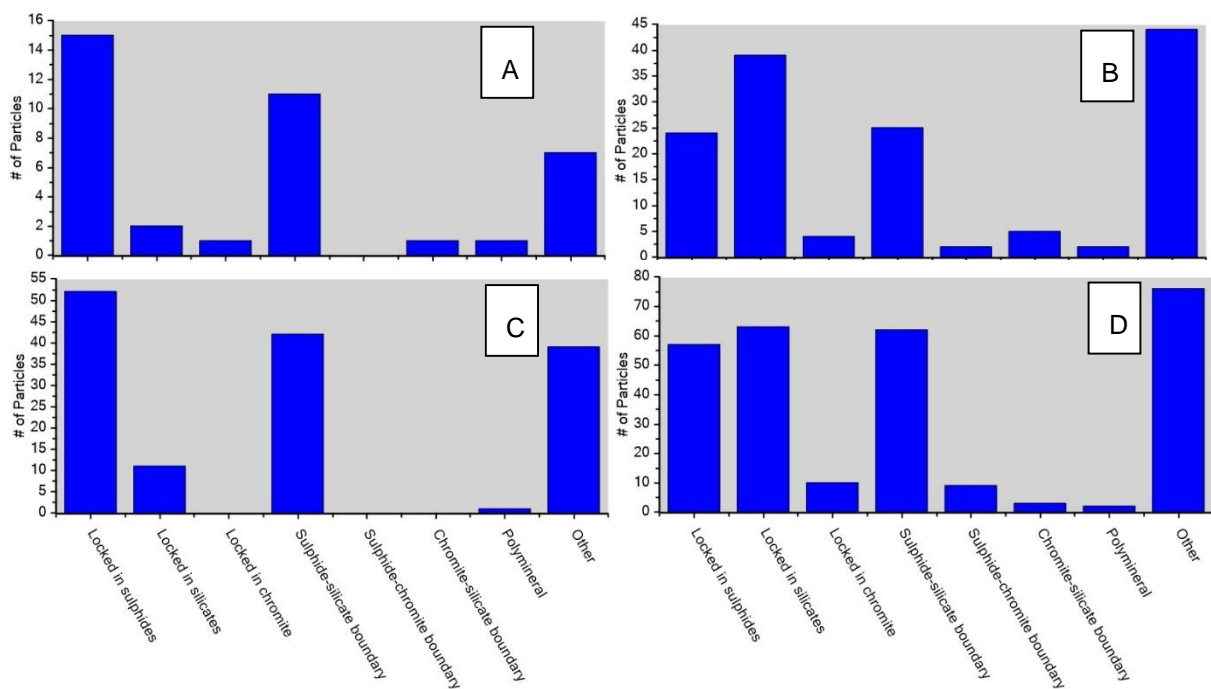
**Figure 13** – Grain size and shape distribution of PGM grains identified with QEMSCAN analysis ( $n=610$ ). Each PGM grain is displayed as a discrete red particle).





**Figure 14** - BSE images of selected PGM (bright white phase) with BMS (medium grey), Chromite (dark grey) and silicates (black). **(a)** PtIrRh-sulphide (left) and PtNi-sulphide (right) with Ni-sulphide, **(b)** Multiple Pt-sulphide grains with Ni-sulphide, **(c)** PtIrRh-sulphide with Ni-sulphide, **(d)** PtPd-sulphide with chalcopyrite + Ni-sulphide, **(e)** Pt-sulphide and Ru-sulphide (stringer) with Ni-sulphide + chalcopyrite + pyrite, **(f)** PtPd-sulphide near Ni-sulphide.

The mode of occurrence for PGM exhibits similar trends between all samples taken throughout the chromitite units of the main ore zone (Fig. 15). There is a strong predominance for PGM to occur either on the inside or outside of BMS grain boundaries (Figs. 14a, b, c, d & e). Additionally, all samples showed a large proportion of the PGM contents to be associated with titanium-phases, apatite and uvarovite (“other” category), especially within the mid UL and lower UM units (Figs. 15b & c). A large proportion of the PGM from the mid UL and upper UM units also occur associated solely with silicate minerals (Fig. 15 b & d). The specific proportions of the minerals which constitute the groupings; ‘silicate’, ‘sulphide’ and ‘other’ as presented for PGM mode of occurrence in Figure 15 are defined in Table 4. Please consult Figure 43, Appendix A for a schematic breakdown of the mineral associations presented in Figure 15.

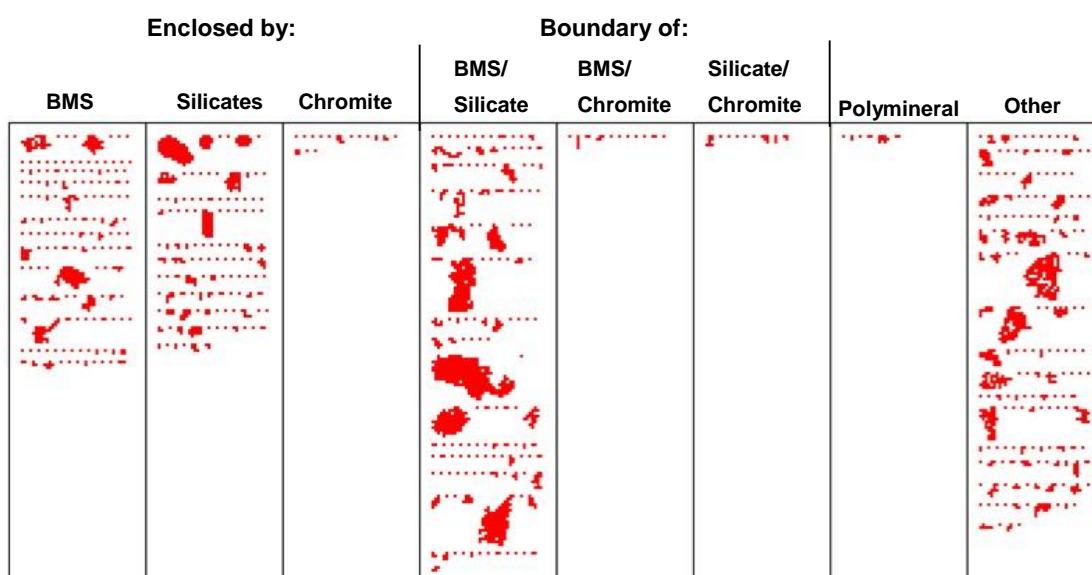


**Figure 15** – PGM mode of occurrence data from QEMSCAN, A) mid UT2 unit, B) mid UL unit, C) upper UM unit, D) lower UM unit.

**Table 4** - Proportions of mineral phase constituting each phase grouping (silicate, sulphides and "other") illustrated in Figure 15 and 16 for PGM mode of occurrence.

Silicates	%	Sulphides	%	"Other"	%
		Cu-sulphides	23		
Feldspar	60	Ni-sulphides	26	Ti-minerals (Rutile, sphene)	49
Orthopyroxene	36	Fe-sulphides	4	Apatite	42
Hydrous silicates	3	Bismuth phases	42	Uvarovite	8
		Silver	5		

The compiled statistics for PGM mode of occurrence, with grain size taken into account, derived from QEMSCAN analysis (Fig. 16) show that the most important relationship (i.e. largest PGM grains and the greatest proportions) for PGM is on the outside boundary of BMS. The second most important mode of occurrence is for PGM to occur with apatite and/or titanium-phases as well as associated with the silicate fractions of the UG2 reef. Many grains situated within grain boundaries of BMS and/or silicate minerals tend to be very small grains (<2  $\mu\text{m}$ ) except for some slightly larger grains (4-6  $\mu\text{m}$ ). The occurrence of small (1  $\mu\text{m}$ ) PGM within the grain boundaries of the various minerals may represent a proportion of PGE contents which are hosted in solid solution or as nano-particles within the UG2 reef. This interpretation will be discussed in section 6.1.3.

**Figure 16** – PGM association as a function of grain size for each category of association (Booyesdal). Each identified PGM grain is represented by a discrete red particle.

### 4.3. Mineral Chemistry and Relative Proportions

The mineral compositions of chromite, sulphide and PGM are described below. Individual mineral compositions were obtained from SEM whereas statistics on the various mineral groups (i.e. chromite, sulphide and PGM populations) were obtained from QEMSCAN. Hydrous silicates, sometimes referred to as 'alteration minerals', are dominated by chlorite, tremolite and mica phases (Table 5).

**Table 5** - Proportions of hydrous silicate mineral contents of the Booyendal samples (normalised to total alteration silicate contents).

Alteration mineral	%
Chlorite (Clinochlore)	36.10
Amphibole (Tremolite, Hornblende)	32.20
Mica (Muscovite, Biotite)	30.20
Talc	1.30
Serpentine (Antigorite, Clinochrysotile)	0.20

#### 4.3.1. Chromite

Although chromite grains throughout the three chromitite units of the mining cut are compositionally quite similar, certain trends do present themselves which make it possible to differentiate between the chromitite units (Fig. 17). Average aluminium values (weight %) within the UT2 unit are lower than the UL and UM units (13.67 vs. 15.29 & 15.42 respectively) (Fig. 17b). Average Fe<sup>3+</sup> values show an increasing trend from the bottom to the top of the main ore zone (UM=5.63 %; UL=5.99 % & UT2=6.64 %) (Fig. 17a). The Mg# (100Mg/Mg+Fe) also displays the lowest average values within the UT2 unit (28.96) compared to the UL (33.11) and UM (31.51) units (Fig. 17c).

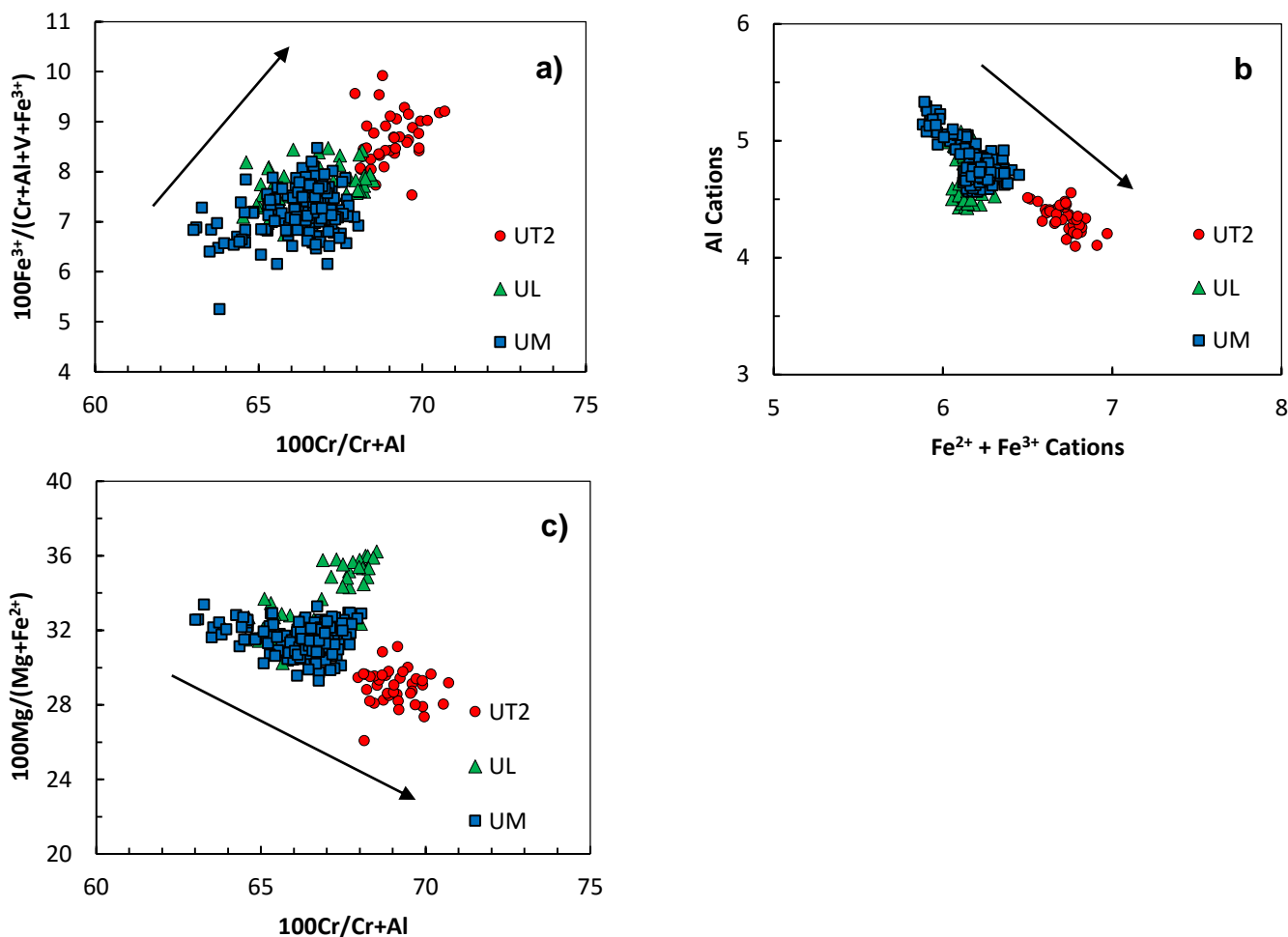


**Figure 17** – Chemical differentiation of individual chromite compositions obtained from SEM from Booyssendal.

#### 4.3.2. Sulphides

Overall, the sulphide mineral contents are dominated by millerite (48 %) and chalcopyrite (39 %) compositions with lesser proportions of pyrite (Fig. 18) as well as minor silver- and lead-bearing minerals. The terms chalcopyrite, millerite and pyrite are used to refer to all variations of copper-, nickel- and iron-sulphides respectively. QEMSCAN results also report the presence of minor proportions of bismuth- and silver-bearing phases. The UT2 unit contains elevated chalcopyrite relative to the UL and UM units (Fig. 18). Millerite remains a dominant phase within the other samples. The top of the UM unit (Fig. 18c) has a strongly millerite-dominated sulphide assemblage whereas chalcopyrite and millerite are in nearly equal proportion to each other in the lower UM unit (Fig. 18d). Pyrite remains a minor phase, with increased proportions in the UL and lower UM units (Figs. 18b & d). Individual mineral compositions for common sulphide minerals compiled from SEM analysis are reported

in Table 6. The compositions range from millerite (Samples B, D, E, G, H & K) and pentlandite (Sample A) to chalcopyrite (Sample C, F & I) and pyrite (Sample J).

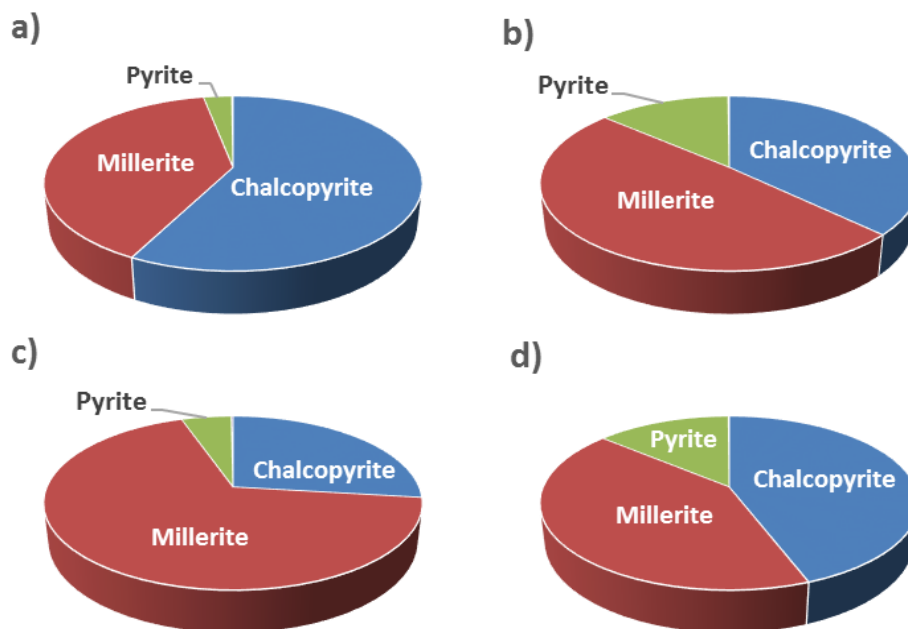


**Figure 18** – BMS split for each QEMSCAN sample; a) UT2 unit, b) mid UL unit c) upper and d) lower

**Table 6** - Individual sulphide mineral compositions analysed by SEM.

Sample #	A	B	C	D	E	F	G	H	I	J	K
Unit	UPEG (upper)	UT2	UT2	UP1	UP1	UL	UL	UL	UM	UM	UM
<b>Ni</b>	42.03	63.09		3.91	62.08	0.58	62.47	63.44	-	-	62.75
<b>Fe</b>	23.22	0.73	29.75	43.07	1.35	30.03	1.47	0.36	30.42	45.82	0.39
<b>Cu</b>	-	-	34.24	-	-	33.90	-	-	34.10	-	-
<b>Co</b>	1.67	0.80	-	-	0.65	-	0.78	0.79	-	-	0.83
<b>S</b>	32.96	36.20	35.58	53.45	35.73	35.00	35.11	35.01	35.38	53.52	35.95
<b>Total (wt. %)</b>	99.88	100.82	99.57	100.42	99.81	99.50	99.83	99.60	99.90	99.34	99.92



### 4.3.3. PGM

Examples of compositions for common PGM minerals identified within the Booyendal samples are reported in Table 7. Many of the identified grains that were analysed with SEM were PGE-sulphide minerals ( $\pm$ Ni, Fe) in the form of Pt,Pd-sulphides (Samples A, B, C, D, F, G, H, I) and Ru-sulphides (Sample E). Table 8 details the types of PGM that were analysed with SEM and includes a detailed description of the PGMs associational characteristics. PGM had a strong association with Ni-sulphides (~55 %). Many of the grains that were identified were found in close association with chromite grains (~80 %) and very often these chromite grains and/or the silicate minerals in the vicinity of the PGM (~80 %) were affected by alteration phases (occurring in association with an alteration mineral).

**Table 7** - Individual mineral compositions for PGM identified with SEM analysis.

<b>Sample #</b>	A	B	C	D	E	F	G	H	I
<b>Unit</b>	UT2	UL	UL	UM	UM	UM	UM	UM	UM
<b>Pt</b>	24.75	44.75	58.84	55.92	-	41.44	41.15	6.35	56.98
<b>Pd</b>	20.30	11.37	15.78	19.83	-	-	-	47.87	15.66
<b>Rh</b>	-	-	-	-	-	15.09	15.27	-	-
<b>Ru</b>	-	-	-	-	51.08	-	-	-	-
<b>Ir</b>	-	-	-	-	4.92	-	-	-	-
<b>Os</b>	-	-	-	-	6.69	-	-	-	-
<b>Au</b>	-	-	-	-	-	-	-	-	10.38
<b>Co</b>	-	-	-	-	-	1.03	0.93	-	-
<b>Cu</b>	-	-	0.80	-	-	13.34	13.04	-	-
<b>Ni</b>	28.49	20.54	4.60	5.92	-	2.18	2.29	18.95	5.11
<b>Fe</b>	-	1.31	1.47	0.49	0.52	0.63	0.67	0.89	-
<b>S</b>	26.43	22.11	18.77	18.33	36.13	26.11	26.21	25.61	19.06
<b>Total (Wt. %)</b>	99.97	100.08	99.46	100.01	99.34	99.83	99.57	99.66	101.35

Data from QEMSCAN indicate that in general the Booyendal samples are dominated by PGE-sulphide compositions (Fig. 19). The UT2 and UL units show a stronger predominance of ferroplatinum compositions within the samples (Figs. 19a & b). PGE-sulphides are still well represented within the UT2 unit (Fig. 19a), but show a marked decrease in proportion within the UL unit (Fig. 19b). The UM unit (Figs. 19c & d), which also contains the highest numbers of identified PGM grains, is dominated by PGE-sulphide compositions.

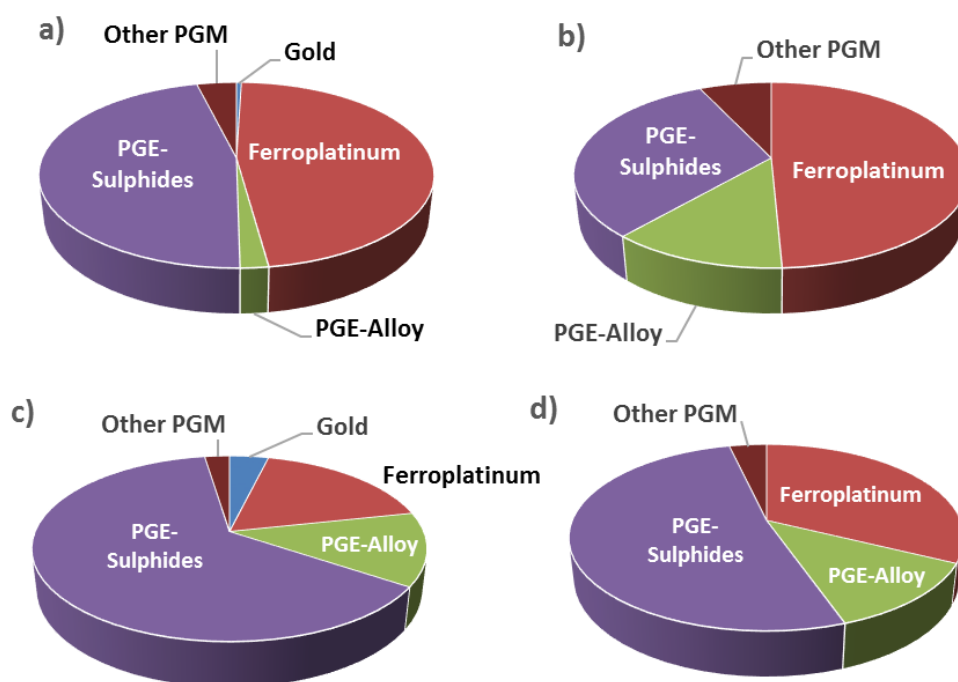


**Figure 19** – Relative abundance of various PGM identified during QEMSCAN analysis **a)** Unit: mid UT2 (n=38) **b)** Unit: mid UL (n=145) **c)** Unit: upper UM (n=145) **d)** Unit: lower UM (n=282).

**Table 8** - Compiled statistics of PGM analysed during qualitative SEM analysis including the mode of occurrence for the identified mineral. The presence of any alteration phases is also reported. The list is sorted by unit starting from the top of the main ore zone.

Type	Unit	BMS Host	BMS Occurrence	Gangue/Host	Alteration Present
Pt,Pd,Ni-S	UT2	Ni-Sulphide	Chr/Chr	Chromite	Yes
Pt,Pd,Ni-S	UT2	Ni-Sulphide	Chr/Sil	Chromite	Yes
Pt,Pd,Ni-S	UT2	Ni-Sulphide	Chr/Sil	Chromite	No
Pt,Pd,Ni-S	UT2	Ni,Fe-Sulphide	Chr/Sil	Chromite	Yes
Pt,Pd,Ni-S	UT2	-	Sil	Near Chromite	Yes
Pt,Pd,Ni-S	UT2	Ni-Sulphide	Chr/Sil	Chromite	Yes
Pt,Pd-Bi,Te	UT2	Ni-Sulphide	Chr/Sil	Chromite	Yes
Ru,Pt,Ir,Os,Fe,Ni-S	UT2	Pyrite	Chr/Sil	Chromite	Yes
Pt-S	UP1	-	Chr/Sil	Chromite	Yes
Pt,Pd,Ni-S	UL	Ni-Sulphide	-	Silicate	No
Pt,Pd,Ni-S	UL	Ni-Sulphide	-	Silicate	Yes
Pt,Pd,Ni-S	UL	Pyrite	Chr/Sil	Chromite	No
Pt,Pd,Ni-S	UL	Pyrite	Chr/Sil	Chromite	Yes
Pt,Pd, Ni,Fe-S	UL	Pyrite	Chr/Sil	Chromite	Yes
Pt-S	UL	-	-	Silicate	No
Ru,Ir,Os,Fe-S	UL	Ni-Sulphide	Sil	Silicate	Yes
Pt,Pd,Ni-S	UM	Ni-Sulphide	Chr/Sil	Chromite	Yes
Pt,Pd,Ni-S	UM	Ni-Sulphide	Chr/Sil	Chromite	Yes
Pt,Pd,Ni-S	UM	-	Chr/Sil	Chromite	Yes
Pt,Pd,Ni-S	UM	Ni-Sulphide	Chr/Chr	Chromite	No
Pt,Pd,Ni-S	UM	Ni-Sulphide	Chr/Chr	Chromite	Yes
Pt,Pd,Ni-S	UM	Chalcopyrite	Chr/Chr	Chromite	Yes
Pt,Pd,Ni-S	UM	Ni-Sulphide	Chr/Chr	Chromite	Yes
Pt,Pd,Ni-S	UM	Chalcopyrite	Chr/Chr	Chromite	Yes
Pt,Pd,Ni-S	UM	Ni-Sulphide	Chr/Chr	Chromite	Yes
Pt,Pd,Ni-S	UM	-	Chr/Sil	Chromite	Yes
Pt,Pd,Ni-S	UM	Ni-Sulphide	Chr/Sil	Chromite	No
Pt,Pd,Ni-S	UM	Ni-Sulphide	Chr/Sil	Chromite	Yes
Pt,Pd, Ni,Fe-S	UM	Pyrite	Chr/Sil	Chromite	Yes
Pt,Pd,Cu,Ni,Fe-S	UM	Chalcopyrite	Chr/Sil	Chromite	Yes
Pt,Pd,Cu,Ni,Fe-S	UM	Chalcopyrite	Chr/Sil	Chromite	Yes
Pt,Pd,Cu,Ni,Fe-S	UM	Chalcopyrite	Chr/Sil	Chromite	Yes
Pt,Pd,Au,Ni-S	UM	Chalcopyrite	Chr/Chr	Chromite	Yes
Pt,Pd-S	UM	Ni-Sulphide	Chr/Sil	Chromite	Yes
Pt,Pd-S	UM	-	Chr/Sil	Chromite	No
Pt,Pd-S	UM	Pyrite	Chr/Sil	Chromite	No
Pt,Pd-S	UM	-	Sil	Near chromite	Yes
Pd,Ni-S	UM	Ni-Sulphide	Chr/Chr	Chromite	No
Ru,Ir,Os-S	UM	-	Sil	Silicate	No
Ru,Ir-As-S	UM	-	Sil	Near chromite	Yes
Pt,Rh,Cu,Ni-S	UM	Ni-Sulphide	Chr/Sil	Chromite	Yes
Pt,Rh,Cu-S	UM	Ni-Sulphide	Chr/Chr	Chromite	Yes
Pt,Rh,Cu-S	UM	Ni-Sulphide	Chr/Sil	Chromite	No
Pt,Rh,Ni,Cu-S	UM	Ni-Sulphide	Chr/Sil	Chromite	Yes
Pt,Pd,Rh,Cu-S	UM	Ni-Sulphide	Chr/Sil	Silicate	Yes
Pt,Pd,Ni,Cu-As,S	UM	Ni-Sulphide	Chr/Sil	Chromite	Yes
Pt,Pd,Te,Ni-As,S	UM	Ni-Sulphide	Chr/Sil	Chromite	Yes
Pt,Ir,Rh,Cu,Fe-As,S	UM	-	Chr/Sil	Chromite	Yes

## 4.4. Bulk Rock Geochemistry

### 4.4.1. Differentiation between Mining Units

A whole rock SiO<sub>2</sub> % vs. MgO % plot effectively discriminates between the various units based on the dominant mineral assemblage (Fig. 20). The FW unit plots further towards plagioclase than the other silicic units, suggesting that it contains a higher proportion of plagioclase (this infers that the rock type is of an intermediary anorthositic to pyroxenitic composition). The chromitite units (UT2, UL and UM) plot as expected near chromite with the silicic component most likely dominated by plagioclase and not orthopyroxene. This trend is consistent with petrographic observations. The outlier from the UP1 unit cluster is representative of a sample which immediately underlies the UT2 unit. It is suggested that this unit contains elevated chromite contents which is also consistent with petrographic observations.

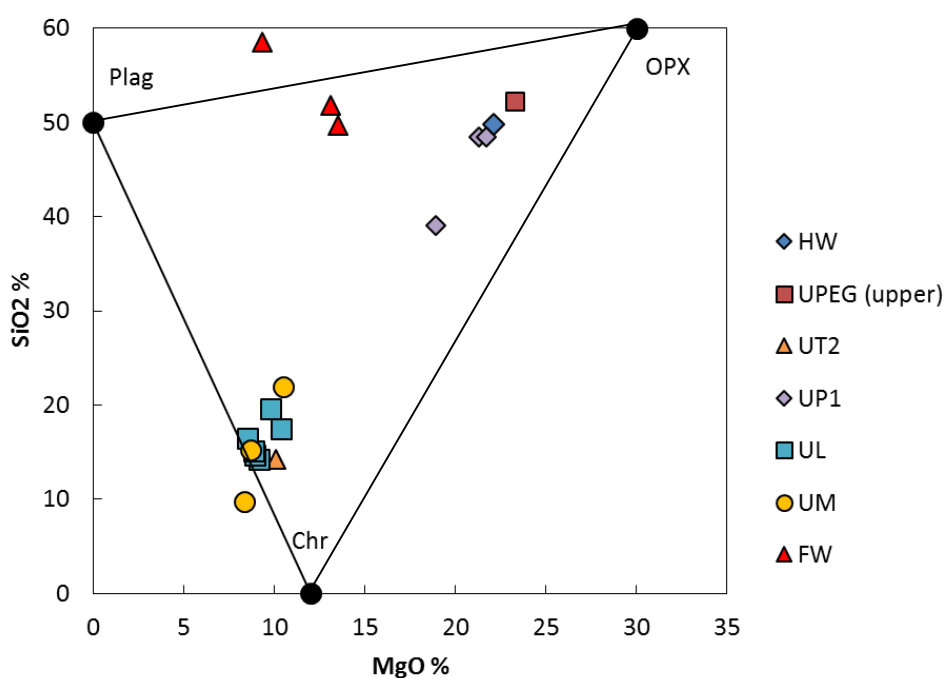


**Figure 20** – Bulk SiO<sub>2</sub> % vs. MgO % plot. The apices of the triangle represent the ideal compositions of orthopyroxene, plagioclase and chromite.

#### 4.4.2. Stratigraphic Variation

Normalised 4PGE (Pt, Pd, Ru, Rh) grade values (Fig. 21a) are elevated within the chromitite units (UT2, UL and UM). PGE grade values are normalised to the average PGE grade over the entire mining cut. The values 'spike' within the lower portion of the UL unit (bottom-loaded) and the upper and lower portions of the UM (top and bottom loaded). PGE grade shows an immediate decrease just below the UM unit within the footwall section. The Pt/Pd ratio (Fig. 21b) is highest within the UL unit (>7) (except within the middle section), is lower within the UM unit (2-5) and the lowest values are recorded in the footwall section (<1). The UP1 unit, although containing very low PGE grade, shows high Pt/Pd ratios, except for the portion just above the UL unit.

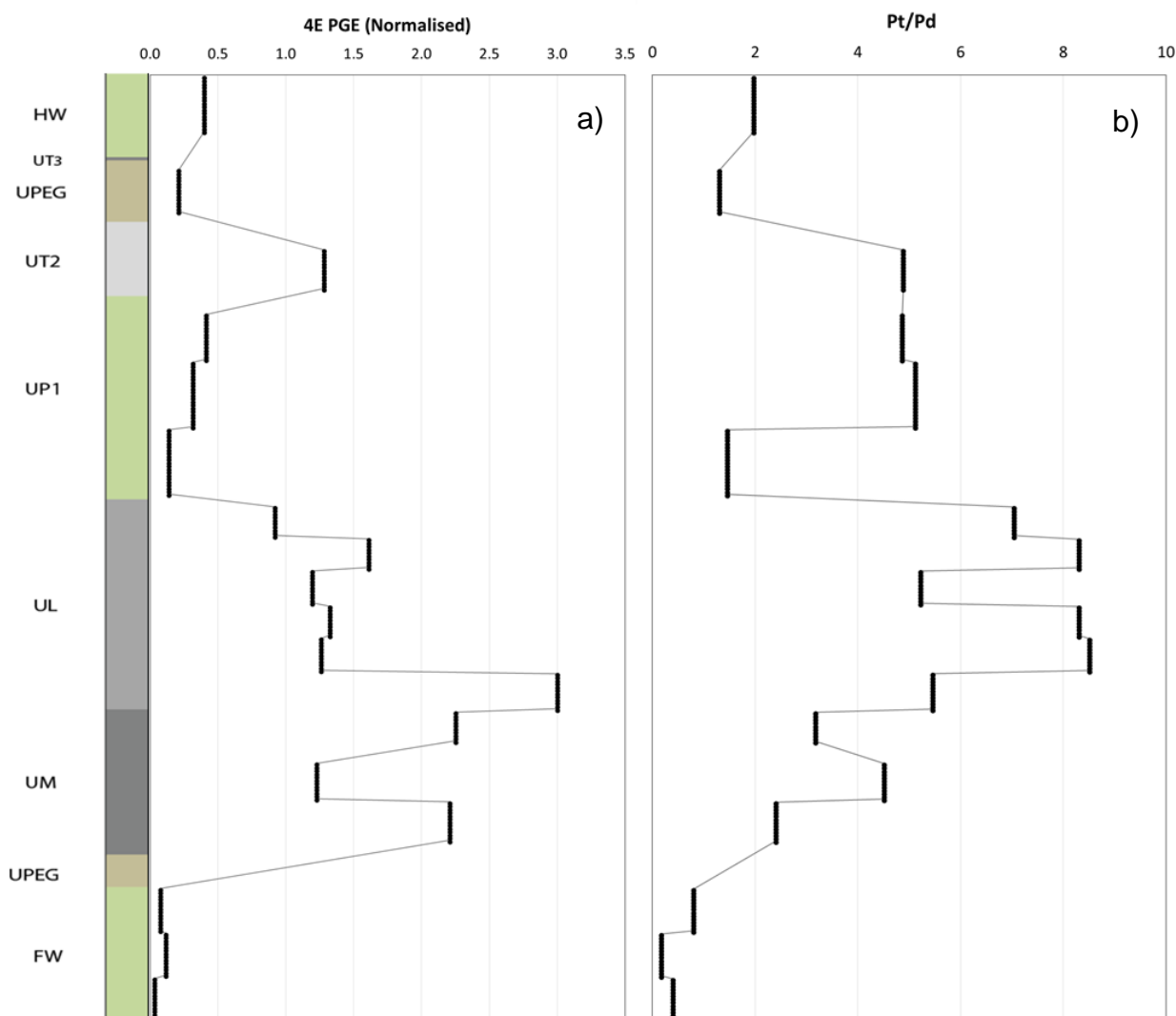


**Figure 21** – Geochemical assay values through the Booyendal mining cut for a) 4PGE (normalised) and b) Pt/Pd.

A plot of copper + nickel (Fig. 22a) is used as a proxy for sulphide mineral distribution. The concentrations are highest within the UT2 (~250 ppm) and lower sections of the UL and UM units (~190 ppm). The UL unit shows an upward decreasing trend (from 200 ppm near the base to 150 ppm at the top). The lowest concentrations are observed at the UL/UM transition (~100 ppm) and within the footwall section (~50-100 ppm). The Cu/Ni ratio (Fig. 22b) remains relatively constant throughout the UG2 at Booyssendal (0.4). This ratio illustrates a slightly higher proportion of nickel throughout the main ore zone with copper dominating the HW and FW units (>0.8).

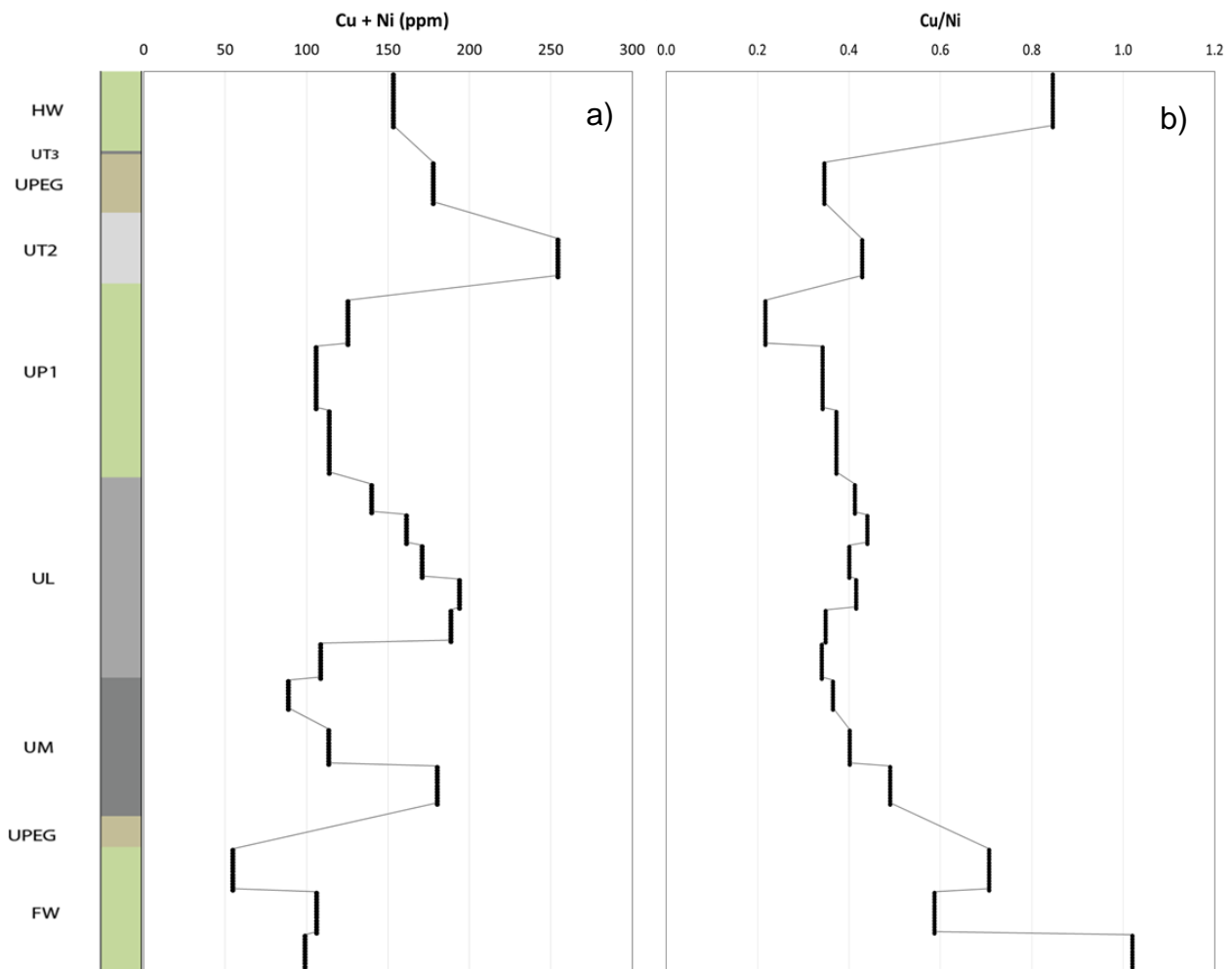


**Figure 22** - Geochemical assay values through the Booyssendal mining cut for a) Cu + Ni (ppm) and b) Cu/Ni.

The Mg# (defined as the cation ratio; Mg/Mg+Fe) (Fig. 23a) is highest within the silicic units (0.6-0.7) whilst in the chromitite units Mg# values are lower (~0.3), showing slight elevations within the lower section of the UL unit and top of the UM unit. The lowest Mg# values were recorded at the base of the UM unit (~0.25). Cr<sub>2</sub>O<sub>3</sub> contents within the chromitite units increase upwards within the UL and decrease upwards within the UM unit (Fig. 23b). The highest Cr<sub>2</sub>O<sub>3</sub> contents are recorded within the UT2 unit (~32 %), at the top of the UL unit (~32 %) and at the base of the UM unit (~35 %).

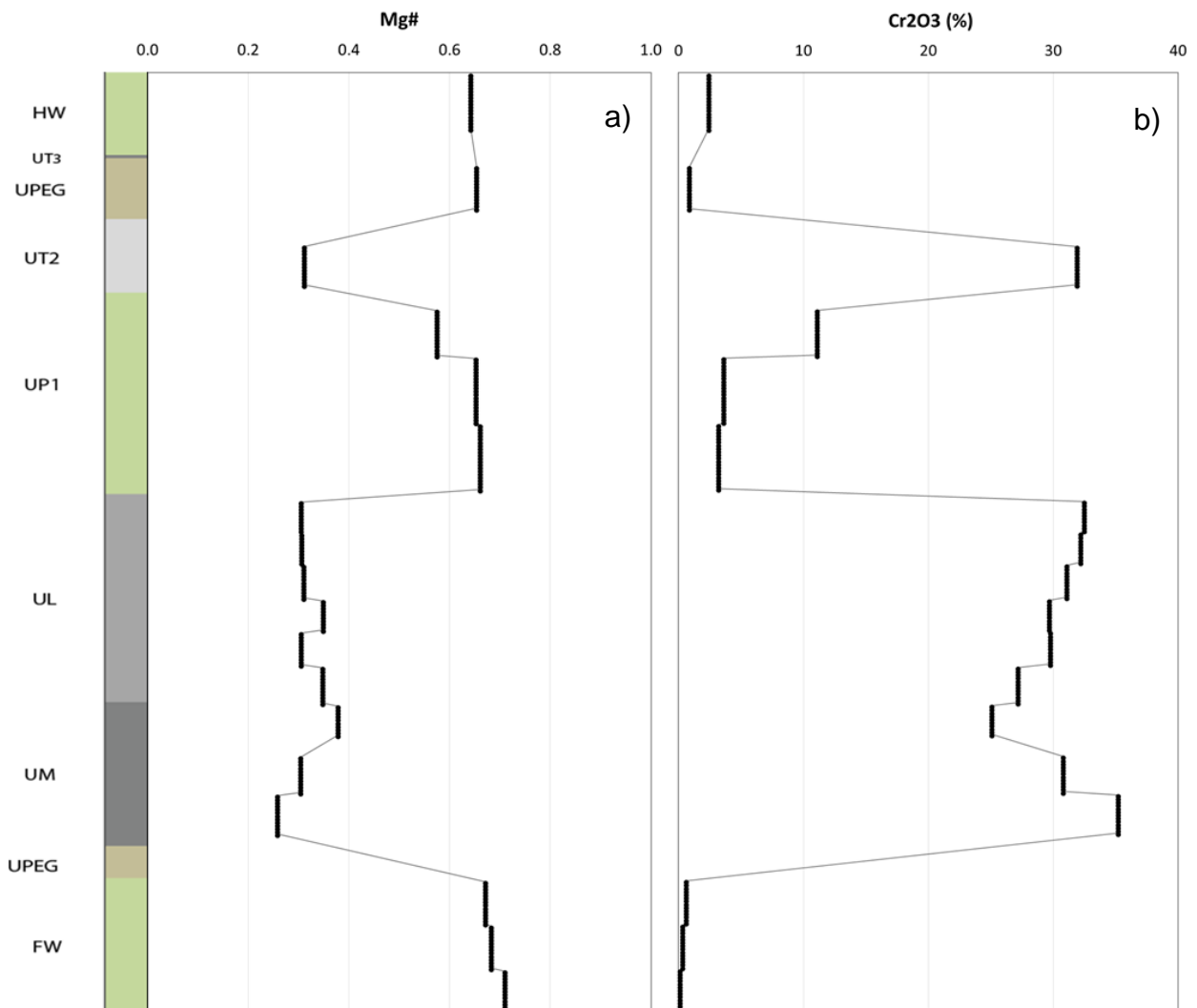


**Figure 23** - Geochemical assay values through the Booyensdal mining cut for a) Mg# and b) Cr<sub>2</sub>O<sub>3</sub> (%).

## 4.5. 3-D $\mu$ XCT Analysis

Samples were scanned with a particular focus on the distribution and grain size characteristics of chromite and PGM through the chromitite units (UT2, UL and UM). Due to the inability of 3-D  $\mu$ XCT analysis to constrain individual mineral compositions, the phases assumed to be PGM in this section are representative of the highest density fraction. This assumption is reinforced by the QEMSCAN results which show minor amounts of high density minerals that are not either PGM or minerals associated with PGM.

### 4.5.1. *Chromite Texture and 3-D Distribution of PGM*

PGM have a heterogeneous and disseminated distribution in 3D space (Figs. 24 & 25). Figure 24 is representative of the middle of the UM unit whilst Figure 25 represents the lower sections of the UM unit. The PGM contents are observed occurring in discrete accumulations (“nugget effect”) or spread out throughout the analysed section. No steadfast correlation can be drawn between the texture of chromite and the distribution of PGM. Some analysed sections of core exhibit areas with dense, compacted chromite textures that are associated with high PGM concentrations (bottom of Fig. 25) and other sections exhibit a disseminated chromite texture in conjunction with elevated PGM concentrations (middle of Fig. 24).

The texture of chromite changes from bands of dense, compact accumulations, such as at the top of Figure 24 and bottom of Figure 25, to disseminated grains with larger proportions of intercumulate silicate phases in other sections. Taking into account all sections which were analysed with 3-D  $\mu$ XCT, chromite textures are highly variable in their distribution throughout the chromitite units. Larger chromite grains tend to form blocky grain shapes whereas the smaller grain size fraction exhibit predominantly rounded grain shapes. When comparing Figures 24 and 25, the overall chromite grain size is larger in the latter and coincides with an increase in the thickness of the bands of compacted chromite. Refer to Figure plate 53 which presents 2-D images of chromite texture as ‘snapshot views’ throughout the stratigraphic height of the chromitite units from top to bottom.



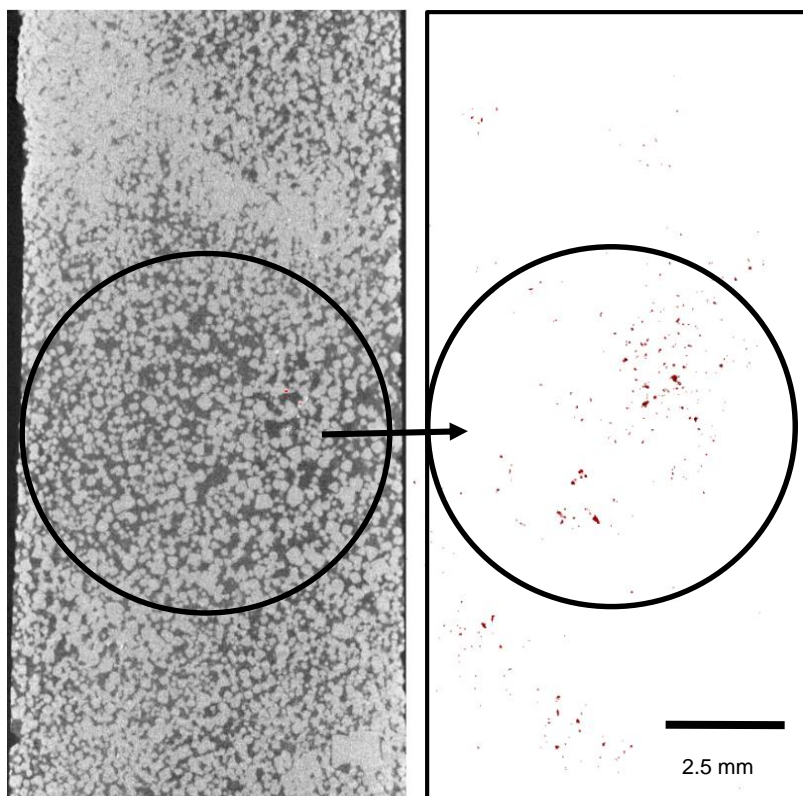


**Figure 24** - 2D slice image of chromite texture (left) juxtaposed with the 3D distribution of PGM (right - red dots). Sample XCT 2 (mid UM unit) shows an area with a disseminated chromite texture correlating with high proportions of PGM.

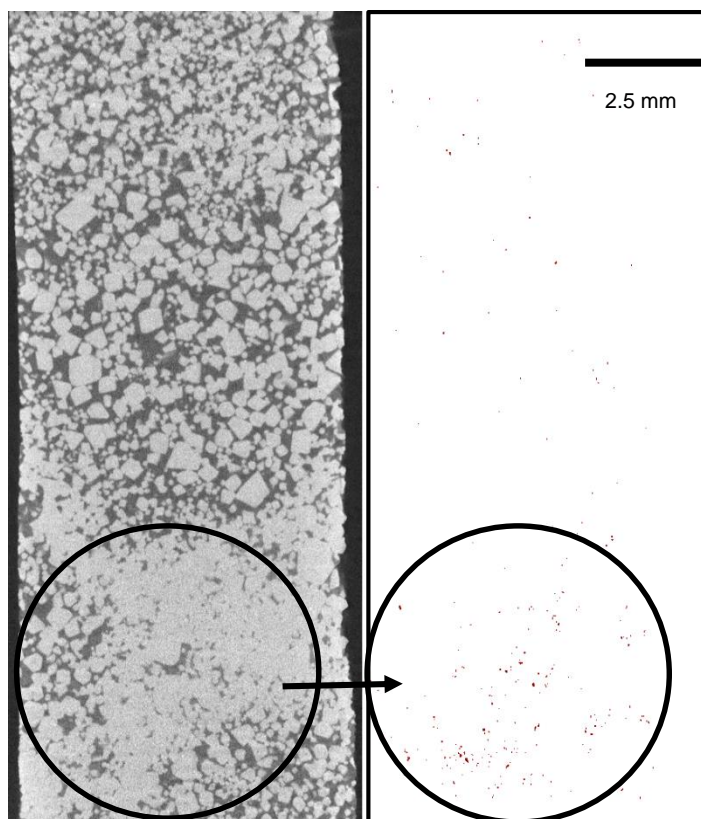


**Figure 25** – 2D slice image of chromite texture (left) juxtaposed with the 3D distribution of PGM (right - red dots). Sample XCT 7 (lower UM unit) showing an area with compacted chromite correlating with high proportions of PGM.

#### 4.5.2. PGM Grain Size Characteristics

The majority of PGM grains are reported to be in the 40-59  $\mu\text{m}$  size fraction (~50 %) within all the analysed sections (Fig. 26). Most of the remaining grains either fall into the smaller (20-39  $\mu\text{m}$ ) or the larger (60-79  $\mu\text{m}$ ) fractions. Although some larger grains do exist (>80  $\mu\text{m}$ ), they constitute a very small proportion of the total PGM contents (10-20 %). Sample “XCT 10” (top of the UL unit) contains a larger proportion of grains within the 20-39  $\mu\text{m}$  size fraction. The voxel resolution of 10  $\mu\text{m}$  allows for a realistic determination of discrete PGM grains with a lower size of limit of 20  $\mu\text{m}$ . Grain size is reported as equivalent spherical diameter (ESD) which differs from conventional equivalent circle diameter (ECD) used for 2D petrographic descriptions.

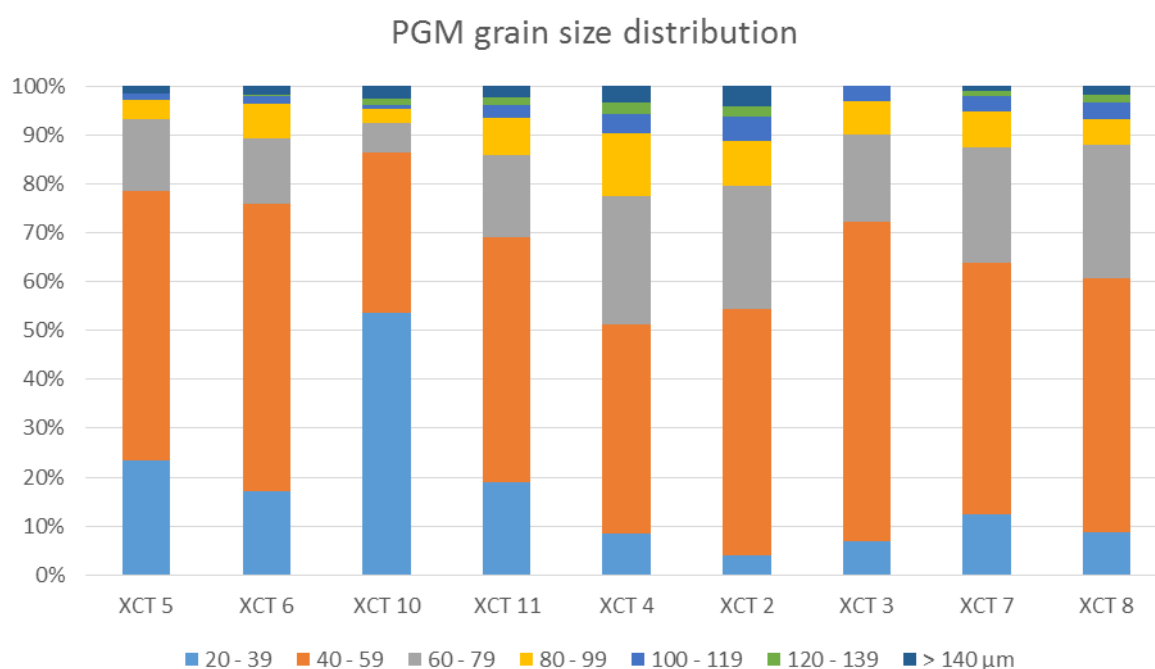


**Figure 26** – Grain size (ESD) distribution of dense mineral phases attained from 3-D  $\mu\text{XCT}$  analysis (10  $\mu\text{m}$  voxel resolution) (Booyse *et al.*)

\* ESD = diameter of a sphere that fully encloses the grain of interest.

## Chapter 5: ZONDEREINDE UG2

The core is representative of a ‘normal UG2’ reef mining cut from Zondereinde mine, western Bushveld Complex. The hanging wall is pyroxenitic to olivine-pyroxenitic and the footwall pyroxenitic. The main ore zone is dominated by chromitite layers with thin pyroxenite partings. The core is divided into eight units based on the distinct mineralogical contrasts. Figure 27 indicates what units are contained within the hanging wall, footwall and main ore zone sections and Figure 28 illustrates the position from which samples were taken and for which analytical technique they were used.

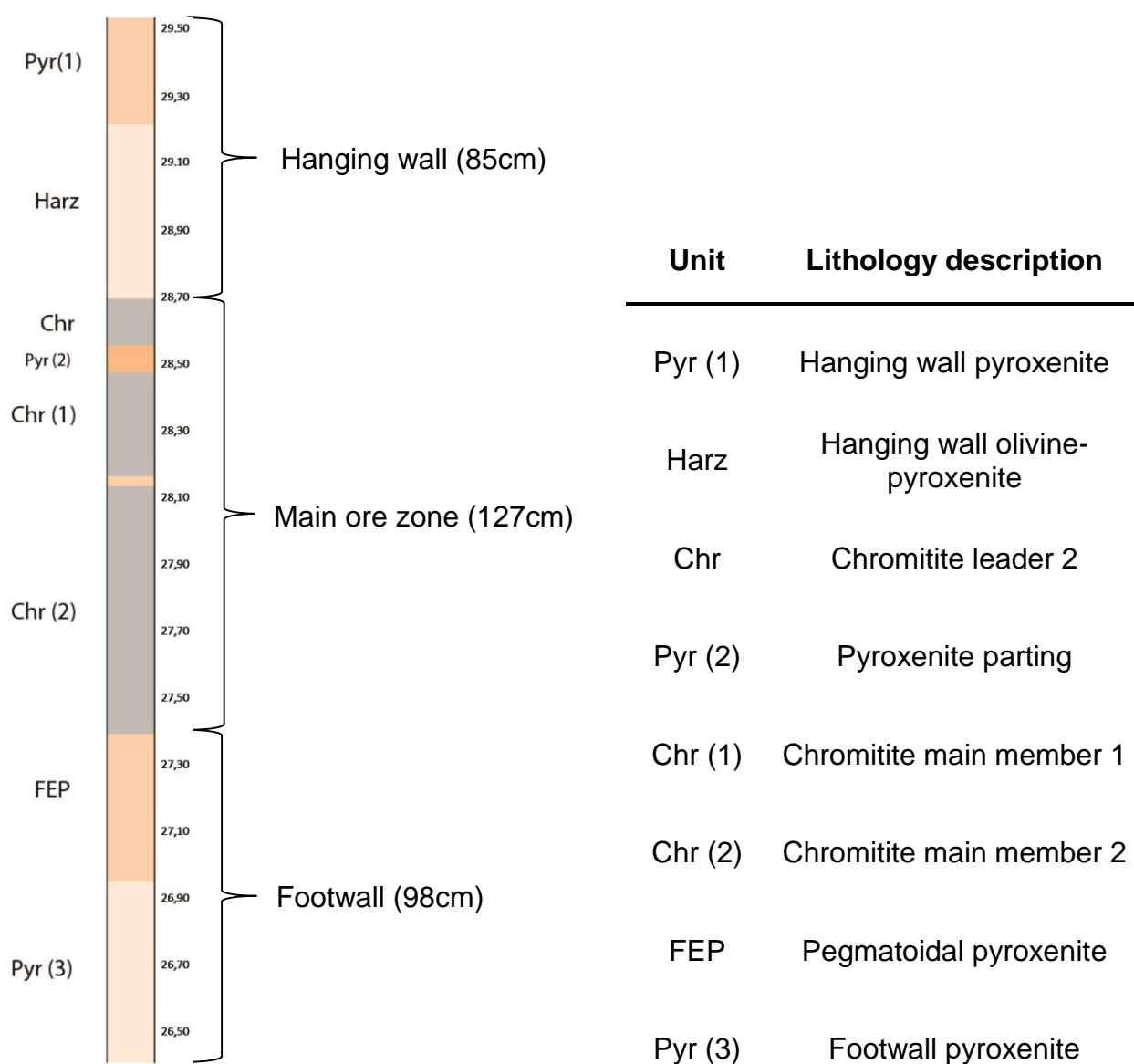


**Figure 27** – Schematic illustration of the Zondereinde core set used in this study. The core is divided into 3 broad sections namely; hanging wall, main ore zone and footwall based on the prevalence of PGE grade within the various units.

## 5.1. Structure and Bulk Mineralogy

The core set consists of, from top to bottom, 85 cm of hanging wall, underlain by 127 cm of main ore zone, followed by 98 cm of footwall (Figure 27). The hanging wall section consists of 32 cm of pyroxenite (Pyr (1)) and 53 cm of olivine-pyroxenite (Harz). XRD data reports the bulk mineralogy of both units to consist of enstatite, forsterite and anorthite with minor amounts of hydrous alteration silicates; talc, antigorite (serpentine) and muscovite. Although the Pyr (1) and Harz units appear to be quite similar, naming conventions at Zondereinde mine suggests that the Harz unit contains elevated olivine proportions compared to the overlying Pyr (1). Mine geologists at Zondereinde recognise the presence of a darker brown/black mineral as olivine and delineate the Harz unit from the Pyr (1) unit. This nomenclature is maintained for simplicity sake throughout this study but this differentiation will be assessed in section 5.4. and discussed in Chapter 6.

The main ore zone is divided into 5 units which are essentially 3 chromitite layers split by two pyroxenite units. At the top is a 14 cm thick chromitite unit (Chr) underlain by a pyroxenite parting (8 cm) and then a 31 cm thick chromitite (Chr (1)) unit. A thin pyroxenite parting (~3 cm) separates the Chr (1) unit and the lowermost chromitite unit (Chr (2)) which is 74 cm thick. The very thin nature of the pyroxenite parting, combined with the brittle nature of the rock meant that this unit could not be analysed as part of this study (see section 3.2.). The chromitite units comprise dominantly Fe-rich magnesio-chromite and minor proportions of an unnamed 'copper-magnesium oxide', enstatite and talc.

The footwall sections are comprised of a 44 cm pegmatoidal pyroxenite (FEP) underlain by a 54 cm pyroxenite (Pyr (3)). The bulk mineralogy of the footwall rocks is similar, but the FEP unit has a larger average grain size. The units are dominated by enstatite and anorthite with minor alteration minerals talc, antigorite and muscovite.

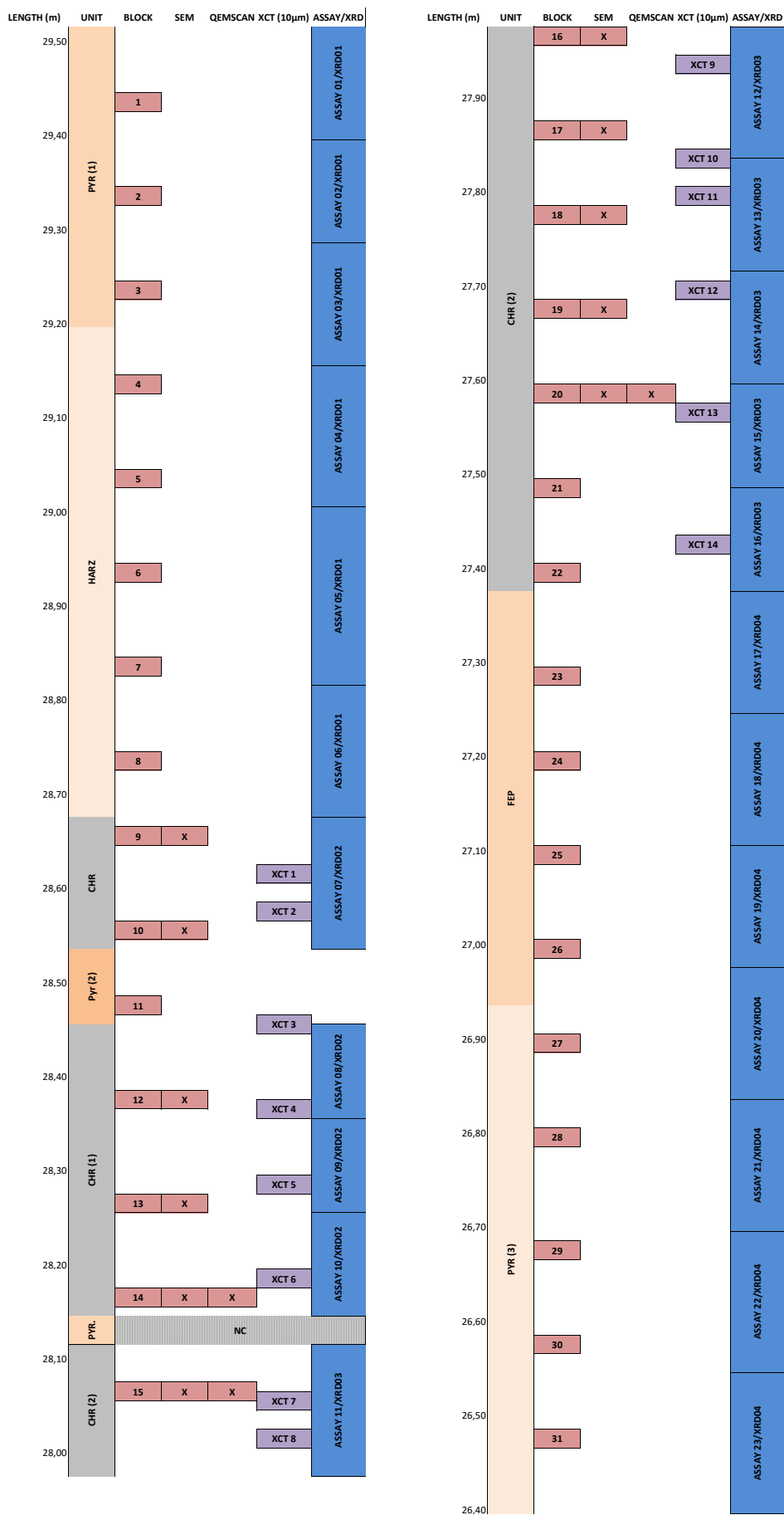


Figure 28 - Schematic illustration of sample localities for petrographic, compositional, geochemical and 3-D analytical techniques. \*NC – No core.

## 5.2. Textural Relationships

The Pyr (1) unit is dominated by cumulus orthopyroxene grains (~70 modal %) with intercumulus plagioclase. The Harz unit contains less cumulus orthopyroxene (~55 modal %) with an increased proportion of plagioclase compared to Pyr (1). Sulphide mineralisation which is minimal within Pyr (1) and displays an upward decrease within the Harz unit. Hydrous alteration phases are prevalent in both units, but show a marked increase within the Harz unit, affecting primary silicate phases (orthopyroxene and olivine) (Fig. 29b & c). Small chromite grains exist as a minor phase within both hanging wall units.

The chromitite units of the main ore zone (Chr, Chr (1), Chr (2)) exhibit differing textural characteristics based upon the proportion and grain size of chromite (this will be discussed in greater detail in section 5.5.2.). The main ore zone, with the exception of the pyroxenite parting Pyr (2), is dominated by Fe-rich magnesio-chromite grains (80-90 modal %) with intercumulus plagioclase, orthopyroxene and talc. The Pyr (2) unit is characterised by large orthopyroxene grains which exhibit extensive alteration features in the form of cross cutting veins and fractures and replacement of orthopyroxene along cleavage planes (Fig. 29a, b, c & d). Sulphide minerals are found in low proportions in the main ore zone relative to the hanging wall section, with slightly elevated concentrations in the Chr (1) unit, occurring as a fine dusting or as small aggregates of different BMS phases. The footwall units (FEP and Pyr (3)) are dominated by orthopyroxene grains with intercumulus plagioclase. The FEP unit contains enlarged orthopyroxene grains (relative to all other units), giving it a pegmatoidal texture. There are extensive alteration features within the FEP unit which increase toward the top contact with the main ore zone. Alteration features are minimal within the Pyr (3) unit. Sulphide minerals, which are rare, are fine grained and occur disseminated throughout both of the footwall units.

### 5.2.1. Silicates

Orthopyroxene grains within the hanging wall units are 3-5 mm in size and are euhedral/subhedral in shape. The Harz unit contains less orthopyroxene than the Pyr (1) unit and is complimented by an increase in olivine and intercumulus plagioclase contents. The plagioclase grains remain relatively unaffected by alteration and are in

the size range of 1-3 mm, with slightly larger grain sizes within the Harz unit. Hydrous alteration features are found in greater proportions within the hanging wall units (~10 modal %) when compared to the rest of the mining cut. Maximum proportions were recorded at the base of the unit and exhibit an upwardly decreasing trend. They occur as the partial alteration of orthopyroxene grains, along cleavage planes (Fig. 29b) and are often found in close association with chromite grain boundaries as a fine coating around the rim of the grain or enclosing BMS minerals (Figs. 29c & d).

The silicic component of the main ore zone is predominantly hosted within the pyroxenite parting (Pyr (2)). This unit contains pegmatoidal orthopyroxene (3-7 mm) which is affected by high degrees of alteration. Hydrous alteration phases affect a large proportion of the silicates, occurring as large patches that replace orthopyroxene grains and often enclose, or are associated with, chromite and sulphide minerals (Figs. 29c & d). Plagioclase grains are small and occur intercumulus to the primary mineral assemblage (chromite and orthopyroxene). Within the chromitite units (Chr, Chr (1)) the silicate mineralogy consists mainly of hydrous silicates which have replaced the primary silicate assemblage in large patches. It is often found enclosing sulphide minerals or occurring around the boundary of chromite grains as a micron scale coating. The silicic portion of the Chr (2) unit, which comprises intercumulus plagioclase with minor cumulus orthopyroxene, does not experience the same degree of alteration as the above units. However, where alteration features are present it affects chromite grains on their grain boundaries or within cross cutting vein-like structures.

The footwall units (FEP, Pyr (3)) are dominated by cumulus orthopyroxene (~70 modal %) and intercumulus plagioclase. The FEP unit is characterised by pegmatoidal orthopyroxene (5-8 mm) which is extensively affected by hydrous silicate minerals. The hydrous phases affect up to ~15 modal % of the FEP unit, preferentially occurring along cleavage planes of orthopyroxene (sometimes completely replacing the primary mineral) and filling fractures which cross-cut the primary mineral assemblage (Fig. 29a & c). Plagioclase grains are relatively unaffected by the alteration features.



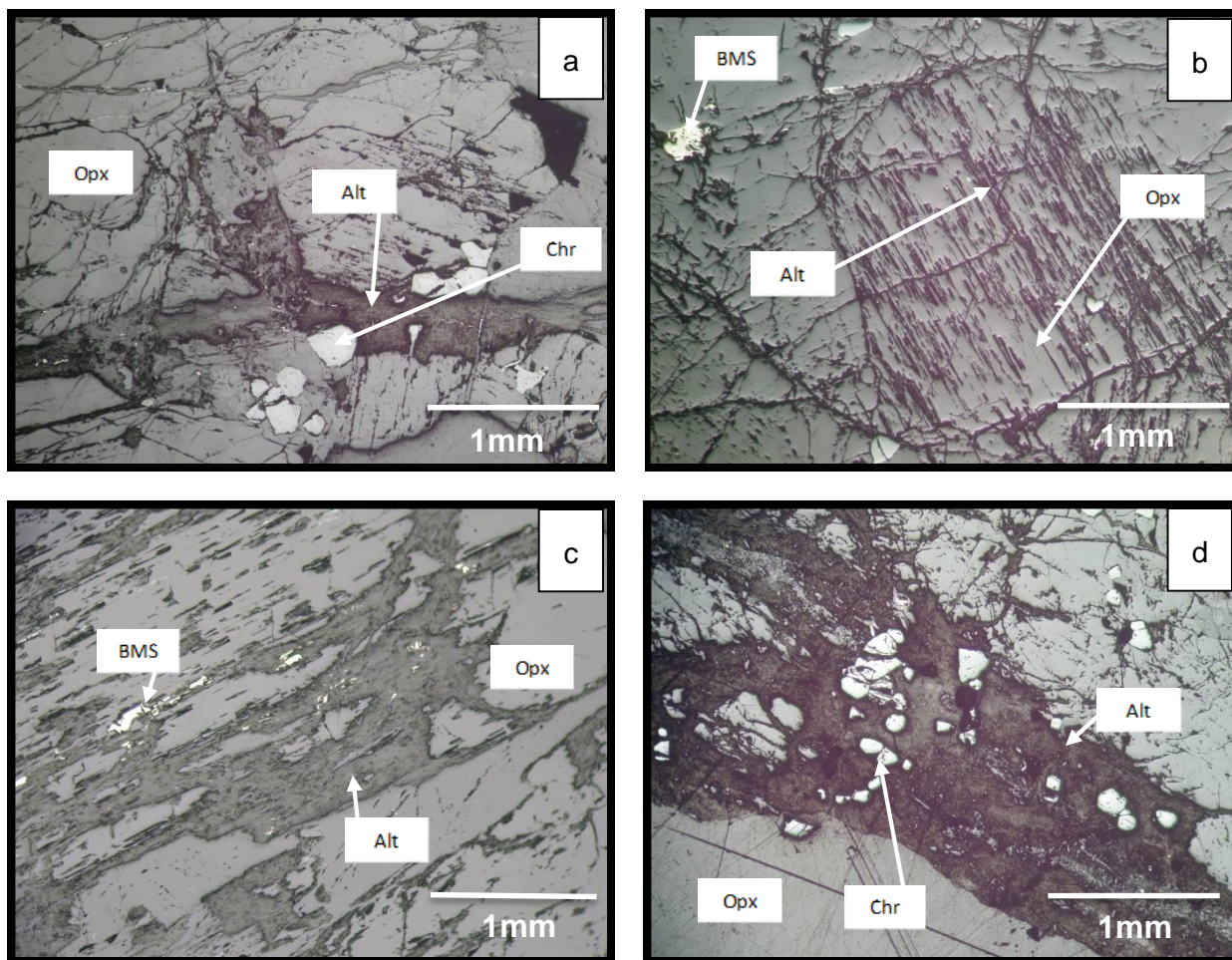


**Figure 29** - Examples of silicate alteration mineral features as observed throughout the Zondereinde mining cut. **(a)** Alteration minerals cross cutting and replacing multiple opx grains with a vein-like texture (Pyr (2)), **(b)** partial replacement, occurring along cleavage planes of opx (Pyr (1)), **(c)** alteration phases enveloping BMS mineralisation (FEP), **(d)** intense alteration of primary silicate grains, enclosing relict chromite with a vein-like mode of occurrence (Pyr (2)).

### 5.2.2. Chromite

Chromite in the hanging wall units exists as a minor phase, often occurring as accumulations of small grains or as singular grains (0.1-1 mm). Where grains are in contact, they can display annealed grain boundaries (Fig. 30c). The main ore zone units, except for Pyr (2), are dominated by euhedral/rounded chromite grains (80-90 modal %) which have a wide grain size distribution ranging from 0.1-1 mm in diameter. The Chr, Chr (1) and Chr (2) units are dominated by large interlocking chromite grains with almost no interstitial minerals in these sections (Figs. 30a & d), although less commonly. There are also sections within the main ore zone chromitites which exhibit a disseminated texture (Figs. 30b & e). When chromite grains exhibit an interlocking texture, grains are of a predominantly larger size (>0.5 mm) (Fig. 30a) than in sections with a disseminated chromite texture (Fig. 30b). In addition, the interlocking grains



tend to have a blocky to euhedral grain shape (Fig. 30a) whereas the more disseminated grains are rounded (Figs. 30b & e). Chromite grains which border on silicate minerals often have hydrous alteration phases around the outside boundary of the grain (Fig. 30f).

The middle of Chr (1) unit exhibits pitting textures (Fig. 31a) on some chromite grain surfaces. This section also contains elevated hydrous alteration phase features which occur in large patches distributed throughout the unit (Fig. 30b). These alteration features are observed completely enclosing chromite and sulphide grains. The Chr (2) unit contains a larger proportion of annealed chromite grain boundaries, especially within the smaller size fraction (Fig. 30c). Within this unit, bands of tightly interlocking chromite grains alternate with areas where chromite grains exhibit a more disseminated texture. The Pyr (2) unit contains minor chromite, which is often found to be associated with alteration phases. These grains form small accumulations or thin horizontal strings of annealed chromite grains. The grain sizes within the Pyr (2) unit are generally small and do not exceed ~0.3 mm in diameter. The footwall units (FEP, Pyr (3)) seem to be devoid of any chromite grains.

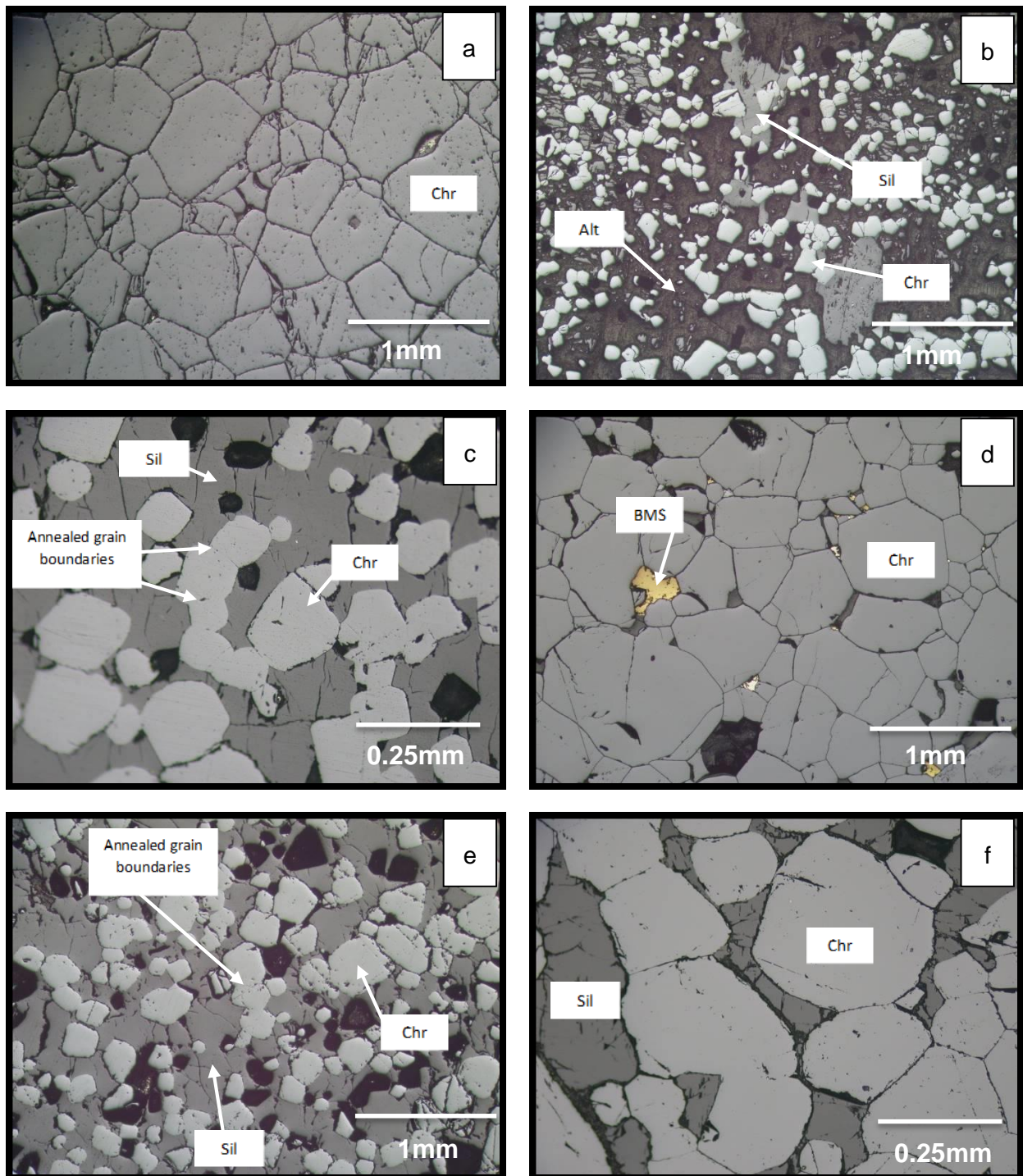


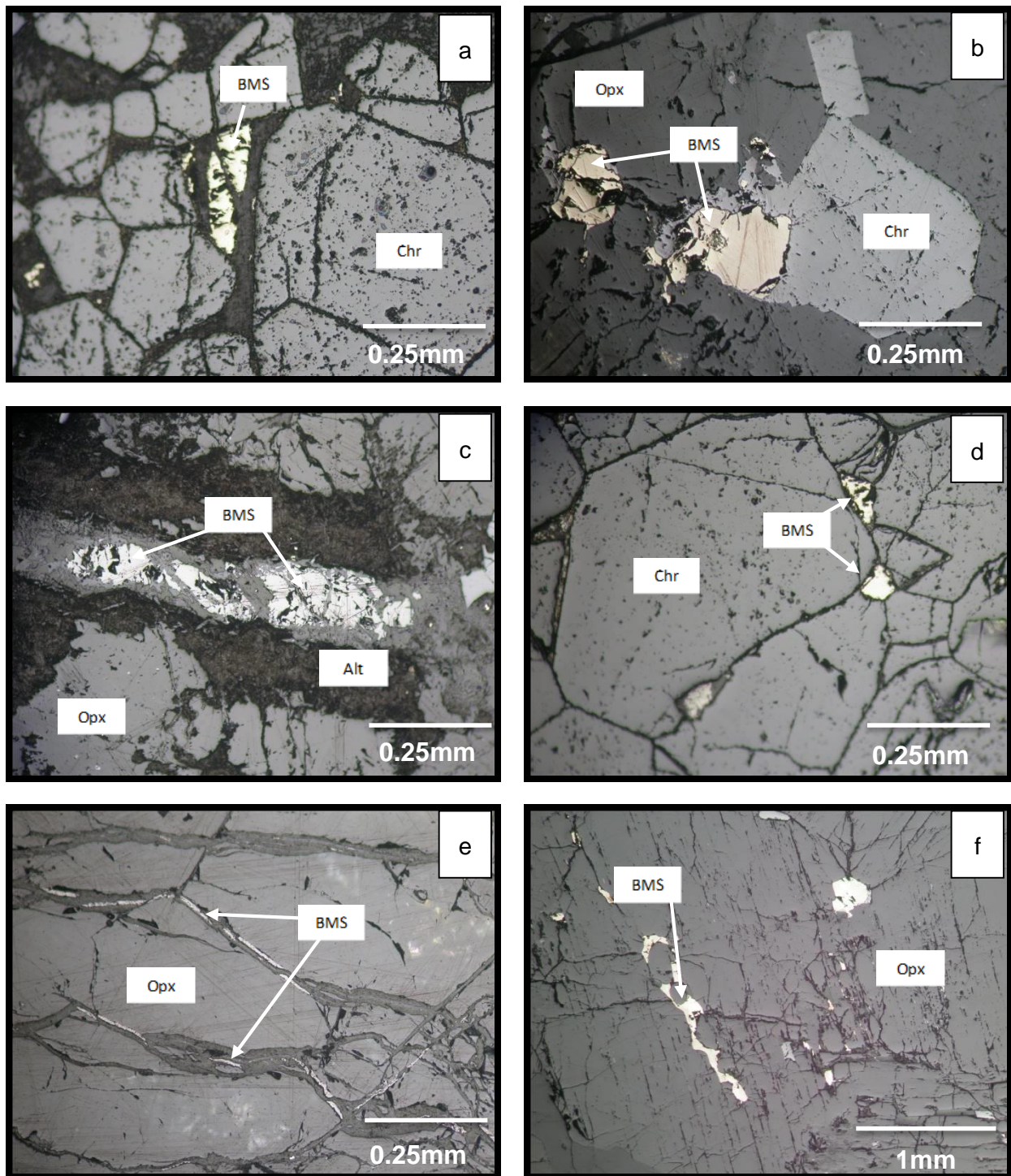
**Figure 30** - Examples of chromite mineral textures and associations throughout the Zondereinde mining unit. **(a)** compact, interlocking chromite grains with no interstitial silicate phase (Chr), **(b)** small, disseminated chromite grains associated with intense alteration of the primary interstitial silicate proportion (Chr (1)), **(c)** disseminated chromite with annealed grain boundaries (Chr (2)), **(d)** compact, interlocking chromite grains with varying grain sizes, BMS grains locked in at chr/chr interstices (Chr (1)), **(e)** disseminated chromite with a small grain size and partial annealing of grains which are in contact with each other (Chr (2)), **(f)** partial annealing of chromite grains with alteration phases affecting the outside boundaries of the grains (Chr (2)).

### 5.2.3. Sulphides

The sulphide mineral contents of the hanging wall units decrease upwards, with the greatest proportions of BMS occurring within the Harz unit. Within the Pyr (1) unit, sulphide mineralisation is observed as a fine dusting of small grains or accumulations of grains (<0.1 mm-0.5 mm) and filling fractures (Figs. 31c, e & f) which are often associated with hydrous alteration phases. The sulphide minerals are highly irregular in shape and are often found along or near chromite grain boundaries (Fig. 31a & b).

Within the main ore zone, sulphide minerals have a small grain size (<0.1-0.3 mm), are closely associated with chromite grains and may be fully enclosed by hydrous alteration phases (Fig. 31a) or near to alteration features (Fig. 31c). Where chromite grains exhibit a tightly packed interlocking structure, BMS grains occur locked in at the interstices between chromite grains (Fig. 31d). Grain shapes range from highly irregular to rounded, with grains taking on the shape of the spaces that they fill, especially in the case of BMS situated at chromite/chromite grain interstices (Fig. 31d). The Chr (1) unit has maximum sulphide concentrations at its base with decreasing contents towards the top of the unit. Sulphides within the Chr (2) unit are very small in size (<0.2 mm) and are low in abundance when compared to all other units throughout the mining cut. The footwall units contain minor BMS mineralisation relative to the above units (hanging wall and main ore zone sections). Where observed, they occur as a finely disseminated dusting of grains occurring on silicate mineral boundaries and locked within silicate grain boundaries (predominantly hydrous alteration phases).

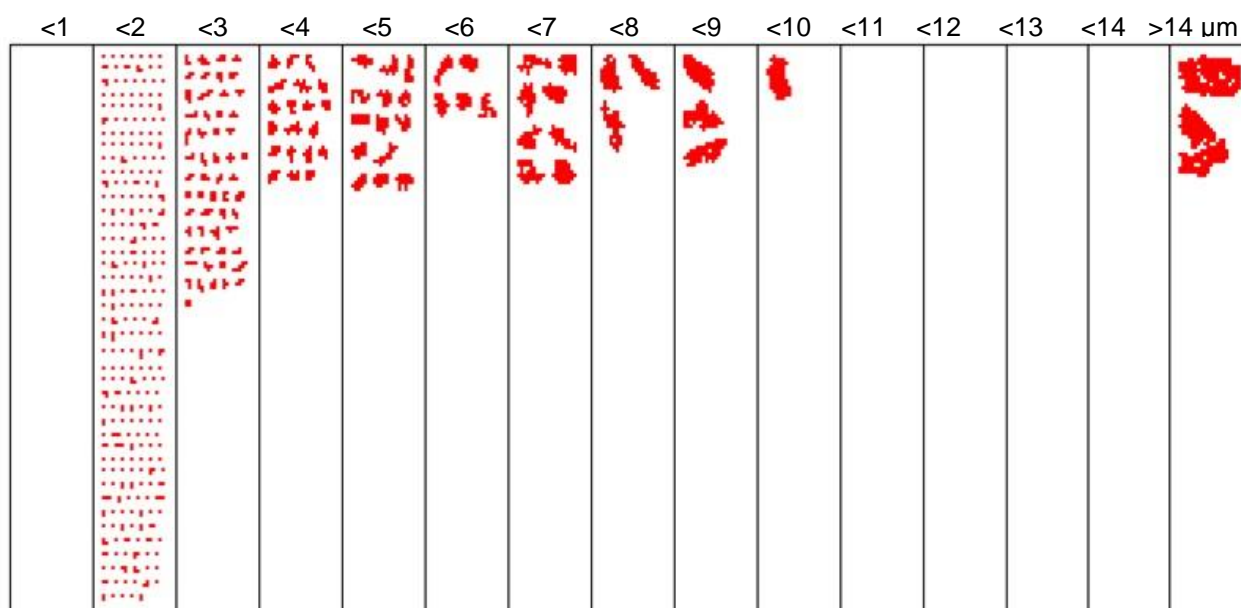




**Figure 31** - Examples of sulphide mineral textures and association throughout the height of the Zondereinde mining cut. **(a)** BMS grain situated within alteration phases at chr/chr grain boundaries, all phases exhibit a “pitting” texture on the surface of the grains (Chr (1)), **(b)** BMS in close association with the outside boundary of chromite (Pyr (1)), **(c)** BMS occurring within a slither of preserved primary silicate which has otherwise been intensely replaced by alteration minerals (Pyr (2)), **(d)** BMS grains locked between the interstices of compact, interlocking chromite grains. The chromite has been affected by alteration along the outside boundary of the grains and also exhibits a slight “pitting” texture on the surface of the grain (Chr), **(e)** BMS occurring as very thin, elongate shapes in vein-like textures of alteration minerals which have replaced primary interstitial plag (Pyr (1)), **(f)** BMS occurring as elongate grains which appear to have overprinted the primary silicate grains. Some BMS grains are enveloped by alteration minerals (Pyr (1)).

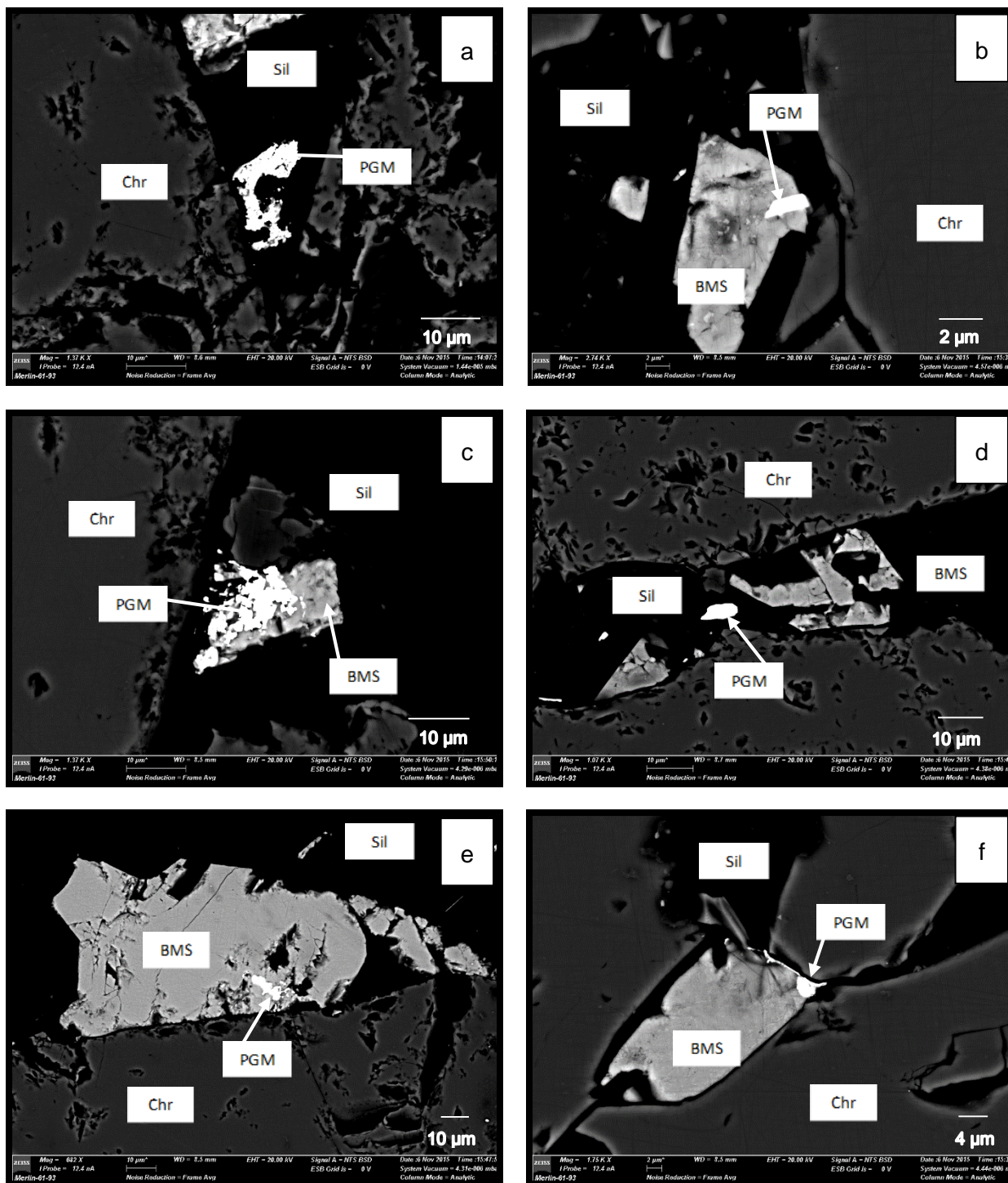
#### 5.2.4. PGM

A total of 384 PGM grains were identified during QEMSCAN analysis. The majority of PGM are  $<3\ \mu\text{m}$  in size (Fig. 32). The size fraction which contains the highest number of grains is the  $1\text{-}2\ \mu\text{m}$  category ( $\sim 70\%$ ) with a decreasing abundance of grains with increasing grain size. No grains were identified in the  $10\text{-}14\ \mu\text{m}$  size fractions, with only two grains identified which are larger than  $14\ \mu\text{m}$  in size. The “ $<1\ \mu\text{m}$ ” category is not populated as the resolution of analysis was set at a  $1\ \mu\text{m}$  pixel spacing meaning that some grains that are identified in the  $1\text{-}2\ \mu\text{m}$  fraction may in fact be smaller than  $1\ \mu\text{m}$ . Grains shapes are predominantly elongate (Figs. 33a, b & e) to sub-rounded (Fig. 33f). Irregularly shaped grains (Figs. 33a & c) make up a smaller portion of the total analysed PGM population.



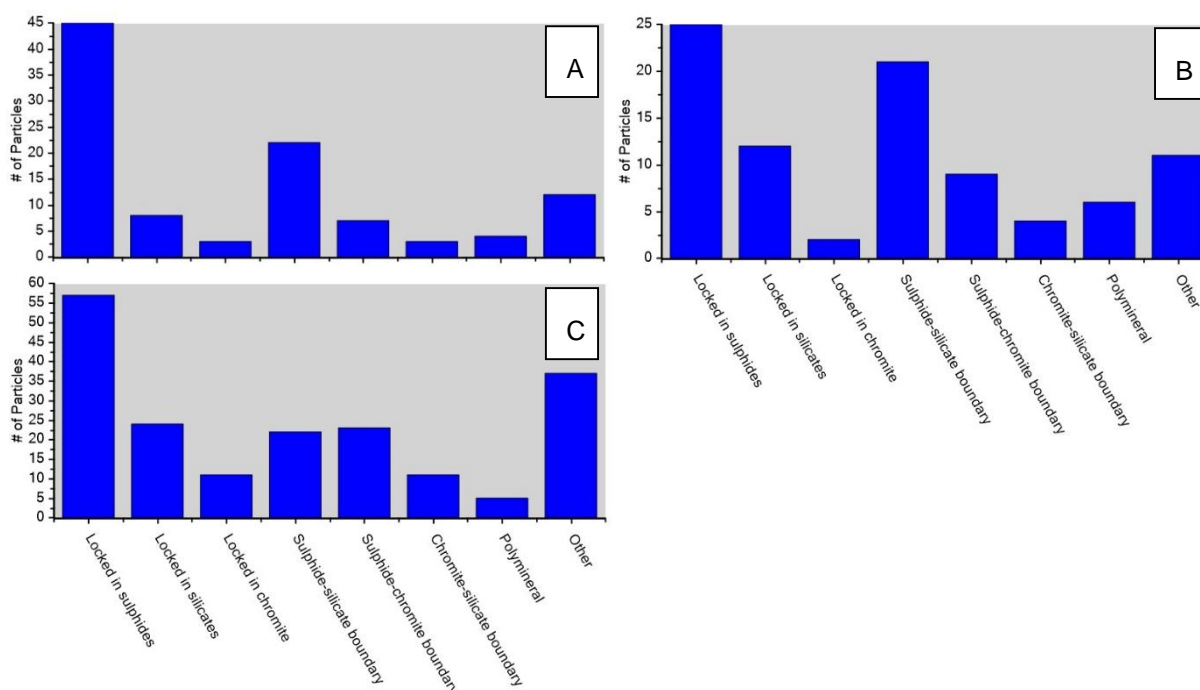
**Figure 32** - Grain size and shape distribution of PGM grains identified with QEMSCAN analysis ( $n=384$ ). Each PGM grain is displayed as a discrete red particle.





**Figure 33** - BSE images of selected PGM (bright white), chromite (dark grey), BMS (light grey) and silicates (black). **(a)** PtFe alloy near chromite boundary, **(b)** PtPb-sulphide with chalcopyrite, **(c)** PtFe alloy with Ni-sulphide, **(d)** Pt-sulphide with Ni-sulphide, **(e)** PdPb alloy with Ni-sulphide, **(f)** PtFe alloy with Ni-sulphide.

Although PGM are found to be associated, to varying degrees, with all minerals in the UG2 reef at Zondereinde (Fig. 34), the predominant mode of occurrence for PGM grains is locked within BMS grains (Figs. 33c & e). Other important associations include PGM occurring on BMS grain boundaries (Fig. 33b), associated with silicates (Fig. 33d), with “other” phases (i.e. calcite and rutile/sphene) and at the boundary between BMS and chromite grains (Fig. 33f). The specific proportions of the minerals which constitute the groupings ‘silicate’, ‘sulphide’ and ‘other’ as presented for the association of PGM in Figure 34 are defined in Table 9. Please consult Figure 43, Appendix A for a schematic breakdown of the mineral associations presented in Figure 34.

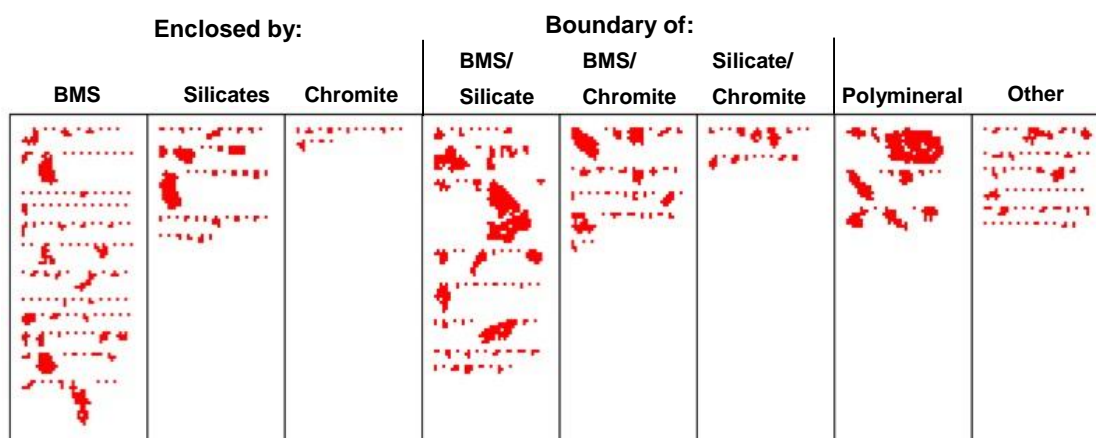


**Figure 34** – PGM association data from QEMSCAN analysis. A) Lower Chr (1) unit, B) upper Chr (2) unit and C) lower Chr (2) unit.

**Table 9** - Proportions of mineral phase constituting each phase grouping (silicate, sulphides and "other") illustrated in Figure 34 and 35 for PGM mode of occurrence.

Silicates	%	BMS	%	"Other"	%
		Cu-sulphides	43		
Feldspar	47	Ni-sulphides	42	Calcite	86
Orthopyroxene	41	Fe-sulphides	4	Ti-minerals (Rutile, Sphene)	12
Hydrous silicates	12	Bismuth phases	9		
		Silver	1		
		Pb phases	0.8		

The compiled statistics for PGM mode of occurrence, with grain size taken into account (Fig. 35), show that the most important association (i.e. largest PGM grain size and greatest proportion) is on the outside boundaries of BMS and silicate phases. Other important relationships include PGM which are contained within the grain boundaries of BMS and silicate phases, although many of these grains are small in size (1-2  $\mu\text{m}$ ), with a few exceptionally large grains (>5  $\mu\text{m}$ ). The association of PGM with "polyminerals" (i.e. BMS-silicate-chromite) boundaries is also important when considering the large size of these particular grains. Although some PGM are also associated with calcite and Ti-bearing phases (rutile and sphene), many of the grains are of a significantly smaller average grain size (<2  $\mu\text{m}$ ).

**Figure 35** - PGM association as a function of grain size for each category of association (Zondereinde). Each identified PGM grain is represented by a discrete red particle.



### 5.3. Mineral Chemistry and Relative Proportions

The mineral compositions of chromite, sulphide and PGM are described below. Individual mineral compositions were obtained from SEM whereas statistics on the various mineral groups (i.e. chromite, sulphide and PGM populations) were obtained from QEMSCAN. Hydrous silicates, sometimes referred to as ‘alteration minerals’, are dominated by chlorite and amphibole phases (Table 10).

**Table 10** - Proportions of hydrous silicate mineral contents of the Zondereinde samples (normalised to total alteration silicate contents).

Mineral	%
Chlorite (Clinochore)	48.10
Amphibole (Tremolite, Hornblende)	50.40
Mica (Muscovite, Biotite)	1.50

#### 5.3.1. Chromite

Chromite grains from each of the chromitite units (Chr, Chr (1) and Chr (2)) exhibit certain trends which make it possible to differentiate between the units (Fig. 36). Chromium contents decrease with stratigraphic height (from the bottom to the top of the main ore zone). Average  $\text{Cr}_2\text{O}_3$  values for chromite grains for each unit (in compound %) are Chr (2) = 45.55; Chr (1) = 44.81; Chr = 43.70 (Fig. 36a). Average  $\text{Al}^{3+}$  values display an opposite trend to chromium values, increasing from the bottom to the top of the main ore zone. Chromite from the Chr unit contains elevated  $\text{Fe}^{3+}$  contents relative to the Chr (1) and Chr (2) units (Figure 36b). Average  $\text{Fe}^{3+}$  values are highest within the Chr unit (6.38 %) compared to 5.62 % and 5.78 % for the Chr (1) and Chr (2) units, respectively. Although the spread of Mg# values is widespread across the chromitite units, the Chr (2) unit displays the maximum value (35.59) whilst the Chr (1) unit displays intermediate values and the Chr unit displays the minimum value (28.16). This trend, although weak, suggests decreasing Mg# values with increasing stratigraphic height (Fig. 36c).

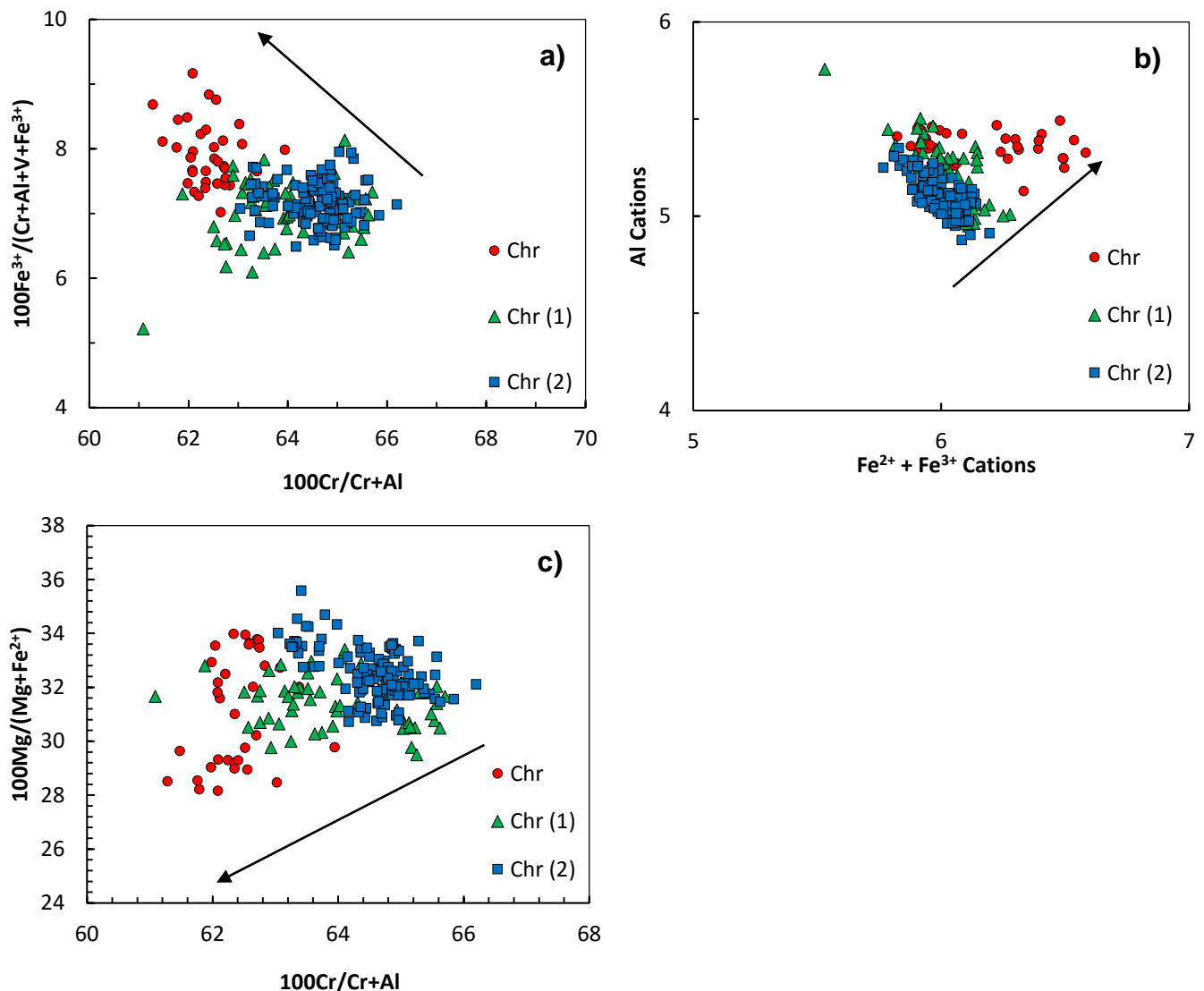


**Figure 36** – Chemical differentiation of individual chromite grains obtained from SEM analysis from Zondereinde.

### 5.3.2. Sulphides

Overall, the BMS budget is dominated by chalcopyrite (48 %) and pentlandite (47 %) (Fig. 37). Pentlandite, the major nickel-sulphide, is the dominant BMS within the lower Chr (1) and upper Chr (2) units (Figs. 37a & b). Chalcopyrite proportions increase substantially within the lower Chr (2) unit in comparison to the two overlying chromitite units (Fig. 37c). The terms chalcopyrite, pentlandite and pyrite are used to refer to all copper-, nickel- and iron-sulphides assemblages, respectively. Lead-, bismuth- and silver-bearing phases are also found in small proportions, relative to the total sulphide contents. Individual mineral compositions for common BMS and alloy minerals which were analysed within the chromitite units are reported in Table 11. These minerals

include chalcopyrite (Samples G & H), chalcocite (Sample D), pentlandite (Samples B, C, I & J), with lead occurring as either a sulphide (Sample F), an alloy with nickel (Sample A) or as native lead (Sample E).

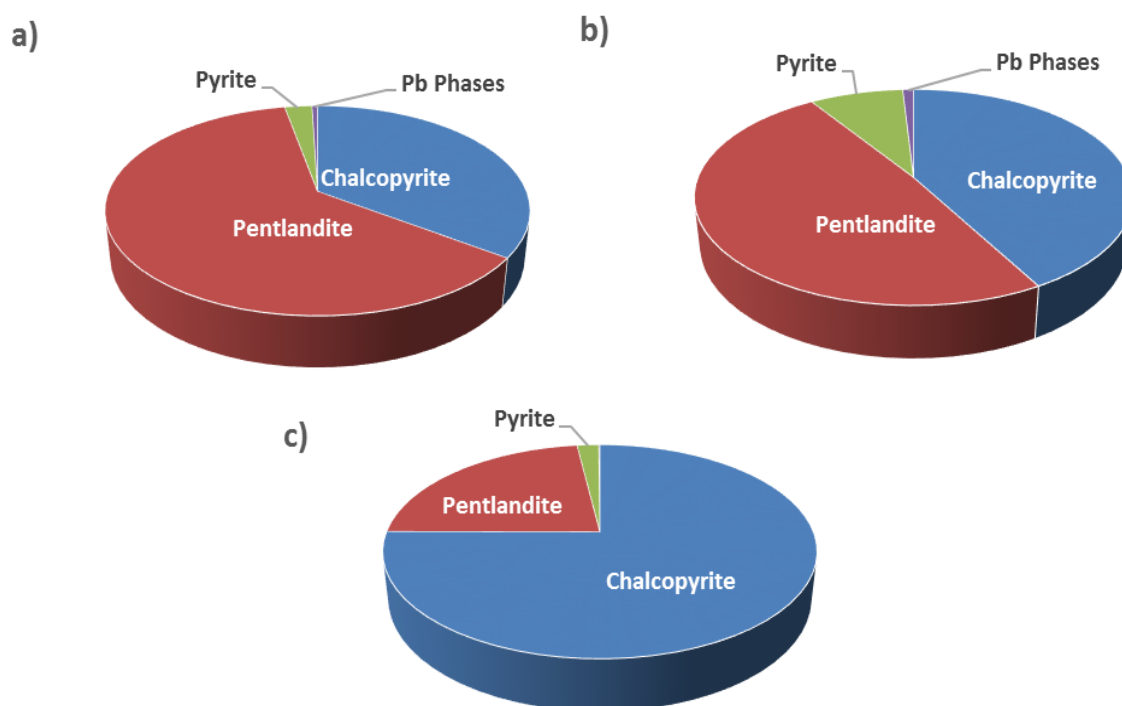


**Figure 37** – BMS split for each QEMSCAN sample; a) lower Chr (1) unit, b) upper and c) lower Chr (2) unit.

**Table 11** - Individual BMS and alloy mineral compositions from the Zondereinde samples.

Sample #	A	B	C	D	E	F	G	H	I	J
Unit	Chr	Chr	Chr	Chr (1)	Chr (2)	Chr (2)	Chr (2)	Chr (2)	Chr (2)	Chr (2)
<b>Ni</b>	24.97	39.07	37.66	3.26	0.52	0.56	0.67	1.26	33.67	35.29
<b>Fe</b>	0.87	26.93	28.31	4.13	0.99	9.79	30.36	29.00	30.88	26.75
<b>Cu</b>	-	-	-	70.28	-	4.04	34.02	35.21	-	-
<b>S</b>	-	33.38	34.22	23.12	-	13.09	35.63	34.82	34.70	38.15
<b>Pb</b>	74.72	-	-	-	98.78	71.83	-	-	-	-
<b>Total (wt. %)</b>	100.56	99.39	100.18	100.80	100.29	99.32	100.67	100.29	99.25	100.20

### 5.3.3. PGM

Typical mineral compositions of PGM that were analysed within the Zondereinde samples are presented in Table 12. These compositions range from ferroplatinum (Samples B, D, F & G) to PGE-sulphides ( $\pm$ Fe, Ni) (Samples A, & H) and PGE-alloys with lead (Samples C, E & I). Table 13 details some of the individual PGM that were analysed with SEM and describes the particular mode of occurrence for each analysis. Most of the PGM were found intimately associated with Ni-sulphide grains (~65 %). BMS which were found in association with PGM had an overwhelming relationship with chromite grains (~95 %), often occurring with chromite grains either locked between two or more grains, on the outer grain boundary or occurring near a chromite grain. A vast majority of the PGM were also found to be closely associated with hydrous silicate alteration (~70 %) which often surround the BMS grains or form a thin coating around the outer edge of chromite grain boundaries.

**Table 12** - Individual mineral compositions for PGM identified with SEM analysis.

Sample #	A	B	C	D	E	F	G	H	I
Unit	Chr (1)	Chr (1)	Chr (1)	Chr (1)	Chr (1)	Chr (2)	Chr (2)	Chr (2)	Chr (2)
<b>Pt</b>	61.62	87.77	4.93	87.20	-	89.73	86.08	-	-
<b>Pd</b>	-	2.21	58.27	-	-	-	2.26	-	45.71
<b>Rh</b>	-	-	-	-	1.58	-	-	-	-
<b>Ru</b>	-	-	-	-	-	-	-	55.96	-
<b>Ir</b>	-	-	-	-	-	-	-	-	-
<b>Pb</b>	-	-	37.50	-	96.26	-	-	-	30.68
<b>Cu</b>	-	-	-	-	-	-	0.88	-	-
<b>Ni</b>	10.43	-	-	1.10	-	-	0.80	-	9.05
<b>Fe</b>	15.24	10.41	-	10.73	2.06	10.87	10.80	2.65	8.71
<b>S</b>	12.47	-	-	-	-	-	-	41.42	5.86
<b>Total (Wt. %)</b>	99.77	100.39	100.70	99.03	99.90	100.60	100.82	100.03	100.01

**Table 13** - Compiled statistics of PGM analysed during qualitative SEM analysis including the mode of occurrence for the identified mineral. The presence of any alteration phases is also reported. The list is sorted by unit starting from the top of the main ore zone.

Type	Unit	BMS Host	BMS Occurrence	Gangue/Host	Alteration Present
Pd,Pb Alloy	Chr	Ni-Sulphide	Chr/Chr	Chromite	Yes
Pt,Pd,Fe,Ni,Cu Alloy	Chr	Ni-Sulphide	Chr/Chr	Chromite	Yes
Pd,Pb Alloy	Chr (1)	Ni-Sulphide	Chr/Chr	Chromite	Yes
Pd,Pb Alloy	Chr (1)	Ni-Sulphide	Chr/Sil	Chromite	Yes
Pd,Pt,Pb Alloy	Chr (1)	with Silicate	-	Silicate	Yes
Pd,Pt,Pb Alloy	Chr (1)	Ni-Sulphide	Chr/Chr	Chromite	Yes
Pd,Pt,Pb,Fe Alloy	Chr (1)	Ni-Sulphide	Chr/Chr	Chromite	Yes
Pd,Pt,Pb,Fe,Ni Alloy	Chr (1)	Ni-Sulphide	Chr/Sil	Chromite	Yes
Pt,Pb,Cu,Fe Alloy	Chr (1)	Ni-Sulphide	Chr/Chr	Chromite	Yes
Pt,Fe Alloy	Chr (1)	Ni-Sulphide	Chr/Sil	Chromite	Yes
Pt,Fe Alloy	Chr (1)	with Silicate	-	Silicate	Yes
Pt,Fe Alloy	Chr (1)	-	Chr/Sil	Chromite	No
Pt,Fe Alloy	Chr (1)	-	Chr/Sil	Chromite	No
Pt,Fe Alloy	Chr (1)	-	Chr/Sil	Chromite	No
Pt,Fe Alloy	Chr (1)	-	Chr/Sil	Chromite	Yes
Pt,Pd,Fe Alloy	Chr (1)	Ni-Sulphide	Chr/Sil	Chromite	Yes
Pt,Ni,Fe-S	Chr (1)	Ni-Sulphide	Near Chromite	Chromite	No
Pt,Ni,Fe-S	Chr (1)	Ni-Sulphide	Chr/Chr	Chromite	Yes
Pt,Ni,Fe-S	Chr (1)	-	Chr/Sil	Chromite	No
Pt,Rh,Ni,Fe-S	Chr (1)	-	-	Chromite	No
Pt,Cu,Fe-S	Chr (1)	Ni-Sulphide	Chr/Chr	Chromite	Yes
Pd,Pb,Ni,Fe-S	Chr (1)	Ni-Sulphide	Chr/Chr	Chromite	Yes
Pd,Pb,Ni,Fe-S	Chr (1)	Ni-Sulphide	Chr/Chr	Chromite	Yes
Pd,Bi-Te	Chr (1)	Ni-Sulphide	Chr/Sil	Chromite	Yes
Pt,Pd,Fe,Bi-Te	Chr (1)	-	Chr/Sil	Chromite	No
Ru,Ir,Os,Y,Fe-S	Chr (1)	Ni-Sulphide	Chr/Sil	Chromite	Yes
Pd,Pb Alloy	Chr (2)	Ni-Sulphide	Chr/Chr	Chromite	No
Pd,Pt,Pb,Fe Alloy	Chr (2)	Ni-Sulphide	Chr/Chr	Chromite	Yes
Pd,Pt,Pb,Fe Alloy	Chr (2)	Ni-Sulphide	Chr/Sil	Chromite	Yes
Pd,Pt,Pb,Fe,Ni Alloy	Chr (2)	Chalcopyrite	Chr/Sil	Chromite	Yes
Pd,Pt,Pb,Fe,Ni Alloy	Chr (2)	Ni-Sulphide	Chr/Sil	Chromite	Yes
Pd,Pt,Pb,Fe,Ni Alloy	Chr (2)	Ni-Sulphide	Chr/Chr	Chromite	Yes
Pd,Pt,Pb,Fe,Ni,Hg Alloy	Chr (2)	Ni-Sulphide	Chr/Sil	Chromite	Yes
Pt,Fe Alloy	Chr (2)	Ni-Sulphide	Chr/Chr	Chromite	No
Pt,Fe Alloy	Chr (2)	Ni-Sulphide	Chr/Chr	Chromite	Yes
Pt,Fe Alloy	Chr (2)	Chalcopyrite	Chr/Sil	Chromite	Yes
Pt,Fe Alloy	Chr (2)	Chalcopyrite	Chr/Sil	Chromite	Yes
Pt,Fe Alloy	Chr (2)	-	Chr/Sil	Chromite	Yes
Pt,Fe Alloy	Chr (2)	Ni-Sulphide	Chr/Chr	Chromite	No
Pt,Pd,Fe,Ni Alloy	Chr (2)	Ni-Sulphide	Chr/Chr	Chromite	Yes
Pd,Pb,Ni,Fe-S	Chr (2)	Ni-Sulphide	Chr/Chr	Chromite	Yes
Ru,Ir,Fe-S	Chr (2)	Ni-Sulphide	Chr/Chr	Chromite	No
Ru,Ir,Y,Fe-S	Chr (2)	Ni-Sulphide	Chr/Chr	Chromite	Yes
Ru,Y-S	Chr (2)	-	Chr/Sil	Chromite	Yes
Rh,Ni,Fe-S	Chr (2)	-	Chr/Sil	Chromite	Yes

The PGM budget for samples from the Zondereinde chromitite units show a clear predominance for PGE-alloy, more specifically, ferroplatinum compositions (~53 % of all analysed PGM) which increase proportionately from the bottom to the top of the main ore zone (Fig. 38). PGE-sulphides are the second most abundant PGM species (~35 %). Gold contents and PGE-alloys, besides ferroplatinum, are elevated within the lower Chr (2) unit (Fig. 38c) relative to the other samples.

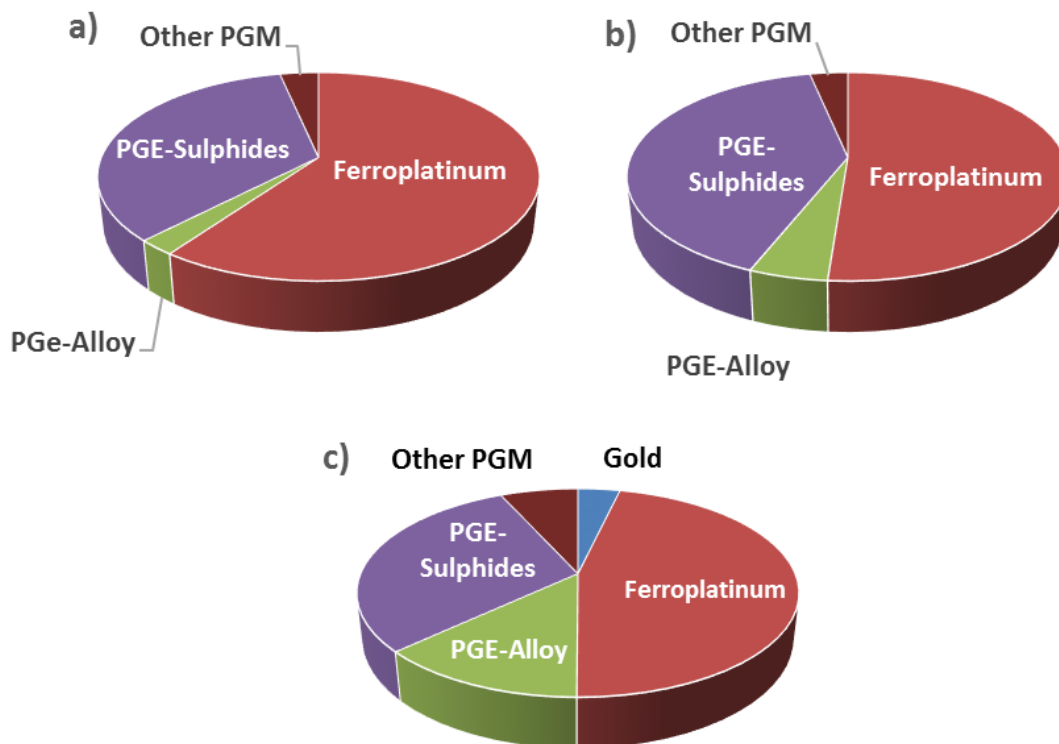
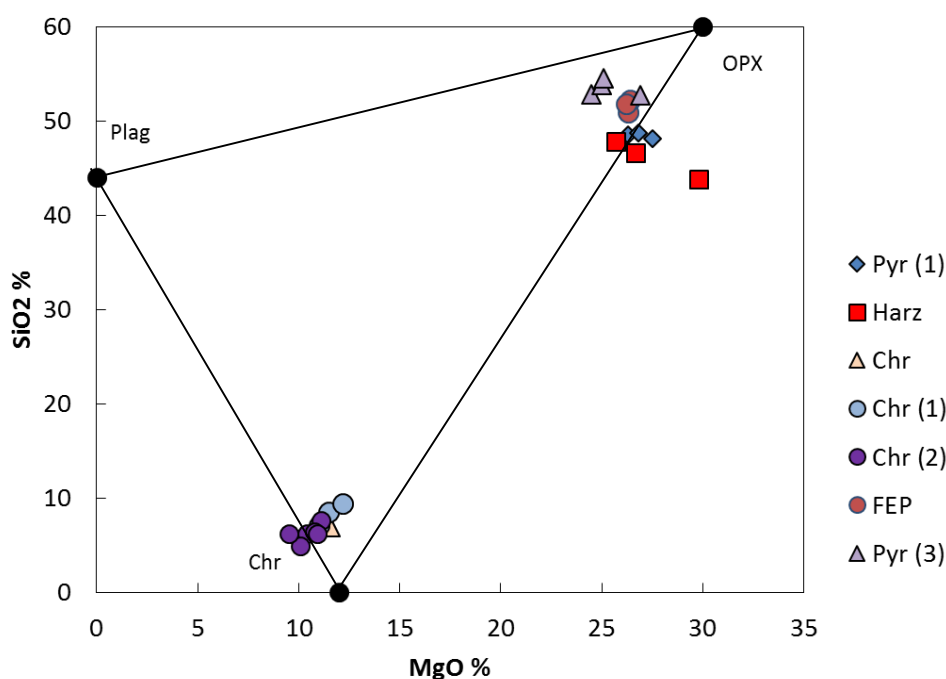


**Figure 38** – Relative abundance of various PGM identified during QEMSCAN analysis **a)** Unit: lower Chr (1) (n=104) **b)** Unit: upper Chr (2) (n=90) **c)** Unit: lower Chr (2) (n=190).

## 5.4. Bulk Rock Geochemistry

### 5.4.1. Differentiation between Mining Units

A whole rock SiO<sub>2</sub> % vs. MgO % plot illustrates the bulk mineralogy of the units (Fig. 39). The chromitite units plot near to chromite whilst the silicic units of the hanging and footwall display a dominant orthopyroxene assemblage. The Harz unit outlier plots towards an ideal forsterite composition (~57 % (MgO) & ~43 % (SiO<sub>2</sub>)), suggesting elevated olivine proportions. The particular data point is representative of the middle of the Harz unit. Figure 39 illustrates the similarity of the rock type between the hanging and footwall units. There also does not seem to be much variation within the chromitite units of the main ore zone. The Chr (2) plots towards plagioclase and not orthopyroxene suggesting that the silicic component of these units is plagioclase-dominated whereas the position of the Chr (1) unit data points suggest the highest proportion of orthopyroxene when compared to the other chromitite units.



#### 5.4.2. Stratigraphic Variation

Normalised 4PGE (Pt, Pd, Ru, Rh) values (Fig. 40a) are highest in the chromitite layers but also within the top section of the FEP unit immediately underlying the main ore zone. PGE grade values are normalised to the average PGE grade over the entire mining cut. The Chr (2) unit can be described as top- and bottom-loaded with the lowest concentrations at the centre of the Chr (2) unit. Both the hanging wall and footwall units contain low PGE grade relative to the main ore zone. Pt/Pd peaks are observed within the Chr unit (~3.8) and at the centre of the Chr (2) unit (~5.3). The Chr unit as well as the top and bottom sections of the Chr (2) unit have elevated 4PGE concentrations combined with higher than average Pt/Pd ratios (~3-4) (Fig. 40b).

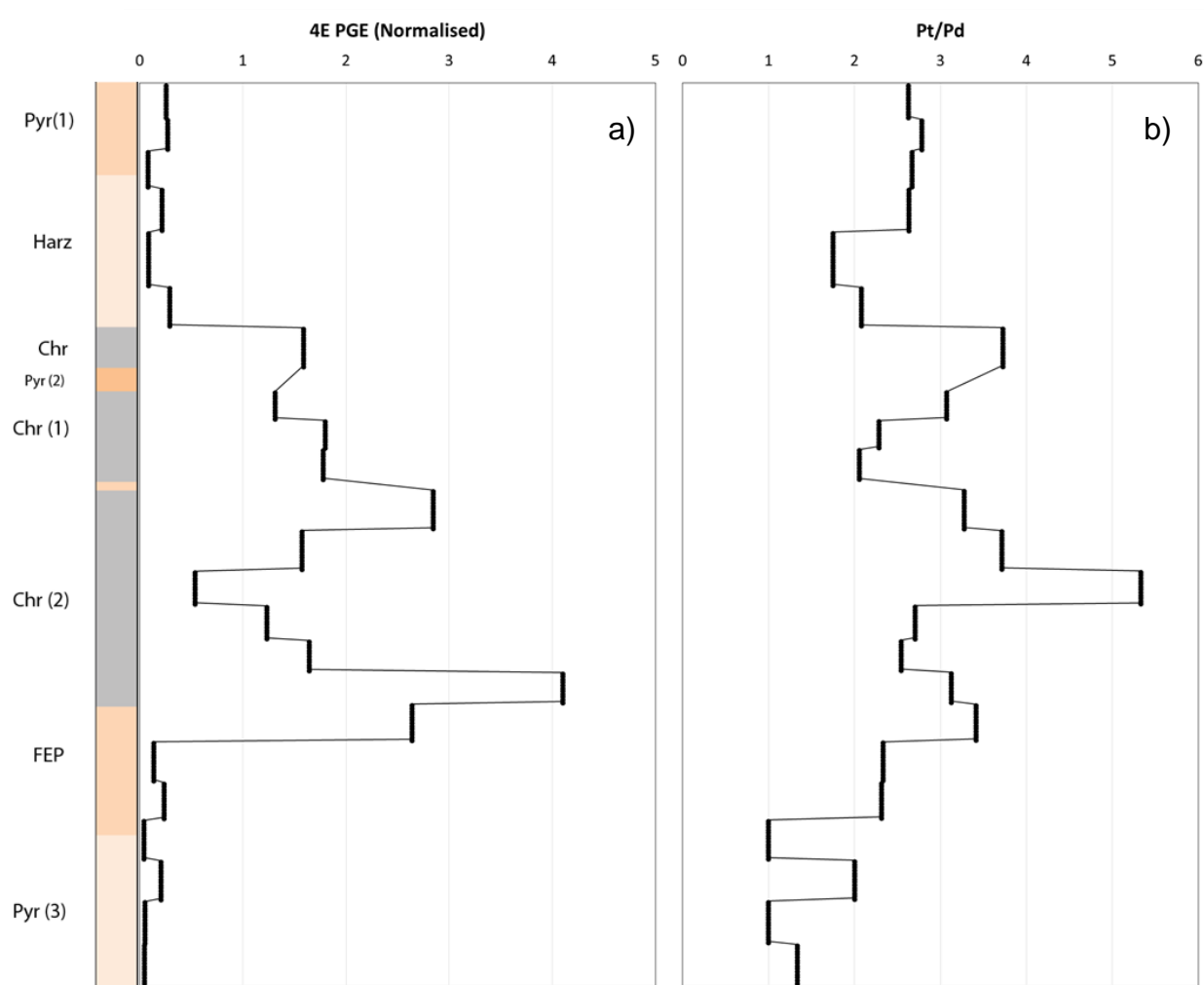


**Figure 40** - Geochemical assay values through the Zondereinde mining cut for a) 4PGE (normalised) and b) Pt/Pd.



Copper + nickel values, which serve as a proxy for sulphide mineral concentrations, are elevated within the lower Harz unit (~1200 ppm). Overall, copper and nickel values exhibit a downward decreasing trend in the mining cut (Fig. 41a). Other high values are recorded within both of the hanging wall units (>600 ppm), within the lower half of Chr (1) unit (~600 ppm) and in the section immediately underlying the main ore zone (~500 ppm). The Cu/Ni ratio is lowest within the hanging wall units (<0.1) and is relatively constant at between 0.2-0.4 within the main ore zone and footwall units. A large 'spike' in this ratio is recorded within the FEP unit (>0.8), just below the main ore zone (Fig. 41b). This area corresponds with elevated 4PGE, Cu+Ni concentrations and Pt/Pd ratio.

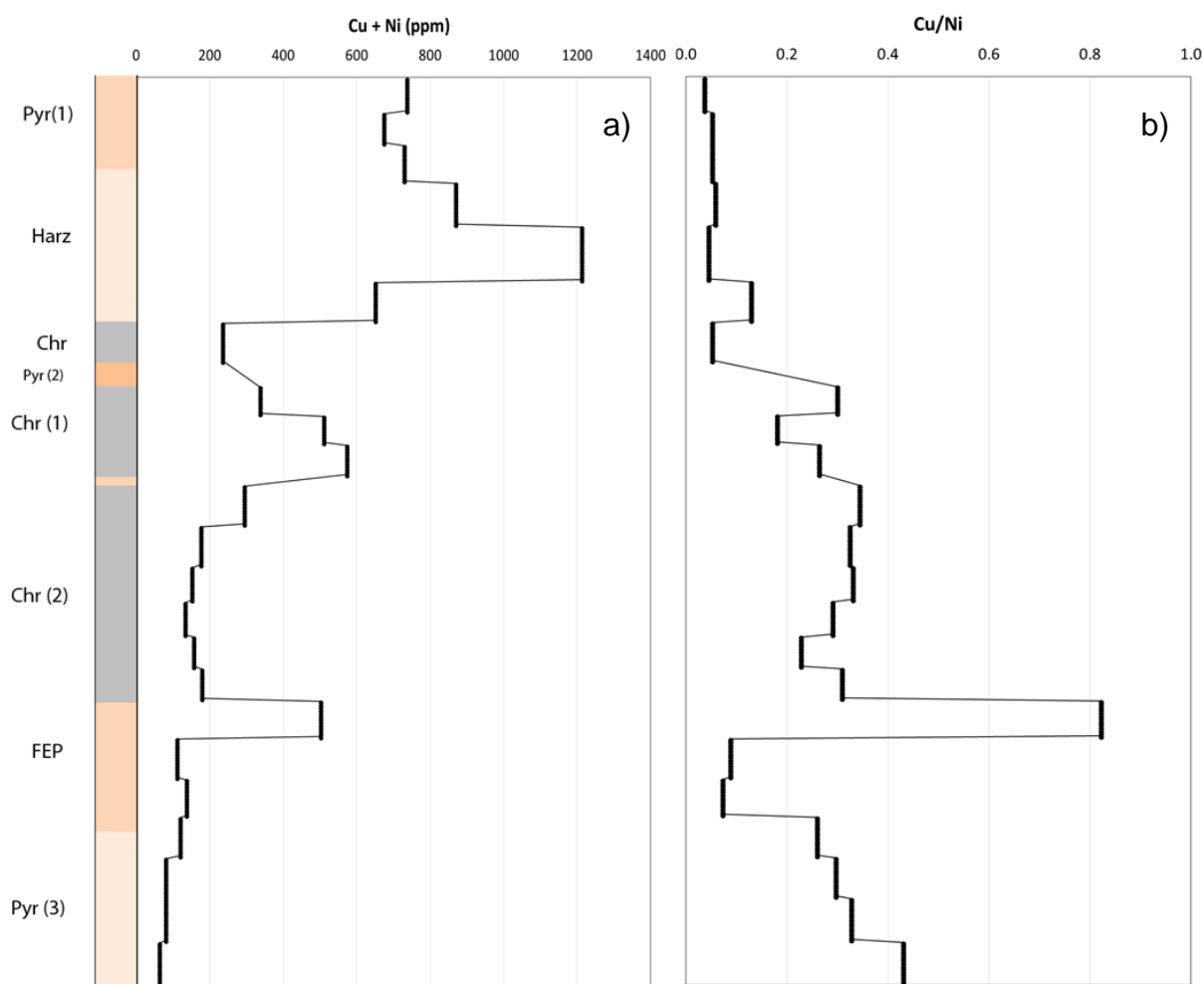


**Figure 41** - Geochemical assay values through the Zondereinde mining cut for a) Cu +Ni (ppm) and b) Cu/Ni.

The bulk rock Mg# (defined as the cation ratio (Mg/Mg+Fe)) throughout the main ore zone exhibits a slightly increasing trend from the bottom to the top. The hanging wall section exhibits constant values (~0.68) whilst the footwall section exhibits a slightly decreasing trend from the bottom to the top (Fig. 42a). Cr<sub>2</sub>O<sub>3</sub> concentrations are relatively consistent throughout the chromitite units, ranging between 36-40 % (Fig. 42b). The Chr (1) unit exhibits a weakly increasing trend whilst the Chr (2) unit exhibits a weakly decreasing trend, from the bottom to the top of the respective units.

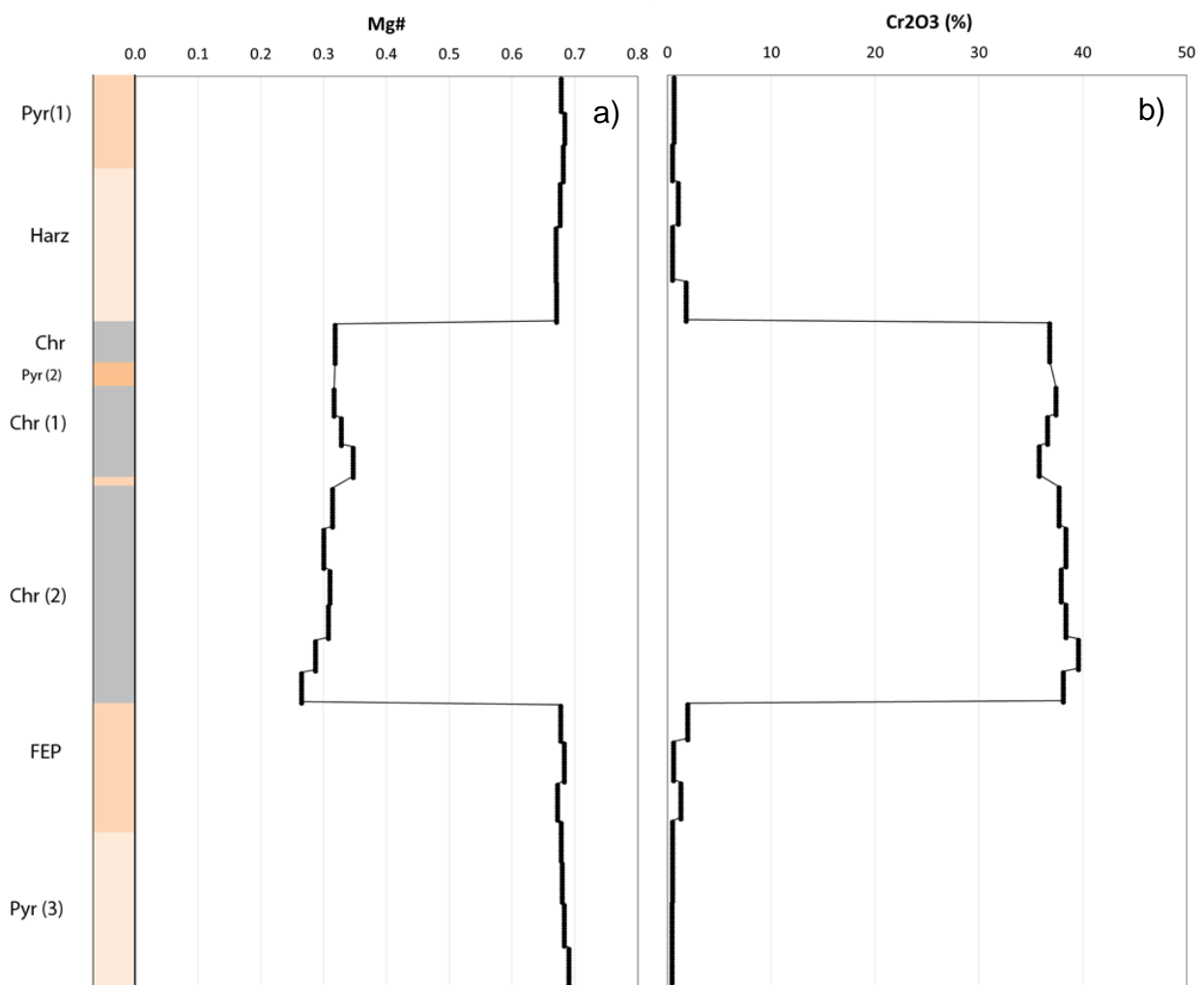


**Figure 42** - Geochemical assay values through the Zondereinde mining cut for a) Mg# and b) Cr<sub>2</sub>O<sub>3</sub> (%).

## 5.5. 3-D $\mu$ XCT Analysis

Samples were scanned with a particular focus on the distribution and grain size characteristics of PGM and chromite minerals through the main ore bearing units (Chr, Chr (1) and Chr (2)). Due to the inability of 3-D  $\mu$ XCT to obtain any compositional data, the phases referred to as PGM in this section are representative of the highest density fraction within the samples. This assumption is reinforced by the QEMSCAN results which show minor amounts of high density minerals that are not either PGM or minerals associated with the PGM contents.

### 5.5.1. *Chromite Texture and 3-D Distribution of PGM*

Figures 43 and 44 represents images of the lower section of the Chr and Chr (1) units, both of which exhibit dense, compact chromite textures. The distribution of PGM within the analysed sections is heterogeneous (Figs. 43 & 44). PGM tend to be disseminated throughout areas which exhibit dense, compacted chromite textures (Figs. 43 & 44). Chromite textures within Figures 43 & 44 show dense packages of compacted chromite which contain pockets of less dense, disseminated chromite grain textures (~3 mm in height). These pockets of low chromite contents show a paucity of PGM grains when compared to the dense chromite sections. Refer to Figure plate 53, which present 2-D images as snapshot views of chromite texture from the top to the bottom of the main ore zone chromitites.

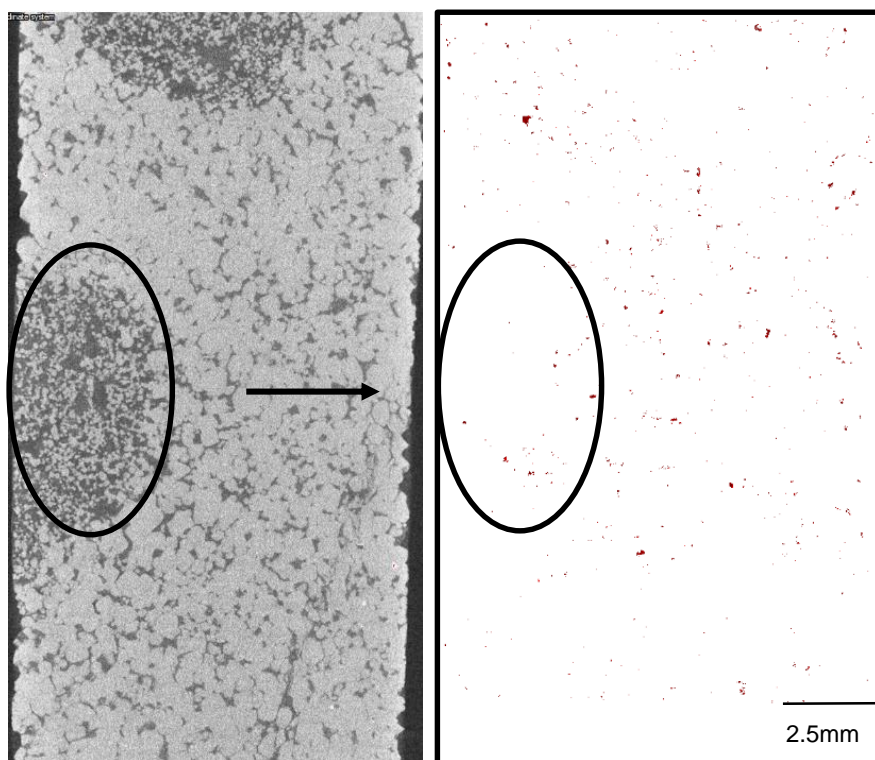


**Figure 43** – 2-D slice image of chromite texture (left) juxtaposed with 3-D PGM distribution (right) (red dots) of the same field of view. XCT 6 (lower Chr (1)), the highlighted areas show sections with a disseminated chromite texture correlating with a paucity of PGM content in comparison to the rest of the sample.

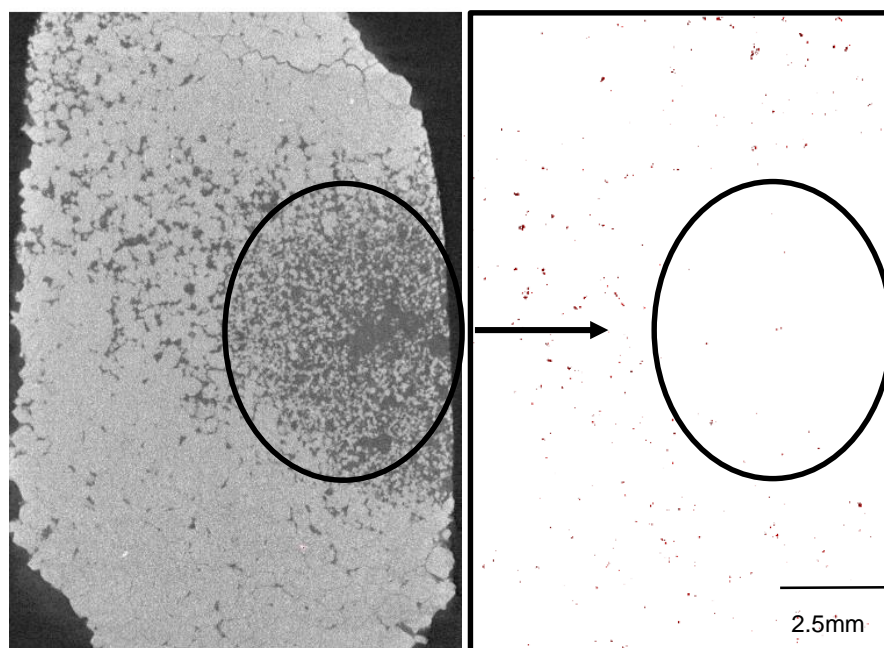


**Figure 44** - 2-D slice image of chromite texture (left) juxtaposed with 3-D PGM distribution (right) (red dots) of the same field of view. XCT 2 (lower Chr), the highlighted areas show sections with a disseminated chromite texture correlating with a paucity of PGM content in comparison to the rest of the sample.

### 5.5.2. PGM Grain Size Characteristics

3D grain size statistics show that most PGM (~50 %) are within the 40-59  $\mu\text{m}$  size fraction (Fig. 45). This trend changes slightly within the 'XCT 4' sample, representative of the upper to mid Chr (1) unit. This section contains a higher proportion of PGM which are in the 20-39  $\mu\text{m}$  size fraction. Overall, as grain size increases the proportion of PGM decreases with only 10-20 % of PGM occurring as grains larger than 80  $\mu\text{m}$  in diameter. The voxel resolution of 10  $\mu\text{m}$  allows for a realistic determination of discrete PGM grains with a lower size of limit of 20  $\mu\text{m}$ . Grain size is reported as equivalent spherical diameter (ESD) which differs from conventional equivalent circle diameter (ECD) used for 2D petrographic descriptions.

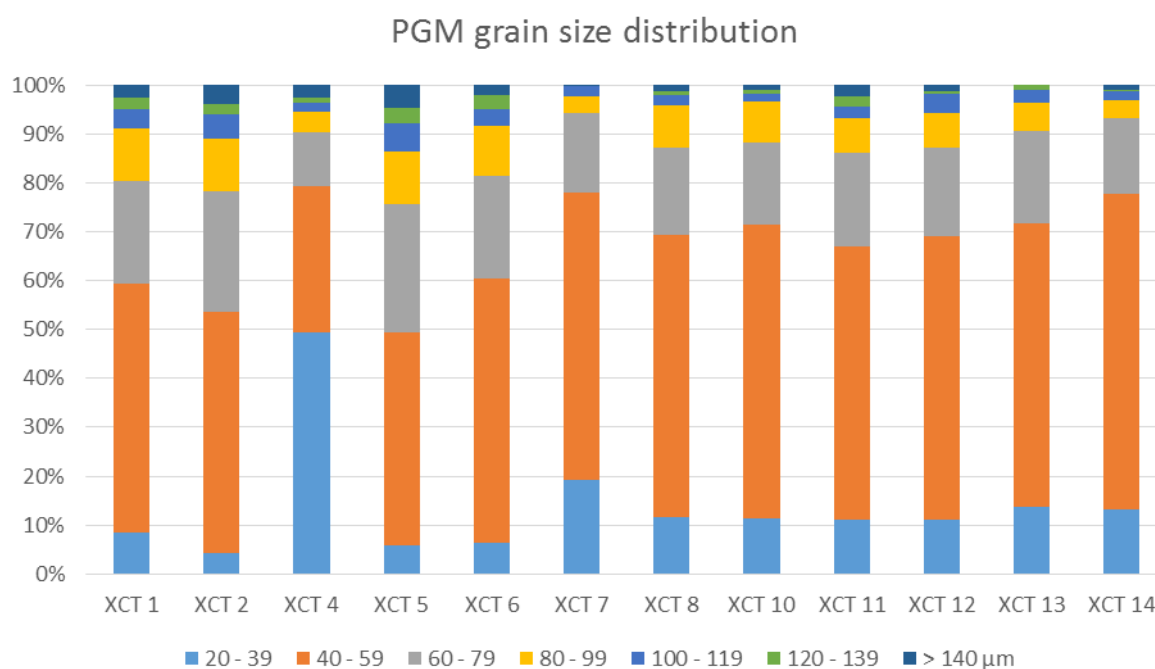


**Figure 45** - Grain size (ESD) distribution of dense mineral phases attained from 3-D  $\mu\text{XCT}$  analysis (10  $\mu\text{m}$  voxel resolution) (Zondereinde).

\* ESD = diameter of a sphere that fully encloses the grain of interest.

## Chapter 6: DISCUSSION

This section will first summarize the most important characteristics of each UG2 mining cut followed by a broader discussion on the relationships between chromite, BMS and PGM. The characteristics of each UG2 reef will then be evaluated within the context of traditional PGM beneficiation techniques. Lastly, the validity of 2-D and 3-D analytical techniques will be discussed, highlighting possible advantages and shortcomings of each within the scope of this study.

### 6.1. Mineralogical and Textural Characterisation of UG2

#### 6.1.1. *Booyseendal*

The main ore zone is characterised by varying proportions of cumulate Fe-rich magnesio-chromite and enstatite, intercumulate anorthite, minor concentrations of BMS mineralisation (100-250 ppm) and hydrous silicate alteration minerals and trace amounts of PGE (3-10 ppm). Chromite grains show a chemical evolution of increasing Fe<sup>3+</sup> values from the bottom to the top of the main ore zone, combined with the lowest average Mg# and Al<sup>3+</sup> values in the UT2 unit (Fig. 17). Texturally, chromite grains occur either as small (0.1-0.3 mm), sub-rounded and disseminated grains, which often exhibit annealed grain boundaries, or as larger, compact, blocky and interlocking grains (0.3-1 mm). The latter texture is observed in greater proportion towards the bottom of the UM unit, but also occurs as 1-3 mm scale horizontal bands within the UT2 and UL units (Figure plate 53). Hydrous silicate alteration features, in the form of minerals such as chlorite, talc, illite, tremolite, serpentine, muscovite and biotite affect all mineral phases within the UG2 reef, with proportionate increases in sections with higher silicic contents. These mineral are predominantly observed as the replacement of orthopyroxene (sometimes complete) along cleavage planes, in cross cutting veins, as fine micron-scale coatings around chromite grains or fully enveloping BMS grains.

2-D QEMSCAN analysis reports that discrete PGM, which are mostly <3 µm in size (~90 %), preferentially associate themselves with BMS, apatite, rutile and sphene grains (Fig. 46). 3-D grain size data reports that (~50 %) of PGM are within the 40-59 µm size fraction. However, the validity of this statistic is uncertain and will be discussed in section 6.3. Sulphide mineral contents are highest within the UT2 unit (~250 ppm) and display an upward decreasing trend within the UL and UM units. The sulphide

budget is dominated by millerite (48 %) and chalcopyrite compositions (39 %) (Fig. 47a). Sulphide mineralisation often occurs as aggregates of two or more BMS which are <0.1-0.4 mm in size. PGE grade is elevated within all three of the chromitite units, but show significant 'spikes' within the lower section of the UL unit as well as at the top and bottom of the UM unit. The PGM budget of the Booyensdal UG2 reef is characterised by high proportions of PGE-sulphide (54 %) and ferroplatinum (28 %) compositions (Fig. 47b).

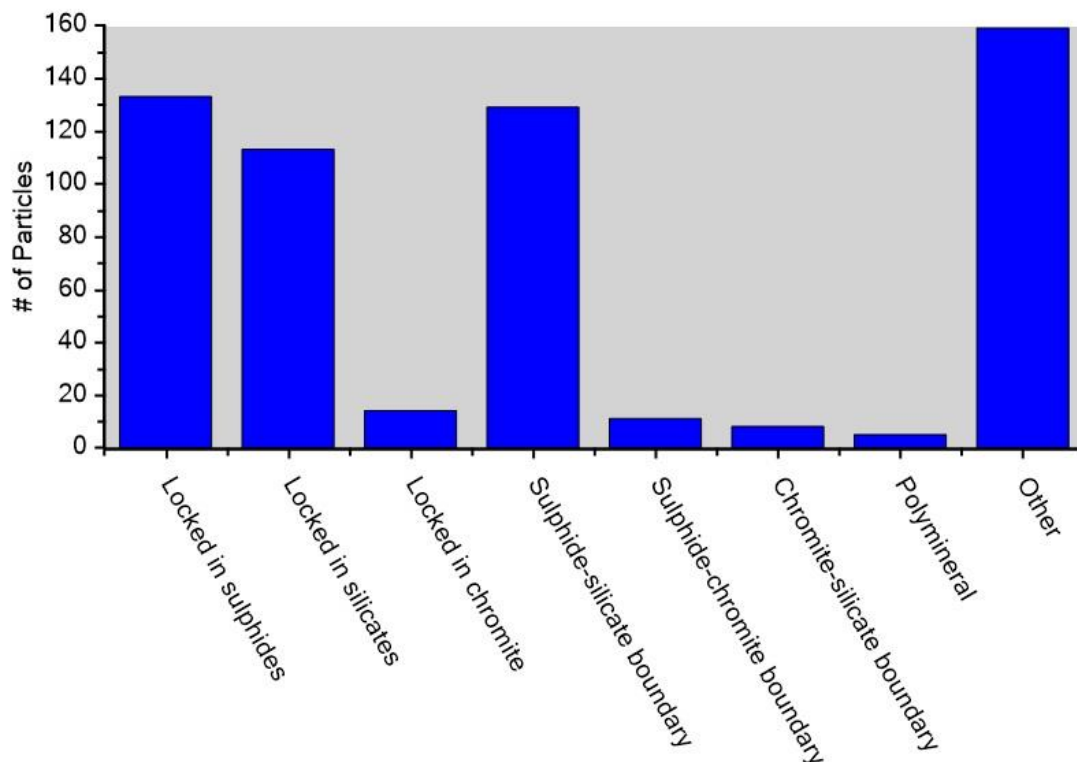


**Figure 46** – Compiled PGM mode of occurrence data as determined via QEMSCAN from the chromitite units (UT2, UL and UM) of the main ore zone from the Booyensdal UG2 reef (n=610).

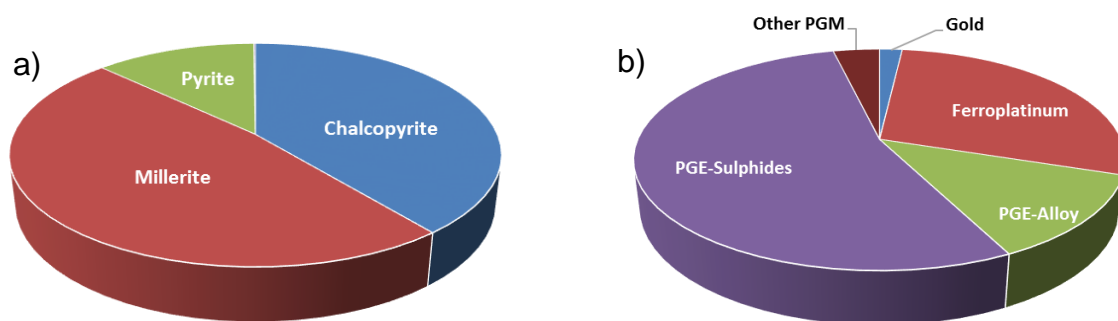


**Figure 47** – Relative modal abundances of the a) BMS and b) PGM budget (n=610) of the Booyensdal UG2 reef as determined with QEMSCAN analysis of the chromitite units from the main ore zone.



The UL and UM units are juxtaposed (Fig. 8), making the clear delineation of the contact between the two units difficult, especially with conventional petrographic techniques. This is due to no observable mineralogical changes at the current unit boundaries. However, the contact may be further interrogated based on variations in bulk geochemical indicators. PGE grade shows a large peak in the section just above the current contact between the UL and the UM units and an abrupt decrease at the top of the UM unit. Copper and nickel contents, which are used as a proxy for sulphide mineral concentrations, increase steadily towards the bottom of the UL unit and decrease abruptly at the top of the UM unit. Cu/Ni values exhibit an overall downward decreasing trend throughout the UL unit whereas at the current transition to the UM unit, the values start to increase and do so all the way into the FW rocks. Mg# remains relatively constant throughout the UL unit whereas a decreasing trend is recorded from the top to the bottom of the UM unit. Taking these geochemical trends into account, it suggests that the delineation of the UL/UM contact, which was indicated on original core logs by Northam Platinum was appropriately delineated.

#### 6.1.2. Zondereinde

The main ore zone is characterised by varying proportions of cumulate Fe-rich magnesio-chromite and enstatite, intercumulate anorthite, minor concentrations of BMS mineralisation (180-750 ppm) and hydrous silicate alteration minerals and trace amounts of PGE (2-13 ppm). Chromite shows a upward decreasing trend for Cr<sup>3+</sup> and Mg# values, whilst Al<sup>3+</sup> and Fe<sup>3+</sup> values increase across the chromitite units from the bottom of the Chr (2) to the top of the Chr unit (Fig. 36). For the most part, chromite grains (0.1-1 mm in size) occur with a compact texture within all of the of the chromitite units, with small mm-scale pockets of disseminated chromite occurring in lower proportions within the upper halves of each chromitite unit (Figure plate 53). Annealed grain boundaries are common with the smaller (0.1-0.3 mm), sub-rounded grain size fraction whilst the larger size fractions (>0.5 mm) tend to form blocky and euhedral habits.

Hydrous silicate alteration features, in the form of minerals such as talc, antigorite, clinochrysotile, tremolite and muscovite, affect all mineral phases within the UG2 reef, with proportionate increases in sections with higher silicic contents. These minerals are predominantly observed as the replacement of orthopyroxene (sometimes

complete) along cleavage planes and in cross cutting veins, as fine micron-scale coatings around chromite grains and fully enveloping BMS grains. Sulphide mineral contents which are highest within the hanging wall section (>600 ppm) display an upward decreasing trend, but also show elevated values (>300 ppm) in the Chr (1) unit and in uppermost section of the FEP unit (~500 ppm). The sulphide budget which often occurs as aggregates of two or more BMS grains (<0.1-0.5 mm) is dominated by pentlandite and chalcopyrite minerals in nearly equal proportions (47 % and 48 % respectively) (Fig. 48a).

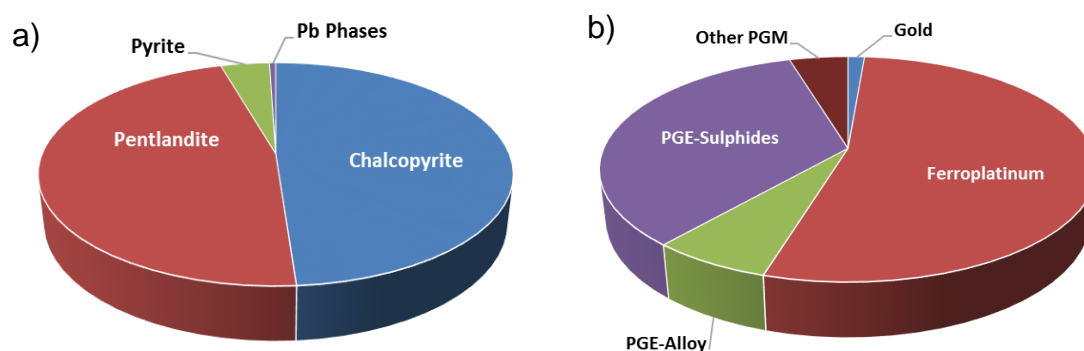


**Figure 47** – Relative modal abundances of the a) BMS and b) PGM budget ( $n=384$ ) of the Zondereinde UG2 reef as determined with QEMSCAN analysis of the chromitite units from the main ore zone

PGE grades are elevated within all three of the chromitite units, but shows the highest values at the top and bottom sections of the Chr (2) unit (up to ~13 ppm). Discrete PGM are dominated by ferroplatinum (53 %) and PGE-sulphide (34 %) compositions (Fig. 48b) which form elongate or irregular grain shapes. 2-D QEMSCAN results report that ~70 % of the identified grains are within the 1-2  $\mu\text{m}$  fraction, with decreasing proportions as grain size increases and predominantly occur locked within, or at the grain boundaries of BMS (Fig. 49). 3-D  $\mu\text{XCT}$  data suggests that the majority of PGM are within the 40-59  $\mu\text{m}$  size fraction (50-60 %). Due to the uncertainty surrounding the validity of this characteristic, it will be interrogated further in section 6.5. below.

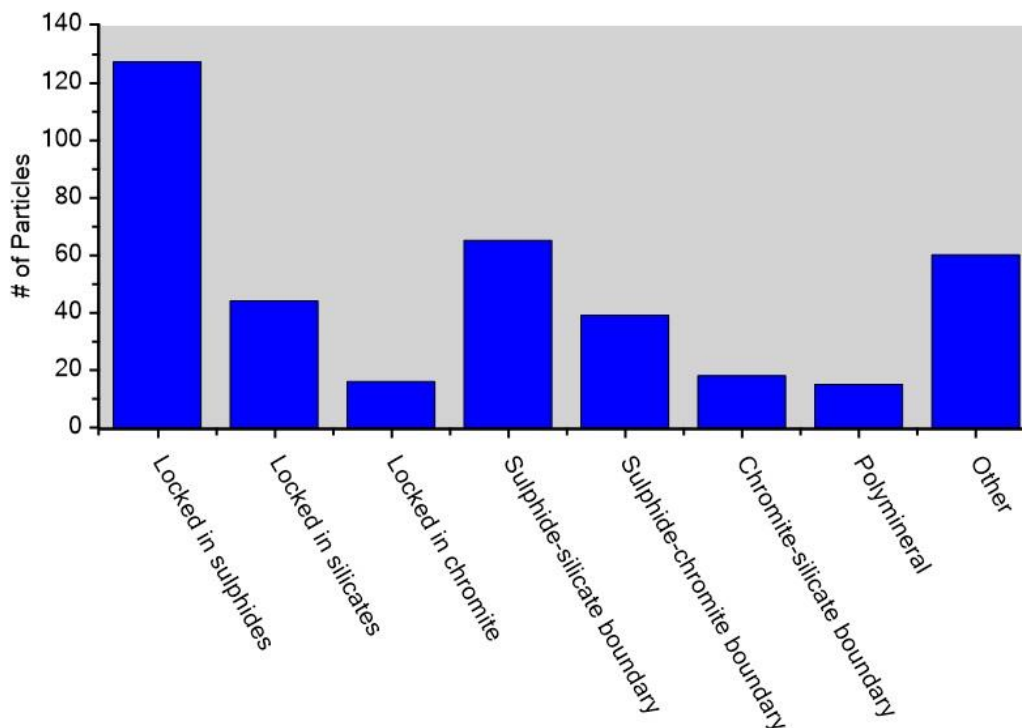


**Figure 48** – Compiled PGM mode of occurrence statistics as determined via QEMSCAN from the chromitite units (Chr, Chr (1), Chr (2)) of the main ore zone from the Zondereinde UG2 reef (n=384).

## 6.2. Relationship between Chromite, Sulphides and PGE Grade

There is an unequivocal textural relationship between PGM and BMS within the UG2 reefs from both locations. However, it is interesting to note that high Cu+Ni values (used as proxy for sulphide mineralisation concentration) do not correlate well with high PGE grade (Figs. 50a & b). In the context of each mining cut, the highest values of PGE grade within the Booyendal samples correlate with relatively intermediate to high Cu+Ni values (100-200 ppm) (Fig. 50a) whilst the highest PGE values within the Zondereinde samples correlate with intermediate to low Cu+Ni values (200-600 ppm) (Fig. 50b). The Zondereinde samples contain much higher proportions of Cu+Ni compared to the Booyendal samples (up to 1200 ppm in the Harz unit). However, the average and maximum PGE grades within the chromitite units is similar between the two locations with average concentrations for both locations ~4-10 ppm and maximum concentrations of 10 ppm (Booyendal) and ~13 ppm (Zondereinde). The close association of BMS with chromite often manifests in the coating of BMS grains around

the grain boundaries of chromite, a texture which may relate to the mechanisms of sulphide mineral emplacement.

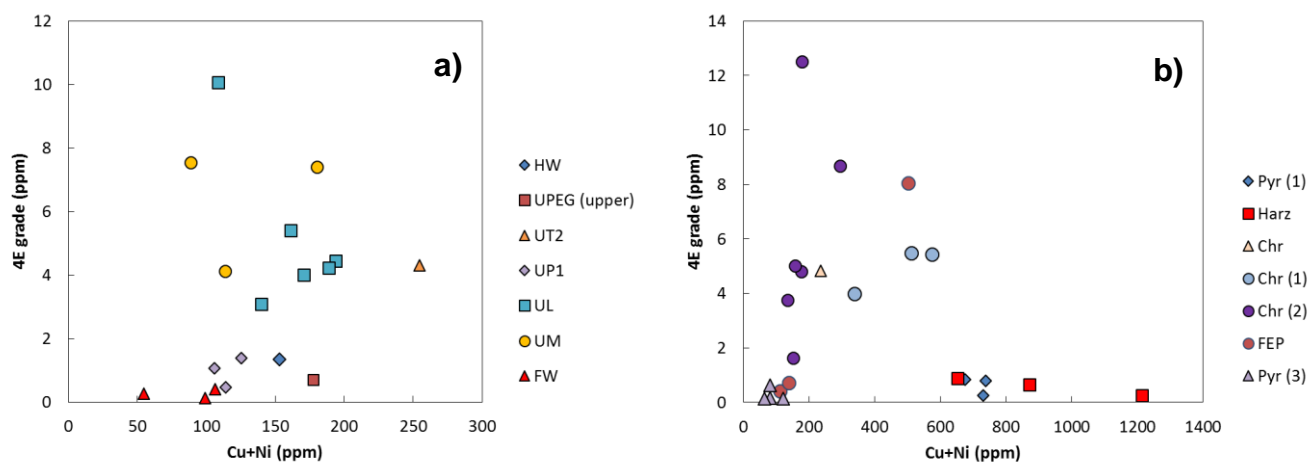


**Figure 49** – Bulk PGE grade vs. Cu + Ni content for a) Booyensdal and b) Zondereinde.

In the case of bulk chromite contents plotted against PGE grade (Fig. 51a and b), high proportions of chromite, as seen within the chromitite units from both locations, shows some degree of correlation with high proportions of PGE grade. The Booyensdal samples have the highest PGE contents within the UL and UM unit which range from 25 - 35 % ( $\text{Cr}_2\text{O}_3$ ) (Fig. 51a). The Zondereinde samples exhibit a clearer relationship between chromite content and PGE grade coupled with consistent  $\text{Cr}_2\text{O}_3$  concentrations (~40 %). The samples from the chromitite units of the main ore zone correlate with the highest PGE grades (Fig 51b). An interesting outlier exists for the FEP unit of the footwall section where although the unit is not considered a chromitite unit, it contains very high proportions of PGE (~8 ppm). It must be noted that upon petrographic investigation, the FEP unit of the Zondereinde UG2 contained anomalous proportions of chromite considering that it is not a chromitite unit whereas no chromite, nor any significant PGE grade, was recorded within the Booyensdal footwall section.

The strong association of PGE with BMS and that of BMS along the outside boundary of chromite suggests that whilst a sulphide liquid most likely played host to the PGE mineralisation, it was the chromitite layers which acted as a trap, concentrating PGE grade within the UG2 reef. This is supported by observations of the “coating” of BMS aggregates along the boundaries of chromite (Fig. 12b & e) and BMS grains often

inheriting the shape of the interstitial spaces they fill when locked between chromite grains (Fig. 31d & f). The overall distribution of PGE grade within the chromitite layers can be described as top- and bottom-loaded with decreasing proportions towards the centre of each chromitite layer. This distribution suggests that PGE mineralisation may have percolated from the layers above and below and into the chromitite layers during compaction of the RLS. This may have been due to the weight of the overlying crystal pile becoming greater when new batches of magma were emplaced above.

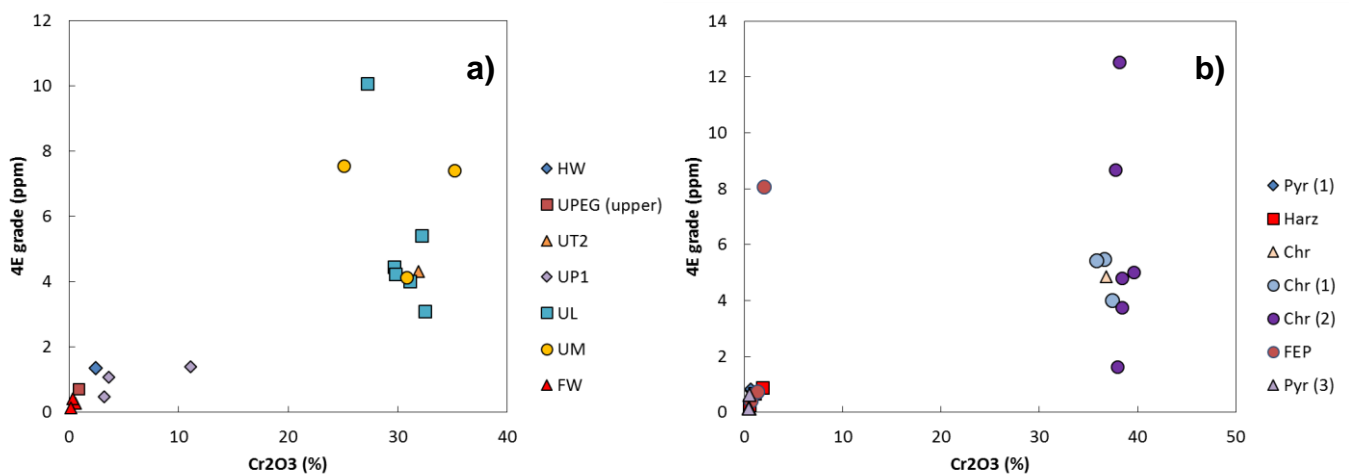


**Figure 50** – Bulk PGE grade vs. chromite contents for a) Booyensdal and b) Zondereinde.

Bulk mineralogy from XRD analysis of the Zondereinde samples did not identify plagioclase as a constituent of the chromitite layers. The lack of this intercumulate phase correlates well with the compact texture of chromite throughout the chromitite layers. The texture of chromite in the chromitite layers of the Booyensdal samples however, varies substantially from disseminated to compact in areas with concomitant variations in intercumulate silicate proportions (See Figure plate 53). The bulk textural differences of chromite from predominantly disseminated within the Booyensdal UG2 compared to the compact, interlocking texture within the Zondereinde UG2 reef may be directly related to the thickness of each locations main ore zone. The combined thicknesses of the three main chromitite units within the Booyensdal samples is 133 cm compared to the 119 cm of the Zondereinde samples. If the assumption is made that the UG2 reef at the two mines were initially of similar thicknesses, the Zondereinde UG2 reef may have undergone a significant degree of compaction in comparison to

the Booyendal UG2 reef. This hypothesis is complemented by the large disparity in the combined thicknesses of the pyroxenite partings which separate the chromitite units of each UG2 reefs main ore zone (Booyendal-63 cm vs. Zondereinde-11 cm). It is however unlikely that the UG2 reef thicknesses were the same considering the geographic distance which separates the two mines.

### **6.3. Two-Dimensional vs. Three-Dimensional Analysis**

The low concentration, small grain sizes and difficulty in detection in combination with issues of finding representative samples are typical problems encountered when dealing with a mineralogical investigation of this nature (Hofmeyr, 1998; Paktunc, 1990; Peyerl, 1983; and Wirth et al., 2013). In addition, the wide compositional variation, shape, size and associational characteristics present further complications to the metallurgist when it comes to plant design and optimization processes to maximise recovery of PGE. Producing pre-concentrates for mineralogical investigation has proven to be useful in order to build confidence in decision making. However, processing methods, such as milling, destroys the primary characteristics of an ore, which may prove to be vital in increasing knowledge of an ore and improve plant recoveries. This abovementioned reason was the motivation behind the study of in-situ UG2 reef samples and, in addition to this, the combination of 2-D and 3-D technologies to investigate any shortcomings of conventional 2-D petrographic techniques.

There are inherent stereological issues related to 2-D descriptions of PGM size and shape characteristics especially when one considers the highly irregular grain shapes of PGM. This can be mitigated by drawing on a large statistical databases from which to describe mineralogical characteristics. But to accomplish this one has to do substantial amounts of analysis which increases the cost of mineralogical investigations. The researcher needs to evaluate whether this is necessary by considering the cost/benefit ratio. Conventional 2-D techniques have proven themselves over time when it comes to determining mineral compositions and describing textures. The introduction of QEMSCAN has greatly enhanced the ability to gather large, reliable statistics which can be used when it comes to both setting up

and adjusting processing circuits to best suit a particular ore type. There are, however, certain associated limitations with 2-D techniques especially when it comes to describing the distribution, grain shapes and sizes of minerals. The quantification of mineral phase proportions in this study was accomplished via a TMS, with a field size of 500 x 500  $\mu\text{m}$ . While these statistics are very important in terms of describing the mode of occurrence of PGM grains, the technique suffers from a lack of data on the rest of the sample. Hence, descriptions of the mineralogy, other than that of PGM and closely associated minerals, may not be representative of the reef package as a whole.

The petrography of polished block mounts in conjunction with reflected light microscopy is not useful for describing the silicate mineralogy, therefore these descriptions are not in great detail. What was important to recognise was the extent and association of alteration phases and the texture of sulphide and chromite phases. Other silicates phases such as orthopyroxene and plagioclase were not selected for detailed compositional analysis. This was done so as to prioritise the characterisation of the minerals which are more important in terms of their known close association with PGM. However, it would have been nice to say more about the silicate fraction of these rocks if the scope of the project would have allowed for it. Mineralisation within the hanging and footwall lithologies is minor when compared to the chromitite units. This is coupled with the fact that the high proportions of silicates in these units contribute to the overall proportions of Mg-bearing minerals (orthopyroxene and olivine) and alteration phases such as talc and chlorite being processed in the flotation circuit, which is ultimately detrimental to plant efficiency.

The ability of 3-D  $\mu\text{XCT}$  to discriminate between individual PGM grains and describe their characteristics such as grain size and shape is weak due to inherent resolution restrictions which is intimately linked to sample size. This problem is exacerbated by the small average grain size of PGM within the UG2 reef. The voxel resolution of 10  $\mu\text{m}$  effectively means that PGM particles with grain sizes of  $>20 \mu\text{m}$  can be identified. Previous literature and the results of this study found that grain sizes of PGM are in fact much smaller than 20  $\mu\text{m}$  meaning that although 3-D  $\mu\text{XCT}$  can identify PGM grains within 3-D space, their grain size characteristics are grossly overestimated (due to partial volume effects) therefore many grains may be entirely overlooked. However, the technique does afford a good indication of the spatial distribution of the different



mineral groups, such as silicate, oxide/BMS and PGM within in 3-D space. The technique is particularly useful for determining the 3-D distribution and size information of chromite (Fig. 52). To compile the accurate descriptions of individual PGM, such as those from the UG2 reef, lengthy scan times (~3-4 hours) and small sample sizes (<5 mm<sup>2</sup>) are inherent limitations and even if this is done, the resulting voxel resolution will be ~5 µm, which may allow for more accurate imaging of the larger size fractions of the PGM population (>10 µm). 3-D µXCT has the ability to image larger sections of core than what is afforded with conventional microscopy techniques. This has given a better overall picture of the textural characteristics of the UG2 reef. The researcher needs to carefully decide on the outcomes of his/her study (i.e. is the required information compositional, textural or associational in nature) and evaluate which techniques will yield the best results with budget and time constraints taken into consideration. It is prudent to state that the combination of 2-D and 3-D techniques, such as in this study, has proven to be invaluable in terms of the characterisation of the UG2 reef as a whole due to each technique having advantages over the other.

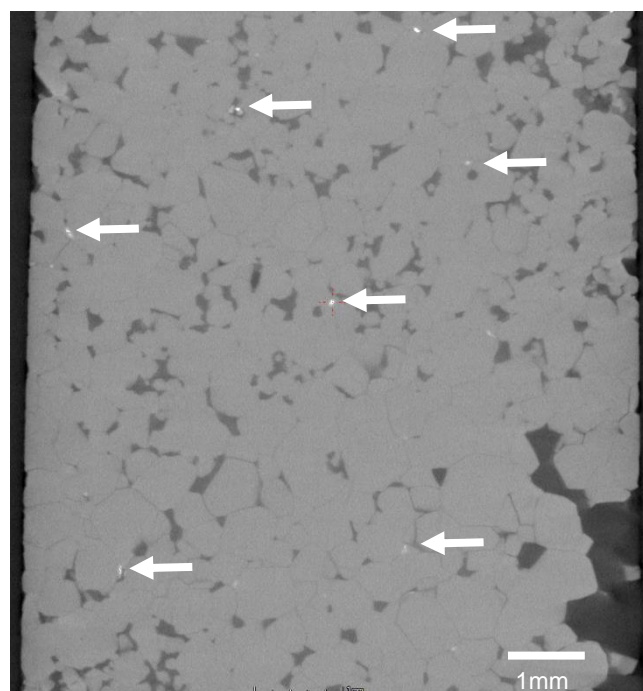


**Figure 51** – 2-D slice image from 3-D µXCT analysis of chromite (light grey) texture with interstitial PGM (bright white).

#### 6.4. Implications for PGM Beneficiation

Chromite texture will influence the grinding regime which ultimately aims to efficiently liberate BMS and PGM particles. The overall texture for chromite from the main ore zone at Zondereinde is dense and compact (refer to Figure plate 53). This suggests that a large amount of BMS and PGM will be locked in at the boundaries of chromite grains and as a result the liberation of these particles may be more difficult to achieve than those of the Booyendal UG2 reef where disseminated chromite textures are more common. With this being said, a grinding regime will most likely be implemented based on the predominant texture of an ore, which makes the consideration for the Booyendal UG2 more difficult due to the variation that is present throughout the height of the chromitite units.

Alteration features were observed in greater proportions within the siliceous hanging and footwall units and within the chromitite units where there are elevated intercumulate silicate phase contents. With the abovementioned differences in chromite textures taken into account, it is suggested that the Zondereinde UG2 chromite units might contribute less alteration mineral contents to the flotation cell than that of the Booyendal UG2. It is also recommended, due to lack of PGE grade and high proportions of gangue, that as little of the hanging and footwall units from both the Booyendal and Zondereinde UG2 reefs are included in the mining cut. The possible benefits include the decrease in waste rock being hauled to surface, increased PGE head grade, lower MgO contents within the flotation circuit and lower proportions of naturally floating gangue (talc and chlorite). This may all be possible without sacrificing PGE contents due to the well constrained nature of the PGE grade to the main ore zone section within both UG2 reef sample sets. However, it is important to state that the uppermost section of the FEP unit of the Zondereinde UG2 reef contains a high concentration of PGE and should not be excluded from the mining cut. The particular textural feature of naturally floatable hydrous alteration minerals occurring as thin micron-scale rims on the outer boundary of chromite grains is detrimental to beneficiation efficiency. This feature was observed throughout the main ore zones of both the Booyendal and Zondereinde UG2 reef and has the potential to increase the proportions of inadvertent chromite recovery. This increase in chromite is detrimental to flotation efficiency as well as smelting techniques and needs to be

accounted for by adjusting the reagent suite that is used during flotation (Becker et al., 2009).

The Booyendal samples are dominated by PGE-sulphide phases whereas the Zondereinde samples are dominated by ferroplatinum phases. Study of previous literature suggests that the presence of PGE-alloys (including ferroplatinum) may be the result of secondary processes suggesting that the Zondereinde UG2 reef has been subjected to post-magmatic modification of the reef. Taking composition and association into account, PGE-sulphides occurring with BMS from the Booyendal UG2 reef are more likely to be recovered first in comparison to the slower floating PGE-alloy dominated species of the Zondereinde UG2 reef. There was no observed difference in the size of PGM particles, with both locations having ~90 % of identified grains with a grain size of less than three microns. This characteristic has in the past and will continue to present problems for the study and beneficiation of the PGM contents of the UG2 reef.

PGM have a very strong affinity for BMS, especially Ni-sulphides, in both the Booyendal and Zondereinde UG2 reef. This association is important when one considers the difficulty in floating liberated PGM with average grain sizes such as those identified in this study ( $<3 \mu\text{m}$ ). Composite BMS-PGM grains have a greater flotation potential due to the increase in grain sizes and the susceptibility of sulphide minerals to flotation. However, it was found that most BMS are situated on or near to the boundaries of chromite grains. This close association of BMS with chromite is an important characteristic to consider when evaluating and implementing the appropriate milling and flotation parameters. Some composite chromite-BMS-PGM particles may report to tailings because of poor BMS-PGM liberation or as a result of the attempt to suppress chromite recovery. The rejection of these composite particles would depend on the overall physio-chemical properties of the particular particle. Within both sample sets, PGM have a strong association with phases such as apatite, rutile and sphene (Booyendal) and calcite, rutile and sphene (Zondereinde). This association has not been previously reported in the literature in terms of the effect on beneficiation and this paucity of information warrants further investigation in terms of the behaviour of these phases during flotation. The occurrence of small ( $1\text{-}2 \mu\text{m}$ ) PGM grains within the grain boundaries of sulphide minerals may be related to the prevalence of nano-

particles within BMS as reported by Wirth et al. (2013). This possible artefact/limitation is due to the nature of QEMSCAN analysis during a TMS. Spot analysis within a BMS grain of a nano-particle or PGE in the crystal lattice of the BMS may yield significant spectral highs of PGE and hence may report the identified pixel as a discrete PGM. This limitation needs further validation in order to constrain the effect of this phenomena.

The PGM contents of dunite pipes within the Bushveld Complex are often beneficiated by means of gravity recovery methods. Dunite pipes, which are known to occur throughout the Bushveld Complex, are considered an important resource due to their often highly elevated PGE contents (up to 2000 ppm) (Xiao and Laplante, 2004). The PGM budget of these post-magmatic intrusive bodies is often dominated by PGE-alloys, especially ferroplatinum (~50 %). This example may hold some benefit for other Bushveld Complex ore deposits where the PGM budget is known to be PGE-alloy dominated, such as the Zondereinde UG2 reef. A possible solution would be to use the gravity recovery method as a secondary process within the beneficiation circuit which attempts to scavenge PGM contents that were not initially concentrated during froth flotation.

## Chapter 7: CONCLUSIONS

### 7.1. Conclusions

The purpose of this study was to evaluate the mineralogical and geochemical variations of the UG2 reef at Booyendal and Zondereinde mines. There was a particular focus on the mineralogical, textural and chemical properties of PGM and associated mineral populations, with a discussion on how the characteristics, and any variation thereof, may influence conventional beneficiation processes such as milling and froth flotation. No beneficiation experiments were conducted to validate any of the interpretations discussed in Chapter 6, therefore the emphasis was directed at carefully, and as far as possible, accurately describing the nature of the UG2 reef at Booyendal and Zondereinde. In addition to the above-mentioned aims, this study also aimed at interpreting and comparing the validity of results obtained via traditional 2-D petrographic techniques (RLM, SEM and QEMSCAN) with those of 3-D  $\mu$ XCT.

From this study, the following conclusions can be made:

- The mineralogical, textural and chemical characteristics of chromite grains within both UG2 reef samples are similar in nature. The main ore zones from both Booyendal and Zondereinde are characterised by Fe-rich magnesio-chromite grains which display variations in grain size and the degree of compaction of the cumulate pile. The overall width of the main ore zone from Zondereinde is thinner in comparison to that of Booyendal (130 cm vs. 196 cm) possibly because the Zondereinde main ore zone had a higher degree of compaction.
- All mineral phases throughout the mining cut of Booyendal and Zondereinde are affected to some extent by alteration of the primary silicate proportion, resulting in mineral assemblages such as chlorite, amphibole, serpentine, mica and talc. These hydrous alteration minerals predominantly affect orthopyroxene grains, sometimes resulting in the complete replacement of the primary mineral assemblage. This alteration also occurs in close association with chromite, occurring as fine micron-scale rims around their grain boundaries, and is also observed in close association with BMS, sometimes completely enveloping the sulphide mineral aggregates. Alteration minerals are observed in greater

proportions in sections where the silicic content of the reef is higher (i.e. the hanging and footwall units). The consequence of the interrelationships between hydrous alteration minerals and chromite/silicate phases is a degree of increased flotation potential of gangue due to the fact that some of these hydrous alteration minerals are naturally floatable.

- QEMSCAN data suggests that there are higher modal proportions of alteration mineral assemblages within silicate fractions of the Zondereinde main ore zone chromitite units compared to Booyendal. However, these sections also contained significantly less silicate proportions in the same sections when compared to the Booyendal main ore zone. It is suggested that this is due to the compact nature of the Zondereinde chromitites. The compaction of the reef package may have resulted in the 'squeezing out' of the intercumulate silicate phases leaving behind what is reported to be 'higher concentrations' of alteration minerals.
- The BMS budget of the Booyendal UG2 reef is dominated by millerite (48 %) and chalcopyrite (39 %) whilst the Zondereinde UG2 reef is dominated by pentlandite (47 %) and chalcopyrite (48 %) assemblages. The proportion of Cu+Ni contents, which served as a proxy for BMS mineralisation, within the Zondereinde core is significantly higher when compared to the Booyendal core. The average contents within the main ore zone ranges from 100-200 ppm (Booyendal) vs. 400-600 ppm with even higher values in the hanging wall units of Zondereinde, ranging from 600-1200 ppm.
- As millerite forms from pentlandite, it is suggested that the predominance of millerite in the Booyendal UG2 reef, when compared to that of Zondereinde, serves as an indication that the reef package has been exposed to fluid infiltration and metasomatic processes.
- The PGM budget of both Booyendal and Zondereinde is characterised by a predominance of small (<3 µm), discrete mineral grains which occur in close association with BMS grains (especially Ni-sulphides), either locked within or at the outer edge of grain boundaries. The Booyendal UG2 reef is dominated by PGE-sulphide assemblages (54 %) whilst the Zondereinde UG2 reef is dominated by PGE-alloys, in particular ferroplatinum (53 %). The flotation potential of the PGM from Booyendal is therefore considered to yield better

recoveries within the fast-floating concentrates compared to that of Zondereinde, assuming high degrees of PGM liberation.

- The close association of PGM with BMS, and that of BMS with chromite grains, presents an interesting situation in terms of beneficiation due to the need to limit chromite contents which report to flotation concentrates. If milling parameters are not carefully refined, the result may either be a net-loss of composite BMS-chromite grains to tailings or conversely the net-gain of chromite reporting to concentrates depending on the physio-chemical response of the composite particle during flotation.
- 3-D imaging techniques reported a larger average grain size of PGM within both core sets (~50 % within the 40-59  $\mu\text{m}$  fraction). The validity of these statistics is questioned due to inherent resolution limitations that are faced with such a technique. However, the most powerful aspect of this new technology, within the scope of this study, lies in its ability to accurately image the textural characteristics of chromite and the broad distribution of PGM phases in samples (3 cm x 1 cm) with a voxel resolution of 10  $\mu\text{m}$  with relatively quick scan times (~1 hour).

## 7.2. Recommendations

In light of this study, the following recommendations can be made:

- In order to minimise the proportions of alteration mineral assemblages being processed with the core, ultimately affecting the efficiency of flotation techniques, it is recommended to limit the amount of hanging wall and footwall units that are included in the mining cut. This is due to the higher than average alteration mineral proportions and minimal PGE grade within these sections. There are practical mining constraints which need to be considered before a minimum mining width can be decided on. Due to the lack of PGE grade within the FW unit (Booyendal) and Pyr (3) unit (Zondereinde) it is suggested that the first reduction in the mining width come from these above-mentioned units.
- It is recommended that bench-scale milling and flotation tests are conducted in order to constrain the effect that the observed hydrous alteration features have



on the gangue mineral populations of both the Booyendal and Zondereinde UG2 reefs. Ultimately, the results of this study may be combined with the results of the additional beneficiation work, to fully characterise the UG2 reef from its primary in-situ state through to the concentration of PGM after milling and flotation. This has the potential to not only advance our understanding of the UG2 reef as a whole, but to also improve the plant efficiencies for Northam Platinum and other platinum producers too.

- The implementation of 3-D  $\mu$ XCT in terms of broad characterisation of chromite texture and PGM distribution within high grade sections has proven to be an invaluable asset due to the relatively cost-effective and quick turn-around times. This is compared to the often laborious and time consuming 2-D petrographic techniques which are traditionally used. It is important, however, to emphasise that 3-D  $\mu$ XCT cannot replace these techniques in terms of mineral composition data as well as resolution (mineral discrimination).
- Further scope is available to investigate the prevalence of calcite, apatite and Ti-bearing phases within the UG2 reef and their behaviour during the flotation stages, especially since there is a strong association with PGM.
- The high proportion of PGM minerals that are reported to occur within the grain boundaries of BMS by QEMSCAN analysis warrants further investigation into the validity of these statistics in light the recent work by Wirth et al. 2013 on PGM nano-particles. These small ( $\sim 1 \mu\text{m}$ ) PGM may be an artefact of the resolution limitations of the techniques employed in this study.

## References

- Armitage, P. E. B., McDonald, I., Edwards, S. J., & Manby, G. M. (2002). Platinum-group element mineralization in the Platreef and calc-silicate footwall at Sandsloot, Potgietersrus District, South Africa. *Transactions of the Institution of Mining and Metallurgy*, 307, 36-45.
- Ballhaus, C., & Sylvester, P. (2000). Noble Metal Enrichment Processes in the Merensky Reef, Bushveld Complex. *Journal of Petrology*, 41(4), 545-561.
- Barnes, S.-J., & Maier, W. D. (2002). Platinum-Group Element Distributions in the Rustenburg Layered Suite of the Bushveld Complex, South Africa. *The Geology, Geochemistry, Mineralogy and Mineral Beneficiation of Platinum-Group Elements*, 54(Special Volume), 431-458.
- Becker, M., & Brough, C. (2008). Geometallurgical characterisation of the Merensky Reef at Northam Platinum Mine: Comparison of normal pothole and transitional reef types. *9th International Congress for Applied Mineralogy*, 79(1989), 3-5.
- Becker, M., Harris, P. J., Wiese, J. G., & Bradshaw, D. J. (2009). Mineralogical characterisation of naturally floatable gangue in Merensky Reef ore flotation. *International Journal of Mineral Processing*, 93(3-4), 246-255.
- Becker, M., Mainza, a. N., Powell, M. S., Bradshaw, D. J., & Knopjes, B. (2008). Quantifying the influence of classification with the 3 product cyclone on liberation and recovery of PGMs in UG2 ore. *Minerals Engineering*, 21(7), 549-558.
- Becker, M., Yorath, G., Ndlovu, B., Harris, M., Deglon, D., & Franzidis, J. P. (2013). A rheological investigation of the behaviour of two Southern African platinum ores. *Minerals Engineering*, 49, 92-97.
- Boudreau, A. E. (2008). Modeling the Merensky reef, Bushveld Complex, Republic of South Africa. *Contributions to Mineralogy and Petrology*, 156(4), 431-437.
- Boudreau, A.E. and McCallum, I.S. (1992) Concentration of Platinum-group elements by magmatic fluids in layered intrusions. *Economic Geology*, 87, 1830-1848.

- Brough, C. P., Bradshaw, D. J., & Becker, M. (2010). A comparison of the flotation behaviour and the effect of copper activation on three reef types from the Merensky reef at Northam. *Minerals Engineering*, 23(11-13), 846-854.
- Cawthorn, R. G. (1999). The platinum and palladium resources of the Bushveld Complex. *South African Journal of Science*, 95(11-12), 481-489.
- Cawthorn, R. G. (2002). The Role of Magma Mixing in the Genesis of PGE Mineralization in the Bushveld Complex: Thermodynamic Calculations and New Interpretations-a Discussion. *Economic Geology*, 97(3), 663-666.
- Cawthorn, R. G. (2005). Pressure fluctuations and the formation of the PGE-rich Merensky and chromitite reefs, Bushveld Complex. *Mineralium Deposita*, 40(2), 231-235.
- Cawthorn, R. G. (2010). The platinum group element deposits of the bushveld complex in South Africa. *Platinum Metals Review*, 54(4), 205-215.
- Cawthorn, R. G. (2011). Geological interpretations from the PGE distribution in the Bushveld Merensky and UG2 chromitite reefs. *Journal of the Southern African Institute of Mining and Metallurgy*, 111(2), 67-79.
- Cawthorn, R. G., & Webb, S. J. (2001). Connectivity between the western and eastern limbs of the Bushveld complex. *Tectonophysics*, 330(3-4), 195-209.
- Cawthorn, R. G., Lee, C. A., Schouwstra, R. P., & Mellowship, P. (2002). Relationship between PGE and PGM in the Bushveld Complex. *Canadian Mineralogist*, 40(2), 311-328.
- Chetty, D., Gryffenberg, L., Lekgetho, T. B., & Molebale, I. J. (2009). Automated SEM study of PGM distribution across a UG2 flotation concentrate bank: Implications for understanding PGM floatability. *Journal of the Southern African Institute of Mining and Metallurgy*, 109(10), 587-593.

- Cnudde, V., & Boone, M. N. (2013). High-resolution X-ray computed tomography in geosciences: A review of the current technology and applications. *Earth-Science Reviews*, 123, 1-17.
- Cousins, C. A., & Vermaak, C. F. (1976). The contribution of southern African ore deposits to the geochemistry of the platinum group metals. *Economic Geology*, 71(1), 287-305.
- Crundwell, F., Moats, M., Ramachandran, V., Robinson, T., & Davenport, W. G. (2011). *Extractive Metallurgy of Nickel, Cobalt and Platinum Group Metals*. Elsevier.
- Dzvinamurungu, T., Viljoen, K. S., Knoper, M. W., & Mulaba-Bafubiandi, A. (2013). Geometallurgical characterisation of Merensky Reef and UG2 at the Marikana Mine, Bushveld Complex, South Africa. *Minerals Engineering*, 52, 74-81.
- Eales, H. V. and Cawthorn, R. G. (1996). The Bushveld Complex. *Developments in Petrology*, 15, 181-229.
- Ekmekçi, Z., Bradshaw, D. J., Allison, S. A., & Harris, P. J. (2003). Effects of frother type and froth height on the flotation behaviour of chromite in UG2 ore. *Minerals Engineering*, 16(10), 941-949.
- Gain, S. B. (1985). The geologic setting of the platiniferous UG-2 chromitite layer on the farm Maandagshoek, eastern Bushveld complex. *Economic Geology*, 80(4), 925-943.
- Gauert, C., Kotzé, E., & Beukes, J. J. (1995). Reef disturbances of Critical Zone rocks of the eastern Bushveld Complex in the vicinity of the Steelpoort fault, South Africa- petrogenetic implications.
- Godel, B. M., Barnes, S. J., & Barnes, S. J. (2013). Deposition mechanisms of magmatic sulphide liquids: Evidence from high-resolution x-ray computed tomography and trace element chemistry of komatiite-hosted disseminated sulphides. *Journal of Petrology*, 54(7), 1454-1481.

- Godel, B., Barnes, S. J., & Maier, W. D. (2006). 3-D distribution of sulphide minerals in the Merensky Reef (Bushveld Complex, South Africa) and the J-M Reef (Stillwater Complex, USA) and their relationship to microstructures using x-ray computed tomography. *Journal of Petrology*, 47(9), 1853-1872.
- Godel, B., Barnes, S. J., & Maier, W. D. (2007). Platinum-group elements in sulphide minerals, platinum-group minerals, and whole-rocks of the Merensky Reef (Bushveld Complex, South Africa): Implications for the formation of the reef. *Journal of Petrology*, 48(8), 1569-1604.
- Godel, B., Barnes, S. J., Barnes, S. J., & Maier, W. D. (2010). Platinum ore in three dimensions: Insights from high-resolution X-ray computed tomography. *Geology*, 38(12), 1127-1130.
- Greet, C. J. (2009). The significance of grinding environment on the flotation of UG2 ores. *Journal of the Southern African Institute of Mining and Metallurgy*, 109(1), 31-37.
- Hay, M. P. (2010). A case study of optimising UG2 flotation performance part 2: Modelling improved PGM recovery and Cr<sub>2</sub>O<sub>3</sub> rejection at Northam's UG2 concentrator. *Minerals Engineering*, 23, 868-876.
- Hay, M. P., & Roy, R. (2010). A case study of optimising UG2 flotation performance. Part 1: Bench, pilot and plant scale factors which influence Cr<sub>2</sub>O<sub>3</sub> entrainment in UG2 flotation. *Minerals Engineering*, 23, 855-867.
- Helmy, H. M., Ballhaus, C., Fonseca, R. O. C., Wirth, R., Nagel, T., & Tredoux, M. (2013). Noble metal nanoclusters and nanoparticles precede mineral formation in magmatic sulphide melts. *Nature Communications*, 4, 2405.
- Hutchinson, D., Foster, J., Prichard, H., & Gilbert, S. (2015). Concentration of Particulate Platinum-Group Minerals during Magma Emplacement; a Case Study from the Merensky Reef, Bushveld Complex. *Journal of Petrology*, 56(1), 113-159.

- Jasieniak, M., & Smart, R. S. C. (2010). Surface chemical mechanisms of inadvertent recovery of chromite in UG2 ore flotation: Residual layer identification using statistical ToF-SIMS analysis. *International Journal of Mineral Processing*, 94(1-2), 72-82.
- Junge, M., Oberthür, T., & Melcher, F. (2014). Cryptic variation of chromite chemistry, platinum group element and platinum group mineral distribution in the UG-2 chromitite: An example from the karee mine, western Bushveld complex, South Africa. *Economic Geology*, 109(3), 795-810.
- Junge, M., Wirth, R., Oberthür, T., Melcher, F., & Schreiber, A. (2015). Mineralogical siting of platinum-group elements in pentlandite from the Bushveld Complex, South Africa. *Mineralium Deposita*, 50(1), 41-54.
- Ketcham, R. A., & Carlson, W. D. (2001). Acquisition, optimization and interpretation of x-ray computed tomographic imagery: Applications to the geosciences. *Computers and Geosciences*, 27(4), 381-400.
- Kinloch, E. D. (1982). Regional trends in the platinum-group mineralogy of the critical zone of the Bushveld complex, South Africa. *Economic Geology*, 77(6), 1328-1347.
- Kinnaird, J. (2005). The Bushveld large igneous province. Retrieved from <http://www.largeigneousprovinces.org/sites/default/files/BushveldLIP.pdf>
- Kinnaird, J. A, Kruger, F. J., Nex, P. A. M., & Cawthorn, R. G. (2002). Chromitite formation — a key to understanding processes of platinum enrichment. *Applied Earth Science*, 1, 23-35.
- Lee, C. A. (1996). A Review of Mineralization in the Bushveld Complex and some other Layered Intrusions. *Developments in Petrology*, 15(C), 103-145.
- Li, C., Ripley, E. M., & Merino, E. (2007). Replacement of base metal sulfides by actinolite, epidote, calcite, and magnetite in the UG2 and Merensky reef of the Bushveld Complex, South Africa. *Economic Geology*, 99(1), 173-184.

- Lotter, N. O., Bradshaw, D. J., Becker, M., Parolis, L. A. S., & Kormos, L. J. (2008). A discussion of the occurrence and undesirable flotation behaviour of orthopyroxene and talc in the processing of mafic deposits. *Minerals Engineering*, 21(12-14), 905-912.
- Maier, W. D. (2005). Platinum-group element (PGE) deposits and occurrences: Mineralization styles, genetic concepts, and exploration criteria. *Journal of African Earth Sciences*, 41(3), 165-191.
- Maier, W. D., Barnes, S., & Groves, D. I. (2012). The Bushveld Complex, South Africa : formation of platinum-palladium, chrome- and vanadium-rich layers via hydrodynamic sorting of a mobilized cumulate slurry in a large, relatively slowly cooling, subsiding magma chamber, *Mineralium Deposita*, 48(1), 1-56.
- Maier, W., & Barnes, S. (1999). Platinum-group elements in silicate rocks of the Lower, Critical and Main Zones at Union Section, western Bushveld Complex. *Journal of Petrology*, 40(11), 1647.
- Mathez, E. A., & Mey, J. L. (2005). Character of the UG2 chromitite and host rocks and petrogenesis of its pegmatoidal footwall, northeastern Bushveld Complex. *Economic Geology*, 100(8), 1617-1630.
- McLaren, C. H., & De Villiers, J. P. R. (1982). The platinum-group chemistry and mineralogy of the UG-2 chromitite layer of the Bushveld complex. *Economic Geology*, 77(6), 1348-1366.
- Mondal, S. K., & Mathez, E. A. (2007). Origin of the UG2 chromitite layer, Bushveld Complex. *Journal of Petrology*, 48(3), 495-510.
- Naldrett, A. J., & Von Gruenewaldt, G. (1989). Association of platinum-group elements with chromitite in layered intrusions and ophiolite complexes. *Economic Geology*, 84(1), 180-187.



- Naldrett, A. J., Wilson, A., Kinnaird, J., & Chunnett, G. (2009). PGE tenor and metal ratios within and below the Merensky Reef, Bushveld Complex: Implications for its genesis. *Journal of Petrology*, 50(4), 625-659.
- Naldrett, A. J., Wilson, A., Kinnaird, J., Yudovskaya, M., & Chunnett, G. (2012). The origin of chromitites and related PGE mineralization in the Bushveld Complex: New mineralogical and petrological constraints. *Mineralium Deposita*, 47(3), 209-232.
- Naldrett, T., Kinnaird, J., Wilson, A., & Chunnett, G. (2008). Concentration of PGE in the Earth's Crust with Special Reference to the Bushveld Complex. *Earth Science Frontiers*, 15(5), 264-297.
- Ndlovu, B., Forbes, E., Farrokhpay, S., Becker, M., Bradshaw, D., & Deglon, D. (2013). A preliminary rheological classification of phyllosilicate group minerals. *Minerals Engineering*, 55, 190-200.
- Penberthy, C. J., Merkle, R. K. W. (1999). Lateral variations in the platinum-group element content and mineralogy of the UG2 chromitite layer, Bushveld Complex. *South African Journal of Geology*, 102(3), 240-250.
- Penberthy, C. J., Oosthuizen, E. J., & Merkle, R. K. W. (2000). The recovery of platinum-group elements from the UG-2 chromitite, Bushveld Complex - a mineralogical perspective. *Mineralogy and Petrology*, 68(1-3), 213-222.
- Reid, D. L., & Basson, I. J. (2002). Iron-rich ultramafic pegmatite replacement bodies within the Upper Critical Zone, Rustenburg Layered Suite, Northam Platinum Mine, South Africa. *Mineralogical Magazine*, 66(6), 895-914.
- Rule, C., & Schouwstra, R. P. (2011). Process mineralogy delivering significant value at Anglo Platinum concentrator operations. *10th International Congress for Applied Mineralogy*, 613-621.
- Schouwstra, R. P., Kinloch, E. D., & Lee, C. A. (2000). A Short Geological Review of the Bushveld Complex. *Platinum Metals Review*, 44(1), 33-39.

- Scoon, R. N., & Mitchell, A. A. (2005). The platiniferous dunite pipes in the eastern limb of the Bushveld complex: Review and comparison with unmineralized discordant ultramafic bodies: Discussion. *South African Journal of Geology*, 108(4), 587-589.
- Smith, A. J. B., Viljoen, K. S., Schouwstra, R., Roberts, J., Schalkwyk, C., & Gutzmer, J. (2013). Geological variations in the Merensky Reef at Bafokeng Rasimone Platinum Mine and its influence on flotation performance. *Minerals Engineering*, 52, 155-168.
- Smith, D. S., & Basson, I. J. (2006). Shape and distribution analysis of Merensky Reef potholing, Northam Platinum Mine, western Bushveld Complex: Implications for pothole formation and growth. *Mineralium Deposita*, 41(3), 281-295.
- Smith, D. S., Basson, I. J., & Reid, D. L. (2004). Normal Reef Subfacies of the Merensky Reef at Northam Platinum mine, Zwartklip facies, western Bushveld Complex, South Africa. *Canadian Mineralogist*, 42(2), 243-260.
- Solomon, N., Becker, M., Mainza, A., Petersen, J., & Franzidis, J. P. (2011). Understanding the influence of HPGR on PGM flotation behaviour using mineralogy. *Minerals Engineering* 24, 1370-1377.
- Vermaak, C. F. (1995). The Platinum-Group Metals - A Global Perspective. Mintek, Randburg, pp. 247.
- Viljoen, M. J., & Scoon, R. N. (1985). The distribution and main geologic features of discordant bodies of iron-rich ultramafic pegmatite in the Bushveld Complex. *Economic Geology*, 80(4), 1109-1128.
- Viring, R. G. and Cowell, V. (1999). The Merensky reef on Northam Platinum Limited. *South African Journal of Geology*, 102(3), 192-208.
- Von Gruenewaldt, G., & Merkle, R. K. W. (1995). Platinum group element proportions in chromitites of the Bushveld complex: implications for fractionation and magma mixing models. *Journal of African Earth Sciences*, 21(4), 615-632.

- Von Gruenewaldt, G., Hatton, C. J., & Merkle, R. K. W. (1986). Platinum-group element-chromitite associations in the Bushveld Complex. *Geology*, *81*, 1067-1079.
- Von Gruenewaldt, G., Sharpe, M. R., & Hatton, C. J. (1985). The Bushveld complex: introduction and review. *Economic Geology*, *80*(4), 803-812.
- Voordouw, R. J., Gutzmer, J., & Beukes, N. J. (2010). Zoning of platinum group mineral assemblages in the UG2 chromitite determined through in situ SEM-EDS-based image analysis. *Mineralium Deposita*, *45*(2), 147-159.
- Webb, S. J., Cawthorn, R. G., Nguuri, T., & James, D. (2004). Gravity modeling Bushveld complex connectivity supported by Southern African Seismic Experiment results. *South African Journal of Geology*, *107*(1-2), 207-218.
- Wesseldijk, Q. I., Reuter, M. A., Bradshaw, D. J., & Harris, P. J. (1999). Flotation behaviour of chromite with respect to the beneficiation of UG2 ore. *Minerals Engineering*, *12*(10), 1177-1184.
- Wills, B. A. (2011). *Wills' mineral processing technology: an introduction to the practical aspects of ore treatment and mineral recovery*. Butterworth-Heinemann.
- Wirth, R., Reid, D., & Schreiber, A. (2013). Nanometer-sized platinum-group minerals (PGM) in base metal sulfides: New evidence for an orthomagmatic origin of the Merensky reef PGE ore deposit, Bushveld Complex, South Africa. *Canadian Mineralogist*, *51*(1), 143-155.
- Xiao, Z., & Laplante, A. R. (2004). Characterizing and recovering the platinum group minerals - A review. *Minerals Engineering*, *17*(9-10), 961-979.

## Appendix A

**Table 14** - Selected mineral standards for SEM analysis.

Mineral	Formula	Element
<b>SILICATES</b>		
Albite	NaAlSi <sub>3</sub> O <sub>8</sub>	Silica (Si), Sodium (Na)
Anorthite	CaAl <sub>2</sub> Si <sub>2</sub> O <sub>8</sub>	Aluminium (Al)
Diopside	CaMgSi <sub>2</sub> O <sub>6</sub>	Calcium (Ca)
Olivine	(Mg, Fe <sup>2+</sup> ) <sub>2</sub> SiO <sub>4</sub>	Magnesium (Mg)
<b>SULPHIDES/OXIDES</b>		
Chromite	Fe <sup>2+</sup> Cr <sub>2</sub> O <sub>4</sub>	Chromium (Cr)
Ilmenite	Fe <sup>2+</sup> TiO <sub>3</sub>	Iron (Fe), Titanium (Ti), Manganese (Mn)
Marcasite	FeS <sub>2</sub>	Sulphur (S)
Pentlandite	(Fe, Ni) <sub>9</sub> S <sub>8</sub>	Nickel (Ni)
Sphalerite	(Zn, Fe)S	Zinc (Zn)
Cuprite	Cu <sub>2</sub> O	Copper (Cu)
<b>OTHER</b>		
Bismuth Selenide	Bi <sub>2</sub> Se <sub>3</sub>	Bismuth (Bi)

Pure elemental standards were used for iridium (Ir), osmium (Os), palladium (Pd), platinum (Pt), rhodium (Rh), ruthenium (Ru) and tellurium (Te).

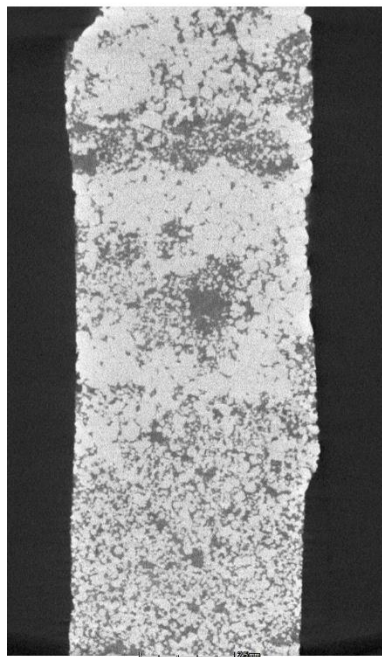
**Table 15** - Mineral properties used to discriminate between phase groupings during 3-D  $\mu$ XCT analysis.

Mineral	Chemical Formula	Specific Gravity (g/cm <sup>3</sup> )	Average Atomic Number (Z)
<u>SILICATES</u>			
Orthopyroxene	MgSiO <sub>3</sub> - FeSiO <sub>3</sub>	3.2 - 3.9	10.6 - 16.7
Anorthite	CaAl <sub>2</sub> Si <sub>2</sub> O <sub>8</sub>	2.7	12
Olivine	Mg <sub>2</sub> SiO <sub>4</sub> - Fe <sub>2</sub> SiO <sub>4</sub>	3.2 - 4.4	10.4 - 18.6
<u>SULPHIDES/OXIDES</u>			
Pyrrhotite	Fe <sub>(1-x)</sub> S (x = 0 - 0.17)	4.6 - 4.7	22.4
Chalcopyrite	CuFeS <sub>2</sub>	4.1 - 4.3	23.5
Pentlandite	(Fe, Ni) <sub>9</sub> S <sub>8</sub>	4.6 - 5	23.4
Chromite	Fe <sup>2+</sup> Cr <sub>2</sub> O <sub>4</sub>	4.5 - 4.8	19.9
Galena	PbS	7.2 - 7.6	73.4
<u>PGM</u>			
Braggite	(Pt, Pd, Ni)S	10	69.2
Sperrylite	PtAs <sub>2</sub>	10.6	58.5
Moncheite	Pt,Pd(Bi,Te) <sub>2</sub>	8.6	70.3 ±2.5
Cooperite	PtS	9.5	69.2

**Table 16** – Summary of the bulk mineralogy for the Booyendal and Zondereinde samples (XRD analysis).

<b><u>Booyendal</u></b>		
<b><u>Unit</u></b>	<b><u>Minerals (Major)</u></b>	<b><u>Minerals (Minor)</u></b>
HW	Enstatite ( <b>OPX</b> ), Anorthite ( <b>Plag</b> )	Talc, Illite
UPEG	Enstatite ( <b>OPX</b> ), Anorthite ( <b>Plag</b> )	Talc, Illite
UT2	Fe-rich Magnesio-chromite ( <b>Oxide</b> ),	Cu,Mg,Mn <b>Oxide</b> , Enstatite ( <b>OPX</b> ), Anorthite ( <b>Plag</b> )
UP1	Enstatite ( <b>OPX</b> ), Anorthite ( <b>Plag</b> )	Talc, Illite
UL	Fe-rich Magnesio-chromite ( <b>Oxide</b> ),	Cu,Mg,Mn <b>Oxide</b> , Enstatite ( <b>OPX</b> ), Anorthite ( <b>Plag</b> )
UM	Fe-rich Magnesio-chromite ( <b>Oxide</b> ),	Cu,Mg,Mn <b>Oxide</b> , Enstatite ( <b>OPX</b> ), Anorthite ( <b>Plag</b> )
UPEG	Enstatite ( <b>OPX</b> ), Anorthite ( <b>Plag</b> )	Illite
FW	Enstatite ( <b>OPX</b> ), Anorthite ( <b>Plag</b> )	Illite
<b><u>Zondereinde</u></b>		
<b><u>Unit</u></b>	<b><u>Minerals (Major)</u></b>	<b><u>Minerals (Minor)</u></b>
Pyr (1)	Enstatite ( <b>OPX</b> ), Anorthite ( <b>Plag</b> )	Forsterite ( <b>Ol</b> ), Talc, Clinochrysotile, Muscovite
Harz	Enstatite ( <b>OPX</b> ), Anorthite ( <b>Plag</b> )	Forsterite ( <b>Ol</b> ), Talc, Clinochrysotile, Muscovite
Chr	Fe-rich Magnesio-chromite ( <b>Oxide</b> )	Cu,Mg,Mn <b>Oxide</b> , Enstatite ( <b>OPX</b> ), Talc
Chr (1)	Fe-rich Magnesio-chromite ( <b>Oxide</b> )	Cu,Mg,Mn <b>Oxide</b> , Enstatite ( <b>OPX</b> ), Talc
Chr (2)	Fe-rich Magnesio-chromite ( <b>Oxide</b> ),	Cu,Mg,Mn <b>Oxide</b> , Enstatite ( <b>OPX</b> )
FEP	Enstatite ( <b>OPX</b> ), Anorthite ( <b>Plag</b> )	Talc, Antigorite, Muscovite
Pyr (3)	Enstatite ( <b>OPX</b> ), Anorthite ( <b>Plag</b> )	Talc, Antigorite, Muscovite

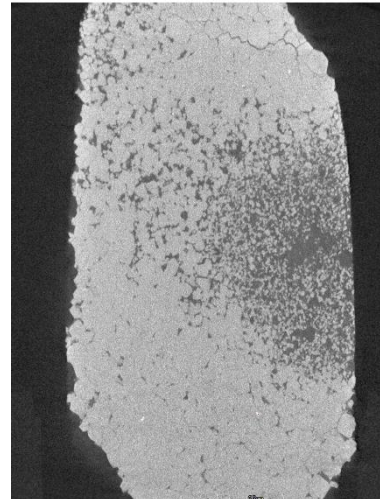




BOY XCT  
6

Mid UT2

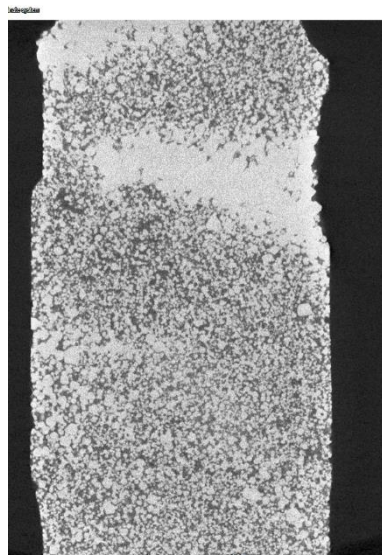
—————  
2.5 mm



ZON XCT  
2

Lower Chr

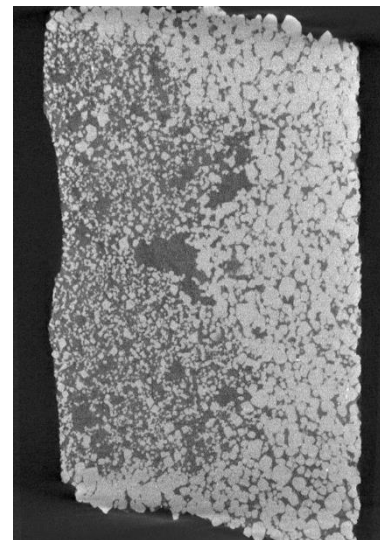
—————  
2.5 mm



BOY XCT  
10

Top UL

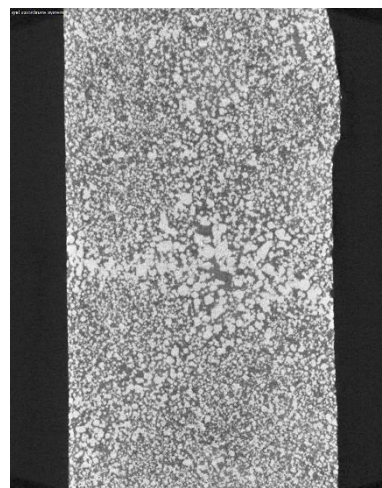
—————  
2.5 mm



ZON XCT  
5

Mid Chr  
(1)

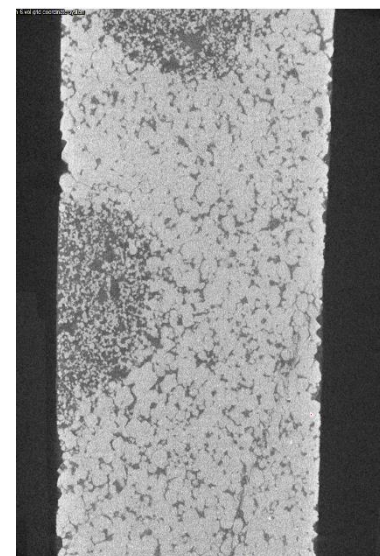
—————  
2.5 mm



BOY XCT  
11

Bottom  
UL

—————  
2.5 mm



ZON XCT  
6

Bottom Chr  
(1)

—————  
2.5 mm

**Figure plate 52** – Chromite textures from 3-D XCT analysis (moving down in stratigraphic height).Booysendal (left) and Zondereinde (right).



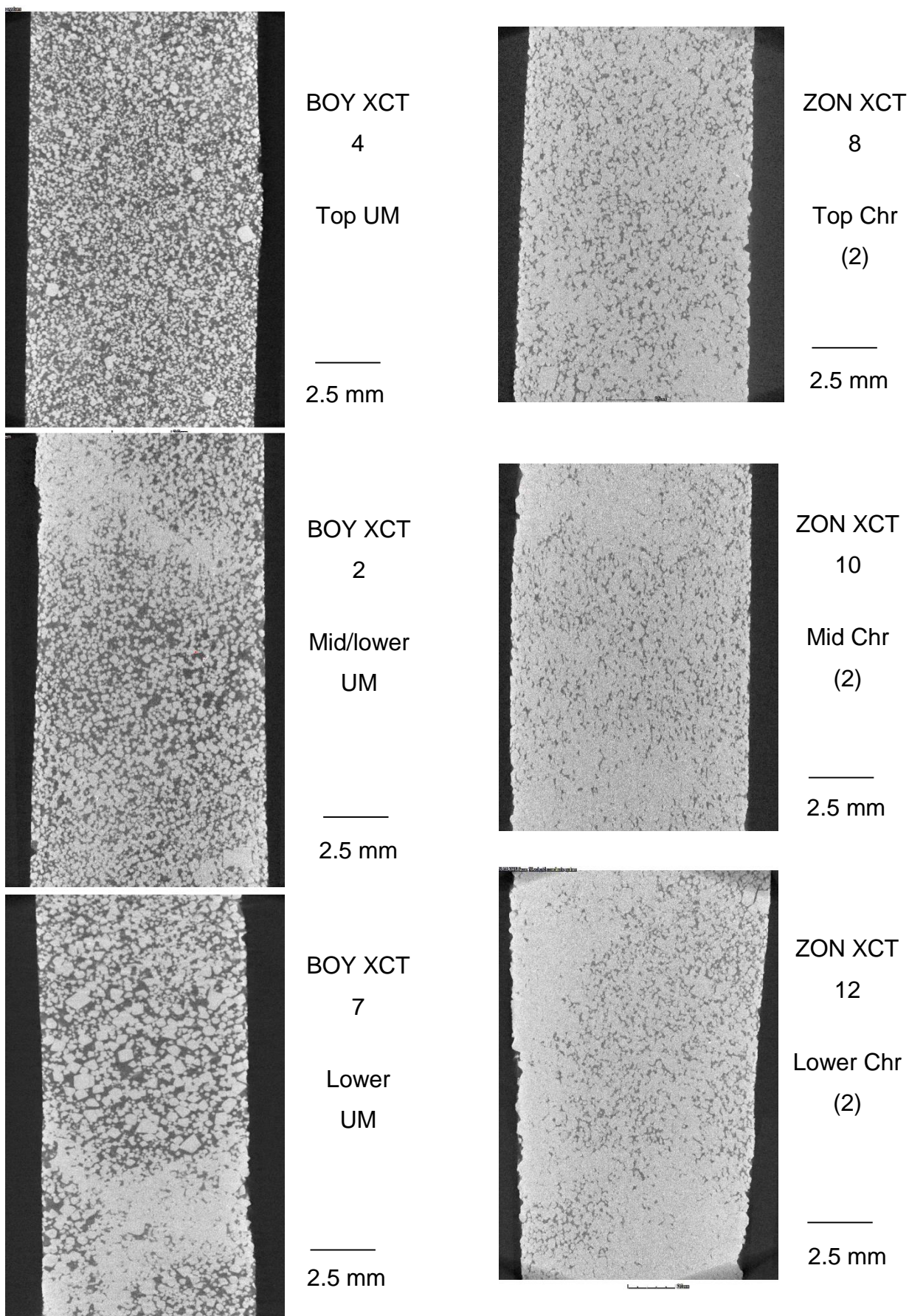


**Figure plate 52 cont.** – Chromite textures from 3-D XCT analysis (moving down in stratigraphic height). Booyensdal (left) and Zondereinde (right).

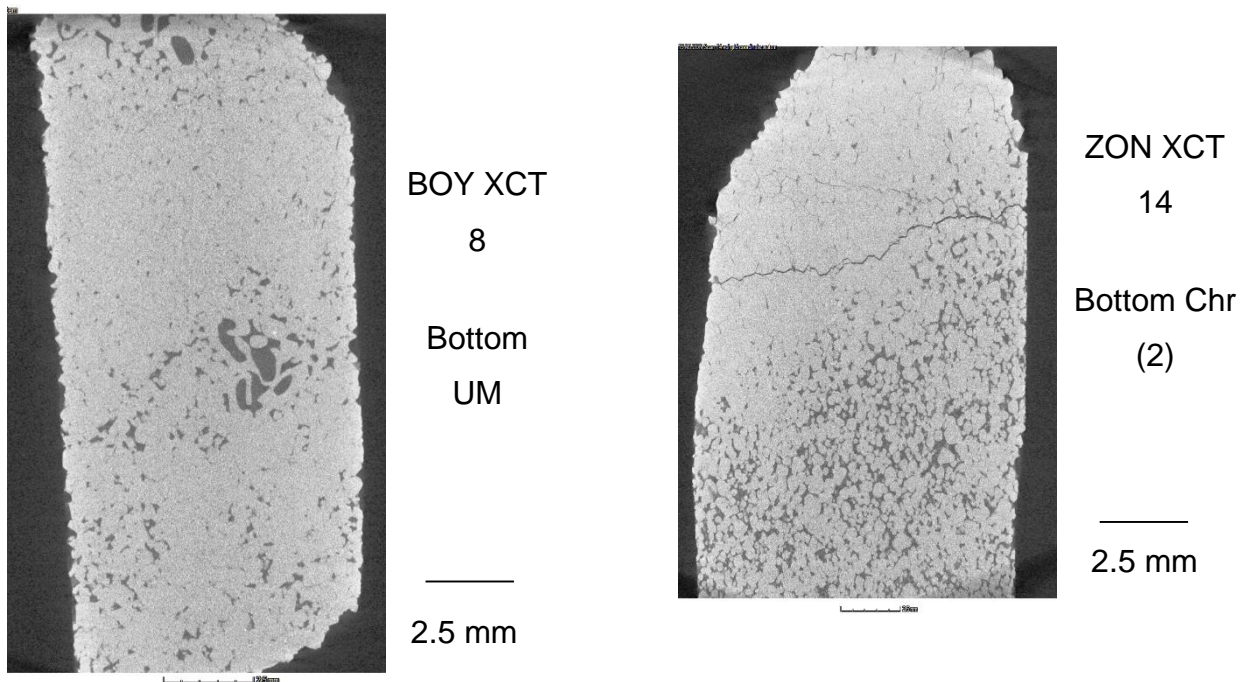


**Figure plate 52 cont.** – *Chromite textures from 3-D XCT analysis (moving down in stratigraphic height). Booyendal (left) and Zondereinde (right).*

## Generalised PGM mode of occurrence

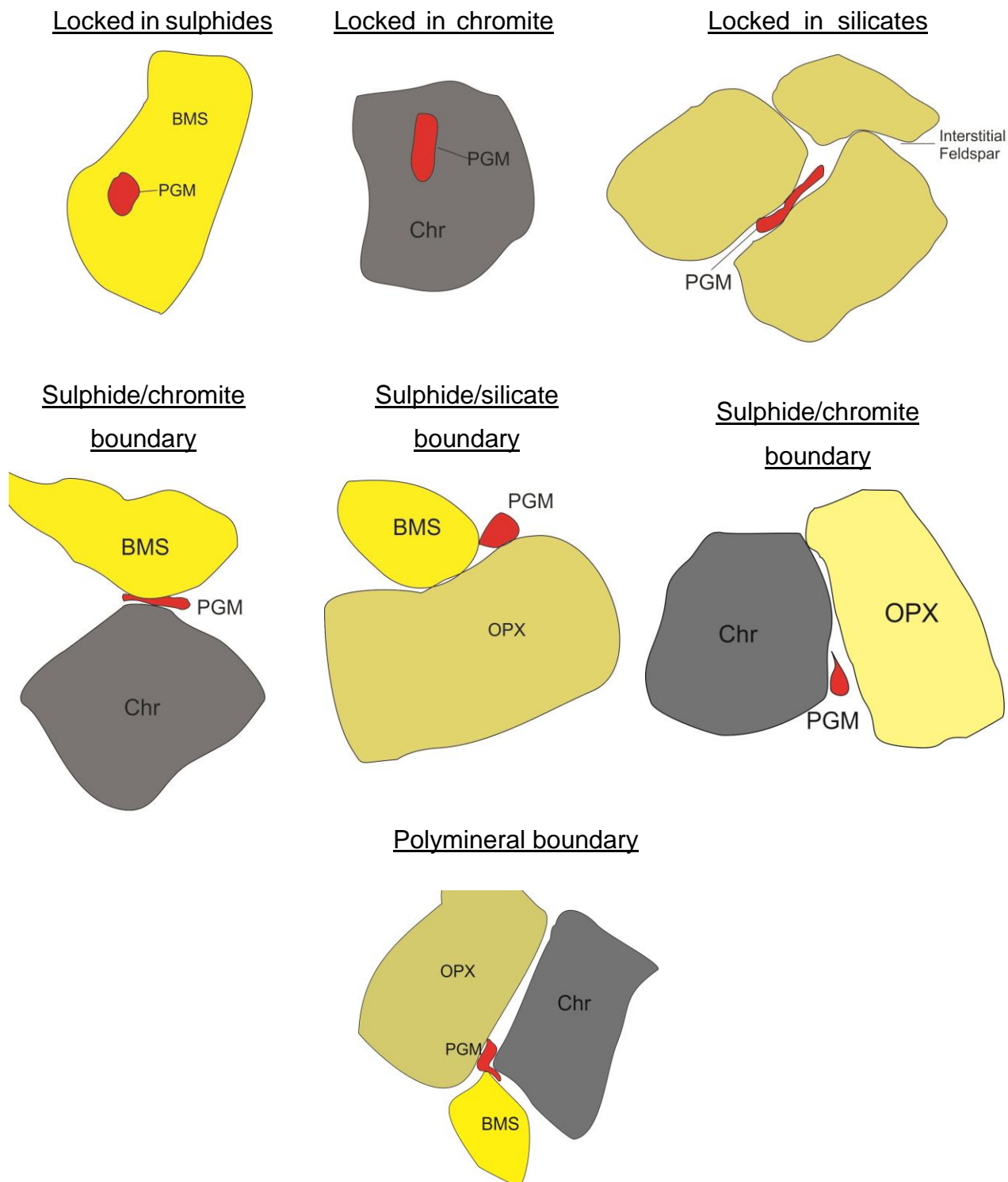


**Figure 53** – Generalised PGM mode of occurrence based on the categories presented in Figures 15, 34, 47 and 49.

**Table 17 - Assay results (Booyendal)**

	Au	Pt	Pd	Rh	Ru	Ir	Cu	Ni	Zn	SiO2	Al2O3	CaO	MgO	Fe2O3	K2O	MnO	Na2O	P2O5	TiO2	Cr2O3	V2O5	LOI	
UNITS	PPM	PPM	PPM	PPM	PPM	PPM	PPM	PPM	PPM	%	%	%	%	%	%	%	%	%	%	%	%	%	%
LDL	0.02	0.02	0.02	0.02	0.02	0.13	0.5	1	0.5	0.05	0.05	0.01	0.05	0.01	0.01	0.01	0.05	0.01	0.01	0.01	0.01	0.01	-50
UDL	1000	1000	1000	1000	1000	1000	10000	10000	10000	100	100	100	100	100	100	100	100	100	100	100	100	100	100
<b>NO.13</b>	0.02	0.73	0.37	0.10	0.14	<0.13	70.2	83	5.9	49.80	6.13	3.86	22.10	13.70	0.10	0.27	0.50	<0.01	0.31	2.44	0.07	0.07	-0.43
<b>NO.14</b>	0.03	0.34	0.26	0.05	0.06	<0.13	45.7	132	11.1	52.20	3.85	2.97	23.30	13.70	0.19	0.21	0.33	0.03	0.23	0.86	0.04	0.04	0.33
<b>NO.1</b>	0.04	2.44	0.50	0.47	0.89	0.20	76.4	178	10.2	14.20	15.40	2.93	10.10	24.80	0.06	0.20	0.40	<0.01	0.82	31.90	0.28	0.28	-0.94
<b>NO.15</b>	0.03	0.73	0.15	0.18	0.33	<0.13	22.3	103	5.9	39.10	9.19	3.25	18.90	15.50	0.06	0.21	0.46	<0.01	0.40	11.10	0.13	0.13	-0.20
<b>NO.11</b>	0.02	0.41	0.08	0.08	0.49	<0.13	27	79	6.4	48.50	7.74	4.23	21.30	12.60	0.09	0.22	0.59	0.02	0.25	3.63	0.06	0.06	-0.02
<b>NO.12</b>	0.02	0.19	0.13	0.07	0.08	<0.13	30.9	83	3	48.40	7.14	4.22	21.70	12.40	0.08	0.22	0.59	0.01	0.24	3.21	0.05	0.05	-0.09
<b>NO.5</b>	0.03	1.76	0.25	0.35	0.73	0.20	40.9	99	17.2	14.20	17.20	2.85	9.14	23.10	0.07	0.17	0.60	0.02	0.76	32.50	0.36	0.36	-1.30
<b>NO.4</b>	0.07	2.16	0.26	0.40	2.58	0.20	49.3	112	14.1	14.70	18.10	3.19	8.93	22.50	0.08	0.21	0.64	<0.01	0.76	32.20	0.34	0.34	-1.23
<b>NO.6</b>	0.16	2.30	0.44	0.43	0.84	0.20	48.9	122	17.7	15.10	18.30	3.38	8.89	22.00	0.09	0.18	0.73	<0.01	0.74	31.10	0.34	0.34	-1.19
<b>NO.7</b>	0.03	2.66	0.32	0.41	1.05	0.20	57	137	9.3	17.50	17.70	3.06	10.40	21.60	0.12	0.22	0.68	<0.01	0.71	29.70	0.31	0.31	-1.12
<b>NO.8</b>	0.02	2.64	0.31	0.41	0.87	0.20	48.8	140	25.4	16.50	18.40	3.72	8.53	21.60	0.13	0.20	0.75	<0.01	0.74	29.80	0.27	0.27	-1.15
<b>NO.9</b>	0.04	6.33	1.16	0.77	1.80	0.30	27.6	81	8.5	19.60	18.50	4.18	9.77	20.30	0.08	0.17	0.64	<0.01	0.65	27.20	0.25	0.25	-0.98
<b>NO.2</b>	0.03	4.26	1.34	0.71	1.24	0.20	23.7	65	15.2	21.90	18.00	4.18	10.50	19.20	0.11	0.18	0.75	<0.01	0.60	25.10	0.22	0.22	-0.92
<b>NO.3</b>	0.00	2.35	0.52	0.48	0.77	0.20	32.5	81	14.8	15.20	17.50	3.15	8.71	22.20	0.11	0.19	0.62	<0.01	0.86	30.80	0.31	0.31	-1.21
<b>NO.10</b>	0.03	3.75	1.56	0.73	1.36	0.30	59.3	121	14	9.82	15.60	1.80	8.35	26.70	0.09	0.20	0.46	<0.01	1.14	35.20	0.41	0.41	-1.59
<b>NO.16</b>	0.02	0.08	0.10	0.05	0.03	<0.13	22.6	32	1.4	49.70	16.70	8.88	13.50	7.36	0.12	0.11	1.45	<0.01	0.12	0.60	0.02	0.02	-0.02
<b>NO.17</b>	0.02	0.05	0.29	0.04	0.02	<0.13	39.3	67	4.1	51.80	16.40	8.16	13.10	6.75	0.42	0.12	1.53	0.01	0.14	0.34	0.02	0.02	0.22
<b>NO.18</b>	0.04	0.02	0.05	0.03	0.02	<0.13	50	49	12.7	58.50	16.70	7.19	9.36	4.24	1.49	0.09	1.62	0.02	0.20	0.14	<0.01	<0.01	0.35

**Table 18 - Assay results (Zondereinde)**

	Au	Pt	Pd	Rh	Ru	Ir	Cu	Ni	Zn	SiO2	Al2O3	CaO	MgO	Fe2O3	K2O	MnO	Na2O	P2O5	TiO2	Cr2O3	V2O5	LOI	
LDL	0.02	0.02	0.02	0.02	0.02	0.13	0.5	1	0.5	0.05	0.05	0.01	0.05	0.01	0.01	0.01	0.05	0.01	0.01	0.01	0.01	0.01	-50
UDL	1000	1000	1000	1000	1000	1000	10000	10000	10000	100	100	100	100	100	100	100	100	100	100	100	100	100	100
UNITS	PPM	PPM	PPM	PPM	PPM	PPM	PPM	PPM	PPM	%	%	%	%	%	%	%	%	%	%	%	%	%	%
NO 1	<0.02	0.21	0.08	0.25	0.25	0.30	26.3	712	21.9	48.10	4.24	3.65	27.50	14.50	0.14	0.23	0.38	0.04	0.22	0.63	0.03	0.35	
NO 2	<0.02	0.39	0.14	0.18	0.12	0.10	33.7	641	22.5	48.50	5.97	3.53	26.30	13.50	0.07	0.24	0.56	0.02	0.14	0.66	0.01	0.34	
NO 3	<0.02	0.16	0.06	0.03	0.00	<0.13	36.4	694	26.9	48.70	5.54	3.78	26.80	13.90	0.09	0.24	0.49	0.00	0.14	0.51	0.00	0.43	
NO 4	<0.02	0.29	0.11	0.13	0.13	0.20	48	823	35.5	46.60	5.34	3.60	26.70	14.20	0.08	0.24	0.44	0.00	0.13	1.06	0.02	0.96	
NO 5	<0.02	0.14	0.08	0.04	0.00	<0.13	52.2	1161	37.4	43.80	3.76	3.08	29.80	16.30	0.08	0.26	0.40	0.01	0.15	0.48	0.01	1.92	
NO 6	<0.02	0.50	0.24	0.08	0.07	<0.13	74.9	577	11.8	47.80	4.45	2.88	25.70	14.00	0.13	0.22	0.32	0.01	0.26	1.82	0.04	1.71	
NO 7	<0.02	2.72	0.73	0.55	0.84	0.20	11.9	224	6.7	6.87	16.40	0.66	11.60	27.60	0.02	0.24	0.17	0.00	0.72	36.80	0.32	-1.14	
NO 8	<0.02	2.06	0.67	0.48	0.79	0.30	78.1	260	7.8	7.15	16.30	0.66	11.00	26.40	0.07	0.24	0.00	0.00	0.69	37.40	0.29	-0.78	
NO 9	<0.02	2.74	1.20	0.58	0.97	0.30	78.5	433	12.3	8.51	15.80	0.63	11.50	26.20	0.06	0.26	0.00	0.00	0.64	36.60	0.31	-0.76	
NO 10	<0.02	2.59	1.26	0.61	0.97	0.30	120	454	6.4	9.43	15.10	0.68	12.20	25.50	0.04	0.23	0.06	0.00	0.63	35.80	0.27	0.36	
NO 11	<0.02	5.31	1.62	0.76	0.99	0.20	75.8	220	13.9	7.61	15.70	0.94	11.10	26.90	0.03	0.23	0.14	0.00	0.70	37.70	0.32	-1.47	
NO 12	<0.02	2.97	0.80	0.46	0.57	0.20	43.5	134	6.2	6.22	15.50	0.82	10.40	27.00	0.05	0.24	0.10	0.00	0.71	38.40	0.34	-1.42	
NO 13	<0.02	0.16	0.03	0.59	0.86	0.30	38.1	115	5.5	6.46	15.40	0.83	10.80	26.70	0.04	0.22	0.06	0.00	0.71	37.90	0.31	-1.20	
NO 14	<0.02	1.92	0.71	0.42	0.71	0.20	30.3	104	5.2	6.23	15.80	0.75	10.90	27.30	0.03	0.21	0.21	0.00	0.74	38.40	0.30	-1.20	
NO 15	<0.02	2.29	0.90	0.50	1.32	0.30	29.2	128	8.9	4.92	16.90	0.88	10.10	27.90	0.03	0.24	0.36	0.00	0.76	39.60	0.31	-1.54	
NO 16	<0.02	6.84	2.19	1.49	2.00	0.50	42.4	137	9.1	6.27	16.80	1.07	9.50	29.30	0.03	0.23	0.28	0.00	1.01	38.10	0.31	-1.68	
NO 17	<0.02	4.06	1.19	1.60	1.21	0.40	227	276	745	50.90	2.77	1.98	26.30	13.90	0.23	0.23	0.18	0.01	0.31	1.95	0.06	0.90	
NO 18	<0.02	0.21	0.09	0.05	0.07	<0.13	9.1	103	24.8	52.20	2.35	1.96	26.40	13.60	0.13	0.23	0.10	0.00	0.17	0.60	0.02	0.24	
NO 19	<0.02	0.37	0.16	0.09	0.11	<0.13	9.4	129	11.5	51.80	2.34	1.88	26.20	14.20	0.21	0.26	0.18	0.00	0.22	1.28	0.04	0.31	
NO 20	<0.02	0.05	0.05	0.03	0.00	<0.13	25	96	8.9	52.70	1.72	2.28	26.90	14.20	0.13	0.27	0.13	0.00	0.23	0.50	0.03	-0.19	
NO 21	<0.02	0.18	0.09	0.04	0.32	<0.13	18.7	63	6.3	52.80	4.96	3.57	24.50	12.80	0.07	0.24	0.30	0.00	0.19	0.49	0.03	-0.16	
NO 22	<0.02	0.05	0.05	0.00	0.06	<0.13	20	61	5.7	53.80	4.45	3.49	25.00	12.90	0.11	0.25	0.30	0.00	0.21	0.43	0.03	-0.16	
NO 23	<0.02	0.08	0.06	0.00	0.00	<0.13	19.4	45	8.6	54.50	4.77	3.33	25.10	12.50	0.06	0.24	0.38	0.00	0.19	0.46	0.03	-0.20	



**Booyendal chromite compositions 1/15****UT2**

	1	2	3	4	5	6	7	8	9	10	11	12	13	14	15	16	17	18	19
<b>Analysed totals</b>																			
Cr <sub>2</sub> O <sub>3</sub>	45.42	44.55	44.89	44.52	45.35	45.30	45.43	45.17	44.96	45.42	44.86	45.60	45.07	45.26	45.19	45.50	45.22	45.24	45.40
Al <sub>2</sub> O <sub>3</sub>	13.11	13.13	13.71	13.54	13.29	13.05	12.73	13.16	13.62	13.78	13.43	13.17	13.21	13.53	14.17	12.65	12.89	13.29	13.11
V <sub>2</sub> O <sub>3</sub>	0.89	0.74	0.70	0.70	0.39	0.59	0.89	0.83	0.67	0.85	0.61	0.78	0.46	0.84	0.57	0.60	0.72	0.51	0.79
TiO <sub>2</sub>	1.14	1.06	0.94	0.87	1.13	1.05	0.96	1.14	0.92	0.84	1.10	1.11	1.07	1.15	0.68	0.99	1.15	1.17	1.12
FeO	23.95	23.12	23.51	23.32	23.78	24.38	23.97	23.74	23.54	23.52	23.71	24.22	23.63	23.80	24.10	23.29	23.34	23.99	23.90
Fe <sub>2</sub> O <sub>3</sub>	6.37	6.98	6.30	7.57	6.51	6.80	6.94	6.73	6.78	6.19	6.55	6.43	6.90	6.37	6.16	6.93	6.80	6.47	6.64
MgO	6.92	7.01	6.79	7.04	6.95	6.57	6.59	6.98	6.84	6.90	6.84	6.70	6.81	6.79	6.45	6.73	6.91	6.86	6.97
MnO	0.00	0.35	0.34	0.31	0.00	0.00	0.00	0.19	0.40	0.28	0.22	0.16	0.33	0.36	0.22	0.27	0.28	0.00	0.00
NiO	0.00	0.00	0.00	0.00	0.00	0.00	0.27	0.00	0.00	0.00	0.00	0.00	0.00	0.24	0.00	0.30	0.27	0.00	0.00
<b>Total</b>	<b>97.80</b>	<b>96.95</b>	<b>97.18</b>	<b>97.88</b>	<b>97.41</b>	<b>97.73</b>	<b>97.78</b>	<b>97.95</b>	<b>97.74</b>	<b>97.79</b>	<b>97.33</b>	<b>98.16</b>	<b>97.48</b>	<b>98.34</b>	<b>97.55</b>	<b>97.27</b>	<b>97.57</b>	<b>97.54</b>	<b>97.93</b>
<b>Cations</b>																			
Cr	9.78	9.66	9.70	9.55	9.79	9.79	9.82	9.71	9.67	9.75	9.69	9.80	9.74	9.69	9.74	9.88	9.77	9.76	9.76
Al	4.21	4.25	4.42	4.33	4.28	4.20	4.10	4.22	4.37	4.41	4.33	4.22	4.26	4.32	4.55	4.10	4.15	4.28	4.20
V	0.22	0.18	0.17	0.17	0.09	0.15	0.22	0.20	0.16	0.21	0.15	0.19	0.11	0.20	0.14	0.15	0.18	0.13	0.19
Ti	0.23	0.22	0.19	0.18	0.23	0.21	0.20	0.23	0.19	0.17	0.23	0.23	0.22	0.23	0.14	0.20	0.24	0.24	0.23
Fe <sub>3+</sub>	1.30	1.44	1.30	1.55	1.34	1.40	1.43	1.38	1.39	1.26	1.35	1.31	1.42	1.30	1.26	1.43	1.40	1.33	1.36
Fe <sub>2+</sub>	5.45	5.30	5.37	5.30	5.43	5.57	5.48	5.39	5.36	5.34	5.42	5.50	5.40	5.39	5.49	5.35	5.33	5.48	5.44
Mg	2.81	2.87	2.77	2.85	2.83	2.67	2.69	2.83	2.77	2.79	2.78	2.71	2.77	2.74	2.62	2.76	2.81	2.79	2.82
Mn	0.00	0.08	0.08	0.07	0.00	0.00	0.00	0.04	0.09	0.07	0.05	0.04	0.08	0.08	0.05	0.06	0.06	0.00	0.00
Ni	0.00	0.00	0.00	0.00	0.00	0.00	0.06	0.00	0.00	0.00	0.00	0.00	0.00	0.05	0.00	0.07	0.06	0.00	0.00
<b>Total</b>	<b>24.00</b>	<b>24.00</b>	<b>24.00</b>	<b>24.00</b>	<b>24.00</b>	<b>24.00</b>	<b>24.00</b>	<b>24.00</b>	<b>24.00</b>	<b>24.00</b>	<b>24.00</b>	<b>24.00</b>	<b>24.00</b>	<b>24.00</b>	<b>24.00</b>	<b>24.00</b>	<b>24.00</b>	<b>24.00</b>	<b>24.00</b>
<b>Cation allocation</b>																			
2+	8.26	8.25	8.22	8.22	8.26	8.25	8.17	8.26	8.22	8.20	8.26	8.25	8.25	8.21	8.17	8.17	8.21	8.27	8.26
3+	15.74	15.75	15.78	15.78	15.74	15.75	15.83	15.74	15.78	15.80	15.74	15.75	15.75	15.79	15.83	15.83	15.79	15.73	15.74
<b>Major cation ratios</b>																			
100Mg/Mg+Fe <sub>2+</sub>	29.06	30.01	28.26	29.58	29.13	27.36	28.03	29.40	28.50	28.62	28.56	27.90	28.73	28.20	26.07	29.18	29.65	28.62	29.29
100Cr/Cr+Al	69.91	69.46	68.71	68.79	69.59	69.95	70.53	69.71	68.88	68.84	69.13	69.90	69.59	69.16	68.13	70.70	70.17	69.54	69.90
100Fe <sub>3+</sub> /Cr+Al+V+Fe <sub>3+</sub>	8.42	9.28	8.32	9.92	8.63	9.01	9.18	8.88	8.91	8.09	8.69	8.47	9.15	8.36	8.05	9.21	9.02	8.58	8.76

2/15

UT2

	20	21	22	23	24	25	26	27	28	29	30	31	32	33	34	35	36	37	38	39
<b>Analysed totals</b>																				
Cr2O3	45.90	45.75	46.20	45.32	46.83	45.35	45.91	45.33	46.09	45.57	46.11	45.62	46.35	46.66	46.26	45.52	45.51	45.56	46.10	46.57
Al2O3	13.81	14.09	13.78	13.92	14.48	13.64	14.20	14.34	13.69	14.27	13.97	14.19	13.87	13.94	14.14	13.91	14.23	14.18	14.47	13.59
V2O3	0.70	0.58	0.79	0.86	0.50	0.75	0.74	0.56	0.88	0.79	0.50	0.71	0.75	0.74	0.76	0.55	0.76	0.61	0.53	0.66
TiO2	1.03	0.99	0.79	1.59	0.85	1.01	1.00	0.91	1.07	1.05	0.94	1.10	1.19	0.88	1.18	0.96	1.25	1.04	1.13	1.10
FeO	24.24	24.01	23.75	24.32	23.86	23.91	24.47	23.60	23.88	23.68	23.77	23.95	23.77	24.72	24.23	23.28	24.28	24.20	23.73	24.46
Fe2O3	6.50	6.81	7.07	5.90	6.34	7.00	6.42	7.48	6.75	6.44	6.52	6.95	6.77	6.63	6.53	7.40	6.55	6.55	6.30	5.78
MgO	7.04	7.15	7.13	7.23	7.34	7.04	7.01	7.24	7.21	7.28	7.27	7.28	7.56	6.91	7.34	7.42	7.17	6.99	7.35	6.85
MnO	0.00	0.15	0.33	0.16	0.00	0.19	0.00	0.23	0.33	0.33	0.00	0.34	0.22	0.00	0.19	0.21	0.27	0.20	0.24	0.00
NiO	0.00	0.00	0.00	0.00	0.23	0.00	0.00	0.35	0.00	0.00	0.00	0.00	0.00	0.00	0.00	0.22	0.00	0.00	0.24	0.00
<b>Total</b>	<b>99.21</b>	<b>99.53</b>	<b>99.83</b>	<b>99.31</b>	<b>100.44</b>	<b>98.88</b>	<b>99.75</b>	<b>100.03</b>	<b>99.90</b>	<b>99.41</b>	<b>99.07</b>	<b>100.14</b>	<b>100.48</b>	<b>100.48</b>	<b>100.63</b>	<b>99.49</b>	<b>100.00</b>	<b>99.33</b>	<b>100.08</b>	<b>99.01</b>
<b>Cations</b>																				
Cr	9.72	9.64	9.72	9.56	9.76	9.64	9.66	9.50	9.69	9.59	9.75	9.55	9.66	9.77	9.63	9.59	9.54	9.62	9.64	9.90
Al	4.36	4.43	4.32	4.38	4.50	4.32	4.45	4.48	4.29	4.48	4.41	4.43	4.31	4.35	4.39	4.37	4.45	4.47	4.51	4.31
V	0.17	0.14	0.19	0.21	0.12	0.18	0.18	0.13	0.21	0.19	0.12	0.17	0.18	0.18	0.18	0.13	0.18	0.15	0.13	0.16
Ti	0.21	0.20	0.16	0.32	0.17	0.20	0.20	0.18	0.21	0.21	0.19	0.22	0.24	0.18	0.23	0.19	0.25	0.21	0.22	0.22
Fe3+	1.31	1.37	1.42	1.19	1.26	1.42	1.28	1.49	1.35	1.29	1.31	1.38	1.34	1.32	1.29	1.48	1.31	1.32	1.25	1.17
Fe2+	5.43	5.35	5.29	5.43	5.26	5.38	5.45	5.23	5.31	5.27	5.32	5.30	5.24	5.48	5.34	5.19	5.38	5.41	5.25	5.50
Mg	2.81	2.84	2.83	2.88	2.88	2.82	2.78	2.86	2.86	2.89	2.90	2.87	2.97	2.73	2.88	2.95	2.83	2.78	2.90	2.75
Mn	0.00	0.03	0.07	0.04	0.00	0.04	0.00	0.05	0.07	0.08	0.00	0.08	0.05	0.00	0.04	0.05	0.06	0.04	0.05	0.00
Ni	0.00	0.00	0.00	0.00	0.05	0.00	0.00	0.07	0.00	0.00	0.00	0.00	0.00	0.00	0.00	0.05	0.00	0.00	0.05	0.00
<b>Total</b>	<b>24.00</b>	<b>24.00</b>	<b>24.00</b>	<b>24.00</b>	<b>24.00</b>	<b>24.00</b>	<b>24.00</b>	<b>24.00</b>	<b>24.00</b>	<b>24.00</b>	<b>24.00</b>	<b>24.00</b>	<b>24.00</b>	<b>24.00</b>	<b>24.00</b>	<b>24.00</b>	<b>24.00</b>	<b>24.00</b>	<b>24.00</b>	<b>24.00</b>
<b>Cation allocation</b>																				
2+	8.24	8.23	8.19	8.34	8.15	8.24	8.23	8.14	8.24	8.24	8.22	8.25	8.27	8.20	8.26	8.18	8.28	8.24	8.20	8.25
3+	15.76	15.77	15.81	15.66	15.85	15.76	15.77	15.86	15.76	15.76	15.78	15.75	15.73	15.80	15.74	15.82	15.72	15.76	15.80	15.75
<b>Major cation ratios</b>																				
100Mg/Mg+Fe2+	28.69	29.05	29.42	29.34	29.55	29.07	28.09	29.47	29.78	29.63	29.79	29.52	31.12	27.74	29.60	30.85	28.81	28.19	29.66	28.00
100Cr/Cr+Al	69.03	68.53	69.22	68.58	68.44	69.03	68.43	67.95	69.31	68.17	68.88	68.31	69.15	69.18	68.68	68.69	68.21	68.30	68.11	69.69
100Fe3+/Cr+Al+V+Fe3+	8.42	8.77	9.05	7.73	8.04	9.10	8.25	9.56	8.69	8.30	8.42	8.91	8.67	8.46	8.35	9.53	8.45	8.47	8.07	7.53



## UP1

3/15

	1	2	3	4	5	6	7	8	9	10
<b>Analysed totals</b>										
Cr <sub>2</sub> O <sub>3</sub>	46.23	47.53	46.48	47.22	46.45	46.80	46.64	47.49	46.79	46.71
Al <sub>2</sub> O <sub>3</sub>	11.58	11.13	10.77	9.88	9.64	10.04	9.21	10.00	9.80	9.77
V <sub>2</sub> O <sub>3</sub>	0.95	0.89	0.93	0.94	0.79	1.20	1.09	0.87	0.95	1.06
TiO <sub>2</sub>	1.26	1.29	2.23	0.97	1.56	1.47	1.49	1.42	1.30	1.50
FeO	26.44	26.47	27.95	27.52	27.41	27.22	28.06	27.83	27.34	27.83
Fe <sub>2</sub> O <sub>3</sub>	8.04	7.82	6.37	8.71	9.49	8.49	9.64	8.21	8.63	8.20
MgO	5.76	5.61	4.99	4.49	5.05	5.09	4.61	4.81	4.77	4.58
MnO	0.00	0.24	0.27	0.28	0.25	0.32	0.29	0.12	0.25	0.24
NiO	0.00	0.21	0.00	0.00	0.00	0.00	0.00	0.00	0.00	0.00
<b>Total</b>	<b>100.26</b>	<b>101.19</b>	<b>99.98</b>	<b>100.02</b>	<b>100.64</b>	<b>100.63</b>	<b>101.02</b>	<b>100.76</b>	<b>99.82</b>	<b>99.88</b>
<b>Cations</b>										
Cr	9.88	10.11	10.05	10.29	10.04	10.09	10.09	10.25	10.20	10.19
Al	3.69	3.53	3.47	3.21	3.11	3.23	2.97	3.22	3.19	3.18
V	0.23	0.21	0.23	0.23	0.19	0.29	0.27	0.21	0.23	0.26
Ti	0.26	0.26	0.46	0.20	0.32	0.30	0.31	0.29	0.27	0.31
Fe <sup>3+</sup>	1.64	1.58	1.31	1.81	1.95	1.74	1.99	1.69	1.79	1.70
Fe <sup>2+</sup>	5.98	5.95	6.39	6.34	6.27	6.21	6.43	6.35	6.30	6.42
Mg	2.32	2.25	2.03	1.84	2.06	2.07	1.88	1.96	1.96	1.88
Mn	0.00	0.05	0.06	0.07	0.06	0.07	0.07	0.03	0.06	0.06
Ni	0.00	0.04	0.00	0.00	0.00	0.00	0.00	0.00	0.00	0.00
<b>Total</b>	<b>24.00</b>	<b>24.00</b>	<b>24.00</b>	<b>24.00</b>	<b>24.00</b>	<b>24.00</b>	<b>24.00</b>	<b>24.00</b>	<b>24.00</b>	<b>24.00</b>
<b>Cation allocation</b>										
2+	8.30	8.26	8.49	8.25	8.38	8.35	8.37	8.34	8.32	8.36
3+	15.70	15.74	15.51	15.75	15.62	15.65	15.63	15.66	15.68	15.64
<b>Major cation ratios</b>										
100Mg/Mg+Fe <sup>2+</sup>	23.99	23.71	20.61	19.29	21.93	21.94	20.01	20.43	20.64	19.61
100Cr/Cr+Al	72.80	74.12	74.33	76.21	76.37	75.77	77.25	76.10	76.19	76.23
100Fe <sup>3+</sup> /Cr+Al+V+Fe <sup>3+</sup>	10.59	10.26	8.70	11.62	12.76	11.35	12.96	10.98	11.62	11.10

4/15

UL

	1	2	3	4	5	6	7	8	9	10	11	12	13	14	15	16	17	18	19	20	
<b>Analysed totals</b>																					
Cr2O3	46.25	46.34	46.40	46.07	46.31	46.59	46.52	46.74	46.06	46.07	45.84	46.30	46.09	45.85	46.23	46.04	45.25	45.69	46.36	46.16	
Al2O3	14.48	14.84	14.30	14.39	14.46	14.70	14.41	14.96	14.48	14.39	14.94	14.76	14.37	15.06	14.85	14.88	15.03	14.77	14.65	14.49	
V2O3	1.06	1.34	1.00	1.23	1.31	1.37	1.13	1.34	1.27	1.11	1.48	1.21	1.05	1.36	1.35	1.27	1.40	1.41	1.32	0.98	
TiO2	0.91	1.06	1.17	1.17	1.23	1.07	1.22	0.93	1.08	1.30	0.96	1.01	1.10	0.85	1.02	0.81	1.03	1.03	1.09	1.16	
FeO	22.14	22.55	22.22	22.41	22.53	22.47	22.55	22.84	22.58	22.73	22.19	22.34	22.34	22.54	22.67	22.22	22.14	22.73	22.56	22.63	
Fe2O3	6.67	5.99	6.14	5.96	6.27	6.03	6.28	6.06	6.61	6.04	6.22	6.25	6.16	6.79	6.25	6.64	6.39	6.45	6.22	5.96	
MgO	8.60	8.58	8.62	8.47	8.67	8.67	8.63	8.46	8.53	8.41	8.69	8.64	8.45	8.56	8.52	8.61	8.70	8.39	8.59	8.33	
MnO	0.00	0.00	0.00	0.00	0.00	0.00	0.00	0.00	0.00	0.00	0.00	0.00	0.00	0.00	0.00	0.00	0.00	0.00	0.00	0.00	
NiO	0.00	0.00	0.00	0.00	0.00	0.00	0.00	0.00	0.00	0.00	0.00	0.00	0.00	0.00	0.00	0.00	0.00	0.00	0.00	0.00	
<b>Total</b>	<b>100.11</b>	<b>100.70</b>	<b>99.84</b>	<b>99.69</b>	<b>100.76</b>	<b>100.91</b>	<b>100.73</b>	<b>101.34</b>	<b>100.61</b>	<b>100.06</b>	<b>100.32</b>	<b>100.51</b>	<b>99.57</b>	<b>101.01</b>	<b>100.89</b>	<b>100.47</b>	<b>99.94</b>	<b>100.47</b>	<b>100.77</b>	<b>99.71</b>	
<b>Cations</b>																					
Cr	9.58	9.53	9.64	9.58	9.53	9.56	9.58	9.56	9.50	9.56	9.44	9.54	9.60	9.40	9.49	9.49	9.35	9.43	9.53	9.61	
Al	4.47	4.55	4.43	4.46	4.44	4.50	4.42	4.56	4.45	4.45	4.59	4.53	4.46	4.60	4.55	4.57	4.63	4.55	4.49	4.50	
V	0.25	0.31	0.24	0.29	0.31	0.32	0.26	0.31	0.30	0.26	0.35	0.28	0.25	0.32	0.32	0.30	0.33	0.33	0.31	0.23	
Ti	0.18	0.21	0.23	0.23	0.24	0.21	0.24	0.18	0.21	0.26	0.19	0.20	0.22	0.17	0.20	0.16	0.20	0.20	0.21	0.23	
Fe3+	1.31	1.17	1.21	1.18	1.23	1.18	1.23	1.18	1.30	1.19	1.22	1.23	1.22	1.32	1.22	1.30	1.26	1.27	1.22	1.18	
Fe2+	4.85	4.90	4.88	4.93	4.90	4.88	4.91	4.94	4.93	4.99	4.84	4.87	4.92	4.89	4.92	4.84	4.84	4.96	4.91	4.98	
Mg	3.36	3.33	3.37	3.32	3.36	3.36	3.35	3.26	3.31	3.29	3.37	3.35	3.32	3.31	3.30	3.34	3.39	3.27	3.33	3.27	
Mn	0.00	0.00	0.00	0.00	0.00	0.00	0.00	0.00	0.00	0.00	0.00	0.00	0.00	0.00	0.00	0.00	0.00	0.00	0.00	0.00	
Ni	0.00	0.00	0.00	0.00	0.00	0.00	0.00	0.00	0.00	0.00	0.00	0.00	0.00	0.00	0.00	0.00	0.00	0.00	0.00	0.00	
<b>Total</b>	<b>24.00</b>	<b>24.00</b>	<b>24.00</b>	<b>24.00</b>	<b>24.00</b>	<b>24.00</b>	<b>24.00</b>	<b>24.00</b>	<b>24.00</b>	<b>24.00</b>	<b>24.00</b>	<b>24.00</b>	<b>24.00</b>	<b>24.00</b>	<b>24.00</b>	<b>24.00</b>	<b>24.00</b>	<b>24.00</b>	<b>24.00</b>	<b>24.00</b>	
<b>Cation allocation</b>																					
2+	8.21	8.23	8.26	8.25	8.26	8.23	8.26	8.20	8.24	8.28	8.21	8.22	8.24	8.19	8.22	8.19	8.23	8.23	8.24	8.25	
3+	15.79	15.77	15.74	15.75	15.74	15.77	15.74	15.80	15.76	15.72	15.79	15.78	15.76	15.81	15.78	15.81	15.77	15.77	15.76	15.75	
<b>Major cation ratios</b>																					
100Mg/Mg+Fe2+	36.00	35.18	36.24	35.36	35.99	35.78	35.89	34.31	35.34	34.85	35.79	35.67	35.34	34.86	34.82	35.53	35.76	34.35	35.41	34.47	
100Cr/Cr+Al	68.17	67.68	68.51	68.23	68.24	68.00	68.41	67.68	68.08	68.22	67.29	67.78	68.26	67.13	67.61	67.48	66.87	67.47	67.97	68.12	
100Fe3+/Cr+Al+V+Fe3+	8.42	7.54	7.82	7.60	7.92	7.57	7.94	7.56	8.34	7.71	7.81	7.87	7.86	8.47	7.84	8.32	8.07	8.13	7.83	7.61	

5/15	UL																			
	21	22	23	24	25	26	27	28	29	30	31	32	33	34	35	36	37	38	39	40
<b>Analysed totals</b>																				
Cr2O3	45.19	44.83	44.07	45.49	45.11	44.67	44.50	44.64	44.23	44.58	44.85	44.85	44.33	44.85	44.43	45.01	44.88	45.45	43.94	43.95
Al2O3	15.47	15.32	15.70	15.33	15.45	15.51	15.87	15.66	15.71	15.23	15.41	15.10	15.15	15.20	15.00	15.17	15.22	15.15	15.82	15.66
V2O3	0.97	0.80	0.90	0.69	0.77	0.86	0.93	0.66	0.86	0.80	0.73	0.71	0.75	0.82	0.88	0.62	0.66	0.77	0.95	0.69
TiO2	0.98	0.96	0.99	0.98	0.89	0.92	0.99	0.90	1.05	1.02	1.13	1.00	1.12	1.18	1.06	1.01	0.96	1.01	0.97	0.99
FeO	22.80	22.31	22.38	22.76	22.29	22.31	22.47	22.33	22.56	22.94	22.97	22.79	22.63	23.30	22.44	22.74	22.52	23.00	22.48	21.93
Fe2O3	5.59	5.85	6.33	5.29	5.62	5.86	5.45	5.60	5.98	5.79	5.62	5.89	5.65	5.57	6.33	5.89	5.56	5.76	6.05	6.28
MgO	7.93	8.02	8.16	7.83	7.90	8.13	8.05	7.90	7.99	7.68	7.96	7.75	7.79	7.67	7.81	7.84	7.88	7.78	8.07	8.26
MnO	0.11	0.14	0.24	0.00	0.34	0.16	0.28	0.13	0.35	0.00	0.00	0.22	0.22	0.14	0.34	0.21	0.09	0.25	0.20	0.30
NiO	0.18	0.19	0.00	0.23	0.20	0.00	0.00	0.25	0.00	0.20	0.00	0.00	0.00	0.00	0.27	0.00	0.00	0.00	0.00	0.00
<b>Total</b>	<b>99.23</b>	<b>98.42</b>	<b>98.77</b>	<b>98.60</b>	<b>98.56</b>	<b>98.42</b>	<b>98.53</b>	<b>98.06</b>	<b>98.73</b>	<b>98.23</b>	<b>98.68</b>	<b>98.32</b>	<b>97.64</b>	<b>98.74</b>	<b>98.55</b>	<b>98.51</b>	<b>97.77</b>	<b>99.16</b>	<b>98.49</b>	<b>98.06</b>
<b>Cations</b>																				
Cr	9.43	9.43	9.21	9.56	9.48	9.38	9.32	9.41	9.26	9.42	9.41	9.47	9.41	9.43	9.36	9.48	9.51	9.52	9.21	9.24
Al	4.82	4.80	4.89	4.81	4.84	4.86	4.96	4.92	4.90	4.80	4.82	4.75	4.79	4.77	4.71	4.76	4.81	4.73	4.95	4.91
V	0.23	0.19	0.21	0.17	0.18	0.21	0.22	0.16	0.20	0.19	0.17	0.17	0.18	0.20	0.21	0.15	0.16	0.18	0.23	0.17
Ti	0.20	0.19	0.20	0.20	0.18	0.18	0.20	0.18	0.21	0.20	0.23	0.20	0.23	0.24	0.21	0.20	0.19	0.20	0.19	0.20
Fe3+	1.11	1.17	1.26	1.06	1.12	1.17	1.09	1.12	1.19	1.16	1.12	1.18	1.14	1.12	1.27	1.18	1.12	1.15	1.21	1.26
Fe2+	5.03	4.96	4.95	5.06	4.95	4.96	4.98	4.98	5.00	5.13	5.10	5.09	5.08	5.18	5.00	5.07	5.05	5.10	4.98	4.88
Mg	3.12	3.18	3.22	3.10	3.13	3.22	3.18	3.14	3.16	3.06	3.15	3.08	3.12	3.04	3.10	3.11	3.15	3.07	3.19	3.28
Mn	0.02	0.03	0.05	0.00	0.08	0.04	0.06	0.03	0.08	0.00	0.00	0.05	0.05	0.03	0.08	0.05	0.02	0.06	0.05	0.07
Ni	0.04	0.04	0.00	0.05	0.04	0.00	0.00	0.05	0.00	0.04	0.00	0.00	0.00	0.00	0.06	0.00	0.00	0.00	0.00	0.00
<b>Total</b>	<b>24.00</b>	<b>24.00</b>	<b>24.00</b>	<b>24.00</b>	<b>24.00</b>	<b>24.00</b>	<b>24.00</b>	<b>24.00</b>	<b>24.00</b>	<b>24.00</b>	<b>24.00</b>	<b>24.00</b>	<b>24.00</b>	<b>24.00</b>	<b>24.00</b>	<b>24.00</b>	<b>24.00</b>	<b>24.00</b>	<b>24.00</b>	<b>24.00</b>
<b>Cation allocation</b>																				
2+	8.18	8.17	8.22	8.16	8.16	8.21	8.22	8.15	8.23	8.18	8.25	8.22	8.25	8.26	8.18	8.23	8.21	8.22	8.22	8.22
3+	15.82	15.83	15.78	15.84	15.84	15.79	15.78	15.85	15.77	15.82	15.75	15.78	15.75	15.74	15.82	15.77	15.79	15.78	15.78	15.78
<b>Major cation ratios</b>																				
100Mg/Mg+Fe2+	31.67	32.55	32.69	31.44	31.93	32.79	31.97	31.69	31.86	30.82	31.75	31.32	31.55	30.56	31.95	31.68	31.93	31.24	32.10	33.46
100Cr/Cr+Al	66.20	66.24	65.31	66.55	66.20	65.88	65.28	65.65	65.38	66.25	66.13	66.58	66.25	66.43	66.52	66.55	66.41	66.80	65.06	65.30
100Fe3+/Cr+Al+V+Fe3+	7.13	7.51	8.09	6.79	7.20	7.51	6.97	7.20	7.65	7.47	7.23	7.59	7.36	7.19	8.16	7.58	7.19	7.37	7.74	8.07

6/15

UL

	41	42	43	44	45	46	47	48	49	50	51	52	53	54	55	56	57	58	59	60
<b>Analysed totals</b>																				
Cr2O3	45.40	45.05	44.71	44.81	44.84	46.18	44.49	44.49	45.20	44.92	43.93	44.93	44.76	45.76	45.34	45.09	45.22	45.59	44.94	44.64
Al2O3	15.83	15.82	15.68	16.15	15.64	14.55	15.33	16.40	16.03	15.95	16.13	15.96	15.96	15.39	15.54	16.00	16.25	15.17	16.01	16.17
V2O3	0.85	0.87	0.59	0.73	0.77	0.86	0.83	0.71	0.42	0.76	0.65	0.83	0.64	0.00	0.76	0.86	0.68	0.50	0.65	0.57
TiO2	1.03	1.14	1.18	0.87	0.94	1.10	1.09	1.00	1.06	0.97	1.00	1.06	1.04	0.81	0.97	1.10	0.89	1.03	1.01	0.83
FeO	23.27	22.73	23.30	22.56	22.76	23.23	23.03	22.77	22.47	22.98	22.29	22.70	22.70	22.34	22.64	22.95	22.17	22.48	22.71	22.73
Fe2O3	5.31	5.89	5.51	5.75	6.23	5.98	6.61	5.60	5.81	5.51	6.44	5.74	5.79	6.32	6.05	5.90	6.00	6.61	5.51	5.76
MgO	7.79	8.31	7.71	8.12	7.96	7.94	8.07	8.11	8.31	8.00	8.26	8.21	8.10	8.05	8.14	8.35	8.52	8.29	8.09	8.03
MnO	0.29	0.22	0.20	0.20	0.35	0.00	0.00	0.19	0.27	0.00	0.35	0.22	0.22	0.00	0.27	0.00	0.29	0.26	0.19	0.00
NiO	0.00	0.00	0.00	0.00	0.00	0.00	0.00	0.00	0.00	0.00	0.00	0.00	0.00	0.27	0.00	0.00	0.00	0.00	0.00	0.00
<b>Total</b>	<b>99.77</b>	<b>100.02</b>	<b>98.87</b>	<b>99.20</b>	<b>99.49</b>	<b>99.84</b>	<b>99.44</b>	<b>99.25</b>	<b>99.57</b>	<b>99.09</b>	<b>99.04</b>	<b>99.64</b>	<b>99.21</b>	<b>98.96</b>	<b>99.72</b>	<b>100.26</b>	<b>100.04</b>	<b>99.93</b>	<b>99.12</b>	<b>98.73</b>
<b>Cations</b>																				
Cr	9.43	9.30	9.37	9.32	9.33	9.63	9.27	9.24	9.36	9.36	9.14	9.31	9.32	9.58	9.41	9.28	9.31	9.45	9.36	9.33
Al	4.90	4.87	4.90	5.01	4.86	4.52	4.76	5.08	4.95	4.96	5.00	4.93	4.95	4.81	4.81	4.91	4.99	4.69	4.97	5.04
V	0.20	0.20	0.14	0.17	0.18	0.20	0.20	0.17	0.10	0.18	0.15	0.19	0.15	0.00	0.18	0.20	0.16	0.12	0.15	0.14
Ti	0.20	0.22	0.24	0.17	0.19	0.22	0.22	0.20	0.21	0.19	0.20	0.21	0.21	0.16	0.19	0.22	0.18	0.20	0.20	0.17
Fe3+	1.05	1.16	1.10	1.14	1.23	1.19	1.31	1.11	1.14	1.09	1.27	1.13	1.15	1.26	1.20	1.15	1.18	1.31	1.09	1.15
Fe2+	5.11	4.96	5.17	4.96	5.01	5.12	5.08	5.00	4.93	5.07	4.91	4.97	5.00	4.95	4.97	5.00	4.83	4.93	5.00	5.02
Mg	3.05	3.23	3.04	3.18	3.12	3.12	3.17	3.18	3.25	3.14	3.24	3.21	3.18	3.18	3.18	3.24	3.31	3.24	3.18	3.16
Mn	0.06	0.05	0.04	0.05	0.08	0.00	0.00	0.04	0.06	0.00	0.08	0.05	0.05	0.00	0.06	0.00	0.06	0.06	0.04	0.00
Ni	0.00	0.00	0.00	0.00	0.00	0.00	0.00	0.00	0.00	0.00	0.00	0.00	0.00	0.06	0.00	0.00	0.00	0.00	0.00	0.00
<b>Total</b>	<b>24.00</b>	<b>24.00</b>	<b>24.00</b>	<b>24.00</b>	<b>24.00</b>	<b>24.00</b>	<b>24.00</b>	<b>24.00</b>	<b>24.00</b>	<b>24.00</b>	<b>24.00</b>	<b>24.00</b>	<b>24.00</b>	<b>24.00</b>	<b>24.00</b>	<b>24.00</b>	<b>24.00</b>	<b>24.00</b>	<b>24.00</b>	<b>24.00</b>
<b>Cation allocation</b>																				
2+	8.22	8.25	8.25	8.19	8.21	8.24	8.24	8.22	8.23	8.21	8.23	8.23	8.23	8.13	8.21	8.24	8.20	8.23	8.22	8.19
3+	15.78	15.75	15.75	15.81	15.79	15.76	15.76	15.78	15.77	15.79	15.77	15.77	15.77	15.87	15.79	15.76	15.80	15.77	15.78	15.81
<b>Major cation ratios</b>																				
100Mg/Mg+Fe2+	30.43	32.88	30.24	31.92	31.64	32.34	32.22	31.51	32.87	31.35	32.69	32.37	31.93	32.58	32.55	32.71	33.69	33.67	31.83	31.43
100Cr/Cr+Al	65.79	65.63	65.65	65.04	65.78	68.03	66.06	64.53	65.41	65.38	64.62	65.37	65.28	66.60	66.18	65.39	65.11	66.84	65.30	64.93
100Fe3+/Cr+Al+V+Fe3+	6.74	7.45	7.08	7.28	7.91	7.63	8.44	7.10	7.36	7.01	8.19	7.27	7.37	8.05	7.67	7.43	7.53	8.38	7.02	7.32

7/15	UM																			
	1	2	3	4	5	6	7	8	9	10	11	12	13	14	15	16	17	18	19	20
<b>Analysed totals</b>																				
Cr2O3	44.44	45.06	44.50	44.83	44.55	44.63	44.80	45.06	45.25	45.07	45.08	44.84	44.82	44.61	44.46	44.67	44.61	44.40	45.00	45.22
Al2O3	15.65	16.74	15.63	15.27	15.08	15.44	15.40	15.10	15.56	15.27	15.19	15.25	14.94	15.34	15.01	14.95	15.32	15.41	15.08	15.08
V2O3	0.74	0.67	0.65	0.68	0.80	0.57	0.59	0.61	0.73	0.62	0.87	0.92	0.64	0.78	0.72	0.69	0.79	0.66	0.73	0.85
TiO2	0.72	0.52	1.00	0.80	0.86	0.86	0.83	0.93	0.79	0.88	0.89	1.00	0.80	0.90	1.00	1.11	1.15	1.08	0.97	1.02
FeO	22.31	22.13	22.59	22.68	22.43	22.56	22.78	22.78	22.63	23.07	22.61	23.33	22.93	23.31	22.93	22.45	22.89	22.59	22.85	23.02
Fe2O3	6.00	5.34	5.62	5.47	5.97	5.40	5.63	6.11	5.77	5.85	5.97	6.32	6.59	5.59	5.99	6.11	5.95	5.81	6.33	5.99
MgO	7.92	7.99	7.83	7.55	7.75	7.67	7.70	7.54	8.01	7.68	7.79	7.81	7.61	7.45	7.51	8.13	7.78	7.87	7.81	7.81
MnO	0.16	0.28	0.33	0.00	0.26	0.16	0.00	0.34	0.00	0.00	0.43	0.00	0.16	0.00	0.30	0.00	0.22	0.00	0.28	0.20
NiO	0.00	0.26	0.00	0.22	0.00	0.00	0.00	0.32	0.00	0.00	0.00	0.00	0.00	0.00	0.00	0.00	0.25	0.31	0.00	0.00
<b>Total</b>	<b>97.94</b>	<b>98.99</b>	<b>98.15</b>	<b>97.49</b>	<b>97.70</b>	<b>97.29</b>	<b>97.73</b>	<b>98.80</b>	<b>98.73</b>	<b>98.42</b>	<b>98.82</b>	<b>99.48</b>	<b>98.49</b>	<b>97.99</b>	<b>97.92</b>	<b>98.11</b>	<b>98.96</b>	<b>98.13</b>	<b>99.05</b>	<b>99.19</b>
<b>Cations</b>																				
Cr	9.38	9.37	9.38	9.54	9.46	9.50	9.50	9.49	9.48	9.50	9.47	9.36	9.47	9.45	9.44	9.43	9.35	9.37	9.44	9.47
Al	4.92	5.19	4.91	4.84	4.77	4.90	4.87	4.74	4.86	4.80	4.76	4.75	4.71	4.85	4.75	4.71	4.79	4.85	4.71	4.71
V	0.18	0.16	0.16	0.16	0.19	0.14	0.14	0.15	0.17	0.15	0.21	0.22	0.15	0.19	0.17	0.17	0.19	0.16	0.17	0.20
Ti	0.15	0.10	0.20	0.16	0.17	0.17	0.17	0.19	0.16	0.18	0.18	0.20	0.16	0.18	0.20	0.22	0.23	0.22	0.19	0.20
Fe3+	1.21	1.06	1.13	1.11	1.21	1.09	1.14	1.23	1.15	1.17	1.19	1.26	1.33	1.13	1.21	1.23	1.19	1.17	1.26	1.19
Fe2+	4.98	4.87	5.04	5.10	5.04	5.08	5.11	5.07	5.01	5.15	5.02	5.15	5.12	5.23	5.15	5.01	5.08	5.04	5.07	5.10
Mg	3.15	3.13	3.11	3.03	3.10	3.08	3.08	2.99	3.16	3.05	3.08	3.07	3.03	2.98	3.01	3.23	3.08	3.13	3.09	3.08
Mn	0.04	0.06	0.07	0.00	0.06	0.04	0.00	0.08	0.00	0.00	0.10	0.00	0.04	0.00	0.07	0.00	0.05	0.00	0.06	0.05
Ni	0.00	0.06	0.00	0.05	0.00	0.00	0.00	0.07	0.00	0.00	0.00	0.00	0.00	0.00	0.00	0.00	0.05	0.07	0.00	0.00
<b>Total</b>	<b>24.00</b>	<b>24.00</b>	<b>24.00</b>	<b>24.00</b>	<b>24.00</b>	<b>24.00</b>	<b>24.00</b>	<b>24.00</b>	<b>24.00</b>	<b>24.00</b>	<b>24.00</b>	<b>24.00</b>	<b>24.00</b>	<b>24.00</b>	<b>24.00</b>	<b>24.00</b>	<b>24.00</b>	<b>24.00</b>	<b>24.00</b>	<b>24.00</b>
<b>Cation allocation</b>																				
2+	8.17	8.06	8.22	8.13	8.20	8.19	8.19	8.14	8.18	8.20	8.20	8.22	8.19	8.20	8.22	8.25	8.20	8.17	8.22	8.23
3+	15.83	15.94	15.78	15.87	15.80	15.81	15.81	15.86	15.82	15.80	15.80	15.78	15.81	15.80	15.78	15.75	15.80	15.83	15.78	15.77
<b>Major cation ratios</b>																				
100Mg/Mg+Fe2+	31.79	31.15	31.25	30.45	31.62	30.85	30.86	30.48	32.03	30.68	31.51	31.05	30.81	29.55	30.37	33.28	31.18	31.66	31.57	31.43
100Cr/Cr+Al	65.57	64.35	65.63	66.32	66.46	65.96	66.11	66.68	66.10	66.43	66.55	66.35	66.79	66.09	66.51	66.71	66.13	65.89	66.69	66.78
100Fe3+/Cr+Al+V+Fe3+	7.68	6.69	7.23	7.07	7.72	7.00	7.26	7.85	7.35	7.51	7.64	8.06	8.47	7.22	7.77	7.90	7.66	7.51	8.10	7.66

8/15

UM

	21	22	23	24	25	26	27	28	29	30	31	32	33	34	35	36	37	38	39	40
<b>Analysed totals</b>																				
Cr2O3	43.97	44.62	45.19	43.76	43.88	44.17	44.74	43.93	43.99	44.26	44.58	44.49	44.72	44.13	44.46	44.45	44.75	43.92	44.45	45.00
Al2O3	15.98	15.55	15.91	16.08	15.64	15.77	15.65	15.51	15.38	15.79	15.84	15.91	16.09	16.05	15.84	15.28	15.50	15.56	15.31	15.61
V2O3	0.59	0.94	0.70	0.53	0.80	0.52	0.60	0.68	0.99	0.67	0.98	0.75	0.64	0.37	0.73	0.70	0.56	0.65	0.58	0.78
TiO2	0.90	0.94	0.88	0.87	0.87	0.97	0.85	1.04	0.95	1.10	0.97	1.06	1.08	1.04	0.95	1.04	0.92	0.90	1.05	0.81
FeO	22.44	22.87	22.83	22.01	22.22	22.23	22.42	22.82	22.53	22.99	22.37	22.72	23.22	22.27	21.84	22.52	22.58	22.88	22.89	22.59
Fe2O3	5.58	5.46	4.80	6.11	5.68	5.86	5.58	5.73	5.92	5.27	5.76	5.33	4.94	5.56	5.56	5.59	5.34	6.10	5.77	5.24
MgO	7.97	7.66	7.83	8.08	7.88	8.04	7.91	7.75	7.86	7.80	8.10	7.93	7.79	7.94	8.16	7.76	7.85	7.70	7.65	7.74
MnO	0.00	0.30	0.00	0.35	0.19	0.00	0.15	0.00	0.15	0.00	0.17	0.21	0.00	0.19	0.29	0.33	0.00	0.00	0.22	0.00
NiO	0.00	0.00	0.00	0.00	0.00	0.25	0.00	0.00	0.00	0.00	0.28	0.00	0.00	0.27	0.25	0.00	0.00	0.00	0.00	0.25
<b>Total</b>	<b>97.43</b>	<b>98.34</b>	<b>98.14</b>	<b>97.79</b>	<b>97.16</b>	<b>97.80</b>	<b>97.91</b>	<b>97.46</b>	<b>97.78</b>	<b>97.89</b>	<b>99.04</b>	<b>98.40</b>	<b>98.47</b>	<b>97.84</b>	<b>98.08</b>	<b>97.66</b>	<b>97.51</b>	<b>97.72</b>	<b>97.93</b>	<b>98.01</b>
<b>Cations</b>																				
Cr	9.31	9.40	9.51	9.22	9.33	9.32	9.45	9.33	9.31	9.35	9.30	9.34	9.38	9.31	9.35	9.43	9.49	9.31	9.41	9.50
Al	5.04	4.88	4.99	5.05	4.96	4.96	4.93	4.91	4.85	4.97	4.92	4.98	5.03	5.05	4.97	4.83	4.90	4.92	4.84	4.92
V	0.14	0.22	0.17	0.13	0.19	0.12	0.15	0.16	0.24	0.16	0.23	0.18	0.15	0.09	0.17	0.17	0.13	0.16	0.14	0.19
Ti	0.18	0.19	0.18	0.17	0.18	0.20	0.17	0.21	0.19	0.22	0.19	0.21	0.22	0.21	0.19	0.21	0.19	0.18	0.21	0.16
Fe3+	1.12	1.10	0.96	1.22	1.15	1.18	1.12	1.16	1.19	1.06	1.14	1.07	0.99	1.12	1.11	1.13	1.08	1.23	1.16	1.05
Fe2+	5.02	5.10	5.08	4.91	5.00	4.97	5.01	5.13	5.04	5.14	4.93	5.04	5.15	4.97	4.86	5.05	5.07	5.13	5.13	5.05
Mg	3.18	3.04	3.11	3.21	3.16	3.20	3.15	3.10	3.14	3.10	3.18	3.14	3.08	3.16	3.23	3.10	3.14	3.08	3.06	3.08
Mn	0.00	0.07	0.00	0.08	0.04	0.00	0.03	0.00	0.03	0.00	0.04	0.05	0.00	0.04	0.07	0.07	0.00	0.00	0.05	0.00
Ni	0.00	0.00	0.00	0.00	0.00	0.05	0.00	0.00	0.00	0.00	0.06	0.00	0.00	0.06	0.05	0.00	0.00	0.00	0.00	0.05
<b>Total</b>	<b>24.00</b>	<b>24.00</b>	<b>24.00</b>	<b>24.00</b>	<b>24.00</b>	<b>24.00</b>	<b>24.00</b>	<b>24.00</b>	<b>24.00</b>	<b>24.00</b>	<b>24.00</b>	<b>24.00</b>	<b>24.00</b>	<b>24.00</b>	<b>24.00</b>	<b>24.00</b>	<b>24.00</b>	<b>24.00</b>	<b>24.00</b>	<b>24.00</b>
<b>Cation allocation</b>																				
2+	8.20	8.21	8.19	8.20	8.20	8.16	8.19	8.23	8.21	8.24	8.15	8.23	8.23	8.17	8.16	8.23	8.21	8.21	8.23	8.13
3+	15.80	15.79	15.81	15.80	15.80	15.84	15.81	15.77	15.79	15.76	15.85	15.77	15.77	15.83	15.84	15.77	15.79	15.79	15.77	15.87
<b>Major cation ratios</b>																				
100Mg/Mg+Fe2+	31.57	30.46	30.84	32.24	31.71	32.22	31.70	30.93	31.70	30.69	32.30	31.31	30.22	31.51	32.92	31.37	31.46	30.63	30.67	30.93
100Cr/Cr+Al	64.85	65.81	65.57	64.61	65.30	65.26	65.71	65.51	65.73	65.27	65.37	65.22	65.08	64.83	65.30	66.11	65.93	65.43	66.06	65.90
100Fe3+/Cr+Al+V+Fe3+	7.20	7.02	6.15	7.84	7.35	7.55	7.16	7.45	7.65	6.82	7.33	6.85	6.34	7.17	7.13	7.25	6.91	7.88	7.48	6.72

9/15	UM																			
	41	42	43	44	45	46	47	48	49	50	51	52	53	54	55	56	57	58	59	60
<b>Analysed totals</b>																				
Cr2O3	44.49	44.13	44.75	44.65	44.11	44.11	44.18	44.14	44.67	44.08	44.69	44.86	44.75	44.94	44.52	44.87	45.18	44.83	45.08	45.13
Al2O3	16.95	17.31	16.46	17.21	17.17	16.96	16.86	16.79	16.89	17.35	16.43	16.49	16.70	16.52	16.46	16.57	16.74	15.84	16.22	16.05
V2O3	0.77	0.79	0.84	0.74	0.81	0.88	0.87	0.90	0.71	0.62	0.94	1.01	0.77	0.79	0.69	0.85	0.63	0.75	0.58	0.84
TiO2	1.03	0.97	1.01	1.04	0.85	0.94	0.99	2.00	1.08	0.91	0.97	0.98	1.13	1.07	1.12	1.01	0.98	1.06	0.93	1.07
FeO	22.59	22.26	22.46	22.65	22.19	22.50	22.43	23.42	22.60	22.13	22.42	22.34	22.52	22.53	22.53	23.03	22.66	22.81	22.44	22.61
Fe2O3	5.13	5.50	5.71	5.11	5.82	5.43	5.53	4.08	5.22	5.44	5.24	5.22	5.18	5.43	5.85	5.27	5.26	5.49	5.40	5.90
MgO	8.37	8.53	8.24	8.32	8.69	8.37	8.40	8.39	8.35	8.51	8.29	8.33	8.48	8.37	8.39	8.20	8.35	8.01	8.12	8.35
MnO	0.15	0.19	0.30	0.22	0.00	0.11	0.00	0.13	0.33	0.29	0.22	0.24	0.17	0.13	0.32	0.00	0.19	0.17	0.14	0.13
NiO	0.00	0.18	0.28	0.21	0.00	0.00	0.24	0.19	0.00	0.00	0.00	0.18	0.00	0.24	0.00	0.00	0.00	0.00	0.24	0.21
<b>Total</b>	<b>99.47</b>	<b>99.86</b>	<b>100.05</b>	<b>100.15</b>	<b>99.64</b>	<b>99.30</b>	<b>99.50</b>	<b>100.04</b>	<b>99.83</b>	<b>99.33</b>	<b>99.20</b>	<b>99.65</b>	<b>99.71</b>	<b>100.00</b>	<b>99.87</b>	<b>99.79</b>	<b>100.00</b>	<b>98.96</b>	<b>99.15</b>	<b>100.29</b>
<b>Cations</b>																				
Cr	9.18	9.05	9.21	9.15	9.06	9.11	9.11	9.06	9.19	9.08	9.27	9.26	9.22	9.25	9.17	9.26	9.29	9.36	9.38	9.28
Al	5.21	5.29	5.06	5.26	5.26	5.23	5.19	5.14	5.18	5.33	5.08	5.08	5.13	5.07	5.06	5.10	5.13	4.93	5.03	4.92
V	0.18	0.18	0.20	0.17	0.19	0.21	0.20	0.21	0.17	0.14	0.22	0.24	0.18	0.19	0.16	0.20	0.15	0.18	0.14	0.20
Ti	0.20	0.19	0.20	0.20	0.17	0.18	0.20	0.39	0.21	0.18	0.19	0.19	0.22	0.21	0.22	0.20	0.19	0.21	0.18	0.21
Fe3+	1.01	1.07	1.12	1.00	1.14	1.07	1.09	0.80	1.02	1.07	1.03	1.03	1.02	1.06	1.15	1.03	1.03	1.09	1.07	1.16
Fe2+	4.93	4.83	4.89	4.91	4.82	4.92	4.90	5.08	4.92	4.82	4.92	4.88	4.91	4.90	4.91	5.03	4.93	5.04	4.94	4.92
Mg	3.25	3.30	3.20	3.22	3.37	3.26	3.27	3.25	3.24	3.31	3.24	3.24	3.29	3.25	3.26	3.19	3.24	3.15	3.18	3.24
Mn	0.03	0.04	0.07	0.05	0.00	0.02	0.00	0.03	0.07	0.07	0.05	0.05	0.04	0.03	0.07	0.00	0.04	0.04	0.03	0.03
Ni	0.00	0.04	0.06	0.04	0.00	0.00	0.05	0.04	0.00	0.00	0.00	0.04	0.00	0.05	0.00	0.00	0.00	0.00	0.05	0.04
<b>Total</b>	<b>24.00</b>	<b>24.00</b>	<b>24.00</b>	<b>24.00</b>	<b>24.00</b>	<b>24.00</b>	<b>24.00</b>	<b>24.00</b>	<b>24.00</b>	<b>24.00</b>	<b>24.00</b>	<b>24.00</b>	<b>24.00</b>	<b>24.00</b>	<b>24.00</b>	<b>24.00</b>	<b>24.00</b>	<b>24.00</b>	<b>24.00</b>	<b>24.00</b>
<b>Cation allocation</b>																				
2+	8.22	8.17	8.16	8.18	8.19	8.20	8.16	8.36	8.23	8.20	8.21	8.17	8.24	8.18	8.24	8.22	8.21	8.23	8.15	8.19
3+	15.78	15.83	15.84	15.82	15.81	15.80	15.84	15.64	15.77	15.80	15.79	15.83	15.76	15.82	15.76	15.78	15.79	15.77	15.85	15.81
<b>Major cation ratios</b>																				
100Mg/Mg+Fe2+	32.09	32.59	32.16	31.61	33.38	32.16	32.41	31.77	32.05	32.56	32.42	32.55	32.82	32.54	32.69	31.51	32.17	31.63	31.93	32.91
100Cr/Cr+Al	63.77	63.10	64.58	63.50	63.27	63.55	63.73	63.81	63.95	63.01	64.58	64.59	64.24	64.59	64.46	64.49	64.41	65.49	65.09	65.35
100Fe3+/Cr+Al+V+Fe3+	6.47	6.88	7.18	6.40	7.28	6.84	6.97	5.25	6.57	6.83	6.63	6.58	6.53	6.83	7.38	6.64	6.60	7.01	6.84	7.43



10/15	UM																			
	61	62	63	64	65	66	67	68	69	70	71	72	73	74	75	76	77	78	79	80
<b>Analysed totals</b>																				
Cr2O3	46.10	46.15	46.32	45.88	46.10	46.48	46.41	46.63	45.88	45.95	45.74	46.13	45.96	45.71	46.03	45.86	45.09	45.57	46.19	45.98
Al2O3	14.78	15.14	14.58	14.69	14.75	15.00	14.69	15.27	14.77	14.69	15.24	15.06	14.67	15.36	15.18	15.17	15.33	15.06	14.94	14.79
V2O3	0.71	0.89	0.66	0.82	0.87	0.92	0.76	0.89	0.85	0.74	0.99	0.81	0.70	0.91	0.90	0.85	0.93	0.94	0.88	0.66
TiO2	0.91	1.06	1.17	1.17	1.22	1.07	1.21	0.93	1.08	1.30	0.96	1.01	1.10	0.85	1.02	0.81	1.03	1.03	1.08	1.16
FeO	22.53	22.94	22.89	22.66	22.88	23.08	23.18	23.33	22.98	23.16	22.80	22.67	22.71	23.02	23.04	22.64	22.58	23.32	23.00	22.94
Fe2O3	6.19	5.51	5.37	5.61	5.83	5.32	5.55	5.48	6.11	5.52	5.52	5.83	5.69	6.21	5.78	6.13	5.86	5.77	5.68	5.56
MgO	8.02	8.00	8.02	7.90	8.07	8.08	8.04	7.88	7.94	7.84	8.09	8.05	7.87	7.98	7.96	8.03	8.10	7.82	8.00	7.77
MnO	0.16	0.28	0.00	0.27	0.36	0.00	0.00	0.00	0.27	0.09	0.00	0.22	0.12	0.17	0.29	0.26	0.23	0.00	0.21	0.27
NiO	0.20	0.00	0.00	0.23	0.00	0.00	0.00	0.18	0.00	0.20	0.00	0.21	0.27	0.00	0.00	0.00	0.00	0.00	0.00	0.17
<b>Total</b>	<b>99.59</b>	<b>99.98</b>	<b>99.02</b>	<b>99.23</b>	<b>100.07</b>	<b>99.95</b>	<b>99.83</b>	<b>100.61</b>	<b>99.89</b>	<b>99.49</b>	<b>99.33</b>	<b>99.99</b>	<b>99.09</b>	<b>100.20</b>	<b>100.19</b>	<b>99.75</b>	<b>99.15</b>	<b>99.52</b>	<b>100.00</b>	<b>99.29</b>
<b>Cations</b>																				
Cr	9.62	9.58	9.72	9.61	9.57	9.65	9.66	9.63	9.55	9.61	9.54	9.57	9.64	9.46	9.54	9.54	9.41	9.51	9.59	9.63
Al	4.60	4.68	4.56	4.59	4.57	4.64	4.56	4.70	4.59	4.58	4.74	4.66	4.59	4.74	4.69	4.71	4.77	4.69	4.63	4.62
V	0.17	0.21	0.16	0.20	0.21	0.22	0.18	0.21	0.20	0.18	0.23	0.19	0.17	0.21	0.21	0.20	0.22	0.22	0.21	0.16
Ti	0.18	0.21	0.23	0.23	0.24	0.21	0.24	0.18	0.21	0.26	0.19	0.20	0.22	0.17	0.20	0.16	0.20	0.20	0.21	0.23
Fe3+	1.23	1.09	1.07	1.12	1.15	1.05	1.10	1.08	1.21	1.10	1.09	1.15	1.14	1.22	1.14	1.21	1.16	1.15	1.12	1.11
Fe2+	4.97	5.04	5.08	5.02	5.03	5.07	5.11	5.09	5.06	5.12	5.03	4.98	5.04	5.04	5.05	4.98	4.99	5.15	5.05	5.08
Mg	3.15	3.13	3.17	3.12	3.16	3.16	3.15	3.07	3.12	3.09	3.18	3.15	3.12	3.11	3.11	3.15	3.19	3.08	3.13	3.07
Mn	0.04	0.06	0.00	0.06	0.08	0.00	0.00	0.00	0.06	0.02	0.00	0.05	0.03	0.04	0.06	0.06	0.05	0.00	0.05	0.06
Ni	0.04	0.00	0.00	0.05	0.00	0.00	0.00	0.04	0.00	0.04	0.00	0.04	0.06	0.00	0.00	0.00	0.00	0.00	0.00	0.04
<b>Total</b>	<b>24.00</b>	<b>24.00</b>	<b>24.00</b>	<b>24.00</b>	<b>24.00</b>	<b>24.00</b>	<b>24.00</b>	<b>24.00</b>	<b>24.00</b>	<b>24.00</b>	<b>24.00</b>	<b>24.00</b>	<b>24.00</b>	<b>24.00</b>	<b>24.00</b>	<b>24.00</b>	<b>24.00</b>	<b>24.00</b>	<b>24.00</b>	<b>24.00</b>
<b>Cation allocation</b>																				
2+	8.16	8.23	8.25	8.20	8.26	8.23	8.26	8.16	8.24	8.23	8.21	8.18	8.18	8.19	8.22	8.18	8.23	8.23	8.23	8.21
3+	15.84	15.77	15.75	15.80	15.74	15.77	15.74	15.84	15.76	15.77	15.79	15.82	15.82	15.81	15.78	15.82	15.77	15.77	15.77	15.79
<b>Major cation ratios</b>																				
100Mg/Mg+Fe2+	32.95	32.20	32.90	32.44	32.93	32.55	32.63	31.32	32.31	31.86	32.57	32.69	32.34	31.82	31.92	32.48	32.68	31.28	32.37	31.62
100Cr/Cr+Al	67.66	67.15	68.05	67.69	67.70	67.52	67.93	67.19	67.56	67.72	66.81	67.25	67.75	66.62	67.04	66.96	66.35	66.99	67.46	67.58
100Fe3+/Cr+Al+V+Fe3+	7.87	7.00	6.92	7.21	7.43	6.76	7.09	6.90	7.79	7.10	7.02	7.39	7.31	7.83	7.31	7.75	7.47	7.37	7.23	7.15

11/15	UM																			
	81	82	83	84	85	86	87	88	89	90	91	92	93	94	95	96	97	98	99	100
<b>Analysed totals</b>																				
Cr2O3	44.98	45.21	44.90	45.24	45.28	45.59	44.76	45.36	46.16	45.66	45.24	45.21	46.08	45.44	46.02	45.49	45.44	45.58	46.06	45.55
Al2O3	14.95	14.74	15.07	14.78	15.08	15.08	14.87	15.23	14.95	15.16	14.78	14.75	15.41	14.84	15.10	15.05	14.90	15.68	14.74	15.03
V2O3	0.85	0.59	0.81	0.87	0.75	0.80	0.85	0.61	0.59	0.77	0.81	0.67	0.96	0.87	0.88	0.77	0.69	0.73	0.61	0.56
TiO2	1.20	1.33	1.28	1.10	1.12	1.34	1.29	1.25	1.40	1.32	1.24	1.03	1.02	1.26	1.24	1.29	1.02	1.07	1.36	1.28
FeO	22.78	23.28	23.31	22.98	23.31	23.38	23.31	23.52	24.04	23.39	23.57	23.04	23.30	23.29	23.35	23.47	22.40	23.11	23.20	23.31
Fe2O3	5.71	5.18	5.31	5.90	5.58	5.61	5.86	6.05	5.53	5.22	5.62	6.22	5.52	5.38	5.33	5.63	5.99	5.52	5.07	5.45
MgO	7.89	7.56	7.54	7.74	7.65	7.77	7.80	7.72	7.62	7.70	7.47	7.65	7.83	7.82	8.01	7.62	7.97	8.09	7.71	7.86
MnO	0.28	0.15	0.34	0.27	0.15	0.22	0.00	0.35	0.19	0.16	0.25	0.26	0.34	0.00	0.00	0.22	0.16	0.00	0.39	0.00
NiO	0.00	0.00	0.00	0.00	0.00	0.24	0.00	0.00	0.00	0.26	0.00	0.00	0.00	0.00	0.00	0.24	0.28	0.00	0.00	0.00
<b>Total</b>	<b>98.65</b>	<b>98.04</b>	<b>98.56</b>	<b>98.89</b>	<b>98.91</b>	<b>100.03</b>	<b>98.74</b>	<b>100.09</b>	<b>100.48</b>	<b>99.63</b>	<b>98.98</b>	<b>98.81</b>	<b>100.47</b>	<b>98.91</b>	<b>99.93</b>	<b>99.79</b>	<b>98.85</b>	<b>99.79</b>	<b>99.15</b>	<b>99.05</b>
<b>Cations</b>																				
Cr	9.46	9.59	9.47	9.51	9.51	9.48	9.42	9.42	9.57	9.52	9.52	9.52	9.52	9.54	9.55	9.49	9.54	9.45	9.67	9.55
Al	4.69	4.66	4.74	4.63	4.72	4.67	4.67	4.72	4.62	4.72	4.64	4.63	4.75	4.65	4.68	4.68	4.67	4.85	4.61	4.70
V	0.20	0.14	0.19	0.21	0.18	0.19	0.20	0.14	0.14	0.18	0.19	0.16	0.23	0.21	0.21	0.18	0.16	0.17	0.15	0.13
Ti	0.24	0.27	0.26	0.22	0.22	0.26	0.26	0.25	0.28	0.26	0.25	0.21	0.20	0.25	0.24	0.26	0.20	0.21	0.27	0.26
Fe3+	1.14	1.05	1.07	1.18	1.12	1.11	1.17	1.20	1.09	1.04	1.13	1.25	1.08	1.08	1.05	1.12	1.20	1.09	1.01	1.09
Fe2+	5.07	5.23	5.20	5.11	5.18	5.14	5.19	5.17	5.27	5.16	5.25	5.14	5.09	5.17	5.13	5.18	4.98	5.07	5.15	5.17
Mg	3.13	3.03	3.00	3.07	3.03	3.04	3.09	3.02	2.98	3.03	2.96	3.04	3.05	3.10	3.13	3.00	3.16	3.16	3.05	3.11
Mn	0.06	0.03	0.08	0.06	0.03	0.05	0.00	0.08	0.04	0.03	0.06	0.06	0.08	0.00	0.00	0.05	0.04	0.00	0.09	0.00
Ni	0.00	0.00	0.00	0.00	0.00	0.05	0.00	0.00	0.00	0.05	0.00	0.00	0.00	0.00	0.00	0.05	0.06	0.00	0.00	0.00
<b>Total</b>	<b>24.00</b>	<b>24.00</b>	<b>24.00</b>	<b>24.00</b>	<b>24.00</b>	<b>24.00</b>	<b>24.00</b>	<b>24.00</b>	<b>24.00</b>	<b>24.00</b>	<b>24.00</b>	<b>24.00</b>	<b>24.00</b>	<b>24.00</b>	<b>24.00</b>	<b>24.00</b>	<b>24.00</b>	<b>24.00</b>	<b>24.00</b>	<b>24.00</b>
<b>Cation allocation</b>																				
2+	8.26	8.29	8.28	8.24	8.24	8.23	8.28	8.27	8.30	8.22	8.27	8.23	8.22	8.27	8.26	8.23	8.17	8.23	8.29	8.28
3+	15.74	15.71	15.72	15.76	15.76	15.77	15.72	15.73	15.70	15.78	15.73	15.77	15.78	15.73	15.74	15.77	15.83	15.77	15.71	15.72
<b>Major cation ratios</b>																				
100Mg/Mg+Fe2+	32.06	30.60	30.17	31.49	30.58	31.00	31.39	30.58	30.11	30.65	29.96	31.09	31.01	31.52	31.97	30.40	32.72	31.90	31.23	31.46
100Cr/Cr+Al	66.86	67.29	66.64	67.24	66.82	66.97	66.87	66.63	67.43	66.88	67.24	67.27	66.73	67.24	67.14	66.96	67.16	66.09	67.69	67.02
100Fe3+/Cr+Al+V+Fe3+	7.38	6.77	6.89	7.60	7.19	7.18	7.60	7.73	7.08	6.71	7.28	8.01	6.96	6.96	6.80	7.23	7.69	7.00	6.56	7.03

12/15

UM

	101	102	103	104	105	106	107	108	109	110	111	112	113	114	115	116	117	118	119	120
<b>Analysed totals</b>																				
Cr2O3	44.85	44.98	45.36	45.69	45.65	44.77	46.27	45.67	45.30	46.08	44.72	45.23	45.56	45.13	45.34	45.79	44.90	45.46	45.73	45.74
Al2O3	15.51	15.21	15.16	15.17	15.24	15.19	15.38	15.32	15.09	15.30	15.02	15.70	15.18	15.70	15.46	15.49	15.36	15.32	15.49	15.45
V2O3	1.06	0.93	0.94	0.87	0.91	0.92	0.60	1.08	0.83	0.89	1.03	0.92	0.57	0.78	1.04	0.59	0.96	0.69	0.89	0.85
TiO2	1.21	1.15	1.17	1.19	0.94	1.29	1.33	1.50	1.46	1.17	1.24	0.96	1.24	1.13	1.36	1.23	1.08	1.28	1.17	1.21
FeO	23.33	23.13	23.29	23.19	23.19	23.11	23.35	23.61	22.97	23.31	22.77	22.85	22.99	23.24	23.38	23.12	22.87	23.22	23.31	23.64
Fe2O3	5.53	5.60	5.77	5.81	5.23	5.81	5.68	5.16	5.77	5.18	6.41	5.35	6.00	5.34	5.41	5.82	5.93	5.28	5.69	5.19
MgO	7.72	7.79	7.96	7.98	7.74	7.90	8.08	7.86	8.03	7.86	7.99	7.91	8.01	7.84	8.00	8.04	7.99	7.87	7.97	7.83
MnO	0.40	0.19	0.00	0.26	0.00	0.27	0.37	0.19	0.30	0.27	0.27	0.25	0.35	0.17	0.25	0.17	0.21	0.22	0.30	0.00
NiO	0.00	0.00	0.00	0.00	0.00	0.00	0.00	0.28	0.30	0.00	0.30	0.00	0.00	0.00	0.00	0.25	0.00	0.00	0.00	0.00
Total	99.61	98.99	99.65	100.16	98.90	99.25	101.06	100.66	100.05	100.06	99.75	99.17	99.90	99.32	100.24	100.50	99.29	99.36	100.54	99.92
<b>Cations</b>																				
Cr	9.34	9.43	9.44	9.47	9.58	9.36	9.50	9.42	9.40	9.56	9.31	9.43	9.46	9.41	9.37	9.45	9.37	9.49	9.43	9.49
Al	4.82	4.75	4.71	4.69	4.77	4.73	4.71	4.71	4.67	4.73	4.66	4.88	4.70	4.88	4.77	4.77	4.78	4.77	4.76	4.78
V	0.25	0.22	0.22	0.21	0.22	0.22	0.14	0.25	0.20	0.21	0.24	0.22	0.13	0.18	0.24	0.14	0.23	0.16	0.21	0.20
Ti	0.24	0.23	0.23	0.24	0.19	0.26	0.26	0.29	0.29	0.23	0.25	0.19	0.24	0.22	0.27	0.24	0.21	0.26	0.23	0.24
Fe3+	1.10	1.12	1.14	1.15	1.05	1.16	1.11	1.01	1.14	1.02	1.27	1.06	1.19	1.06	1.07	1.14	1.18	1.05	1.12	1.03
Fe2+	5.14	5.13	5.13	5.08	5.15	5.11	5.07	5.15	5.04	5.11	5.01	5.04	5.05	5.13	5.11	5.05	5.05	5.13	5.09	5.19
Mg	3.03	3.08	3.12	3.12	3.06	3.11	3.13	3.06	3.14	3.07	3.14	3.11	3.14	3.08	3.12	3.13	3.14	3.10	3.10	3.06
Mn	0.09	0.04	0.00	0.06	0.00	0.06	0.08	0.04	0.07	0.06	0.06	0.06	0.08	0.04	0.05	0.04	0.05	0.05	0.07	0.00
Ni	0.00	0.00	0.00	0.00	0.00	0.00	0.00	0.06	0.06	0.00	0.06	0.00	0.00	0.00	0.00	0.05	0.00	0.00	0.00	0.00
Total	24.00	24.00	24.00	24.00	24.00	24.00	24.00	24.00	24.00	24.00	24.00	24.00	24.00	24.00	24.00	24.00	24.00	24.00	24.00	24.00
<b>Cation allocation</b>																				
2+	8.26	8.25	8.25	8.26	8.21	8.28	8.28	8.25	8.25	8.25	8.21	8.21	8.27	8.24	8.29	8.21	8.24	8.27	8.25	8.26
3+	15.74	15.75	15.75	15.74	15.79	15.72	15.72	15.75	15.75	15.75	15.79	15.79	15.73	15.76	15.71	15.79	15.76	15.73	15.75	15.74
<b>Major cation ratios</b>																				
100Mg/Mg+Fe2+	30.43	31.16	31.77	31.90	30.86	31.61	31.97	31.00	32.33	31.22	32.41	31.35	32.14	30.79	31.55	31.87	31.97	31.29	31.45	30.72
100Cr/Cr+Al	65.98	66.48	66.74	66.89	66.77	66.41	66.85	66.65	66.82	66.88	66.63	65.89	66.81	65.84	66.29	66.46	66.21	66.55	66.45	66.49
100Fe3+/Cr+Al+V+Fe3+	7.07	7.20	7.37	7.40	6.70	7.47	7.19	6.58	7.40	6.59	8.20	6.81	7.66	6.82	6.90	7.38	7.58	6.78	7.20	6.61

13/15

UM

	121	122	123	124	125	126	127	128	129	130	131	132	133	134	135	136	137	138	139	140
<b>Analysed totals</b>																				
Cr2O3	44.97	45.24	45.12	45.47	45.53	46.15	45.33	45.54	45.71	46.12	45.83	44.83	46.04	45.06	45.27	45.49	45.72	45.44	46.08	45.45
Al2O3	15.03	14.73	15.10	15.18	15.60	15.28	15.14	15.13	14.95	14.90	15.07	15.38	14.95	15.45	15.28	15.69	15.16	15.18	14.98	14.99
V2O3	0.98	0.97	0.85	0.96	0.83	0.70	0.94	0.97	0.86	0.91	0.64	1.15	0.66	0.94	0.94	0.52	1.09	0.99	1.04	0.76
TiO2	1.08	1.16	1.09	1.08	0.92	0.98	1.21	1.16	0.92	1.01	1.11	0.98	0.89	1.15	1.01	1.15	0.98	1.02	1.05	0.96
FeO	22.81	23.10	23.07	23.63	23.33	23.24	23.69	23.17	22.89	22.99	23.16	22.34	23.08	23.36	22.89	23.29	23.19	23.24	23.29	22.88
Fe2O3	5.82	5.79	6.19	5.02	5.37	5.56	5.07	5.47	5.65	5.21	5.93	6.20	5.54	5.55	5.62	5.08	5.55	5.71	5.54	5.98
MgO	7.92	7.73	7.82	7.51	7.76	7.80	7.40	7.97	7.76	7.90	8.01	8.01	7.75	7.87	8.01	7.87	7.77	7.73	7.72	7.77
MnO	0.17	0.24	0.33	0.00	0.00	0.22	0.29	0.00	0.00	0.00	0.00	0.48	0.00	0.00	0.00	0.00	0.00	0.24	0.14	0.31
NiO	0.00	0.00	0.00	0.00	0.00	0.00	0.00	0.00	0.24	0.00	0.00	0.25	0.00	0.00	0.00	0.00	0.23	0.00	0.24	0.00
Total	98.77	98.96	99.59	98.85	99.35	99.92	99.08	99.40	98.97	99.04	99.74	99.62	98.91	99.38	99.02	99.10	99.69	99.57	100.07	99.10
<b>Cations</b>																				
Cr	9.44	9.51	9.41	9.56	9.50	9.59	9.52	9.50	9.60	9.67	9.54	9.32	9.67	9.40	9.47	9.50	9.53	9.48	9.58	9.53
Al	4.71	4.62	4.70	4.76	4.85	4.74	4.74	4.71	4.68	4.66	4.68	4.77	4.69	4.80	4.77	4.89	4.71	4.72	4.64	4.69
V	0.23	0.23	0.20	0.23	0.20	0.16	0.23	0.23	0.20	0.22	0.15	0.27	0.16	0.22	0.22	0.12	0.26	0.24	0.25	0.18
Ti	0.22	0.23	0.22	0.22	0.18	0.19	0.24	0.23	0.18	0.20	0.22	0.19	0.18	0.23	0.20	0.23	0.19	0.20	0.21	0.19
Fe3+	1.16	1.16	1.23	1.00	1.07	1.10	1.01	1.09	1.13	1.04	1.18	1.23	1.11	1.10	1.12	1.01	1.10	1.13	1.10	1.19
Fe2+	5.07	5.14	5.09	5.25	5.15	5.11	5.26	5.11	5.08	5.10	5.10	4.91	5.13	5.15	5.06	5.15	5.11	5.13	5.12	5.07
Mg	3.13	3.06	3.07	2.98	3.05	3.05	2.93	3.14	3.07	3.12	3.14	3.14	3.07	3.10	3.16	3.10	3.05	3.04	3.02	3.07
Mn	0.04	0.05	0.07	0.00	0.00	0.05	0.07	0.00	0.00	0.00	0.00	0.11	0.00	0.00	0.00	0.00	0.00	0.05	0.03	0.07
Ni	0.00	0.00	0.00	0.00	0.00	0.00	0.00	0.00	0.05	0.00	0.00	0.05	0.00	0.00	0.00	0.00	0.05	0.00	0.05	0.00
Total	24.00	24.00	24.00	24.00	24.00	24.00	24.00	24.00	24.00	24.00	24.00	24.00	24.00	24.00	24.00	24.00	24.00	24.00	24.00	24.00
<b>Cation allocation</b>																				
2+	8.24	8.25	8.24	8.23	8.20	8.21	8.26	8.25	8.15	8.22	8.24	8.16	8.20	8.25	8.22	8.25	8.16	8.22	8.18	8.22
3+	15.76	15.75	15.76	15.77	15.80	15.79	15.74	15.75	15.85	15.78	15.76	15.84	15.80	15.75	15.78	15.75	15.84	15.78	15.82	15.78
<b>Major cation ratios</b>																				
100Mg/Mg+Fe2+	32.06	31.41	31.41	29.74	30.52	31.03	29.30	31.93	31.43	31.99	32.14	32.44	31.26	31.08	32.11	30.89	31.09	30.85	30.97	31.46
100Cr/Cr+Al	66.73	67.31	66.70	66.76	66.19	66.95	66.75	66.87	67.21	67.48	67.10	66.16	67.37	66.17	66.52	66.03	66.92	66.75	67.35	67.03
100Fe3+/Cr+Al+V+Fe3+	7.48	7.47	7.91	6.46	6.83	7.05	6.54	7.00	7.24	6.67	7.56	7.87	7.09	7.09	7.18	6.51	7.06	7.28	7.04	7.66

14/15

UM

	141	142	143	144	145	146	147	148	149	150	151	152	153	154	155	156	157	158	159	160
<b>Analysed totals</b>																				
Cr2O3	45.97	46.05	45.21	45.13	44.86	45.92	44.70	44.82	45.44	44.90	45.81	45.05	45.01	45.38	45.28	45.32	44.99	45.43	45.53	45.48
Al2O3	15.02	15.14	15.24	15.36	15.41	15.39	15.20	15.18	15.27	15.34	15.02	15.17	15.24	15.03	15.07	15.18	15.20	15.17	15.03	15.06
V2O3	0.74	0.90	0.75	0.99	0.67	1.09	0.61	0.82	0.92	0.80	1.02	0.83	0.69	0.77	0.73	1.21	0.87	0.97	0.81	0.63
TiO2	1.07	0.89	1.03	1.08	1.10	1.01	1.00	0.99	1.05	1.05	1.08	1.16	0.98	0.91	1.20	0.97	1.04	1.05	1.04	0.96
FeO	23.23	23.41	23.17	23.06	23.20	23.92	22.79	22.90	23.31	22.90	23.26	23.40	23.13	22.87	22.80	23.37	22.98	23.07	22.85	22.82
Fe2O3	5.58	4.80	5.50	5.88	5.45	5.79	5.78	6.15	6.12	6.09	5.08	6.03	5.44	6.02	5.98	5.63	5.53	5.68	6.24	5.65
MgO	7.78	7.50	7.75	7.90	7.74	7.73	7.68	7.75	7.87	7.88	7.66	7.77	7.48	7.73	7.92	7.75	7.83	7.84	8.03	7.88
MnO	0.18	0.00	0.00	0.28	0.00	0.00	0.24	0.33	0.19	0.31	0.21	0.15	0.26	0.00	0.24	0.00	0.00	0.00	0.22	0.00
NiO	0.00	0.00	0.00	0.00	0.00	0.00	0.00	0.00	0.00	0.00	0.00	0.00	0.00	0.32	0.27	0.00	0.00	0.22	0.00	0.00
Total	99.56	98.69	98.65	99.69	98.43	100.85	98.02	98.94	100.17	99.25	99.14	99.57	98.23	99.02	99.50	99.43	98.45	99.42	99.74	98.48
<b>Cations</b>																				
Cr	9.60	9.70	9.51	9.39	9.45	9.46	9.46	9.41	9.42	9.38	9.60	9.40	9.52	9.53	9.45	9.46	9.47	9.48	9.47	9.58
Al	4.68	4.75	4.78	4.76	4.84	4.73	4.80	4.75	4.72	4.78	4.69	4.72	4.81	4.70	4.69	4.73	4.77	4.72	4.66	4.73
V	0.17	0.22	0.18	0.23	0.16	0.25	0.15	0.19	0.22	0.19	0.24	0.20	0.17	0.18	0.17	0.29	0.21	0.23	0.19	0.15
Ti	0.21	0.18	0.21	0.21	0.22	0.20	0.20	0.20	0.21	0.21	0.22	0.23	0.20	0.18	0.24	0.19	0.21	0.21	0.21	0.19
Fe3+	1.11	0.96	1.10	1.17	1.09	1.14	1.17	1.23	1.21	1.21	1.01	1.20	1.09	1.20	1.19	1.12	1.11	1.13	1.24	1.13
Fe2+	5.13	5.22	5.15	5.07	5.17	5.22	5.10	5.08	5.11	5.06	5.16	5.16	5.17	5.08	5.03	5.16	5.12	5.10	5.03	5.09
Mg	3.06	2.98	3.07	3.10	3.07	3.00	3.07	3.07	3.08	3.10	3.03	3.06	2.98	3.06	3.12	3.05	3.11	3.09	3.15	3.13
Mn	0.04	0.00	0.00	0.06	0.00	0.00	0.05	0.07	0.04	0.07	0.05	0.03	0.06	0.00	0.05	0.00	0.00	0.00	0.05	0.00
Ni	0.00	0.00	0.00	0.00	0.00	0.00	0.00	0.00	0.00	0.00	0.00	0.00	0.00	0.07	0.06	0.00	0.00	0.05	0.00	0.00
Total	24.00	24.00	24.00	24.00	24.00	24.00	24.00	24.00	24.00	24.00	24.00	24.00	24.00	24.00	24.00	24.00	24.00	24.00	24.00	24.00
<b>Cation allocation</b>																				
2+	8.23	8.19	8.23	8.24	8.24	8.22	8.22	8.22	8.23	8.23	8.23	8.25	8.22	8.14	8.20	8.21	8.23	8.18	8.23	8.21
3+	15.77	15.81	15.77	15.76	15.76	15.78	15.78	15.78	15.77	15.77	15.77	15.75	15.78	15.86	15.80	15.79	15.77	15.82	15.77	15.79
<b>Major cation ratios</b>																				
100Mg/Mg+Fe2+	31.24	29.85	30.93	31.49	30.69	30.20	30.96	31.18	31.29	31.54	30.71	30.91	29.89	31.28	32.06	30.84	31.44	31.43	32.49	31.86
100Cr/Cr+Al	67.24	67.11	66.55	66.33	66.12	66.67	66.36	66.45	66.61	66.24	67.17	66.57	66.44	66.95	66.84	66.68	66.49	66.76	67.01	66.94
100Fe3+/Cr+Al+V+Fe3+	7.13	6.15	7.07	7.49	7.03	7.29	7.49	7.89	7.75	7.78	6.51	7.72	7.02	7.70	7.66	7.18	7.12	7.25	7.94	7.26

15/15

UM/UPEG

	1	2	3	4	5	6	7	8	9	10	11	12	13	14	15	16	17	18	19	20
<b>Analysed totals</b>																				
Cr2O3	43.66	43.19	43.85	43.77	43.85	43.38	43.02	42.97	43.28	43.02	43.02	43.10	43.48	43.40	43.46	44.32	44.12	42.88	43.50	42.83
Al2O3	11.21	11.26	11.11	11.07	11.77	11.37	11.32	11.04	12.21	12.32	11.70	12.07	11.94	12.55	12.71	11.85	12.16	12.36	11.68	11.64
V2O3	1.29	1.16	1.14	1.15	1.08	1.37	1.22	0.98	1.19	1.20	1.04	1.46	1.31	1.25	1.24	1.10	1.08	1.07	1.29	1.29
TiO2	1.58	1.53	1.43	1.74	1.54	1.87	1.74	1.63	1.47	1.58	1.59	1.53	1.58	1.32	1.38	1.66	1.55	1.90	1.51	1.66
FeO	26.18	25.58	25.99	26.21	26.17	26.39	25.83	25.82	25.82	25.54	25.82	25.93	26.08	25.50	25.41	25.88	25.81	26.04	25.27	25.95
Fe2O3	9.87	9.93	10.04	10.10	10.07	9.83	10.09	10.76	9.73	9.45	10.20	9.76	9.55	9.62	9.30	9.40	9.98	10.02	9.96	10.40
MgO	6.05	6.10	6.02	6.19	6.27	6.12	6.23	5.94	6.36	6.35	6.22	6.21	6.25	6.44	6.50	6.52	6.69	6.67	6.46	6.26
MnO	0.00	0.19	0.00	0.00	0.00	0.19	0.17	0.30	0.00	0.30	0.18	0.24	0.00	0.16	0.23	0.00	0.00	0.00	0.34	0.18
NiO	0.00	0.00	0.00	0.00	0.00	0.00	0.00	0.22	0.00	0.00	0.00	0.00	0.00	0.00	0.00	0.00	0.00	0.00	0.00	0.00
Total	99.84	98.92	99.59	100.22	100.74	100.52	99.62	99.65	100.05	99.75	99.77	100.30	100.20	100.24	100.22	100.72	101.39	100.94	100.02	100.22
<b>Cations</b>																				
Cr	9.37	9.34	9.44	9.36	9.30	9.24	9.24	9.26	9.21	9.17	9.21	9.16	9.26	9.20	9.20	9.38	9.26	9.03	9.27	9.13
Al	3.59	3.63	3.57	3.53	3.72	3.61	3.62	3.55	3.87	3.92	3.73	3.83	3.79	3.97	4.01	3.74	3.81	3.88	3.71	3.70
V	0.31	0.28	0.28	0.28	0.26	0.33	0.30	0.24	0.29	0.29	0.25	0.35	0.32	0.30	0.30	0.26	0.26	0.26	0.31	0.31
Ti	0.32	0.31	0.29	0.35	0.31	0.38	0.36	0.33	0.30	0.32	0.32	0.31	0.32	0.27	0.28	0.33	0.31	0.38	0.31	0.34
Fe3+	2.02	2.05	2.06	2.06	2.03	1.99	2.06	2.21	1.97	1.92	2.08	1.98	1.93	1.94	1.87	1.89	1.99	2.01	2.02	2.11
Fe2+	5.94	5.85	5.92	5.93	5.87	5.95	5.87	5.88	5.81	5.76	5.85	5.83	5.87	5.72	5.69	5.79	5.73	5.80	5.70	5.85
Mg	2.45	2.49	2.44	2.50	2.51	2.46	2.52	2.41	2.55	2.55	2.51	2.49	2.51	2.57	2.59	2.60	2.65	2.65	2.60	2.52
Mn	0.00	0.04	0.00	0.00	0.00	0.04	0.04	0.07	0.00	0.07	0.04	0.06	0.00	0.04	0.05	0.00	0.00	0.00	0.08	0.04
Ni	0.00	0.00	0.00	0.00	0.00	0.00	0.00	0.05	0.00	0.00	0.00	0.00	0.00	0.00	0.00	0.00	0.00	0.00	0.00	0.00
Total	24.00	24.00	24.00	24.00	24.00	24.00	24.00	24.00	24.00	24.00	24.00	24.00	24.00	24.00	24.00	24.00	24.00	24.00	24.00	24.00
<b>Cation allocation</b>																				
2+	8.39	8.38	8.36	8.42	8.38	8.45	8.43	8.37	8.36	8.38	8.40	8.37	8.38	8.33	8.34	8.39	8.38	8.45	8.38	8.41
3+	15.61	15.62	15.64	15.58	15.62	15.55	15.57	15.63	15.64	15.62	15.60	15.63	15.62	15.67	15.66	15.61	15.62	15.55	15.62	15.59
<b>Major cation ratios</b>																				
100Mg/Mg+Fe2+	25.67	26.23	25.78	26.38	26.14	25.71	26.57	25.60	26.33	26.36	26.19	25.76	25.96	26.59	26.72	27.27	27.76	27.35	27.60	26.35
100Cr/Cr+Al	72.31	72.00	72.58	72.62	71.42	71.89	71.83	72.31	70.39	70.08	71.15	70.53	70.94	69.88	69.62	71.49	70.86	69.94	71.41	71.16
100Fe3+/Cr+Al+V+Fe3+	13.19	13.36	13.41	13.51	13.27	13.13	13.55	14.48	12.85	12.54	13.61	12.90	12.65	12.60	12.18	12.40	13.02	13.23	13.20	13.84

**Zondereinde chromite compositions 1/11****Chr**

	1	2	3	4	5	6	7	8	9	10	11	12	13	14	15	16	17
<b>Analysed totals</b>																	
Cr <sub>2</sub> O <sub>3</sub>	42.30	42.48	42.22	43.41	42.89	43.43	43.50	43.31	42.93	43.31	42.77	42.03	42.44	42.66	42.89	44.14	43.02
Al <sub>2</sub> O <sub>3</sub>	17.54	17.64	17.29	17.08	17.45	17.33	17.61	17.73	17.38	17.41	17.97	17.81	17.46	17.23	17.22	16.69	17.42
V <sub>2</sub> O <sub>3</sub>	0.74	0.57	0.64	0.53	0.65	0.67	0.71	0.69	0.81	0.62	0.68	0.39	0.49	0.58	0.57	0.47	0.82
TiO <sub>2</sub>	0.95	1.05	0.86	0.88	0.96	0.91	0.77	0.87	0.83	0.82	0.92	0.86	0.91	0.92	0.80	1.01	0.92
FeO	23.94	23.65	23.58	23.79	23.50	23.07	23.40	23.43	22.73	23.24	22.97	23.42	23.16	23.45	23.46	23.35	23.44
Fe <sub>2</sub> O <sub>3</sub>	6.71	6.36	7.28	6.68	6.56	6.50	5.99	6.40	6.63	6.41	6.52	6.89	6.72	7.02	6.98	6.34	6.09
MgO	7.71	7.77	7.58	7.65	7.91	8.06	7.90	7.97	8.22	7.98	8.03	7.76	7.78	7.85	7.75	7.83	7.81
MnO	0.00	0.23	0.45	0.18	0.19	0.20	0.10	0.10	0.27	0.15	0.45	0.22	0.21	0.00	0.00	0.23	0.25
NiO	0.00	0.00	0.00	0.00	0.00	0.22	0.00	0.24	0.00	0.00	0.28	0.00	0.25	0.23	0.24	0.19	0.00
<b>Total</b>	<b>99.90</b>	<b>99.76</b>	<b>99.91</b>	<b>100.18</b>	<b>100.09</b>	<b>100.40</b>	<b>99.98</b>	<b>100.75</b>	<b>99.80</b>	<b>99.95</b>	<b>100.59</b>	<b>99.39</b>	<b>99.44</b>	<b>99.94</b>	<b>99.91</b>	<b>100.26</b>	<b>99.77</b>
<b>Cations</b>																	
Cr	8.72	8.76	8.72	8.95	8.82	8.90	8.94	8.84	8.83	8.91	8.73	8.69	8.78	8.80	8.85	9.09	8.87
Al	5.39	5.42	5.33	5.25	5.35	5.30	5.40	5.40	5.33	5.34	5.47	5.49	5.39	5.30	5.30	5.13	5.36
V	0.17	0.13	0.15	0.12	0.15	0.16	0.16	0.16	0.19	0.14	0.16	0.09	0.12	0.14	0.13	0.11	0.19
Ti	0.19	0.21	0.17	0.17	0.19	0.18	0.15	0.17	0.16	0.16	0.18	0.17	0.18	0.18	0.16	0.20	0.18
Fe <sup>3+</sup>	1.32	1.25	1.43	1.31	1.28	1.27	1.17	1.24	1.30	1.26	1.27	1.36	1.32	1.38	1.37	1.24	1.20
Fe <sup>2+</sup>	5.22	5.16	5.15	5.19	5.11	5.00	5.09	5.06	4.94	5.06	4.96	5.12	5.07	5.12	5.12	5.09	5.11
Mg	2.99	3.02	2.95	2.97	3.06	3.11	3.06	3.07	3.19	3.09	3.09	3.03	3.04	3.05	3.02	3.04	3.04
Mn	0.00	0.05	0.10	0.04	0.04	0.04	0.02	0.02	0.06	0.03	0.10	0.05	0.05	0.00	0.00	0.05	0.05
Ni	0.00	0.00	0.00	0.00	0.00	0.05	0.00	0.05	0.00	0.00	0.06	0.00	0.05	0.05	0.05	0.04	0.00
<b>Total</b>	<b>24.00</b>	<b>24.00</b>	<b>24.00</b>	<b>24.00</b>	<b>24.00</b>	<b>24.00</b>	<b>24.00</b>	<b>24.00</b>	<b>24.00</b>	<b>24.00</b>	<b>24.00</b>	<b>24.00</b>	<b>24.00</b>	<b>24.00</b>	<b>24.00</b>	<b>24.00</b>	<b>24.00</b>
<b>Cation Allocation</b>																	
2+	8.21	8.23	8.20	8.20	8.21	8.16	8.17	8.14	8.19	8.19	8.15	8.20	8.15	8.16	8.14	8.19	8.20
3+	15.79	15.77	15.80	15.80	15.79	15.84	15.83	15.86	15.81	15.81	15.85	15.80	15.85	15.84	15.86	15.81	15.80
<b>Major cation ratios</b>																	
100Mg/Mg+Fe <sup>2+</sup>	28.22	28.55	28.16	28.47	29.30	30.22	29.20	29.32	31.01	29.75	29.64	28.52	29.04	29.29	28.95	29.78	28.99
100Cr/Cr+Al	61.79	61.76	62.08	63.02	62.25	62.69	62.35	62.09	62.35	62.52	61.48	61.28	61.97	62.41	62.56	63.94	62.35
100Fe <sup>3+</sup> /Cr+Al+V+Fe <sup>3+</sup>	8.44	8.02	9.16	8.38	8.22	8.12	7.48	7.95	8.29	8.02	8.11	8.68	8.48	8.83	8.76	7.98	7.65



2/11

Chr

	18	19	20	21	22	23	24	25	26	27	28	29	30	31	32	33	34	35
<b>Analysed totals</b>																		
Cr2O3	44.25	44.47	44.06	44.85	44.95	44.27	44.55	44.38	44.51	44.46	44.70	44.00	44.47	44.57	44.30	44.26	44.09	44.54
Al2O3	18.15	17.88	18.12	17.93	17.42	17.65	17.67	17.42	17.84	17.72	17.81	17.99	18.02	18.16	18.14	17.75	18.06	17.73
V2O3	0.50	0.65	0.64	0.66	0.57	0.65	0.61	0.72	0.56	0.56	0.76	0.69	0.71	0.67	0.69	0.56	0.76	0.44
TiO2	0.68	0.71	0.77	0.69	0.73	0.75	0.72	0.68	0.70	0.75	0.65	0.79	0.76	0.76	0.83	0.81	0.76	0.76
FeO	21.91	22.00	22.43	22.64	22.66	21.88	22.39	22.33	21.99	22.14	22.05	22.59	21.89	22.49	23.04	22.12	22.63	22.25
Fe2O3	6.44	6.43	6.08	5.73	6.23	6.28	6.04	6.56	6.37	6.26	6.09	5.95	6.05	5.96	6.29	6.04	6.24	6.12
MgO	8.94	8.99	8.86	8.61	8.48	8.87	8.71	8.61	8.90	8.87	8.93	8.50	9.02	8.77	8.68	8.88	8.68	8.87
MnO	0.20	0.28	0.00	0.17	0.34	0.19	0.09	0.31	0.11	0.00	0.00	0.18	0.19	0.10	0.08	0.10	0.21	0.00
NiO	0.23	0.00	0.00	0.00	0.00	0.20	0.00	0.00	0.25	0.20	0.19	0.18	0.18	0.20	0.00	0.00	0.00	0.00
<b>Total</b>	<b>101.30</b>	<b>101.41</b>	<b>100.97</b>	<b>101.29</b>	<b>101.37</b>	<b>100.74</b>	<b>100.76</b>	<b>101.02</b>	<b>101.23</b>	<b>100.96</b>	<b>101.18</b>	<b>100.88</b>	<b>101.28</b>	<b>101.67</b>	<b>102.05</b>	<b>100.52</b>	<b>101.44</b>	<b>100.71</b>
<b>Cations</b>																		
Cr	8.91	8.96	8.90	9.06	9.10	8.98	9.04	9.01	8.98	9.00	9.02	8.92	8.96	8.96	8.88	8.99	8.89	9.04
Al	5.45	5.37	5.46	5.40	5.26	5.34	5.35	5.27	5.37	5.35	5.36	5.44	5.41	5.44	5.42	5.38	5.43	5.37
V	0.11	0.15	0.15	0.15	0.13	0.15	0.14	0.17	0.13	0.13	0.17	0.16	0.16	0.15	0.16	0.13	0.17	0.10
Ti	0.13	0.14	0.15	0.13	0.14	0.15	0.14	0.13	0.13	0.14	0.12	0.15	0.14	0.14	0.16	0.16	0.15	0.15
Fe3+	1.24	1.23	1.17	1.10	1.20	1.21	1.17	1.27	1.22	1.21	1.17	1.15	1.16	1.14	1.20	1.17	1.20	1.18
Fe2+	4.67	4.69	4.79	4.84	4.85	4.70	4.81	4.79	4.70	4.74	4.71	4.85	4.66	4.78	4.89	4.75	4.82	4.77
Mg	3.40	3.41	3.38	3.28	3.24	3.39	3.33	3.30	3.39	3.38	3.40	3.25	3.42	3.32	3.28	3.40	3.30	3.39
Mn	0.04	0.06	0.00	0.04	0.07	0.04	0.02	0.07	0.02	0.00	0.00	0.04	0.04	0.02	0.02	0.02	0.05	0.00
Ni	0.05	0.00	0.00	0.00	0.00	0.04	0.00	0.00	0.05	0.04	0.04	0.04	0.04	0.04	0.00	0.00	0.00	0.00
<b>Total</b>	<b>24.00</b>	<b>24.00</b>	<b>24.00</b>	<b>24.00</b>	<b>24.00</b>	<b>24.00</b>	<b>24.00</b>	<b>24.00</b>	<b>24.00</b>	<b>24.00</b>	<b>24.00</b>	<b>24.00</b>	<b>24.00</b>	<b>24.00</b>	<b>24.00</b>	<b>24.00</b>	<b>24.00</b>	<b>24.00</b>
<b>Cation Allocation</b>																		
2+	8.11	8.16	8.17	8.15	8.16	8.13	8.16	8.16	8.11	8.13	8.11	8.14	8.13	8.13	8.18	8.18	8.17	8.17
3+	15.89	15.84	15.83	15.85	15.84	15.87	15.84	15.84	15.89	15.87	15.89	15.86	15.87	15.87	15.82	15.82	15.83	15.83
<b>Major cation ratios</b>																		
100Mg/Mg+Fe2+	33.54	33.95	32.93	32.02	32.00	33.78	32.81	32.73	33.64	33.55	33.74	31.60	33.99	32.50	31.82	33.58	32.18	33.47
100Cr/Cr+Al	62.04	62.52	61.98	62.65	63.38	62.71	62.83	63.08	62.59	62.73	62.73	62.12	62.34	62.20	62.08	62.58	62.08	62.74
100Fe3+/Cr+Al+V+Fe3+	7.86	7.85	7.46	7.02	7.65	7.73	7.43	8.07	7.80	7.70	7.43	7.33	7.39	7.27	7.67	7.46	7.64	7.54

**3/11****Chr (1)**

	1	2	3	4	5	6	7	8	9	10	11	12	13	14	15	16
<b>Analysed totals</b>																
Cr2O3	45.06	44.53	44.76	44.31	44.24	44.52	44.51	44.70	44.38	44.60	44.36	44.36	44.07	44.74	45.10	44.54
Al2O3	16.77	16.76	16.81	16.93	17.36	16.98	16.82	17.79	17.37	17.10	17.28	17.52	17.44	17.43	17.08	17.87
V2O3	0.52	0.48	0.40	0.64	0.62	0.79	0.69	0.62	0.50	0.64	0.68	0.56	0.56	0.62	0.57	0.46
TiO2	0.76	0.76	0.74	0.74	0.65	0.67	0.79	0.61	0.77	0.55	0.70	0.78	0.71	0.65	0.80	0.62
FeO	22.42	22.10	21.95	22.38	21.94	22.65	22.75	22.65	22.51	22.84	22.54	23.26	22.76	23.04	22.81	22.74
Fe2O3	5.34	5.78	5.96	6.00	5.88	5.12	5.83	5.29	6.01	5.96	5.75	5.59	6.23	6.11	5.57	5.30
MgO	8.13	8.49	8.56	8.26	8.56	7.93	8.16	8.22	8.40	7.98	8.19	8.01	8.20	8.01	8.04	8.21
MnO	0.38	0.00	0.19	0.12	0.25	0.27	0.16	0.09	0.24	0.24	0.17	0.13	0.29	0.30	0.34	0.15
NiO	0.00	0.00	0.00	0.19	0.00	0.00	0.00	0.23	0.00	0.00	0.21	0.00	0.00	0.23	0.26	0.00
<b>Total</b>	<b>99.37</b>	<b>98.90</b>	<b>99.37</b>	<b>99.57</b>	<b>99.50</b>	<b>98.94</b>	<b>99.72</b>	<b>100.20</b>	<b>100.18</b>	<b>99.91</b>	<b>99.88</b>	<b>100.21</b>	<b>100.25</b>	<b>101.14</b>	<b>100.56</b>	<b>99.90</b>
<b>Cations</b>																
Cr	9.33	9.24	9.24	9.15	9.10	9.25	9.19	9.14	9.09	9.19	9.12	9.10	9.03	9.11	9.24	9.13
Al	5.18	5.19	5.18	5.21	5.33	5.26	5.18	5.43	5.30	5.25	5.30	5.36	5.33	5.29	5.22	5.46
V	0.12	0.11	0.09	0.15	0.14	0.19	0.16	0.14	0.12	0.15	0.16	0.13	0.13	0.14	0.13	0.11
Ti	0.15	0.15	0.15	0.15	0.13	0.13	0.15	0.12	0.15	0.11	0.14	0.15	0.14	0.13	0.16	0.12
Fe3+	1.05	1.14	1.17	1.18	1.15	1.01	1.15	1.03	1.17	1.17	1.13	1.09	1.21	1.18	1.08	1.04
Fe2+	4.91	4.85	4.80	4.89	4.77	4.98	4.97	4.90	4.88	4.98	4.90	5.05	4.93	4.96	4.94	4.93
Mg	3.17	3.32	3.33	3.21	3.32	3.11	3.17	3.17	3.24	3.10	3.18	3.10	3.17	3.08	3.10	3.17
Mn	0.08	0.00	0.04	0.03	0.06	0.06	0.04	0.02	0.05	0.05	0.04	0.03	0.06	0.07	0.07	0.03
Ni	0.00	0.00	0.00	0.04	0.00	0.00	0.00	0.05	0.00	0.00	0.04	0.00	0.00	0.05	0.06	0.00
<b>Total</b>	<b>24.00</b>	<b>24.00</b>	<b>24.00</b>	<b>24.00</b>	<b>24.00</b>	<b>24.00</b>	<b>24.00</b>	<b>24.00</b>	<b>24.00</b>	<b>24.00</b>	<b>24.00</b>	<b>24.00</b>	<b>24.00</b>	<b>24.00</b>	<b>24.00</b>	<b>24.00</b>
<b>Cation Allocation</b>																
2+	8.17	8.17	8.17	8.13	8.15	8.15	8.18	8.09	8.17	8.13	8.11	8.17	8.16	8.10	8.12	8.14
3+	15.83	15.83	15.83	15.87	15.85	15.85	15.82	15.91	15.83	15.87	15.89	15.83	15.84	15.90	15.88	15.86
<b>Major cation ratios</b>																
100Mg/Mg+Fe2+	31.44	33.10	33.41	31.83	32.85	30.33	31.30	30.70	31.87	30.28	31.13	29.77	30.85	30.00	30.56	30.52
100Cr/Cr+Al	64.31	64.05	64.10	63.71	63.08	63.74	63.96	62.76	63.14	63.62	63.26	62.93	62.89	63.25	63.91	62.57
100Fe3+/Cr+Al+V+Fe3+	6.72	7.28	7.47	7.51	7.32	6.45	7.31	6.54	7.47	7.41	7.17	6.97	7.73	7.53	6.92	6.58

4/11 Chr (1)

	17	18	19	20	21	22	23	24	25	26	27	28	29	30	31	32	33	34	35
<b>Analysed totals</b>																			
Cr2O3	44.90	45.68	44.24	44.76	45.17	44.88	45.42	45.28	44.81	45.17	45.41	45.19	44.81	44.85	45.12	44.75	44.93	44.56	45.52
Al2O3	17.64	19.51	17.50	17.84	18.66	17.52	17.14	16.81	17.26	17.98	17.67	17.53	17.23	17.24	17.48	17.39	17.31	17.93	17.19
V2O3	0.55	0.76	0.58	0.65	0.42	0.61	0.70	0.67	0.66	0.66	0.85	0.60	0.79	0.56	0.75	0.60	0.58	0.49	0.91
TiO2	0.92	0.53	0.68	0.98	0.82	0.70	0.78	0.75	0.61	0.60	0.52	0.75	0.77	0.77	0.66	0.67	0.71	0.66	0.54
FeO	23.16	22.49	22.14	22.90	22.82	22.95	22.50	22.32	22.31	22.39	22.52	22.80	22.64	22.13	22.70	22.47	22.46	22.41	22.87
Fe2O3	5.20	4.37	6.12	5.29	6.08	6.06	5.63	5.93	6.37	5.03	4.96	5.74	5.75	5.79	5.99	5.87	5.12	5.50	5.50
MgO	8.26	8.88	8.57	8.54	9.04	8.46	8.46	8.49	8.51	8.54	8.35	8.48	8.31	8.59	8.50	8.45	8.40	8.52	8.23
MnO	0.17	0.42	0.27	0.22	0.14	0.00	0.17	0.32	0.35	0.22	0.24	0.20	0.25	0.17	0.22	0.20	0.00	0.16	0.16
NiO	0.00	0.00	0.00	0.00	0.00	0.00	0.24	0.00	0.00	0.00	0.00	0.00	0.18	0.18	0.00	0.00	0.00	0.00	0.00
<b>Total</b>	<b>100.80</b>	<b>102.64</b>	<b>100.11</b>	<b>101.18</b>	<b>103.14</b>	<b>101.19</b>	<b>101.04</b>	<b>100.57</b>	<b>100.88</b>	<b>100.59</b>	<b>100.51</b>	<b>101.29</b>	<b>100.73</b>	<b>100.29</b>	<b>101.42</b>	<b>100.40</b>	<b>99.50</b>	<b>100.23</b>	<b>100.92</b>
<b>Cations</b>																			
Cr	9.14	9.04	9.05	9.05	8.93	9.10	9.23	9.25	9.12	9.18	9.26	9.15	9.14	9.17	9.13	9.14	9.25	9.09	9.27
Al	5.35	5.76	5.34	5.38	5.50	5.30	5.20	5.12	5.24	5.45	5.37	5.29	5.24	5.25	5.27	5.30	5.31	5.45	5.22
V	0.13	0.17	0.13	0.15	0.09	0.14	0.16	0.16	0.15	0.15	0.20	0.14	0.18	0.13	0.17	0.14	0.14	0.11	0.21
Ti	0.18	0.10	0.13	0.19	0.15	0.13	0.15	0.15	0.12	0.12	0.10	0.14	0.15	0.15	0.13	0.13	0.14	0.13	0.10
Fe3+	1.01	0.82	1.19	1.02	1.14	1.17	1.09	1.15	1.23	0.97	0.96	1.11	1.12	1.13	1.15	1.14	1.00	1.07	1.07
Fe2+	4.99	4.71	4.79	4.90	4.77	4.92	4.84	4.82	4.80	4.81	4.85	4.88	4.88	4.79	4.86	4.86	4.89	4.84	4.93
Mg	3.17	3.31	3.30	3.26	3.37	3.24	3.24	3.27	3.27	3.27	3.21	3.24	3.19	3.31	3.24	3.25	3.26	3.27	3.16
Mn	0.04	0.09	0.06	0.05	0.03	0.00	0.04	0.07	0.08	0.05	0.05	0.04	0.05	0.04	0.05	0.04	0.00	0.04	0.04
Ni	0.00	0.00	0.00	0.00	0.00	0.00	0.05	0.00	0.00	0.00	0.00	0.00	0.04	0.04	0.00	0.00	0.00	0.00	0.00
<b>Total</b>	<b>24.00</b>	<b>24.00</b>	<b>24.00</b>	<b>24.00</b>	<b>24.00</b>	<b>24.00</b>	<b>24.00</b>	<b>24.00</b>	<b>24.00</b>	<b>24.00</b>	<b>24.00</b>	<b>24.00</b>	<b>24.00</b>	<b>24.00</b>	<b>24.00</b>	<b>24.00</b>	<b>24.00</b>	<b>24.00</b>	<b>24.00</b>
<b>Cation Allocation</b>																			
2+	8.19	8.11	8.16	8.21	8.18	8.16	8.12	8.17	8.14	8.13	8.12	8.16	8.13	8.13	8.15	8.15	8.15	8.15	8.12
3+	15.81	15.89	15.84	15.79	15.82	15.84	15.88	15.83	15.86	15.87	15.88	15.84	15.87	15.87	15.85	15.85	15.85	15.85	15.88
<b>Major cation ratios</b>																			
100Mg/Mg+Fe2+	30.65	31.66	32.62	31.68	32.81	31.66	32.32	32.89	32.53	31.88	31.38	31.82	31.55	32.96	31.99	32.03	31.96	31.83	31.12
100Cr/Cr+Al	63.06	61.09	62.90	62.72	61.87	63.20	63.98	64.37	63.52	62.75	63.29	63.35	63.55	63.57	63.38	63.30	63.51	62.50	63.97
100Fe3+/Cr+Al+V+Fe3+	6.44	5.21	7.59	6.53	7.30	7.45	6.95	7.36	7.83	6.17	6.09	7.06	7.12	7.18	7.33	7.26	6.39	6.79	6.76

5/11

Chr (1)

	36	37	38	39	40	41	42	43	44	45	46	47	48	49	50	51	52	53
<b>Analysed totals</b>																		
Cr2O3	44.99	44.84	44.53	44.70	44.68	44.88	45.22	44.05	45.04	45.24	44.88	44.64	44.83	45.01	45.20	44.69	44.44	44.90
Al2O3	16.00	15.98	16.05	16.14	16.04	16.09	16.17	16.60	15.88	15.99	16.22	15.94	15.78	15.81	15.82	16.18	15.94	15.81
V2O3	0.57	0.64	0.57	0.47	0.40	0.54	0.56	0.57	0.60	0.58	0.70	0.58	0.85	0.56	0.53	0.67	0.63	0.60
TiO2	0.69	0.72	0.80	0.70	0.78	0.63	0.77	0.68	0.75	0.67	0.71	0.71	0.61	0.79	0.67	0.67	0.47	0.72
FeO	22.35	22.14	22.46	22.51	22.55	22.94	22.83	22.10	22.77	22.31	22.64	23.06	22.44	22.63	22.35	22.56	22.32	22.30
Fe2O3	5.69	5.32	5.35	5.64	5.21	5.38	5.03	5.47	5.31	5.18	5.72	5.67	5.49	5.45	5.77	6.03	6.41	5.66
MgO	8.01	7.98	7.71	7.86	7.78	7.62	7.81	8.00	7.80	7.81	7.90	7.54	7.87	7.68	7.94	7.94	7.68	8.02
MnO	0.17	0.25	0.25	0.17	0.09	0.00	0.08	0.28	0.00	0.15	0.09	0.13	0.00	0.20	0.25	0.00	0.31	0.09
NiO	0.00	0.00	0.20	0.00	0.00	0.00	0.00	0.00	0.00	0.25	0.22	0.00	0.00	0.19	0.00	0.27	0.18	0.00
<b>Total</b>	<b>98.47</b>	<b>97.87</b>	<b>97.92</b>	<b>98.19</b>	<b>97.53</b>	<b>98.08</b>	<b>98.47</b>	<b>97.74</b>	<b>98.14</b>	<b>98.18</b>	<b>99.07</b>	<b>98.29</b>	<b>97.88</b>	<b>98.33</b>	<b>98.53</b>	<b>99.03</b>	<b>98.38</b>	<b>98.10</b>
<b>Cations</b>																		
Cr	9.43	9.45	9.40	9.40	9.46	9.46	9.48	9.27	9.49	9.52	9.36	9.41	9.46	9.48	9.48	9.32	9.35	9.45
Al	5.00	5.02	5.05	5.06	5.06	5.06	5.06	5.21	4.99	5.02	5.04	5.01	4.97	4.96	4.95	5.03	5.00	4.96
V	0.14	0.15	0.14	0.11	0.10	0.13	0.13	0.14	0.14	0.14	0.17	0.14	0.20	0.13	0.13	0.16	0.15	0.14
Ti	0.14	0.14	0.16	0.14	0.16	0.13	0.15	0.14	0.15	0.13	0.14	0.14	0.12	0.16	0.13	0.13	0.09	0.14
Fe3+	1.13	1.07	1.07	1.13	1.05	1.08	1.00	1.10	1.06	1.04	1.13	1.14	1.10	1.09	1.15	1.20	1.28	1.13
Fe2+	4.96	4.94	5.01	5.01	5.05	5.12	5.06	4.92	5.07	4.97	4.99	5.14	5.01	5.04	4.96	4.98	4.97	4.97
Mg	3.17	3.17	3.07	3.11	3.10	3.03	3.09	3.17	3.10	3.10	3.10	2.99	3.13	3.05	3.14	3.12	3.05	3.18
Mn	0.04	0.06	0.06	0.04	0.02	0.00	0.02	0.06	0.00	0.03	0.02	0.03	0.00	0.05	0.06	0.00	0.07	0.02
Ni	0.00	0.00	0.04	0.00	0.00	0.00	0.00	0.00	0.00	0.05	0.05	0.00	0.00	0.04	0.00	0.06	0.04	0.00
<b>Total</b>	<b>24.00</b>	<b>24.00</b>	<b>24.00</b>	<b>24.00</b>	<b>24.00</b>	<b>24.00</b>	<b>24.00</b>	<b>24.00</b>	<b>24.00</b>	<b>24.00</b>	<b>24.00</b>	<b>24.00</b>	<b>24.00</b>	<b>24.00</b>	<b>24.00</b>	<b>24.00</b>	<b>24.00</b>	<b>24.00</b>
<b>Cation Allocation</b>																		
2+	8.16	8.16	8.14	8.16	8.17	8.14	8.17	8.15	8.17	8.10	8.12	8.16	8.14	8.14	8.16	8.10	8.08	8.17
3+	15.84	15.84	15.86	15.84	15.83	15.86	15.83	15.85	15.83	15.90	15.88	15.84	15.86	15.86	15.84	15.90	15.92	15.83
<b>Major cation ratios</b>																		
100Mg/Mg+Fe2+	31.79	31.82	30.48	30.93	30.69	29.78	30.50	31.32	30.76	31.01	30.92	29.50	31.40	30.49	31.67	31.17	30.55	32.03
100Cr/Cr+Al	65.34	65.30	65.04	65.00	65.13	65.17	65.22	64.03	65.53	65.48	64.99	65.25	65.57	65.62	65.70	64.93	65.15	65.57
100Fe3+/Cr+Al+V+Fe3+	7.23	6.80	6.86	7.19	6.70	6.86	6.40	6.97	6.78	6.60	7.23	7.25	7.01	6.98	7.33	7.62	8.13	7.23

**6/11** **Chr (2)**

	1	2	3	4	5	6	7	8	9	10	11	12	13	14	15	16	17	18	19
<b>Analysed totals</b>																			
Cr2O3	45.82	45.88	45.81	46.07	45.44	45.40	45.82	45.67	45.56	45.40	45.00	45.70	46.06	45.38	46.40	45.68	45.68	45.19	46.22
Al2O3	16.59	16.46	16.49	16.98	16.60	17.04	17.01	16.88	16.81	16.86	16.51	16.56	16.85	16.58	16.94	16.67	16.72	16.79	16.79
V2O3	0.95	0.55	0.67	0.63	0.65	0.47	0.42	0.57	0.70	0.85	0.59	0.51	0.56	0.57	0.58	0.57	0.79	0.58	0.54
TiO2	0.89	0.78	0.70	0.81	0.73	0.80	0.86	0.79	0.84	0.83	1.08	0.82	0.76	0.87	0.78	0.81	0.78	0.78	0.78
FeO	22.86	22.92	22.68	22.62	22.44	22.71	22.81	22.55	22.34	22.45	22.95	22.42	22.92	22.56	22.96	22.69	22.63	22.79	23.07
Fe2O3	5.24	5.43	5.67	5.34	6.09	5.63	5.72	5.96	5.72	5.75	5.28	6.02	5.36	5.94	5.56	5.74	5.89	5.91	5.35
MgO	8.46	8.21	8.30	8.54	8.48	8.38	8.37	8.45	8.60	8.64	8.15	8.58	8.29	8.38	8.56	8.38	8.53	8.29	8.32
MnO	0.00	0.00	0.12	0.00	0.18	0.19	0.12	0.10	0.14	0.17	0.20	0.17	0.15	0.10	0.00	0.00	0.16	0.14	0.00
NiO	0.00	0.00	0.00	0.23	0.00	0.00	0.29	0.36	0.19	0.00	0.00	0.00	0.00	0.25	0.00	0.21	0.00	0.00	0.00
<b>Total</b>	<b>100.82</b>	<b>100.23</b>	<b>100.45</b>	<b>101.23</b>	<b>100.61</b>	<b>100.62</b>	<b>101.42</b>	<b>101.33</b>	<b>100.90</b>	<b>100.94</b>	<b>99.76</b>	<b>100.79</b>	<b>100.95</b>	<b>100.63</b>	<b>101.79</b>	<b>100.74</b>	<b>101.17</b>	<b>100.47</b>	<b>101.07</b>
<b>Cations</b>																			
Cr	9.35	9.44	9.40	9.35	9.29	9.27	9.30	9.28	9.28	9.23	9.29	9.33	9.39	9.29	9.37	9.34	9.29	9.26	9.42
Al	5.05	5.05	5.04	5.14	5.06	5.19	5.15	5.11	5.11	5.11	5.09	5.04	5.12	5.06	5.10	5.08	5.07	5.13	5.10
V	0.22	0.13	0.16	0.14	0.15	0.11	0.10	0.13	0.16	0.20	0.14	0.12	0.13	0.13	0.13	0.13	0.18	0.13	0.13
Ti	0.17	0.15	0.14	0.16	0.14	0.16	0.17	0.15	0.16	0.16	0.21	0.16	0.15	0.17	0.15	0.16	0.15	0.15	0.15
Fe3+	1.02	1.06	1.11	1.03	1.19	1.10	1.10	1.15	1.11	1.11	1.04	1.17	1.04	1.16	1.07	1.12	1.14	1.15	1.04
Fe2+	4.94	4.99	4.92	4.86	4.86	4.91	4.90	4.84	4.81	4.83	5.01	4.84	4.94	4.88	4.91	4.91	4.87	4.94	4.97
Mg	3.25	3.18	3.21	3.27	3.27	3.23	3.20	3.23	3.30	3.31	3.17	3.30	3.19	3.23	3.26	3.23	3.27	3.20	3.19
Mn	0.00	0.00	0.03	0.00	0.04	0.04	0.03	0.02	0.03	0.04	0.04	0.04	0.03	0.02	0.00	0.00	0.03	0.03	0.00
Ni	0.00	0.00	0.00	0.05	0.00	0.00	0.06	0.07	0.04	0.00	0.00	0.00	0.00	0.05	0.00	0.04	0.00	0.00	0.00
<b>Total</b>	<b>24.00</b>	<b>24.00</b>	<b>24.00</b>	<b>24.00</b>	<b>24.00</b>	<b>24.00</b>	<b>24.00</b>	<b>24.00</b>	<b>24.00</b>	<b>24.00</b>	<b>24.00</b>	<b>24.00</b>	<b>24.00</b>	<b>24.00</b>	<b>24.00</b>	<b>24.00</b>	<b>24.00</b>	<b>24.00</b>	<b>24.00</b>
<b>Cation Allocation</b>																			
2+	8.19	8.17	8.16	8.13	8.16	8.18	8.13	8.10	8.14	8.18	8.23	8.18	8.16	8.14	8.17	8.13	8.17	8.17	8.17
3+	15.81	15.83	15.84	15.87	15.84	15.82	15.87	15.90	15.86	15.82	15.77	15.82	15.84	15.86	15.83	15.87	15.83	15.83	15.83
<b>Major cation ratios</b>																			
100Mg/Mg+Fe2+	32.59	31.72	32.19	32.70	32.96	31.95	31.89	32.47	33.28	33.30	31.41	33.42	31.65	32.52	32.57	32.31	32.89	31.81	31.71
100Cr/Cr+Al	64.94	65.15	65.07	64.53	64.73	64.12	64.37	64.46	64.50	64.36	64.63	64.91	64.70	64.74	64.74	64.76	64.69	64.34	64.86
100Fe3+/Cr+Al+V+Fe3+	6.51	6.78	7.05	6.58	7.55	6.99	7.06	7.35	7.09	7.12	6.67	7.47	6.63	7.41	6.82	7.13	7.27	7.35	6.62

7/11	Chr (2)																	
	20	21	22	23	24	25	26	27	28	29	30	31	32	33	34	35	36	37
<b>Analysed totals</b>																		
Cr2O3	46.07	46.04	45.88	45.65	46.21	46.08	46.18	45.54	46.47	45.84	46.37	45.71	45.44	45.75	46.30	45.81	45.84	45.32
Al2O3	16.55	16.64	16.54	16.50	16.29	16.40	16.34	16.41	16.38	16.79	16.80	16.69	16.81	16.81	16.94	16.77	16.97	16.98
V2O3	0.71	0.71	0.85	0.64	0.76	0.70	0.65	0.49	0.67	0.57	0.42	0.64	0.72	0.67	0.68	0.72	0.68	0.73
TiO2	0.77	0.73	0.75	0.90	0.79	0.64	0.84	0.85	0.86	0.79	0.74	0.68	0.86	0.83	0.81	0.73	0.83	0.80
FeO	22.70	22.65	22.94	22.91	22.86	22.61	23.07	22.45	23.35	22.71	23.30	22.96	23.15	23.15	23.33	23.16	23.43	23.10
Fe2O3	5.86	5.80	5.89	5.59	5.83	6.38	5.65	6.40	5.50	6.12	5.62	6.19	5.76	5.46	5.59	5.84	5.85	6.03
MgO	8.39	8.32	8.31	8.24	8.35	8.31	8.22	8.38	8.23	8.49	8.16	8.18	8.21	8.08	8.18	8.15	8.20	8.22
MnO	0.14	0.45	0.00	0.22	0.18	0.30	0.18	0.29	0.00	0.29	0.13	0.13	0.23	0.10	0.18	0.24	0.00	0.15
NiO	0.18	0.00	0.20	0.00	0.00	0.20	0.00	0.26	0.00	0.00	0.00	0.23	0.00	0.26	0.20	0.00	0.22	0.20
<b>Total</b>	<b>101.36</b>	<b>101.33</b>	<b>101.36</b>	<b>100.65</b>	<b>101.26</b>	<b>101.62</b>	<b>101.14</b>	<b>101.08</b>	<b>101.45</b>	<b>101.62</b>	<b>101.55</b>	<b>101.40</b>	<b>101.19</b>	<b>101.11</b>	<b>102.20</b>	<b>101.42</b>	<b>102.01</b>	<b>101.53</b>
<b>Cations</b>																		
Cr	9.37	9.36	9.33	9.35	9.42	9.36	9.43	9.29	9.46	9.29	9.42	9.30	9.25	9.33	9.34	9.32	9.26	9.20
Al	5.02	5.05	5.02	5.04	4.95	4.97	4.98	5.00	4.97	5.07	5.09	5.06	5.11	5.11	5.10	5.09	5.12	5.14
V	0.16	0.16	0.20	0.15	0.18	0.16	0.15	0.11	0.15	0.13	0.10	0.15	0.17	0.15	0.16	0.17	0.16	0.17
Ti	0.15	0.14	0.15	0.17	0.15	0.12	0.16	0.16	0.17	0.15	0.14	0.13	0.17	0.16	0.16	0.14	0.16	0.15
Fe3+	1.13	1.12	1.14	1.09	1.13	1.23	1.10	1.24	1.07	1.18	1.09	1.20	1.12	1.06	1.07	1.13	1.13	1.16
Fe2+	4.88	4.87	4.94	4.97	4.93	4.86	4.98	4.85	5.03	4.87	5.01	4.94	4.99	5.00	4.98	4.98	5.01	4.96
Mg	3.22	3.19	3.19	3.18	3.21	3.18	3.16	3.22	3.16	3.24	3.13	3.14	3.15	3.11	3.11	3.12	3.13	3.14
Mn	0.03	0.10	0.00	0.05	0.04	0.06	0.04	0.06	0.00	0.06	0.03	0.03	0.05	0.02	0.04	0.05	0.00	0.03
Ni	0.04	0.00	0.04	0.00	0.00	0.04	0.00	0.05	0.00	0.00	0.00	0.05	0.00	0.05	0.04	0.00	0.04	0.04
<b>Total</b>	<b>24.00</b>	<b>24.00</b>	<b>24.00</b>	<b>24.00</b>	<b>24.00</b>	<b>24.00</b>	<b>24.00</b>	<b>24.00</b>	<b>24.00</b>	<b>24.00</b>	<b>24.00</b>	<b>24.00</b>	<b>24.00</b>	<b>24.00</b>	<b>24.00</b>	<b>24.00</b>	<b>24.00</b>	<b>24.00</b>
<b>Cation Allocation</b>																		
2+	8.13	8.16	8.13	8.19	8.17	8.11	8.18	8.14	8.18	8.18	8.16	8.11	8.19	8.13	8.13	8.16	8.14	8.14
3+	15.87	15.84	15.87	15.81	15.83	15.89	15.82	15.86	15.82	15.82	15.84	15.89	15.81	15.87	15.87	15.84	15.86	15.86
<b>Major cation ratios</b>																		
100Mg/Mg+Fe2+	32.49	32.14	32.03	31.78	32.46	32.40	31.75	32.76	31.57	32.63	30.96	31.34	31.22	30.75	30.89	31.03	30.87	31.13
100Cr/Cr+Al	65.12	64.97	65.03	64.97	65.54	65.33	65.45	65.04	65.54	64.68	64.92	64.75	64.45	64.61	64.70	64.69	64.43	64.16
100Fe3+/Cr+Al+V+Fe3+	7.23	7.15	7.27	6.97	7.21	7.84	7.02	7.95	6.81	7.53	6.93	7.63	7.14	6.77	6.85	7.20	7.19	7.43

8/11

Chr (2)

	38	39	40	41	42	43	44	45	46	47	48	49	50	51	52	53	54	55
<b>Analysed totals</b>																		
Cr2O3	46.02	45.94	46.28	45.79	45.69	45.82	45.55	46.15	46.37	46.12	45.45	46.19	45.88	46.03	45.86	45.75	46.09	46.18
Al2O3	16.69	17.21	16.96	16.93	16.76	17.04	16.66	16.69	16.57	16.24	16.85	17.28	16.94	16.72	17.18	16.79	15.78	16.47
V2O3	0.59	0.68	0.71	0.71	0.38	0.51	0.69	0.59	0.71	0.49	0.85	0.60	0.67	0.78	0.59	0.55	0.61	0.64
TiO2	0.84	0.79	0.71	0.70	0.82	0.77	0.77	0.81	0.77	0.69	0.82	0.81	0.74	0.84	0.92	0.84	0.73	0.74
FeO	23.07	23.46	23.01	22.92	23.04	23.13	23.01	22.99	23.04	22.35	22.93	22.83	22.56	22.65	22.64	22.78	22.65	22.46
Fe2O3	5.80	5.27	5.48	6.20	5.92	5.69	5.94	5.72	5.84	6.04	5.62	5.86	6.05	5.83	5.78	6.05	5.68	6.47
MgO	8.34	8.23	8.34	8.45	8.24	8.22	8.33	8.27	8.37	8.41	8.37	8.66	8.64	8.67	8.71	8.45	8.09	8.64
MnO	0.16	0.00	0.19	0.18	0.17	0.22	0.00	0.14	0.18	0.28	0.11	0.30	0.22	0.12	0.13	0.30	0.18	0.16
NiO	0.00	0.00	0.00	0.00	0.00	0.00	0.00	0.19	0.00	0.00	0.00	0.00	0.00	0.00	0.22	0.00	0.00	0.19
<b>Total</b>	<b>101.51</b>	<b>101.59</b>	<b>101.69</b>	<b>101.87</b>	<b>101.03</b>	<b>101.41</b>	<b>100.96</b>	<b>101.56</b>	<b>101.84</b>	<b>100.63</b>	<b>100.99</b>	<b>102.52</b>	<b>101.69</b>	<b>101.65</b>	<b>102.03</b>	<b>101.51</b>	<b>99.82</b>	<b>101.97</b>
<b>Cations</b>																		
Cr	9.34	9.31	9.37	9.25	9.32	9.31	9.29	9.37	9.39	9.45	9.26	9.25	9.27	9.31	9.23	9.28	9.55	9.33
Al	5.05	5.20	5.12	5.10	5.10	5.16	5.07	5.05	5.00	4.96	5.12	5.16	5.10	5.04	5.16	5.08	4.88	4.96
V	0.14	0.16	0.16	0.16	0.09	0.12	0.16	0.14	0.16	0.11	0.20	0.14	0.15	0.18	0.14	0.13	0.14	0.15
Ti	0.16	0.15	0.14	0.13	0.16	0.15	0.15	0.16	0.15	0.13	0.16	0.15	0.14	0.16	0.18	0.16	0.14	0.14
Fe3+	1.12	1.02	1.06	1.19	1.15	1.10	1.15	1.11	1.13	1.18	1.09	1.12	1.16	1.12	1.11	1.17	1.12	1.25
Fe2+	4.96	5.03	4.93	4.90	4.97	4.97	4.97	4.94	4.94	4.85	4.94	4.84	4.82	4.85	4.82	4.89	4.96	4.80
Mg	3.19	3.14	3.18	3.22	3.17	3.15	3.20	3.17	3.19	3.25	3.21	3.27	3.29	3.31	3.30	3.23	3.16	3.29
Mn	0.04	0.00	0.04	0.04	0.04	0.05	0.00	0.03	0.04	0.06	0.02	0.06	0.05	0.03	0.03	0.07	0.04	0.03
Ni	0.00	0.00	0.00	0.00	0.00	0.00	0.00	0.04	0.00	0.00	0.00	0.00	0.00	0.00	0.04	0.00	0.00	0.04
<b>Total</b>	<b>24.00</b>	<b>24.00</b>	<b>24.00</b>	<b>24.00</b>	<b>24.00</b>	<b>24.00</b>	<b>24.00</b>	<b>24.00</b>	<b>24.00</b>	<b>24.00</b>	<b>24.00</b>	<b>24.00</b>	<b>24.00</b>	<b>24.00</b>	<b>24.00</b>	<b>24.00</b>	<b>24.00</b>	<b>24.00</b>
<b>Cation Allocation</b>																		
2+	8.18	8.17	8.15	8.16	8.18	8.17	8.17	8.14	8.17	8.16	8.18	8.17	8.16	8.18	8.15	8.18	8.16	8.13
3+	15.82	15.83	15.85	15.84	15.82	15.83	15.83	15.86	15.83	15.84	15.82	15.83	15.84	15.82	15.85	15.82	15.84	15.87
<b>Major cation ratios</b>																		
100Mg/Mg+Fe2+	31.89	30.72	31.69	32.20	31.47	31.08	31.93	31.70	32.13	33.13	31.95	32.71	33.14	33.43	33.13	32.43	32.11	33.71
100Cr/Cr+Al	64.90	64.17	64.66	64.47	64.64	64.33	64.71	64.96	65.23	65.57	64.40	64.19	64.50	64.87	64.15	64.62	66.20	65.28
100Fe3+/Cr+Al+V+Fe3+	7.16	6.49	6.72	7.59	7.34	7.02	7.36	7.05	7.17	7.51	6.96	7.14	7.41	7.18	7.09	7.47	7.14	7.94



9/11	Chr (2)																		
	56	57	58	59	60	61	62	63	64	65	66	67	68	69	70	71	72	73	74
<b>Analysed totals</b>																			
Cr2O3	45.32	45.94	45.56	45.95	45.81	45.68	45.84	45.46	46.07	45.25	46.11	45.89	45.83	46.05	45.90	45.60	46.02	46.05	45.53
Al2O3	17.11	16.70	16.64	16.73	16.61	17.00	16.87	16.88	16.90	17.79	16.57	17.01	16.57	17.03	16.78	16.61	16.73	16.72	17.17
V2O3	0.62	0.50	0.64	0.53	0.55	0.56	0.55	0.48	0.38	0.64	0.67	0.55	0.51	0.50	0.66	0.58	0.74	0.35	0.53
TiO2	0.96	0.84	0.86	0.75	0.90	0.86	0.83	0.79	0.84	0.63	0.81	0.87	0.69	0.83	0.92	0.78	0.86	0.95	0.90
FeO	22.27	22.29	22.60	22.37	22.45	22.57	22.73	22.31	22.58	22.11	22.64	22.74	22.40	22.38	22.73	22.55	22.84	22.40	22.67
Fe2O3	6.24	5.65	5.56	5.54	5.46	5.55	5.68	5.82	5.76	5.80	5.78	5.71	5.90	5.69	5.60	6.08	5.61	6.15	5.77
MgO	8.94	8.60	8.53	8.64	8.56	8.48	8.43	8.66	8.61	9.01	8.51	8.58	8.57	8.71	8.56	8.45	8.49	8.68	8.65
MnO	0.31	0.31	0.00	0.00	0.14	0.19	0.00	0.09	0.00	0.00	0.23	0.23	0.00	0.15	0.20	0.25	0.00	0.33	0.16
NiO	0.00	0.00	0.00	0.00	0.00	0.18	0.28	0.00	0.21	0.00	0.00	0.00	0.00	0.17	0.00	0.00	0.18	0.17	0.00
<b>Total</b>	<b>101.75</b>	<b>100.83</b>	<b>100.40</b>	<b>100.51</b>	<b>100.48</b>	<b>101.09</b>	<b>101.21</b>	<b>100.51</b>	<b>101.35</b>	<b>101.22</b>	<b>101.32</b>	<b>101.57</b>	<b>100.46</b>	<b>101.52</b>	<b>101.34</b>	<b>100.90</b>	<b>101.46</b>	<b>101.79</b>	<b>101.37</b>
<b>Cations</b>																			
Cr	9.13	9.37	9.33	9.39	9.37	9.29	9.32	9.28	9.35	9.13	9.37	9.29	9.38	9.31	9.31	9.31	9.34	9.31	9.22
Al	5.14	5.08	5.08	5.10	5.07	5.15	5.11	5.14	5.11	5.35	5.02	5.13	5.06	5.14	5.08	5.06	5.06	5.04	5.18
V	0.14	0.12	0.15	0.12	0.13	0.13	0.13	0.11	0.09	0.15	0.15	0.13	0.12	0.12	0.15	0.13	0.17	0.08	0.12
Ti	0.18	0.16	0.17	0.15	0.17	0.17	0.16	0.15	0.16	0.12	0.16	0.17	0.13	0.16	0.18	0.15	0.17	0.18	0.17
Fe3+	1.20	1.10	1.08	1.08	1.06	1.07	1.10	1.13	1.11	1.11	1.12	1.10	1.15	1.10	1.08	1.18	1.08	1.18	1.11
Fe2+	4.75	4.81	4.90	4.84	4.86	4.86	4.89	4.82	4.85	4.72	4.87	4.87	4.85	4.79	4.88	4.87	4.90	4.79	4.85
Mg	3.39	3.31	3.29	3.33	3.30	3.25	3.23	3.33	3.29	3.42	3.26	3.27	3.31	3.32	3.27	3.25	3.25	3.31	3.30
Mn	0.07	0.07	0.00	0.00	0.03	0.04	0.00	0.02	0.00	0.00	0.05	0.05	0.00	0.03	0.04	0.05	0.00	0.07	0.04
Ni	0.00	0.00	0.00	0.00	0.00	0.04	0.06	0.00	0.04	0.00	0.00	0.00	0.00	0.04	0.00	0.04	0.04	0.04	0.00
<b>Total</b>	<b>24.00</b>	<b>24.00</b>	<b>24.00</b>	<b>24.00</b>	<b>24.00</b>	<b>24.00</b>	<b>24.00</b>	<b>24.00</b>	<b>24.00</b>	<b>24.00</b>	<b>24.00</b>	<b>24.00</b>	<b>24.00</b>	<b>24.00</b>	<b>24.00</b>	<b>24.00</b>	<b>24.00</b>	<b>24.00</b>	<b>24.00</b>
<b>Cation Allocation</b>																			
2+	8.21	8.18	8.19	8.16	8.19	8.15	8.12	8.17	8.14	8.14	8.18	8.19	8.16	8.14	8.20	8.17	8.15	8.17	8.19
3+	15.79	15.82	15.81	15.84	15.81	15.85	15.88	15.83	15.86	15.86	15.82	15.81	15.84	15.86	15.80	15.83	15.85	15.83	15.81
<b>Major cation ratios</b>																			
100Mg/Mg+Fe2+	34.33	33.45	32.99	33.51	33.25	32.48	32.30	33.47	33.05	34.01	32.96	32.72	33.36	33.46	32.87	32.75	32.60	33.63	32.90
100Cr/Cr+Al	63.98	64.85	64.74	64.81	64.90	64.31	64.57	64.36	64.65	63.04	65.11	64.40	64.97	64.46	64.71	64.80	64.85	64.87	64.01
100Fe3+/Cr+Al+V+Fe3+	7.67	7.00	6.93	6.87	6.81	6.87	7.02	7.23	7.10	7.07	7.14	7.03	7.32	6.99	6.92	7.53	6.92	7.58	7.11

10/11	Chr (2)																		
	75	76	77	78	79	80	81	82	83	84	85	86	87	88	89	90	91	92	93
<b>Analysed totals</b>																			
Cr2O3	44.25	44.07	44.50	44.65	44.52	44.26	44.58	44.68	44.94	44.60	44.47	44.56	44.89	44.61	45.06	44.99	44.82	44.20	44.23
Al2O3	17.11	17.13	16.98	17.19	17.28	17.16	17.19	17.26	16.72	17.39	17.00	17.33	17.09	17.11	17.22	17.41	17.13	17.15	17.22
V2O3	0.56	0.59	0.61	0.57	0.48	0.71	0.71	0.72	0.60	0.81	0.58	0.66	0.54	0.55	0.47	0.67	0.71	0.53	0.68
TiO2	0.85	0.84	0.89	0.72	0.86	0.80	0.82	0.74	0.79	0.82	0.81	0.73	0.84	0.85	0.78	0.86	0.80	0.88	0.78
FeO	22.10	22.00	22.04	21.62	21.84	22.11	21.77	22.26	22.05	22.03	22.16	21.95	21.80	22.08	22.28	21.61	22.27	21.80	22.11
Fe2O3	5.87	6.17	5.78	5.83	5.64	6.19	5.97	5.51	5.85	5.35	5.81	5.85	6.07	5.46	5.90	5.94	5.72	5.96	5.98
MgO	8.70	8.73	8.72	8.81	8.73	8.64	8.85	8.56	8.64	8.78	8.63	8.72	8.93	8.49	8.76	9.22	8.54	8.91	8.72
MnO	0.00	0.11	0.09	0.27	0.11	0.12	0.15	0.09	0.10	0.10	0.00	0.23	0.21	0.14	0.00	0.23	0.29	0.00	0.00
NiO	0.00	0.00	0.00	0.00	0.19	0.17	0.20	0.00	0.00	0.00	0.17	0.00	0.00	0.20	0.00	0.00	0.00	0.00	0.00
<b>Total</b>	<b>99.44</b>	<b>99.64</b>	<b>99.62</b>	<b>99.67</b>	<b>99.65</b>	<b>100.17</b>	<b>100.24</b>	<b>99.83</b>	<b>99.70</b>	<b>99.87</b>	<b>99.64</b>	<b>100.03</b>	<b>100.37</b>	<b>99.49</b>	<b>100.47</b>	<b>100.92</b>	<b>100.28</b>	<b>99.43</b>	<b>99.72</b>
<b>Cations</b>																			
Cr	9.11	9.05	9.15	9.16	9.14	9.06	9.10	9.17	9.25	9.13	9.16	9.11	9.15	9.19	9.19	9.10	9.17	9.09	9.08
Al	5.25	5.25	5.21	5.26	5.29	5.24	5.23	5.28	5.13	5.31	5.22	5.29	5.20	5.26	5.24	5.25	5.22	5.26	5.27
V	0.13	0.14	0.14	0.13	0.11	0.17	0.16	0.17	0.14	0.19	0.14	0.15	0.12	0.13	0.11	0.15	0.17	0.12	0.16
Ti	0.17	0.16	0.17	0.14	0.17	0.16	0.16	0.15	0.16	0.16	0.16	0.14	0.16	0.17	0.15	0.17	0.15	0.17	0.15
Fe3+	1.15	1.21	1.13	1.14	1.10	1.21	1.16	1.08	1.15	1.04	1.14	1.14	1.18	1.07	1.15	1.14	1.11	1.17	1.17
Fe2+	4.81	4.78	4.79	4.69	4.74	4.79	4.70	4.83	4.80	4.77	4.83	4.75	4.70	4.81	4.81	4.62	4.82	4.74	4.80
Mg	3.37	3.38	3.38	3.41	3.38	3.33	3.40	3.31	3.35	3.39	3.35	3.36	3.43	3.30	3.37	3.51	3.29	3.45	3.37
Mn	0.00	0.02	0.02	0.06	0.02	0.03	0.03	0.02	0.02	0.02	0.00	0.05	0.05	0.03	0.00	0.05	0.06	0.00	0.00
Ni	0.00	0.00	0.00	0.00	0.04	0.04	0.04	0.00	0.00	0.00	0.04	0.00	0.00	0.04	0.00	0.00	0.00	0.00	0.00
<b>Total</b>	<b>24.00</b>	<b>24.00</b>	<b>24.00</b>	<b>24.00</b>	<b>24.00</b>	<b>24.00</b>	<b>24.00</b>	<b>24.00</b>	<b>24.00</b>	<b>24.00</b>	<b>24.00</b>	<b>24.00</b>	<b>24.00</b>	<b>24.00</b>	<b>24.00</b>	<b>24.00</b>	<b>24.00</b>	<b>24.00</b>	<b>24.00</b>
<b>Cation Allocation</b>																			
2+	8.19	8.19	8.19	8.16	8.15	8.14	8.14	8.16	8.18	8.18	8.14	8.16	8.18	8.14	8.17	8.19	8.17	8.19	8.17
3+	15.81	15.81	15.81	15.84	15.85	15.86	15.86	15.84	15.82	15.82	15.86	15.84	15.82	15.86	15.83	15.81	15.83	15.81	15.83
<b>Major cation ratios</b>																			
100Mg/Mg+Fe2+	33.53	33.71	33.79	34.25	33.68	33.26	34.27	32.75	33.75	33.61	33.36	33.51	34.69	32.76	33.52	35.59	32.78	34.55	33.49
100Cr/Cr+Al	63.42	63.30	63.73	63.53	63.34	63.36	63.49	63.44	64.32	63.23	63.69	63.28	63.79	63.62	63.70	63.41	63.70	63.35	63.26
100Fe3+/Cr+Al+V+Fe3+	7.35	7.71	7.24	7.26	7.04	7.70	7.42	6.86	7.32	6.65	7.28	7.25	7.52	6.85	7.31	7.31	7.11	7.46	7.45

11/11

Chr (2)

	94	95	96	97	98	99	100	101	102	103	104	105	106	107	108	109	110	111	112	113
<b>Analysed totals</b>																				
Cr2O3	45.09	44.96	45.47	45.78	45.79	45.48	45.49	45.85	45.91	45.06	44.93	45.18	45.39	45.23	45.42	45.78	45.28	45.29	45.52	45.57
Al2O3	16.38	16.74	16.15	16.27	16.56	16.51	16.57	15.95	16.37	16.63	16.45	15.87	16.42	16.44	16.26	16.58	16.46	16.82	16.35	16.73
V2O3	0.57	0.87	0.68	0.56	0.65	0.58	0.85	0.72	0.56	0.48	0.77	0.77	0.78	0.56	0.54	0.57	0.55	0.59	0.63	0.66
TiO2	0.84	0.86	0.92	0.89	0.83	0.87	0.78	0.94	0.89	0.90	0.85	0.84	0.84	0.84	0.93	0.83	0.85	0.87	0.90	0.90
FeO	22.50	22.67	22.98	22.68	22.92	22.78	22.58	23.07	22.70	22.53	22.43	22.86	23.18	22.29	22.80	22.91	22.53	23.10	22.78	23.03
Fe2O3	6.13	5.95	5.56	5.83	5.31	5.81	5.82	5.54	5.50	6.00	6.14	5.95	5.24	6.21	5.49	5.54	5.91	5.48	5.64	5.43
MgO	8.25	8.35	8.16	8.18	8.06	8.33	8.34	8.07	8.25	8.32	8.34	7.99	8.00	8.56	8.24	8.32	8.24	8.22	8.15	8.33
MnO	0.18	0.14	0.00	0.30	0.36	0.14	0.13	0.17	0.10	0.16	0.20	0.19	0.00	0.00	0.00	0.00	0.42	0.00	0.36	0.00
NiO	0.23	0.19	0.00	0.21	0.00	0.00	0.24	0.00	0.24	0.24	0.21	0.00	0.00	0.19	0.00	0.00	0.00	0.00	0.00	0.00
<b>Total</b>	<b>100.16</b>	<b>100.73</b>	<b>99.91</b>	<b>100.70</b>	<b>100.47</b>	<b>100.51</b>	<b>100.81</b>	<b>100.31</b>	<b>100.52</b>	<b>100.32</b>	<b>100.32</b>	<b>99.65</b>	<b>99.86</b>	<b>100.32</b>	<b>99.68</b>	<b>100.52</b>	<b>100.23</b>	<b>100.37</b>	<b>100.35</b>	<b>100.67</b>
<b>Cations</b>																				
Cr	9.28	9.19	9.39	9.39	9.40	9.32	9.30	9.45	9.42	9.25	9.23	9.38	9.38	9.28	9.39	9.38	9.31	9.29	9.36	9.32
Al	5.03	5.10	4.98	4.98	5.07	5.05	5.05	4.90	5.01	5.09	5.04	4.91	5.06	5.03	5.01	5.07	5.05	5.14	5.01	5.10
V	0.13	0.20	0.16	0.13	0.15	0.13	0.20	0.17	0.13	0.11	0.18	0.18	0.18	0.13	0.13	0.13	0.13	0.14	0.15	0.15
Ti	0.16	0.17	0.18	0.17	0.16	0.17	0.15	0.18	0.17	0.18	0.17	0.17	0.17	0.16	0.18	0.16	0.17	0.17	0.18	0.18
Fe3+	1.20	1.16	1.09	1.14	1.04	1.13	1.13	1.09	1.07	1.17	1.20	1.18	1.03	1.21	1.08	1.08	1.16	1.07	1.10	1.06
Fe2+	4.90	4.90	5.02	4.92	4.98	4.94	4.88	5.03	4.93	4.89	4.87	5.02	5.07	4.84	4.99	4.97	4.90	5.01	4.96	4.98
Mg	3.20	3.22	3.18	3.16	3.12	3.22	3.21	3.14	3.19	3.22	3.23	3.13	3.12	3.31	3.21	3.21	3.19	3.18	3.16	3.21
Mn	0.04	0.03	0.00	0.07	0.08	0.03	0.03	0.04	0.02	0.03	0.04	0.04	0.00	0.00	0.00	0.00	0.09	0.00	0.08	0.00
Ni	0.05	0.04	0.00	0.04	0.00	0.00	0.05	0.00	0.05	0.05	0.04	0.00	0.00	0.04	0.00	0.00	0.00	0.00	0.00	0.00
<b>Total</b>	<b>24.00</b>	<b>24.00</b>	<b>24.00</b>	<b>24.00</b>	<b>24.00</b>	<b>24.00</b>	<b>24.00</b>	<b>24.00</b>	<b>24.00</b>	<b>24.00</b>	<b>24.00</b>	<b>24.00</b>	<b>24.00</b>	<b>24.00</b>	<b>24.00</b>	<b>24.00</b>	<b>24.00</b>	<b>24.00</b>	<b>24.00</b>	<b>24.00</b>
<b>Cation Allocation</b>																				
2+	8.14	8.15	8.20	8.15	8.18	8.19	8.12	8.20	8.14	8.15	8.15	8.19	8.18	8.15	8.20	8.18	8.19	8.19	8.20	8.19
3+	15.86	15.85	15.80	15.85	15.82	15.81	15.88	15.80	15.86	15.85	15.85	15.81	15.82	15.85	15.80	15.82	15.81	15.81	15.80	15.81
<b>Major cation ratios</b>																				
100Mg/Mg+Fe2+	32.25	32.18	31.79	31.94	31.07	32.25	32.33	31.56	32.12	32.24	32.59	31.46	30.79	33.57	32.13	32.03	32.10	31.27	31.70	31.86
100Cr/Cr+Al	64.86	64.30	65.37	65.36	64.97	64.88	64.80	65.84	65.28	64.50	64.68	65.62	64.96	64.85	65.20	64.93	64.85	64.36	65.12	64.62
100Fe3+/Cr+Al+V+Fe3+	7.68	7.40	6.99	7.28	6.62	7.25	7.22	6.97	6.87	7.50	7.68	7.52	6.59	7.74	6.92	6.90	7.40	6.84	7.07	6.76